The text of this thesis was typeset in LaTeX but the figures were printed separately, cut out and glued in (yes, really). I have the original LaTeX files and the plotting programs for a few of the figures but lost track of the programs and data for most of the plots. With various formats of data tape becoming obsolete it is now certain that the missing plots can never be recreated as good as new. I have now scanned these plots – unfortunately from photocopies of photocopies, working from the only hardcopy of the thesis I have to hand right now – and have used these with the LaTeX files and surviving plotting programs to construct this electronic version.

One day I may find a better quality hardcopy and construct an even nicer electronic edition but as it's taken me over thirty years to get this far, I wouldn't bank on it. Actually I think the Radcliffe Science Library has a PDF as well as the definitive hardcopy. While some page breaks in my version here differ slightly from the Radcliffe, the LaTeX files were adjusted so that all section and subsection page numberings listed in the contents match the definitive version.

It can be cited, optionally including the title 'The Taurid meteoroid complex', as

Asher D.J. (1992), D.Phil. thesis, University of Oxford

(1991, which it says on the abstract page, wouldn't be totally incorrect but the degree viva examination and subsequent minor corrections were early 1992).

Happy(?) reading.

David Asher 2023 August

Erratum: In Table 4.3, the 1989 VA line should read

1989 VA	0.73	0.59	29	225	3	87.8	18.1	0.342

and be above 1991 CB1.

Some papers which I referred to in the thesis as preprints have since been published as follows:

Hartung, J.B. (1993). "Giordano Bruno, the June 1975 meteoroid storm, Encke and other Taurid Complex objects." *Icarus,* **104,** 280–290.

Hasegawa, I. (1992). "Historical variation in the meteor flux as found in Chinese and Japanese chronicles." *Cel. Mech. Dyn. Astron.,* **54,** 129–142.

Whipple, F.L. (1992). "The activities of comets related to their aging and origin." *Cel. Mech. Dyn. Astron.,* **54,** 1–11.

David Asher 11th May 1994

The Taurid meteoroid complex

D.J. Asher

The Taurid meteoroid complex

David John Asher, New College, Oxford

A thesis submitted for the degree of Doctor of Philosophy

Michaelmas term 1991

ABSTRACT

Current knowledge of the Taurid complex of interplanetary objects is reviewed, with its dominant presence in the inner Solar System for the past twenty thousand years emphasised. The importance of giant comets, of which the Taurid progenitor is the contemporary example, is discussed.

The efficiency and limits to the validity of techniques to be used are evaluated. These techniques are primarily computational, but analytic descriptions that greatly help to understand dynamical simulations are also presented.

The first main subject concerns passages of the Earth through a meteoroidal swarm observed in some years only. This requires material concentrated in part of its orbit; the proposed mechanism is the 7:2 mean motion resonance with Jupiter. A detailed model is developed, satisfactorily explaining the years, and range of dates within years, of swarm detections. The possibility is investigated that the swarm parent object (presumably the source of the entire Taurid Complex) has also given rise to a prominent cometary dust trail. The likely evolution over the past few millennia of such a parent is calculated to examine its consistency with periodic meteoroid production that could yield a 200-year cyclicity in extraterrestrial input to the Earth.

For the second major study an appropriate method of selecting Taurids from available meteor data is described and computer models are compared to see which evolutionary schemes best reproduce the meteor orbital element distributions. The Taurids are shown to have most probably originated through splitting of large fragments from the parent near perihelion and subsequent disintegration of many of these fragments on collisions in the asteroid belt. That the complex extends to large masses is confirmed by demonstrating that a statistically significant number of Apollo asteroid orbits are aligned with the Taurid stream as defined by meteors.

The possible association of zodiacal dust bands with the Taurid Complex, and a photographic plate search for asteroids in the swarm and dust trail, constitute further topics. Future observations are encouraged to test the swarm and trail theories.

Contents

Chapter 1

Giant comets and the Taurid progenitor

The aim of this work is to produce quite a detailed model, consistent with observations, of the evolution of the Taurid complex of interplanetary objects. The evolutionary stages that will be concentrated on are those for which the computational modelling of orbital evolution can be used to the greatest advantage. In this introductory chapter we review the wider context into which the work fits and put forward the main questions that will be addressed, as well as describing what the Taurid Complex actually is and how its various constituents are detected.

1.1 The Taurid Complex is big

1.1.1 The Taurid meteor stream

The Taurid complex of interplanetary objects is named after the meteor stream that is the original and best known signature of it. The Taurids do not produce a spectacular meteor shower but the great breadth of the Taurid stream means that it is a major stream with regard to amount of material. The Taurids were recognised as a shower in 1918 and were soon found to be split into two branches, radiants being evident both north and south of the ecliptic (Kronk 1988). After the first orbits had been calculated from photographic (night-time, in October–November) observations, Whipple (1940) predicted that there should be a post-perihelion (daytime) intersection with the Earth in June–July. The daytime β-Taurids and daytime ζ-Perseids were indeed discovered using radar methods, and they were found to have orbits matching the night-time stream (Almond 1951, Lovell 1954). The radiant of the β-Taurids is south of the ecliptic and so they are more closely associated with the Northern Taurids (orbits passing through the ecliptic

between the pre- and post-perihelion intersections); the ζ-Perseids radiate from north of the ecliptic and are the twin shower of the Southern Taurids.

The real size of the stream is evidenced by the fact that the activity lasts at least three months at both relevant times of year. As observations have been done over the years, new names have been given to showers coming from different longitudes in the sky, the Taurids not having as localised a radiant as many of the well-known and more compact streams. But despite the fact that the orbits of meteors in the various showers are comparatively spread out, they are still well enough aligned, and of similar size and shape, that they must be related (*i.e.* have a common origin), as was suspected soon after photographic meteor orbits were first accurately measured, *e.g.* Wright & Whipple (1950) talk of the Southern Arietids and Southern Taurids as being a continuous stream. Regarding the night-time showers, careful analysis of similarity of orbits by Štohl & Porubčan (1990) has identified sub-streams that give rise to a series of separately named showers spanning a period of more than three months as being part of the Taurid Complex. Similarly detailed work on daytime showers has not been done, but when daytime showers were first detected in the late 1940's, May–August was the time of greatest activity (Lovell 1954), and quite a few of the daytime showers active during this period do appear to be associated with the Taurid Complex. The night-time showers listed in Table 1.1 are those identified by Štohl & Porubčan; various daytime showers that Kronk (1988) states are related to the Taurids are also listed. An orbit from each is drawn projected on to the ecliptic (noting that they have low inclinations) in Figure 1.1. It has to

Southern Arietids	October 8
Northern Piscids	October 12
Southern Taurids	October 30 – November 7
Northern Taurids	November 4–7
Northern χ-Orionids	December 10
Southern χ-Orionids	December 10
ρ-Geminids	January 8
Daytime ε-Arietids	May 9
Daytime ζ-Perseids	June 13
Daytime β-Taurids	June 30

Table 1.1: Taurid Complex showers, with dates of maximum activity given by Kronk (1988).

be borne in mind that the orbits even within each sub-stream are quite spread out; this Figure is simply to give a rough picture of the Taurid stream. We shall take the term "Taurid stream" to include the related streams.

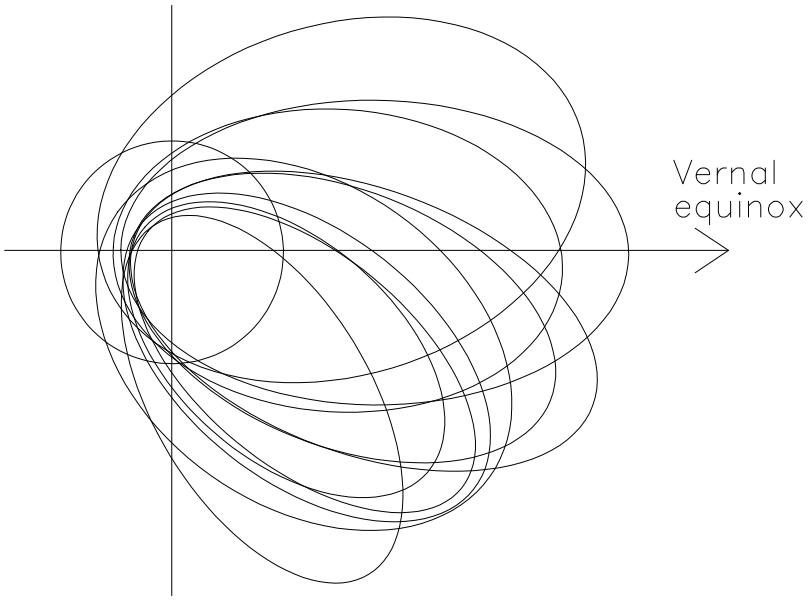

Figure 1.1: A representative orbit from each of the Taurid sub-streams listed in Table 1.1. Orbital elements from Kronk (1988). The circle is the Earth's orbit.

Around three quarters of meteors are sporadic rather than belonging to well-defined streams (see Kresák 1968), although the dividing line is not clear-cut — perhaps 20% of meteors sometimes classified as sporadic actually occur as part of minor showers (Hughes 1990). Indeed some of the Taurid Complex showers listed above are best described as minor showers (Štohl & Porubčan 1990). The proportion of sporadics increases significantly for fainter meteors (Hughes 1978), as expected since as orbital evolution (spreading the meteoroids away from stream orbits) takes place, so will physical (collisional) evolution, producing smaller meteoroids. Thus the meteoric influx to the Earth is dominated by sporadic meteors. The fact that a substantial proportion of the sporadic background (which, depending on one's terminology, may include some of the minor sub-streams mentioned above) in fact constitutes a very broad stream surrounding the more clearly defined Taurid stream, as follows, is one of the most convincing demonstrations of the great amount of material associated with the Taurid Complex.

The apparent radiants of radar meteors (and, at night time, visual and photographic meteors) show significant maxima in helion (HE), *i.e.* a direction coming from the Sun, and antihelion (AH) directions. Strong seasonal variations in these sources find a natural explanation in a huge, diffuse, sporadic stream surrounding (aligned with) the Taurid Complex (Štohl 1984, 1986). That is, the sporadic meteoroids move on similar orbits to meteoroids that are part of what is generally

recognised as the Taurid stream, but there is a somewhat greater dispersion of elements in the sporadic stream. The geometry of stream orbits and radiant directions is shown in Figure 1.2. Both HE (daytime) and AH (night-time) sources have broad

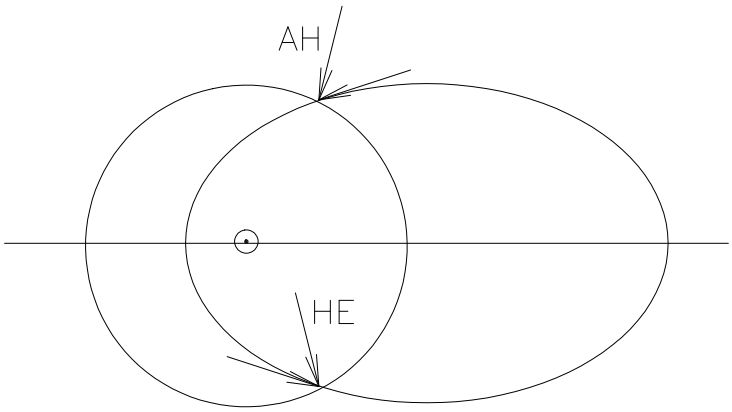

Figure 1.2: A representative orbit in the sporadic meteor stream of Štohl (1984, 1986), with the directions of true radiants, and helion (HE) and antihelion (AH) apparent radiants, shown.

maxima that last for at least three months, for the HE source during April–June and for the AH source during October–December. This picture, deduced from number counts and radiants, of a broad stream to which so many sporadic meteors belong appears to be confirmed by orbital data. We point out the existence of an apex (AP) source (see Štohl 1986) which dominates for fainter (10th magnitude, say) meteors. These AP detections are enhanced due to the Earth's velocity in space (the meteors having a velocity relative to the Earth leading to their coming from the apex direction of the Earth's motion) and are due to lower-eccentricity (e tending to be between 0 and 0.6 for the most part) meteoroids whose orbits have presumably been circularised by the Poynting-Robertson effect, which acts preferentially on smaller particles. These meteoroids essentially belong to the background zodiacal dust cloud (see Section 1.1.2). Thus the broad sporadic stream (with typical eccentricities of $\sim$0.75) surrounding the Taurids is most clearly evident in a size range intermediate between masses relating to stream meteors and masses relating to zodiacal background meteors.

Figure 1.1 shows that there is a tendency for larger orbits in the Taurid stream to be at greater longitudes (*cf.* trends with longitude calculated by Štohl & Porubčan 1990). This is because of the differential effect of Jupiter on the rate of longitude precession on orbits of different sizes and will be considered extensively during this thesis. We shall see in due course that this dispersal in longitude is associated with

a timescale of ∼10 kyr (1 kyr = 1000 years).

Though there are clearly preferred longitudes for Taurid orbits, it is dynamically expected that some orbits will be present at all longitudes, firstly of meteoroids that separated from the parent object at the greatest times in the past and secondly of meteoroids that have the fastest precession rates. Despite the strong seasonal variations in the sporadic meteor flux described above, that there is some activity from these two specific directions, the near-ecliptic HE and AH sources, at all longitudes among radar meteors has been known for some time (*e.g.* see Hawkins 1956, Štohl 1968). Furthermore the distribution of orbits of photographic meteors (*e.g.* see McCrosky & Posen 1961) and fireballs (*e.g.* see Dohnanyi 1978) as a whole shows a prevalence of size, shape and inclination of orbits typical of the Taurid Complex. Although inclinations are generally low, the lack of orbits with i below $\sim 3^\circ$ reported by McCrosky & Posen appears of interest as this i distribution is what is expected of Taurids (Chapter 4).

The discussion so far has concentrated on meteors. The other objects for which accurate orbits exist (and which therefore also provide useful information for orbital models) are those large enough to be observed away from the Earth, *viz.* comets and Apollo asteroids. The best known member of the Taurid Complex is Comet P/Encke which has long been regarded as the parent object of the Taurids. Of Apollos that have similar (low inclination, high eccentricity, similar perihelion distance) orbits to Encke and the Taurid meteors, more are found aligned fairly well with them in longitude than would be expected by chance (see Section 4.4), from which we infer a common origin. Thus the Taurid Complex contains several known Apollo asteroids (Clube & Napier 1984, Olsson-Steel 1987a), and there is the possibility of one other comet (Rudnicki), though the similarity of Rudnicki's perihelion distance and longitude with Encke's may be coincidence (see Olsson-Steel 1987a, Steel 1992). Figure 1.3 shows the orbits, projected on to the ecliptic, of Encke and the asteroids identified as belonging to the Taurid Complex in Section 4.4 of this thesis, and may be compared to Figure 1.1. Tentative evidence for cometary activity on Asteroid 2201 Oljato was presented by McFadden *et al.* (1984). Olsson-Steel (1988) searched radar data for meteoroid streams associated with particular asteroids and found that various individual Taurid asteroids (as opposed to simply the Taurid Complex in general) do indeed possess meteoroid streams.

Accurate orbital data on meteors have been collected for the past fifty years and in many ways accurate orbits are the most useful kind of observational information when constructing dynamical models. When we use these data (Chapter 4), we shall

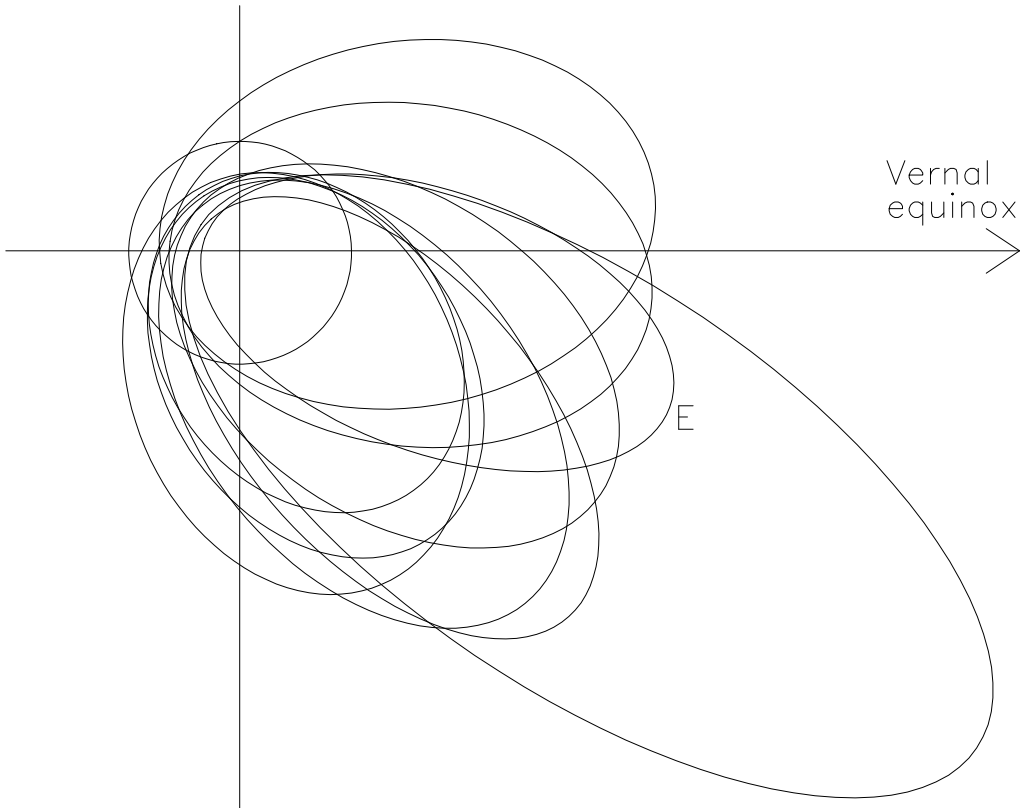

Figure 1.3: Orbits of Encke's Comet (E) and Taurid Complex asteroids; *cf.* Figure 1.1.

simply consider orbital elements rather than the somewhat arbitrary question of what sub-stream (or sporadics) to classify the meteors as. One of the main questions of that chapter will be the mechanism for generating the range in size of orbits (which then undergo differential precession due to Jupiter as described above). We shall see that the distribution of Taurid meteor orbits as detected by photography and radar is best explained by a model in which large cometary fragments split from the parent object (the Encke progenitor) at perihelion and these fragments then undergo catastrophic collisions with objects in the asteroid belt. The importance of violent collisions with asteroids in the evolution of the Taurid stream was first suggested by Whipple & Hamid (1952). The frequent occurrence of catastrophic disruption of cometary fragments is suggestive of a rather fragile parent body, which we now proceed to discuss.

1.1.2 The source of the Taurid Complex

The production of meteoroids during the course of regular fragmentations means that there is a continuous input of material to the zodiacal complex. The broad

sporadic stream surrounding the Taurids is naturally understood as being the intermediary between the more structured Taurid stream and the background zodiacal cloud (Clube 1987), as material gradually disperses, with higher (a, e) meteoroids gradually feeding the lower (a, e) zodiacal background as they undergo both comminution and orbital decay. We envisage a picture whereby material in the inner Solar System not only originates primarily from comets, but is derived from a single large body, as proposed by Whipple (1967).

Some dust must originate from asteroids but the fact that the Pioneer spacecraft in the 1970's found no dust enhancement on passage through the asteroid belt (Humes *et al.* 1974, Fechtig 1984), suggesting that there is no strong concentration at source, casts doubt on any idea that the majority of zodiacal dust and meteoroids is asteroidal. In addition, the model of Dohnanyi (1976) suggests that asteroidal particles in the dust size range are destroyed by collisions with cometary particles at a much faster rate than that at which they are created. Clube (1987) has emphasised how the nature of interplanetary dust particles collected from the stratosphere and the low compressive strength of the commonest fireballs is indicative of a cometary rather than asteroidal origin for the zodiacal complex, and consequently for the mass input to the Earth. This comment about mass input to the Earth does not necessarily extend to material that survives passage through the atmosphere to be collected as meteorites, since here there is a clear selection effect against the weaker material of which comets are composed.

By considering the amount of matter produced by comets and its orbital distribution, Kresák (1980) showed that the presently observable population of active comets is totally insufficient to maintain the zodiacal dust cloud in the inner Solar System at its current density. Meteoroids in the inner Solar System undergo both orbital and physical (collisional) evolution, with radiative effects eventually removing particles from the zodiacal complex altogether. The natural evolutionary sequence of stream meteoroids from short-period comets feeding the sporadic meteoroid component which in turn feeds the background zodiacal cloud requires some major source in the recent ($\sim 10^4$ yr) past (Olsson-Steel 1986). The zodiacal dust cloud is therefore not in a steady state, being replenished by the occasional arrival of exceptional comets, the last of which must have arrived recently enough to produce the current zodiacal dust. The arrivals of these giant comets in the inner Solar System are separated by $\sim 10^5$ yr (Clube & Napier 1984) — though there is a long-term modulation of this rate (Section 1.2.4) — and the mass of the zodiacal cloud undergoes substantial fluctuations on such timescales. Arriving in the inner

Solar System perhaps 20 kyr ago, the contemporary giant comet is almost certainly identified, as suggested by Whipple (1967), with Comet P/Encke, which was (or whose progenitor was) therefore much larger in the past.

Meteor observations, *in situ* satellite experiments, lunar microcraters and zodiacal light observations can be used to determine the mass function and overall particle number density of zodiacal meteoroids. Grün *et al.* (1985) evaluated these quantities and constructed a collisional model of the zodiacal complex, in which particles continually erode and fragment. They found that the observations reveal a deficiency of source particles in the range 10^{-4} g $< m <$ 1 g, assuming a steady-state model, these particles being destroyed by collisions in $\sim 10^4$ yr. If there is a continual replenishing input of meteoroids at these larger masses (*e.g.* from comets), then in the mass range 10^{-10} g $< m < 10^{-5}$ g the particle density is increasing on timescales of 10^{4-5} yr because these particles are created as collision products of the larger meteoroids at a faster rate than that at which they are destroyed or removed by the Poynting-Robertson effect. The fragmenting giant comet evidently provides an adequate replenishing source at these masses during the past 10^4 yr, and the largest fragmentations may cause moderate fluctuations in the zodiacal meteoroid and dust population on $\sim 10^3$ yr timescales (Clube 1987).

The total mass of the zodiacal cloud is in the region of 2.5×10^{19} g, in masses $\lesssim$1 g (Whipple 1967). However, a significant number of dust particles incident on the Earth arrive in swarms and are explained as being due to very weakly bound meteoroids of mass 10^2 g $< m < 10^6$ g that are electrostatically disrupted on passage through the auroral plasma (Fechtig 1982); $\sim$30% of the dust influx to the Earth detected in the HEOS-2 satellite experiment was derived from these few larger meteoroids, and of course over a longer timescale it could well be that a few even larger meteoroids would be detected; the bulk of the mass could be in larger bodies (*cf.* discussion of mass function, Section 4.3).

Gustafson *et al.* (1987) showed that the interplanetary dust distribution was well explained if most of the dust originated during the last few 10^4 yr from Comet Encke. This is an important demonstration of how a source on an Encke-like orbit can generate the *spatial* distribution of the zodiacal dust cloud, but we are here stressing the likelihood of the intermediate *physical* stage of larger meteoroids generated from fragments of the Taurid parent.

In the inner Solar System at the present day, then, we are faced with a huge meteoroidal complex which represents the disintegration products of a single giant comet. We note that the mass of comets is concentrated in the few largest bodies

(Donnison 1986). The Taurid progenitor object may still exist as a substantial (but now devolatilised and hence fragile) core body or may have completely disintegrated leaving no objects larger than asteroids a few km in diameter. It is also possible that the source "object" is a compact (gravitationally bound) swarm of meteoroids with no single dominant object. The size of the original comet may have been as much as ∼100 km (Clube & Napier 1984).

The picture, then, is of a single large source for most of the present zodiacal material. This comet would have been captured into the inner Solar System some 20 kyr ago and would be expected to undergo an initial highly active phase during which most of its volatiles were lost — this material is now quite widely dispersed. For the past ∼10 kyr the comet has been devolatilised (though perhaps weakly reactivated from time to time by violent impacts; Clube 1987) but has regularly generated meteoroids as input to the zodiacal complex. It is dynamical aspects of the latter evolutionary phase that are primarily considered in this thesis.

1.1.3 Swarms of meteoroids

We now describe various detections of meteoroidal swarms (and of some single objects) likely to be associated with the Taurid Complex. In certain years, at one of the two times of year (October–November for the pre-perihelion intersection with the Earth, the latter part of June for post-perihelion) when the Earth-Moon system passes through the core of the complex, swarms of meteoroids have been detected. We use the term "swarm" to refer to members of a stream that are not fully spread round the orbit. If there is a swarm, events are expected that are not repeated every year. In quite a few of the following cases the effect has specifically not been observed in other years (as opposed to simply being missed because no observation was attempted); non-observations can be very important (Chapter 3).

Virtually all the events described here can reasonably be expected to be related to the Taurid Complex. While some of them will be single random encounters, some definitely relate to concentrations of many meteoroids in only part of the orbit. In Chapter 3 we shall consider reasons for this restriction to part of the orbit, in particular the mechanism of the 7:2 mean motion resonance with Jupiter. We shall defer the detailed interpretation of the timings and duration of the various events to the later chapter and for the moment let the description simply take the form of listing a wide variety of phenomena relating to detections of Taurid Complex material. The observations are summarised in Table 1.2.

One of the meteoroidal swarms that has received most attention in recent years

Jun 1178	Bruno crater on Moon
Jun 1890	Farmington meteorite
Jun 1908	Tunguska meteoroid
Jun 1975	Swarm detections with lunar seismometers
Jun 1975	Disturbances to Earth's ionosphere
Oct–Nov 1951	Dutch fireball swarm
Nov 1968	Break-up of large meteoroid
Nov 1974	Submicron dust detection
Nov 1981	Swarm causing localised dayglow obscuration
Feb 1969	Passage of Earth through dust cloud
(Remotely observed)	IRAS dust trail

Table 1.2: Detections of Taurid Complex meteoroids (see text for details).

is that detected during lunar seismometer studies that recorded a series of impacts of objects up to 50 kg in mass on the Moon over several days in late June of 1975 (Dorman *et al.* 1978). The swarm's occurrence was apparent on the Earth because ionisation produced by incoming meteoroids affected the propagation of radio waves in the ionosphere (Kaufmann *et al.* 1989). Oberst (1989) linked the Farmington meteorite of 25 June 1890 to the lunar swarm and although he cast doubt on the Taurid Complex association, the possible significance of Farmington was discussed by Steel *et al.* (1991a).

Regarding large masses, the 50–100 m Tunguska meteoroid of 1908 was almost certainly a Taurid Complex member owing to its date (30 June) and the direction of its radiant (Kresák 1978). Of all extraterrestrial objects to have hit the Earth, this is the largest of which we have direct evidence and recorded observations. Even larger, though, was the object that was observed producing a spectacular event on the Moon in June 1178 and most likely formed the 20 km Giordano Bruno crater (Hartung 1976, 1991).

The Corvid meteor shower, observed only in 1937, was in late June but as the radiant was not near the Sun, it cannot be regarded similarly to the above. However, Hartung (1991) has suggested that as the meteoroids intersect the Earth-Moon system, they could be secondary meteoroids resulting from a recent impact on the Moon (*e.g.* the one in 1178), being material ejected into heliocentric orbits (but not necessarily Taurid orbits).

Turning to November, there was a swarm of very bright Taurid meteors (of magnitudes between 0 and –5, corresponding to masses ∼10 g) observed from Holland and lasting over a week in 1951 (van Diggelen & de Jager 1955). Accurate orbits are

unfortunately not available for these meteors. Observations of other enhancements of bright meteors in the Taurids are discussed in Chapter 3. Bigg & Thompson (1969) reported a photograph of four meteors, much brighter than the near-full Moon, and an accompanying dust cloud taken on 11 November 1968 (in the early morning, but with the meteors coming from the night side of the Earth). These four meteors moved on similar paths which took them only briefly into the region of the atmosphere where trails would be formed, and were apparently released by a single very large meteoroid.

Frank *et al.* (1987) found a substantial increase in the occurrence of transient dark spots in the Earth's ultraviolet dayglow, as observed by satellite, in early November 1981. Their preferred explanation for these "atmospheric holes" is that small cometary objects entered the upper atmosphere and were disrupted, with the resultant water vapour absorbing the dayglow at the appropriate wavelengths. An alternative interpretation is that the energy from incoming meteoroids causes atmospheric oxygen to rise to the heights at which absorption occurs. This alternative results in the overall influx of meteoroids of the relevant masses to the Earth being much larger than what is commonly believed, but a *temporary* enhancement of large meteoroids is clearly not inconsistent with passage through a massive meteoroidal swarm. We point out that though the observations are on the daytime side of the Earth, they are actually looking down on top of the Earth and so can detect meteoroids on Taurid orbits coming from the night-time direction. The most significant point appears to be the similarity of the dates to those of the bright Taurid observations in 1951 (see Chapter 3), suggesting separate encounters with the same swarm.

Considering the dust end of the mass range, detectors on satellites found a significant enhancement of submicron dust related to the Taurids in November 1974 (Singer & Stanley 1980). Roosen *et al.* (1973) showed that a temporary reduction in the Gegenschein in February 1969 could be explained by dust passing through the Earth's shadow, having been blown out by solar radiation pressure from the descending node of Comet Encke (or a dust swarm moving in a similar orbit). This did not happen when the observation was repeated in February 1971, near the time of Encke's nodal passage, possibly suggesting an object or swarm of material in an Encke-like orbit but at a different anomaly.

Finally, a detection not actually at or near the Earth-Moon system but conveniently mentioned here is the very bright dust trail associated with Comet Encke discovered near aphelion by IRAS (the Infra-Red Astronomical Satellite) in 1983

(Sykes 1988). In Chapter 3 the possibility is investigated that the Taurid source object may lie within the trail, *i.e.* that the trail may be largely generated by this object and not by Encke itself. We have mentioned the possibility of a swarm of meteoroids in the 7:2 Jovian resonance; this concentration of meteoroids in a resonant swarm would be presumed to have happened over several kyr, enough time for the swarm to become sufficiently wide that the Earth takes over a week to pass through it (swarm passages in 1951, 1975, 1981; Table 1.2). The source object would be expected to oscillate backwards and forwards through the resonant swarm (Chapter 3) and the trail would represent a more compact concentration of material, released during a more recent period. Encke was not observed before 1786 despite the fact that it should have been detectable (Kronk 1984) and the question arises whether any inferred orbit of the parent object is consistent with Encke splitting off the parent shortly before its (Encke's) discovery, this event giving rise to the trail in addition to Encke.

It can be seen that there are many detected events plausibly connected with the Taurid Complex; nothing like this range of phenomena has been discovered in relation to any other stream. Whilst the probable association of various of the above phenomena with the Taurids has been noted in the past (Brecher 1984, Clube & Asher 1990, Clube & Napier 1984, Hartung 1991, Steel & Clube 1991), this thesis will attempt to produce a more detailed dynamical model of the evolution of the complex to explain the phenomena than has hitherto been done.

1.1.4 The Taurid Complex and the Earth

Up to this point, we have described various presently detectable components of the Taurid Complex, covering the entire size range from submicron dust particles to km-sized asteroids. These observations provide valuable information for investigating the past evolution of the complex, and orbital evolution studies aimed at reproducing the complex's present-day structure (*e.g.* as determined from measured meteor orbits; Babadzhanov *et al.* 1990, Steel *et al.* 1991a) suggest timescales of 10–20 kyr for the age of the complex. There will of course have been considerable mass influx of Taurid Complex material to the Earth over this time and it would be very useful if in addition to observations of the present structure of the complex, we could find direct clues to the structure in the past, as evidenced by the input of extraterrestrial material to the Earth. Possible presently detectable signatures of past meteoroidal input are isotopic and elemental abundances, and, insofar as a substantial influx of meteoroids or dust may be expected to influence the atmospheric temperature,

evidence for past climatic variations, *e.g.* as measured by tree-ring data (Sonett & Suess 1984). We are not immediately insisting that all past, say, ^{14}C abundances and climatic variations must be explained by a mechanism of meteoroidal input to the Earth, but any variation in the past 20 kyr that follows naturally from a model of the evolution of the Taurid progenitor would have to be regarded as significant. Of course, the Taurid Complex is not the only source of dust and meteoroids incident on the Earth, but as discussed so far in this chapter, there is reason to believe that it is currently the dominant one.

A direct association of the Tunguska event with cosmic elemental abundances in the Tunguska region itself and in a South Pole ice core was demonstrated by Ganapathy (1983); material could have been transported to the South Pole through the stratosphere after the explosion; alternatively the large meteoroid could have been in the middle of a sizable dust swarm. As discussed by Clube & Napier (1984, 1987), similar exotic abundances were found in a Greenland ice core corresponding to ages up to 20 kyr ago, making it plausible that the source of the Tunguska object has been around for such a period of time.

The principal long-term climatic effect due to incoming low-density fragile meteoroids that fragment when they enter the atmosphere is expected to be periods of cooling induced by atmospheric dust veils (Clube 1991, Clube & Napier 1984). This does not preclude temporary periods of atmospheric greenhouse enhancement (Clube 1991) during epochs when the mass input is dominated by the most highly friable meteoroids, which can be severely enough disrupted to produce tiny particles that can interact chemically with the atmosphere. It is possible that the friability of meteoroids increases the longer they have been in interplanetary space owing to loss of volatiles.

There is clear evidence for a correlation over the past several kyr between higher ^{14}C levels and cool temperatures (Sonett & Suess 1984), implying some common mechanism. The conventional explanation for isotopic variations invokes modulation of the solar cosmic ray flux. While the necessary nuclear processes may be triggered by solar cosmic rays, it may be that the changing levels are due to varying amounts of the parent species (*e.g.* ^{13}N for ^{14}C production), brought into the terrestrial environment in meteoroidal material. Alternatively, incoming large meteoroids that heat up may produce sufficient temperatures that, although sub-nuclear, still generate neutrons with enough energy to produce ^{14}C (Brown & Hughes 1977). Though a meteoroidal mechanism for isotopic variations is unproven, it is at least plausible.

It seems reasonable to associate the most recent (late-Pleistocene) glaciation (∼20–10 kyr ago) with the most active phase of the Taurid progenitor giant comet (see Clube & Napier 1984). Thus it may have been captured into a small-perihelion, sub-Jovian orbit ∼20 kyr ago and lost most of its volatile material during the first 10 kyr. The devolatilised comet may have continued to provide input to the Taurid Complex since then but at a lesser rate, so that the overall decline in the Δ^{14}C level during the Holocene (Oeschger & Beer 1990) is reasonably understood in terms of enhanced ^{14}C input during the late Pleistocene, correlated with the reduced temperature, followed by a discontinuity in mean temperature and a declining reservoir of ^{14}C on the Earth, the ^{14}C no longer being sufficiently replenished as it decays.

If the Δ^{14}C excess during the ice age is due to the giant comet then it is plausible that irregular and regular modulations of Δ^{14}C, imposed on the overall decline, are also due to the giant comet, *i.e.* mass input to the Earth could be modulated by the largest fragmentations over the past 10 kyr, which would result in random enhancements of the zodiacal complex, and the more predictable effect of intersections of the Taurid parent's precessing orbit with that of the Earth, since concentrations of meteoroids would be expected near the orbit of the parent. In addition there can be short-term cyclicities. Oeschger & Beer (1990) describe a clear 200 yr periodicity in ^{14}C variation in tree rings, in phase with a similar periodicity of ^{10}Be in ice cores. In Chapter 3 we shall be developing the idea of a massive meteoroidal swarm at the core of the Taurid stream, with the parent object librating about the centre of the swarm, and one possible mechanism, that will be dynamically tested in Section 3.4, for generating an appropriate cyclicity, is through impacts of swarm meteoroids on the parent during its passage through the densest part of the swarm resulting in a periodic enhancement of the dust and meteoroid production rate. The critical question is whether the librating source has the correct period and phase.

1.1.5 History

Another line of evidence that has the potential to provide important constraints on models of past evolution is historical information. The various aspects of this and their relevance to the Taurid Complex have been discussed by Clube & Napier (1982a, 1990).

We have already mentioned the 12th century observation of the event that formed the Bruno lunar crater. Perhaps the clearest example of useful historical evidence is spectacular meteor showers observed in historical times, which can provide valuable information if their time of occurrence is known. Astapovič & Terenteva (1968)

investigated past observations of fireballs and found that a thousand years ago the Taurids were the most powerful shower. Furthermore the Northern Taurid branch was twice as strong as the Southern branch, a situation that does not persist today (Hindley 1972). It may be difficult to construct a model of sufficient detail to explain all historical observations associated with the Taurids, nor will a model necessarily be unique, but the possible use of historical records must be kept in mind. A further example of the way in which the effects of the proposed giant comet may have been apparent in historical times is provided by evidence that the zodiacal light was observed to be much brighter in the past (see Clube & Napier 1984, Clube 1987).

Increased meteor or fireball observations in the historical record could result from nodal crossings of the Taurid parent object or any dense meteoroidal swarm with the Earth, or from fragmentations of large Taurid objects which give rise to large new populations of meteoroids. In addition to the recording of astronomical phenomena, and rather more significantly for anyone around at the time, there is the question of catastrophic impacts. In a similar way to the variation in the input of extraterrestrial material to the Earth, discussed above, the Earth may at various epochs have undergone much more intense periods of bombardment than the one Tunguska-size object experienced this century (Clube 1990). Whilst a detailed interpretation of human history along these lines is not straightforward, some events do find a natural explanation in a giant comet which is known to have been disintegrating for the last several millennia.

The fact that the Taurid Complex is the dominant entity in the inner Solar System at present and the fact that it has interacted (and, although the most active evolutionary phase is probably over, may still interact in the future) with the Earth on timescales relevant to human civilisation both provide good reasons for studying it, quite apart from the increase in understanding of the behaviour of small Solar System bodies that is likely to result.

1.2 The origin of Earth-crossing objects

Having surveyed the various stages in the physical decay of the giant comet Taurid progenitor and the Taurid Complex components that have resulted, we now concentrate the discussion on the comet rather than the disintegration products. We consider the initial capture into a short-period orbit and the orbital and physical evolution thereafter. In a wider context, we address the question of cometary origins in general. For a full discussion of the origin of comets and the history of ideas on

the subject see Bailey *et al.* (1990).

The orbital evolution of meteoroids in the Taurid Complex could be investigated without regard to the ultimate source of the progenitor object; we could simply postulate that a giant comet somehow entered a sub-Jovian orbit about 20 kyr ago, and construct a model, consistent with observations, of its evolution from that point. This could be regarded as a little narrow-minded, and we shall here describe a general picture of giant comets, of which the Taurid parent is just one example. Of course, there are questions relating to the orbital origin and physical nature of short-period comets and Earth-crossing asteroids upon which there is not presently universal agreement so that what follows should not be regarded as a definitive statement of current knowledge; indeed we shall describe alternative theories. Nevertheless, the aim will be to present the ideas from the viewpoint that is in best accord with what is known about, and what this thesis will discover about, the evolution of the Taurid progenitor. The main points will be the physical and orbital evolution of giant comets, their importance in providing the population of Earth-crossing objects and their consequent influence on the terrestrial environment, and the long-term patterns of their arrival in the inner Solar System.

1.2.1 Short-period comets

The majority of discovered comets are long-period (LP); see, *e.g.*, Donnison (1986) for relative numbers. The sharpness of the peak at a near-parabolic value in the energy distribution of comets means that the existence of the Oort cloud — a spherically symmetric cloud of comets extending several 10^4 AU from the Sun — is not in doubt, and also that most of these comets are "new", *i.e.* entering the planetary system for the first time (see Section 1.2.4 regarding the mechanism for perturbing new comets into the planetary system), since the energy perturbations during even a single passage through the planetary system would broaden the peak in the distribution (Oort 1950). Indeed because passage through the planetary system disperses the energy, the peak at near-parabolic values is much higher than would be predicted by a steady-state model — the "fading problem" (see, *e.g.*, Bailey 1985), discussed below.

There is apparently a concentration of short-period (SP) comets under the control of Jupiter, with period $P \lesssim 13$ yr (Everhart 1972). The physical lifetime of those SP comets with small perihelion distance is very short compared to the age of the Solar System and so a source and a capture mechanism are needed. The question naturally arises whether SP ($P<200$ yr) comets are simply due to capture of LP

comets by the giant planets, and in particular whether the Jupiter family of comets is due to capture from the Oort cloud LP population by Jupiter, a critical point being whether the isotropic LP population can reproduce the low-inclination prograde orbits typical of the Jupiter family. Provided that the perihelion distance $q \lesssim 6$ AU ($\sim$1 AU outside Jupiter) so that capture may occur on short enough timescales, full numerical integrations of the three-body system Sun-Jupiter-comet are well within current computer technology. Everhart (1972) found that low-i, prograde orbits in the spherically symmetrical Oort cloud were preferentially captured, explaining the observed i distribution of short-period orbits; the period distribution was also reproduced well. Quinn *et al.* (1990) showed that although the capture probability from a near-parabolic orbit eventually to an SP orbit is an order of magnitude greater for low-i ($0 < i < 9^\circ$) than isotropic orbits, these low values of i occupy such a small proportion (<1%) of isotropic phase space that the observed inclinations of Jupiter family comets are not quite reproduced. However, the capture timescales are longer for high-i orbits and comets are not expected to survive arbitrarily many perihelion passages. Restricting their results to comets captured within 1000 perihelion passages, Quinn *et al.* found that 25% of Jupiter family comets have i less than the observed median — still a slight discrepancy, but if one giant comet gave rise through splitting to many Jupiter family comets then the results seem perfectly in accord with observations, capture of one object into such a low-i orbit being wholly unremarkable.

Even if the orbital distribution is correct, though, there is a long-recognised problem (*e.g.* Joss 1973) that the observed number of LP (Oort cloud) comets (presumably constant over the last $\sim 10^5$ yr, the timescale on which the current SP population has been captured) is hopelessly insufficient to produce the observed number of SP comets. However, this problem can be overcome if the actual *number* of comets captured were less but if one or two of these were exceptionally large and, after initial capture, underwent a significant amount of splitting to produce many SP comets, as first suggested by Alexander (1850); cometary splittings are certainly known to occur frequently (Pittich 1972) and may also be necessary to explain steady-state models of the Oort cloud itself. This may well be relevant to the Encke progenitor, and the possibility that this single object gave rise to much of the present Jupiter family of comets should not be overlooked in the future, though the problem of numbers is conventionally overcome by invoking additional cometary reservoirs.

These other populations of comets proposed as the SP comet source are a dense,

isotropic inner core to the Oort cloud, and a trans-Neptunian disc (the Kuiper belt; Kuiper 1951) of comets. These are both plausibly formed with the rest of the Solar System, and comets from both could also be fed outwards into the Oort cloud, helping to solve the problem of the latter's depletion over the age of the Solar System (see Bailey *et al.* 1990), though these are not the only solutions to this problem as comets could be captured by the Sun when it passes through giant molecular clouds (Clube & Napier 1982b).

When new comets from the Oort cloud are perturbed into the planetary system, a uniform distribution of q is expected (Joss 1973) and the studies described above restricted q to being near Jupiter's orbit since Jupiter has a much larger effect than the other planets; for these initial q-values capture timescales are comparatively short. The inner Oort cloud and Kuiper belt reservoirs of comets by definition contain huge numbers of comets with q nearer the edge of the planetary system, with Uranus or Neptune likely to be important in the initial stages of capture; timescales for capture are now so long that when allowing for the effect of these planets, a method of avoiding having to integrate the full equations of motion is necessary. Everhart (1977) derived a probability distribution numerically for the effect of single approaches to each planet; Stagg & Bailey (1989) extended this to allow for more than one planet having an effect at a time, *i.e.* the comet not having to be under the control of single planets in turn, and found that this did affect the results slightly. In contrast, Quinn *et al.* (1990) multiplied the planetary masses by a large factor (10 or more), arguing that if the orbital changes are effectively a diffusion process then the increased masses change merely the rate, but not the result, of the process. They found that orbital elements of Jupiter family comets, in particular the low inclinations, were reproduced by the Kuiper belt source but not by an isotropic source. Stagg & Bailey, however, broadly confirmed the conclusions of Everhart, finding that low i orbits *were* preferentially captured from the inner core to the Oort cloud and suggested that for orbits that take a long time to be captured, the capture process is dominated by a few reasonably large perturbations, *i.e.* a "stochastic" rather than "diffusive" process. Whilst Stagg & Bailey's discussion was aimed primarily at application to the inner Oort cloud, a similar capture mechanism presumably applies also to the conventional Oort cloud.

We probably have to accept that none of the above possibilities for the origin of the Jupiter family of comets has been conclusively eliminated by dynamical studies, but for the reasons discussed in this Section it appears unnecessary to invoke the initial cometary reservoirs. The idea of the conventional Oort cloud as the only

source has the advantage (if this is an advantage) of being a source that is known to exist rather than just one that is cosmogonically plausible. Further evidence in favour of the conventional Oort cloud picture, and the importance of giant comets, is likely to come from a successful theory of geological catastrophism (see Section 1.2.4) since comets are an integral part of this. Under this picture we do not appeal to the inner Oort cloud or Kuiper belt except insofar as they may consist of comets in the process of being captured. We note that these cometary reservoirs are in principle detectable by gravitational effects, stellar occultations or infra-red flux (Bailey 1984).

Having concentrated on dynamical aspects, we focus now on the physical nature of giant comets. LP comets have much brighter absolute magnitudes than SP comets (Donnison 1986), and could typically be 100 times larger. The fading problem (see above) is best explained if comets show a diminishing tendency to disrupt (split) as they evolve; see Table 8 of Oort (1950). In particular, observations seem to be understandable if many new, large comets undergo splitting and effectively disappear. LP comets may also be intrinsically brighter, in accord with evolution of volatile-rich comets into devolatilised ("cometary") asteroids, which, though fragile compared to main-belt ("asteroidal") asteroids, will be less likely to split spontaneously. We put forward the idea of differentiated giant comets, in which the volatiles are concentrated towards the outer layers, perhaps owing to formation in a hot medium (Clube 1988) so that volatiles rose towards the surface, as with meteorite "parent bodies". We apparently deal with inhomogeneous cometary material partitioned between active and inactive (cometary) components (Whipple 1991). Thus as physical evolution occurs, the cometary layers released become gradually less volatile-rich and the comet therefore becomes fainter, eventually becoming extinct and classified as an asteroid, though on a planet-crossing orbit. The whole process thus leads to a natural explanation of Earth-crossing asteroids (*cf.* Öpik 1963).

1.2.2 Apollo asteroids

The number of known Earth-crossing asteroids is rapidly increasing, and is now of the order of 100. Helin & Shoemaker (1979) estimate the total number as about 1300, down to absolute visual magnitude 18. Dynamical lifetimes of Apollos (asteroids that cross to inside the Earth's orbit), *i.e.* their typical orbital survival times as Apollos, are $\sim 10^8$ yr (Öpik 1963), much less than the age of the Solar System, but long enough that remnants of previous giant comets may be expected to be present as Apollo asteroids, until they disintegrate completely. We discuss comets and the

alternative, main-belt asteroids, as the source of the near-Earth asteroids (NEA's); see Wetherill (1988) and references therein.

The orbital process that is perhaps not immediately obvious is for asteroids in apparently stable main-belt orbits to be perturbed into Earth-crossing orbits. Wetherill (1988) describes two chaotic regions of the asteroid belt, *viz.* the 3:1 resonance with Jupiter and the inner region of the belt where there is an interaction of Martian perturbations with one of the strongest secular resonances (ν_6). This model predicts about half the true number of Earth-crossers, though there are considerable uncertainties, *e.g.* 50±30%.

We have seen that quite a few Apollo asteroids are associated with the Taurid Complex, and the fact that the Taurid progenitor has given rise to NEA's gives reason to favour general large comet replenishment of the NEA population. In proposing that many (even most) NEA's originated as cometary, we have to consider both dynamical and physical questions. Physically, a cometary body can become asteroidal either through the primordial or late evolutionary loss of all its volatile material, or through the formation of a non-volatile crust (Weissman *et al.* 1989). Typically it takes only around $300\sqrt{q}$ revolutions, where q is the perihelion distance, for a comet to become extinct (Kresák 1987), though of course the timescale would be considerably increased for a particularly large comet. We envisage (Section 1.1, Chapter 4) that the Taurid progenitor in its later stages of evolution has become devolatilised and fragile and therefore susceptible to fragment on collisions with objects in the asteroid belt. Therefore we may expect NEA's that are the remnants of giant comets to break into smaller bodies on timescales of 10^{4-5} yr; this does not preclude a reasonable fraction of the NEA population being due to the present and perhaps a few past giant comets.

A cometary origin for at least some NEA's seems assured; Weissman *et al.* (1989) list various objects classified as asteroids as strong cometary candidates on a combined basis of orbits, physical properties and association with meteor streams; the probable comets include Chiron and Hidalgo (see Section 1.2.3), Oljato, Hephaistos, and the asteroidal (but probably extinct comet) parent of the Geminid meteor stream, Phaethon. Hartmann *et al.* (1987) showed that various asteroids identified as probable extinct or dormant comets on dynamical grounds only were classified as D, P or C spectral type. These classes are all low albedo and among asteroids in general are found at larger heliocentric distances (C in the outer part of the main asteroid belt, P and D further out). The dark and fairly red nature of D-types in particular has been regarded as indicative of a carbonaceous-rich, cometary-like

composition (Gradie & Veverka 1980). Comet nuclei tend to have albedo <0.1 (Hartmann *et al.* 1987). Physically, then, there is much observational evidence for the NEA population containing several extinct cometary objects. We note also that various NEA's identified (dynamically) as being in non-cometary orbits, *i.e.* typically with only moderate eccentricities, showed a tendency to be S-type and so plausibly perturbed out of the inner asteroid belt (Hartmann *et al.* 1987).

Turning to orbital considerations, we note that most discovered NEA's are on more stable (though still chaotic over long enough timescales) orbits than the Jupiter family of comets, crossing only the orbits of terrestrial planets and being safely inside Jupiter's orbit. Thus we may think in terms of dynamical evolution occurring alongside physical evolution. An "entry corridor" into high-eccentricity, sub-Jovian orbits can be predicted theoretically (see, *e.g.*, Napier 1984), though the aphelion distances of NEA's imply that after this initial capture stage, a further mechanism is needed. Öpik (1963) proposed the inward drift of Jupiter family comets due to the jet deceleration of nuclei in retrograde rotation (essentially momentum conservation when material is lost from the cometary surface; Whipple 1950).

Evolution from cometary to Apollo asteroidal orbits can be predicted, then; that it occurs has also been demonstrated numerically by Milani *et al.* (1989), who integrated actual Earth-crossing asteroids 100 kyr forwards and backwards in time. They point out that, the orbits being chaotic, the results must be treated statistically only; this just means that orbital behaviour we find is the sort of thing that *does* happen rather than necessarily something that *did* happen to a particular asteroid. They define various classes of orbit, and of interest to us here is that transitions occur between orbits typical of comets (defined as orbits reaching the outer Solar System) and two of the classes, Alinda and Oljato (named after objects that spend at least some time in the class). Oljato asteroids are in chaotic orbits characterised by high eccentricity and low inclination and have a clear resemblance to Taurid-like orbits. Alindas are orbits which stay in mean motion resonances with Jupiter for significant periods of time; thus quite a few Taurid orbits would be classified as Alindas. The connections of cometary orbits with the Alinda and Oljato classes, and of the two classes with each other, is of considerable interest in relation to the orbital capture of the Taurid progenitor. In particular, the existence of an entry corridor to a Taurid-like orbit from a longer-period orbit is established. For a numerically integrated example of the kind of Jupiter-induced process of capture into the inner Solar System that we envisage for the Taurid progenitor, see the calculations of the possible past evolution of Comet P/Brooks 1 by Carusi *et al.* (1985). More generally,

Nakamura & Yoshikawa (1991) have shown, from integrations of periodic comets, that orbits with q near Jupiter frequently evolve to have q of 1–2 AU within 1–2 kyr only.

There is nothing to stop a close approach to a terrestrial planet causing the final stage in the capture of the Taurid progenitor, though such an occurrence is *a priori* unlikely, *i.e.* we expect Jupiter to be the main influence. The fact that Comet Encke's aphelion distance Q=4.1 is well inside Jupiter's orbit has often been considered puzzling, and Q of the presently resonant parent object that we propose in Chapter 3 would also be well inside the Jovian orbit. Sekanina's (1972) model of non-gravitational forces on Encke demonstrated that Q=4.7 and a cometary radius (presently ∼3 km; Luu & Jewitt 1990) of about 10 km were plausible 5 kyr ago. This mechanism could have applied to the Taurid parent (we suggest in Section 3.3 that Encke itself only separated from the parent ∼200 yr ago).

To summarise, some NEA's are probably compositionally similar to main-belt asteroids and some will be cometary asteroids. The former may be expected to survive physically for their dynamical lifetimes and provide a fairly constant background to the NEA population; the latter may disintegrate on timescales of, say, 10^5 yr so that the arrival of giant comets in the inner Solar System may cause substantial fluctuations in the number of NEA's. The picture of giant comet evolution is, dynamically, from the orbits of long-period comets to those of short-period comets to those of Apollo asteroids. As this happens, physical evolution occurs, with the object gradually becoming less bright as its more volatile layers are lost. As stated in Section 1.2.1, the idea is of differentiated comets, with the volatiles concentrated towards the outer layers. Though they become extremely bright when cometary activity starts, it is of course possible that the new giant comets have low albedo nuclei.

1.2.3 Chiron — the next giant comet?

Our picture would be strengthened if other giant comets (or objects with the potential to become Earth-crossing giant comets) were found to exist in the inner Solar System, or in orbits such that they had a good chance of eventually being captured into the inner Solar System. Asteroids 944 Hidalgo and 2060 Chiron (Table 1.3) have been identified as large objects and probable comets that are on unstable orbits (Clube & Napier 1984, Olsson-Steel 1987b). Hidalgo's diameter is ∼50 km (Olsson-Steel 1987b), and Chiron is much larger — a recent radiometric determination of its diameter is model-dependent but suggests that it may be bigger and

	a	e	q	Q	i
Hidalgo	5.8	0.66	2.0	9.7	42
Chiron	13.7	0.38	8.5	18.9	7

Table 1.3: Orbital elements of giant comet candidates

darker than previously thought, with a diameter possibly as high as 370 km (Sykes & Walker 1991). Colorimetry places Chiron in asteroid spectral class C, being an object darkened by carbonaceous (kerogen-like) material, but enriched in volatile ices relative to most C-type asteroids (Hartmann *et al.* 1987, 1990). Thus from observations of the nucleus alone it appears to be a comet that has not spent long enough near the Sun to sublimate most of the volatiles, and it was recently found to have developed a cometary coma as it approached perihelion (Hartmann *et al.* 1990).

Chiron's present orbit is Saturn-crossing and certainly chaotic; a set of very similar orbits has been accurately integrated for ±100 kyr by Hahn & Bailey (1990) to derive accurate probabilities for its past and future orbital evolution. They find a probability of about 1 in 4 that it will become a Jupiter family short-period comet within the next 100 kyr, and a slightly higher chance that it was at some time in the last 100 kyr. The chance that it leaves the Solar System within the same amount of time is much less (though not negligible) and since the general pattern of orbital behaviour can presumably be extended, it seems fair to say that Chiron could well, in the next few 10^5 yr, become the next giant comet after the Taurid progenitor that decays in the inner Solar System and has a major effect on the Earth's environment. Hahn & Bailey suggest that the Taurid Complex itself could have been produced by the ejection of material from Chiron's outer layers in the past, a possibility that cannot be excluded, though independent evidence on the Taurids does imply that material in the complex has only been around for a few 10^4 yr at most.

1.2.4 Terrestrial catastrophism

Many aspects of catastrophism are discussed in the book edited by Clube (1989). The idea that there can be extraterrestrial causes for major terrestrial events has become quite well-accepted since the famous paper by Alvarez *et al.* (1980) demonstrating extraterrestrial abundances of iridium in the geological layer corresponding to the Cretaceous-Tertiary mass extinction. Nevertheless, despite the fact that it is an astronomical inevitability that interplanetary bodies will repeatedly hit the

Earth, there has for many years been a reluctance to believe that this can have catastrophic consequences; see Clube & Napier (1986, 1990) for a history of ideas about catastrophism and their lack of acceptance in the past.

Alvarez *et al.* (1980) proposed the impact of a 10 km asteroid with resultant climatic changes to explain the externally induced mass extinction. A number of random encounters with the background Earth-crossing asteroid population are to be expected during the course of Earth history. However, a long-term process dominated by occasional random impacts of large asteroids is not adequate for explaining the existence of various patterns in past geological events. There is strong evidence (see, *e.g.*, Shoemaker & Wolfe 1986) that craterings and extinctions occur not only in bunches but correlated with each other. There are indications that the craterings and extinctions are cyclic with period $\sim$30 Myr (1 Myr = 10^6 years), strongly supported by data on the frequency of magnetic field reversals, which plausibly represent a response of the Earth's interior to the changing figure of the Earth due to climatic (temperature) changes which cause, *e.g.*, redistribution of mass in the oceans towards or away from the poles. There are reasons to believe that perturbations to the Oort cloud may vary on such timescales, resulting in increased comet fluxes to the inner Solar System lasting a few Myr. Thus it seems that comets, by periodically replenishing the population of Earth-crossing objects, are the key astronomical factor modulating the geological processes. Knowledge of the details of this theory should determine the source of the largest short-period comets (*cf.* Section 1.2.1).

The book edited by Smoluchowski *et al.* (1986) contains various ideas to explain the periodicities in the geological record through the mechanism of perturbation of comets into the inner Solar System. These include a tenth planet whose perihelion and aphelion precess through a primordial disc of comets with the appropriate period, a brown dwarf companion star to the Sun, presently orbiting with a period of about 26 Myr, and, which does not require the existence of any as yet unknown body attached to the Solar System, the Sun's vertical motion in the Galaxy. A 15 Myr cycle in the pattern of magnetic field reversals (Mazaud *et al.* 1983), and its phase (after allowing for an appropriate delay for comets to travel into the inner Solar System), are successfully explained by the variation in the smooth galactic field (Clube & Napier, in preparation). It is also possible that the Sun's motion imposes a longer-term (timescales of $\sim 10^8$ yr) variation on the comet flux, and indeed on the comet population of the Oort cloud itself if during the Sun's passage through spiral arms, where giant molecular clouds (GMC's) concentrate, the GMC's provide a re-

plenishing source for the Oort cloud (Clube & Napier 1982b). The idea that comets thus have an interstellar origin is still controversial, but the $^{12}C/^{13}C$ ratio of Comet P/Halley is in agreement with that of the interstellar medium (Clube & Napier, in preparation). Evidence is growing on the differentiated nature of giant comets (Sections 1.2.1 & 1.2.2), but normal ideas about large comet formation, involving accretion and radioactive heating by ^{26}Al, are not likely to result in hot cores being produced — Clube (1988) has suggested that spiral arms represent a hot outflow from the centre of the Galaxy out of which differentiated solid bodies may be expected to condense. Studies of the Taurid Complex and of observed comets and Apollo asteroids are of interest to see whether they are consistent with the theory of differentiated giant comets.

The cometary mass distribution being such that the mass is concentrated in the few largest members, it seems that an influx of comets lasting a few Myr takes the form of a sequence of arrivals of exceptionally large comets in the inner Solar System, typically separated by timescales longer than their disintegration time, rather than a continuous flux of significant comets over the period of a few Myr. Thus the physical decay of each single large object may last a few 10^4 yr, with their arrivals separated by a few 10^5 yr (Clube & Napier 1984). The evolution of the Taurid progenitor represents the most recent example of these fundamental unitary processes (lasting a few 10^4 yr) in Earth history.

A disintegrating comet's terrestrial interaction occurs both through impacts and through the injection of meteoroids and dust with climatic effects. The history of the Taurid Complex suggests that each giant comet's evolution is characterised (Section 1.1.4) by an initial active cometary phase ($\sim 10^4$ yr, corresponding to major glaciation which is probably cosmic dust induced, *i.e.* due to passages through a dense meteoroid stream) followed by a phase in which the comet is largely devolatilised. The latter phase (upon which this work on the Taurids will concentrate) may last a few $\sim 10^4$ yr, during which periods of activity may be modulated by fragmentations, nodal intersections and short-term cyclicities (Section 1.1.4) so that in addition to receiving an underlying dust input the Earth will undergo intermittent Tunguska-type showers (Section 1.1.5). Tunguska showers are equivalent to historical description of armageddon (Clube 1990, Clube & Napier 1982a, 1990) and the picture of the catastrophic effects of the contemporary giant comet, which have occurred during the emergence of human civilisation, is conveniently termed "historical" or "biblical" catastrophism. Clube and Napier have emphasised that the line of argument developed here, involving a single exceptional cometary source for

the Taurid-Arietid complex and the zodiacal dust cloud, has the merit of jointly explaining "biblical catastrophism" (Section 1.1.5) and "geological catastrophism".

Chapter 2

Taurid orbital evolution — general properties

In Chapter 1 we reviewed work that has been done on the Taurid Complex and put forward the main questions of interest that arose, which it will be this work's aim to answer. This will be done primarily in Chapters 3 and 4, but the dynamical modelling therein will depend heavily on various computational techniques. It is the purpose of the present chapter to describe these, and also to give a general picture of patterns of evolution of Taurid orbits, considered in a theoretical sense — the physical modelling and fitting to observations will follow in the later chapters. Basically, the present chapter is the groundwork for what is to be done later. If we know general principles of orbital evolution, then instead of simply accepting the end-results of elaborate dynamical simulations, we can have a clear understanding of how the results come about.

2.1 Computational preliminaries

2.1.1 Choice of integrator

We require a knowledge of how various Taurid orbits evolve under planetary perturbations over timescales of $\sim 10^4$ yr. In the main, this will have to be discovered computationally and so a numerical integrator for solving the (Newtonian) equations of motion is needed. This work is not an exercise in numerical analysis and computation and the aim is not to find the absolutely fastest and most accurate method; it is merely necessary to have an efficient enough method so that the necessary calculations can be carried out within the computing time available. Of course, the complexity of the numerical modelling will be limited by what the computer can do in a reasonable amount of time, but there will usually be a stage where an increase

in the number of particles in a simulation throws no new light on the science and so is unnecessary. A 7th order Runge-Kutta-Nyström method derived by Dormand & Prince (1978) was shown by Fox (1984) to be very efficient for high-eccentricity orbits (like the Taurids) and so was a natural choice, especially as Fox (1984, personal communication to W.M. Napier) had provided a subroutine for implementing this integration procedure.

The procedure whereby one applies the integrator to the full equations of motion (*i.e.* second derivative of position = gravitational acceleration) is called Cowell's method, in contrast to Encke's method, which uses the known solution to the Kepler two-body problem and only integrates the difference in position considering the perturbing acceleration (see, *e.g.*, Roy 1978). With Encke's method, the integration error is less as a proportion of the absolute (as opposed to difference in) position and so the method is often more efficient and accurate. However, its advantage varies considerably from one part of an evolving orbit to another, and from one orbit to another, and it was not thought to be worth the significant extra effort of programming it. Thus Cowell's method was used throughout.

Runge-Kutta-Nyström (RKN) methods are designed to solve second order differential equations in which the expressions for the second derivatives are independent of the first derivatives. They are therefore suitable for work, such as this, where the perturbing forces of interest are the gravitational attractions of the planets. They may also be used to allow for the non-gravitational force on comets (due to the reactive force when mass loss occurs; Whipple 1950), which (Marsden 1972) often appears to be well described by expressions that for any single comet are functions of heliocentric distance only (though an orbital solution can sometimes be improved by allowing for mass loss to occur asymmetrically about perihelion; Yeomans & Chodas 1989). On the other hand, the Poynting-Robertson radiative force on small particles (see, *e.g.*, Burns *et al.* 1979) is velocity dependent and so this is an example for which a different integrator would be required.

RKN methods are single step methods, *i.e.* the position $\mathbf{x}$ and velocity $\mathbf{v}$ evaluated after each successive small time step depend only on the values at the starting time t_0 of that single step. For a step of length h we have the Taylor expansions

$$\mathbf{x}(t_0 + h) = \mathbf{x}(t_0) + h\mathbf{v}(t_0) + \frac{h^2}{2}\mathbf{f}(t_0)$$

$$\mathbf{v}(t_0 + h) = \mathbf{v}(t_0) + h\mathbf{f}(t_0)$$

with $O(h^3)$ and $O(h^2)$ error respectively, $\mathbf{f}$ being the gravitational acceleration. It turns out that if, instead of using the value of $\mathbf{f}$ at t_0, one uses an appropriately

weighted average (weighted differently for $\mathbf{v}$ as for $\mathbf{x}$) of values at certain intermediate values of t between t_0 and $t_0 + h$, then the error can be made proportional to a higher power of h and so smaller. Intermediate values of $\mathbf{x}$, required for the evaluation of $\mathbf{f}(\mathbf{x},t)$, are calculated in a similar way, *i.e.* each using an average of the $\mathbf{f}$'s already evaluated. This particular RKN method is 7th order, meaning that the truncation error[1] on any step is proportional to h^8, leading to an overall error roughly proportional to the 7th power of some (rather vaguely defined) average step size being used.[2] Integrator speeds depend on the number of times that the expression for the force on the integrated particle needs to be evaluated, *i.e.* on the number of intermediate values of t in each step. For this method, there are 9 force evaluations per step, in effect reduced to 8 because the last one can be used as the first for the next step.

The key property of an efficient integrator for highly eccentric orbits is that the step size can be varied in a sensible way, because for a fixed step size, the error is significantly greater at points in the orbit where the position and velocity are most rapidly changing (typically at perihelion). A common way to do this is by embedding a Runge-Kutta method in one of higher order and, the lower order one being much less accurate, the difference between the two can be used as an estimate of the error. Thus the present integrator's value lies in the fact that the values obtained by a 6th order method can be calculated using the *same* intermediate force evaluations as for the 7th order method. If the estimated error is too great compared to some global error control then the calculation is not used and the step is re-computed with a smaller step size; if the step is accepted then the estimated error can still be used to give a sensible step size to try for the next step.

In practice in this work's integrations of Taurid orbits about three quarters of the evaluated steps are actually used. The step size, to achieve some overall limit in the error, is typically thirty times smaller at perihelion than at aphelion, demonstrating the value of a variable step size method. The question arises of how efficient it is to integrate more than one meteoroid simultaneously. This is certainly a good idea if one is going to the trouble of integrating the planetary system at the same time, but this was not in fact the case for most aspects of the present work. Rather,

[1] Truncation error refers to the error due to the scheme being used to approximate the solution of the differential equations, as opposed to rounding error, which occurs because of the finite accuracy to which computers can store numbers.

[2] An expression for the error introduced during a step may be derived by writing out Taylor expansions at all the intermediate points; the intermediate t-values and the weightings for the averages are then chosen so that all terms up to and including h^7 cancel in this error expression, leaving an $O(h^8)$ error.

predetermined planetary orbits were used — but one might still expect there to be a saving if a single set of planetary positions can be calculated and used to evaluate the force on more than one meteoroid. However, in order to use the same planetary positions, exactly the same time steps must naturally be used for the different meteoroids, and the variation in step size round an orbit by a factor of thirty, noting that there will be a general tendency for the meteoroids to get out of phase with each other, means that one fails to take full advantage of the RKN method's automatic step size selection. There will only be a significant gain if more than thirty or so particles are integrated simultaneously and so the usual procedure has been to perform a separate integration for each particle.

The integrator is programmed with an adjustable parameter ε, which is a small positive number to which the estimated error at each step is compared. The integrator allows the number of steps to increase as ε decreases. The error decreases with ε but there is no way to tell in advance precisely what the actual size of the error will be. Consequently the integrator must be tested with different values of ε. Table 2.1 shows the results of some test integrations of the two-body problem. This is convenient for testing the integrator as the solution is known and when it comes to actual simulations with planetary perturbations, this behaviour of the integration errors may be expected to be repeated since the Sun's force is predominant virtually continuously. It turns out that the effect if ε is too large is to make the aphelion distance Q decrease (*cf.* Milani *et al.* 1989); the proportional change $\Delta q/q$ in perihelion distance q is well over an order of magnitude below $\Delta Q/Q$. This systematic change in Q due to integration error is a decrease whether the integration runs forwards or backwards in time.

Inaccuracies appear to set in mainly while the particle is near the Sun (Table 2.1 shows that there is quite a strong dependence of the error on q, for a fixed amount of computer time). This is presumably because all derivatives are greater when the particle is nearer the Sun (and is acted on by a greater force) and the truncation error, expressed by means of various manipulations of Taylor expansions, will depend on certain (fairly high) derivatives.

For large values of ε ($\sim 10^{-6}$), error estimation and consequently error control can be unreliable; in fact in the q=0.1 cases of Table 2.1 more integration steps are used for ε=10^{-6} than for the more accurate case of ε=10^{-8}. For small values of ε ($\lesssim 10^{-14}$) it is generally impossible to achieve any reduction in error, the accuracy being limited by computer rounding error. In fact, for ε below $\sim 10^{-20}$ it becomes impossible to control the step size as the error is estimated as zero, within the limits

	$q_0 = 0.1$ $Q_0 = 3.0$		$q_0 = 0.2$ $Q_0 = 3.0$		$q_0 = 0.4$ $Q_0 = 3.0$	
ε	N	$\Delta Q/Q_0$	N	$\Delta Q/Q_0$	N	$\Delta Q/Q_0$
10^{-6}	230	3×10^{-1}	150	8×10^{-2}	97	3×10^{-2}
10^{-8}	213	4×10^{-3}	176	1×10^{-3}	138	6×10^{-4}
10^{-10}	323	4×10^{-5}	281	6×10^{-6}	235	2×10^{-6}
10^{-12}	570	4×10^{-7}	509	3×10^{-8}	430	7×10^{-9}
10^{-14}	1096	9×10^{-11}	979	2×10^{-12}	832	5×10^{-11}
10^{-16}	2127	1×10^{-11}	1895	6×10^{-12}	1608	3×10^{-12}
	$q_0 = 0.1$ $Q_0 = 4.5$		$q_0 = 0.2$ $Q_0 = 4.5$		$q_0 = 0.4$ $Q_0 = 4.5$	
ε	N	$\Delta Q/Q_0$	N	$\Delta Q/Q_0$	N	$\Delta Q/Q_0$
10^{-6}	144	2×10^{-1}	99	8×10^{-2}	66	1×10^{-2}
10^{-8}	131	5×10^{-3}	111	1×10^{-3}	91	4×10^{-4}
10^{-10}	198	6×10^{-5}	175	6×10^{-6}	150	1×10^{-6}
10^{-12}	344	5×10^{-8}	316	5×10^{-9}	274	7×10^{-9}
10^{-14}	667	5×10^{-11}	606	2×10^{-12}	532	1×10^{-11}
10^{-16}	1294	1×10^{-11}	1175	5×10^{-12}	1028	2×10^{-12}

Table 2.1: Performance of integrator at different accuracies, as measured by the proportional change in Q over 10 kyr, for different values of ε and initial values of q and Q. The number N of integration steps (proportional to the computer time taken) is also shown (in thousands).

of a Fortran double precision program.[3] However, such considerations are irrelevant for physical (dynamical) studies as opposed to studies in computer arithmetic. All that is required is that the integration error is small compared to the error due to physical effects that we have not allowed for, *e.g.* idealisations of the planetary system. The requirement that the systematic error in Q, or equivalently semi-major axis a, be negligible compared to changes in a induced by the planets leads to typical choices of ε of 10^{-9}. The choice will not always be identical, *e.g.* special care is taken to choose ε small enough when q is small.

Just occasionally the program will fail drastically, and the cause may be identified as being that a step is accepted when it should not be, owing to a significant underestimate of the error, the 7th order formula giving a similar solution to that of the embedded 6th order method. This will not happen for very small step sizes, when errors can be predicted to be, *e.g.*, $O(h^8)$, but outside the step size region of convergence the error becomes less predictable and in a particularly unlucky case a serious error may occur. Such errors would usually be obvious and could be cor-

[3]It was also found that performing the force evalutions in single precision made error estimation impossible, the error repeatedly being estimated as zero.

rected by re-running with a lower ε, though a very infrequent error would not be important in a simulation with a large number of particles. We certainly seem to be able to perform $>10^6$ yr of integrations on average per serious error. If, rather than many-particle models, we were interested in an accurate integration of an individual object, we should perform checks at more than one value of ε.

2.1.2 Planetary system

When doing this work, one has the choice of what planetary model to use. The main requirement is that the results that would be obtained if the genuine planetary system were used are accurately simulated. However, it will often be important to find a model planetary system that we can use that is efficient in terms of computer time, since an inefficient method may make it impossible to include a reasonable number of particles in a dynamical model. While I have not been seriously constrained by lack of computer time during the course of this work, it remains extremely useful to establish general principles about which aspects of the results are affected by the choice of planetary model.

The most obvious question is which planets to include, *e.g.* if there is good reason to believe that Jupiter's gravity is the dominant perturbing force then there is no need to include the other planets. We shall see that different applications require different models. For example, the non-Jovian planets have very little effect on the rate at which the Taurid stream as a whole broadens (Chapter 4). On the other hand, in Chapter 3, although we consider particles in a resonance under the control of Jupiter, the effect of the inner planets is crucial in perturbing particles both within, and in and out of, the resonance. Another question is whether to allow for the planets' precession, and if so whether to use pre-calculated elements or actually perform a full integration of the planetary system.

Integrating the planetary system concurrently with the meteoroids takes a considerable amount of computer time. Alternatively pre-derived formulae (*e.g.* see Laskar 1988) can be used to calculate the planetary orbital elements as a function of time. However, it is much faster to have the orbital elements constant than continuously varying because various coefficients (*e.g.* for rotating a planet's position in the plane of its own orbit to the ecliptic frame) need not be repeatedly evaluated. Of course, we may take account of planetary precession without incurring large overheads in computer time if the planetary elements are updated only occasionally.

During any period when planetary elements are constant, one possibility would be to integrate the planets but neglect their mutual interactions (though $P^2 = a^3$

would hold; *cf.* below). By comparison to the calculation of positions as a function of time by standard formulae for bodies moving on ellipses, this is found to be at least as fast for the outer planets (the step sizes for Taurids give virtually zero truncation error for the outer planets) but much slower for planets nearer the Sun. My approach has been to use the usual ellipse formulae.

Even when allowing for planetary precession, then, elements are held constant for certain periods of time. T.R. Quinn (1991, personal communication) has given me planetary orbital elements at $\sim$500 yr intervals. These are smoothed elements, with variations that occur on timescales of $\lesssim$1000 yr removed. Smoothed elements are sufficient to discover general patterns of orbital behaviour (as opposed to calculating very accurate behaviour of single objects for which very precise starting conditions are known). The elements are derived from an integration covering the past 3 Myr described in Quinn *et al.* (1991). There is presently no other comparably accurate integration of all the planets over the period of time ($>10^4$ yr) of relevance to a study of the orbital evolution of the Taurids, *e.g.* the DE102 integration described in Newhall *et al.* (1983) goes back just $\sim$3 kyr.

Except when actually integrating the planetary system, I have used the approximation of constant mean motion for the planets. Provided that the long-term sidereal period is chosen accurately, the error in longitude will be small ($<1^\circ$, say) over the timescales I consider; integrations of the planetary system confirm this point. Constant values of the semi-major axis, calculated by averaging results from Quinn *et al.*'s (1991) integration, have been used. The constant sidereal periods have not been calculated from $P^2 = a^3$ because the perturbing effect of other planets means that Kepler's third law is not precisely obeyed. Sidereal periods are given in Appendix III of Roy (1978) though for the inner planets to get extra significant figures I used the *Explanatory Supplement to the Astronomical Ephemeris* (1961).

It is preferable (although in practice for these studies on the Taurids unlikely to be important) to have small maximum errors in planetary positions, rather than having the longitude systematically deviating by a larger and larger fraction of a revolution, just in case there is, *e.g.*, some subtle effect due to the relative positions of two planets, *e.g.* a resonance with both. However, while maximum errors in planetary positions are useful to know, they do not provide an actual measure of the error in the orbit being integrated. The latter can only truly be ascertained from actual integrations.

We now move to an example. We present integrations backwards in time 20 kyr of the present-day elements of Comet P/Encke for different planetary models;

variations in semi-major axis a, perihelion distance q, inclination i, argument of perihelion ω and longitude of perihelion ϖ are in Figures 2.1, 2.2, 2.3, 2.4 and 2.5 respectively, with the planetary models summarised in Table 2.2. Of course the non-gravitational force on the comet means that they will all differ somewhat from reality, but the purpose here is to compare gravitational models. The integration accuracy is good enough that the differences are just due to the planetary differences. This example is not significantly affected by a strong Jovian resonance (Section 2.2.2).

Jupiter (non-precessing) Circular orbit	Jupiter (non-precessing) Approximation to Kepler motion
Jupiter (non-precessing) Kepler motion	Jupiter Elements updated every 5 kyr
Jupiter Elements updated every 500 yr	Jupiter & Saturn Elements updated every 500 yr
Jupiter, Saturn & 4 inner planets Elements updated every 500 yr	Whole planetary system integrated (Newtonian equations of motion; 9 point masses)

Table 2.2: Explanation of Figures 2.1, 2.2, 2.3, 2.4 and 2.5.

An immediate check on the effect of uncertainty in planetary longitudes is given by a comparison between the plots where Jupiter has Kepler motion and an approximation to it. The approximation, correct to first order in eccentricity e, is that the angular motion about the empty focus is constant (*e.g.* Porter 1952) and leads to a maximum deviation in the longitude of Jupiter, here assumed to have a constant e of 0.048, of 0.1°. The approximation saves a small amount of computer time and the two integrations are seen to produce almost identical results.

As regards the behaviour of a, we see from Figure 2.1 that the crucial factor is whether the inner planets are included. No noticeable long-term change in a is produced by Jupiter or Saturn. The inner planets, which are crossed by the orbit of Encke, produce changes typically of $\sim$0.02 AU over 20 kyr. It will become clear that these changes to a are best thought of as occasional random perturbations; see especially Section 3.1.2 for further discussion (also about the relative importance of the four planets). As far as our choice of planetary model is concerned, we may leave out the inner planets if we are not interested in changes in a below, say, 0.02 AU.

On the other hand, if we are interested in the evolution of q, the crucial parameter of the planetary model is seen to be the orbit of Jupiter; we see in Figure 2.2 that

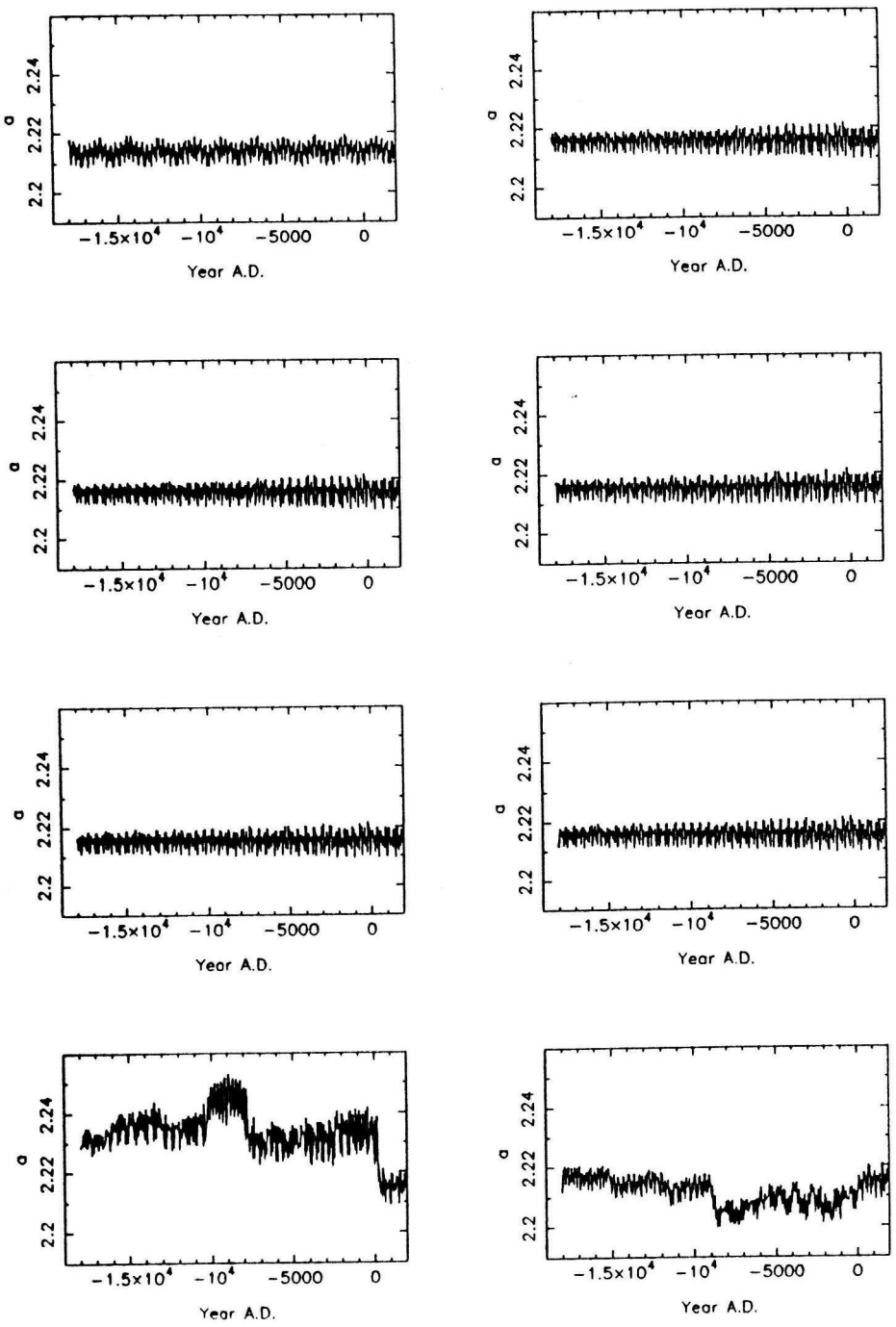

Figure 2.1: Evolution of a over 20 kyr for various planetary models; refer Table 2.2.

the plot that is most different from all the others is the one where Jupiter is in a circular orbit. The important parameters are Jupiter's eccentricity and longitude of perihelion; by checking Jupiter's orbital evolution (not shown here, though we mention that the variation in Jupiter's ϖ is only $\pm 10^\circ$ or so in the last 30 kyr) it is found that a particle's q is smallest (and Q largest) when the the heliocentric distance

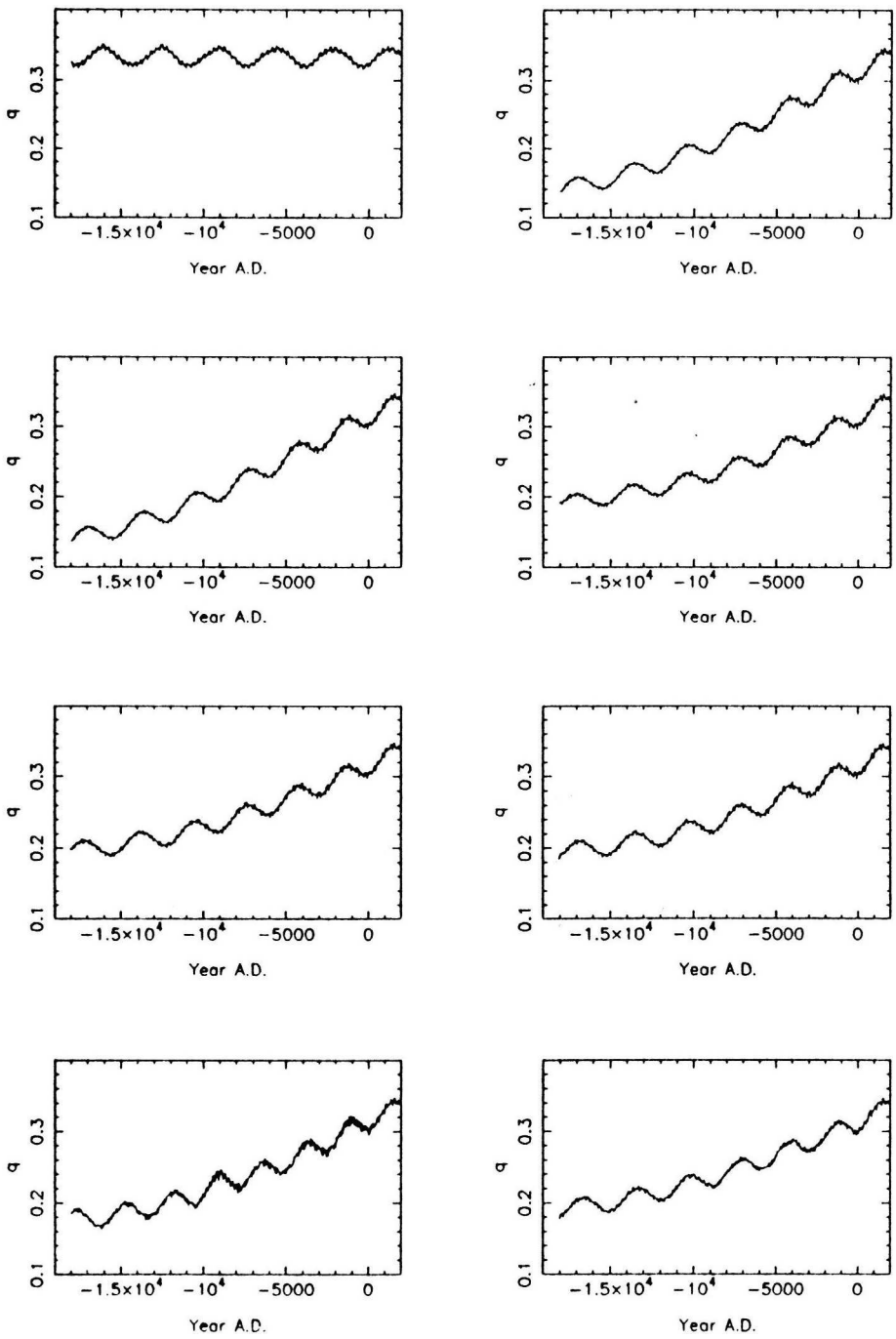

Figure 2.2: Evolution of q over 20 kyr for various planetary models; refer Table 2.2.

of Jupiter's orbit at the particle's aphelion is largest. Essentially, perturbations to q occur because Jupiter's perturbing force acts primarily when the particle is near aphelion. A good approximation, especially over just the past 10 kyr or so, is to take Jupiter in a non-precessing (though non-circular) orbit. It can be seen to be very satisfactory to update Jupiter's elements only every 5 kyr, and clearly the procedure

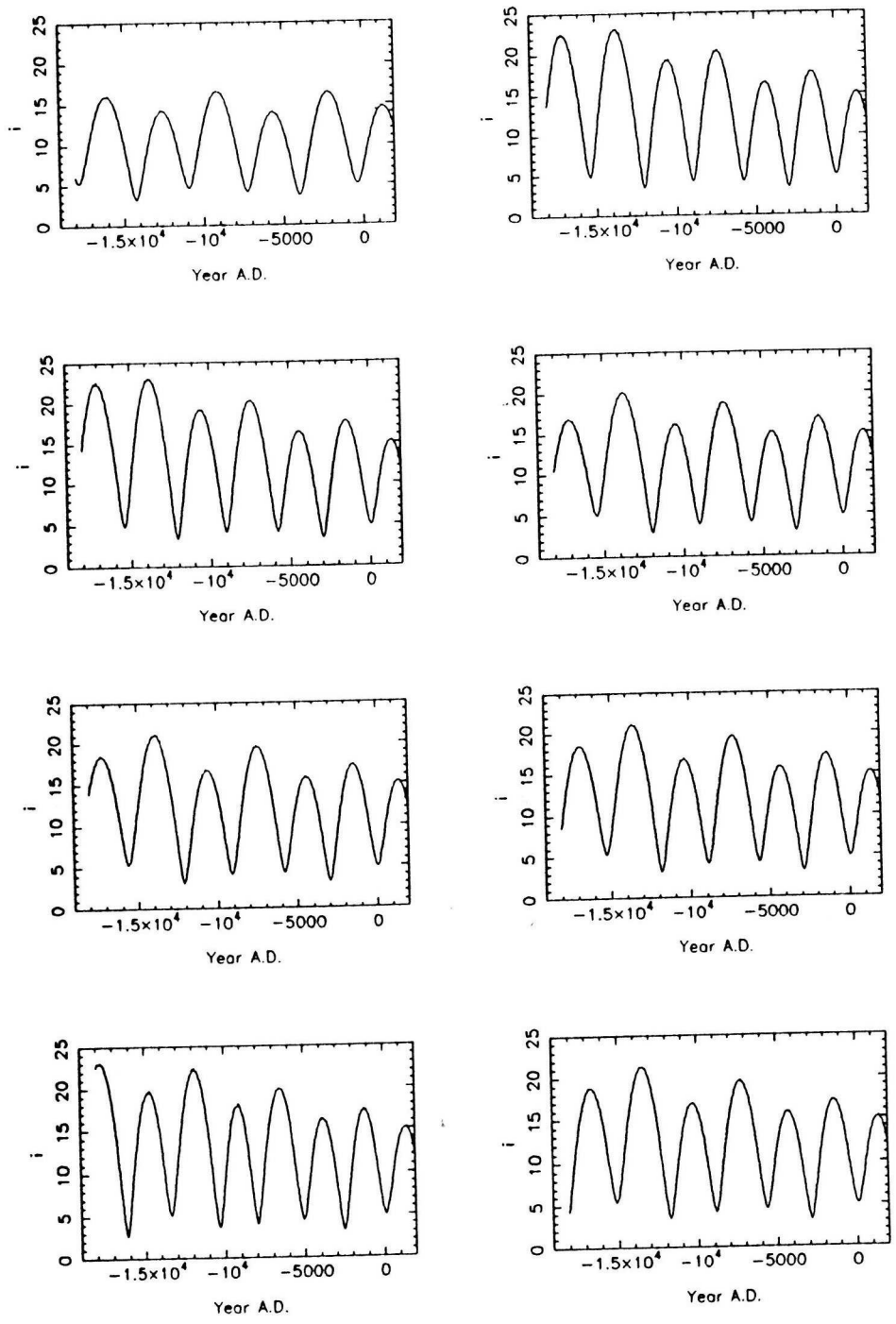

Figure 2.3: Evolution of i over 20 kyr for various planetary models; refer Table 2.2.

of updating elements every 500 yr is reasonable. The resultant small discontinuity in planetary positions is irrelevant for Jupiter, and would only be unfortunate for the inner planets if a close approach were occurring at the time; this extremely unlikely situation could be corrected as it arose, or we could simply argue that it did not

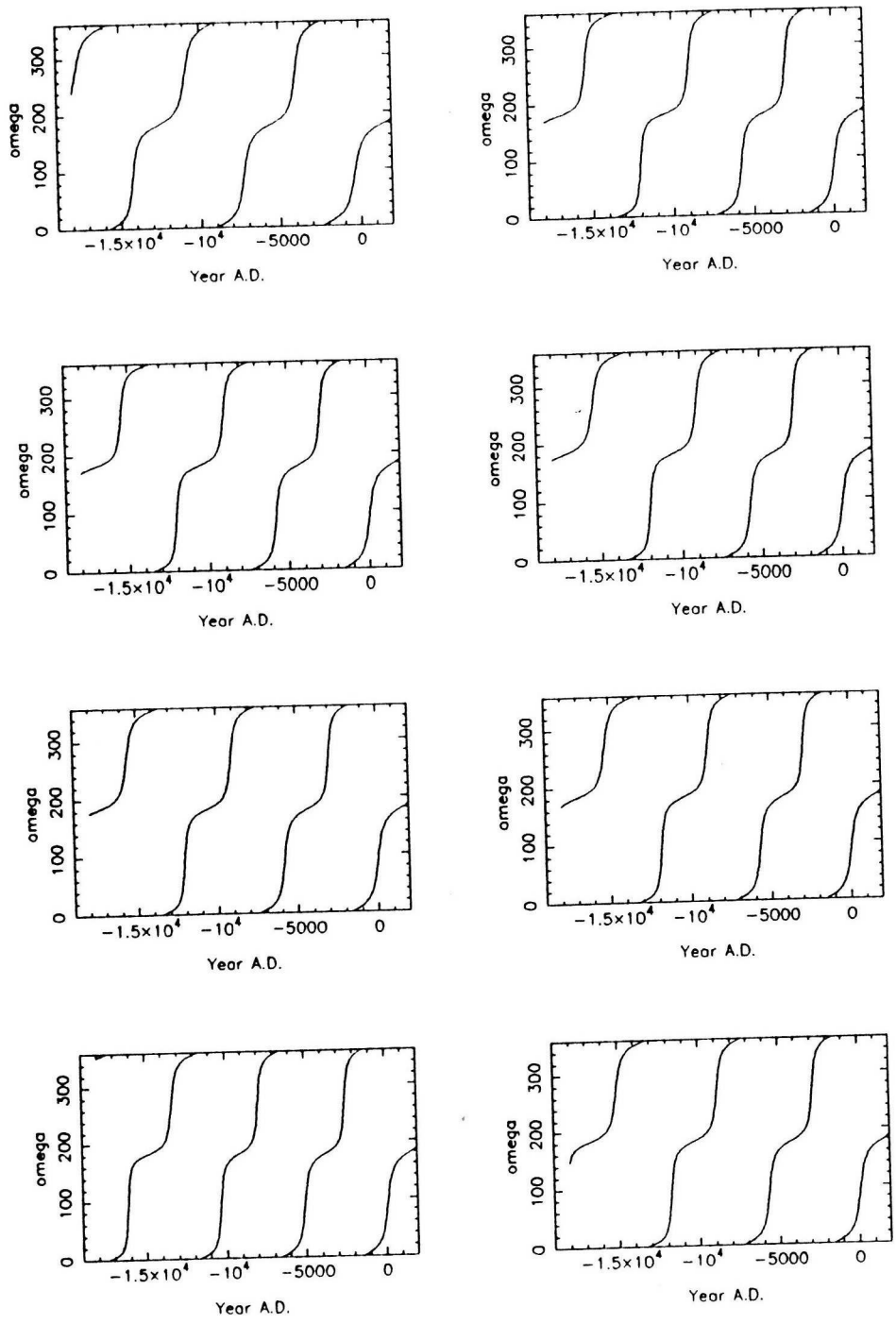

Figure 2.4: Evolution of ω over 20 kyr for various planetary models; refer Table 2.2.

matter as the result of close approaches was unpredictable in any case.

Details of the evolution of angular elements (Figures 2.3, 2.4, 2.5), *e.g.* the way the precession of i and ω are closely coupled, are of great importance in this thesis. We shall discuss the i and ω evolution displayed in Figures 2.3 & 2.4 further

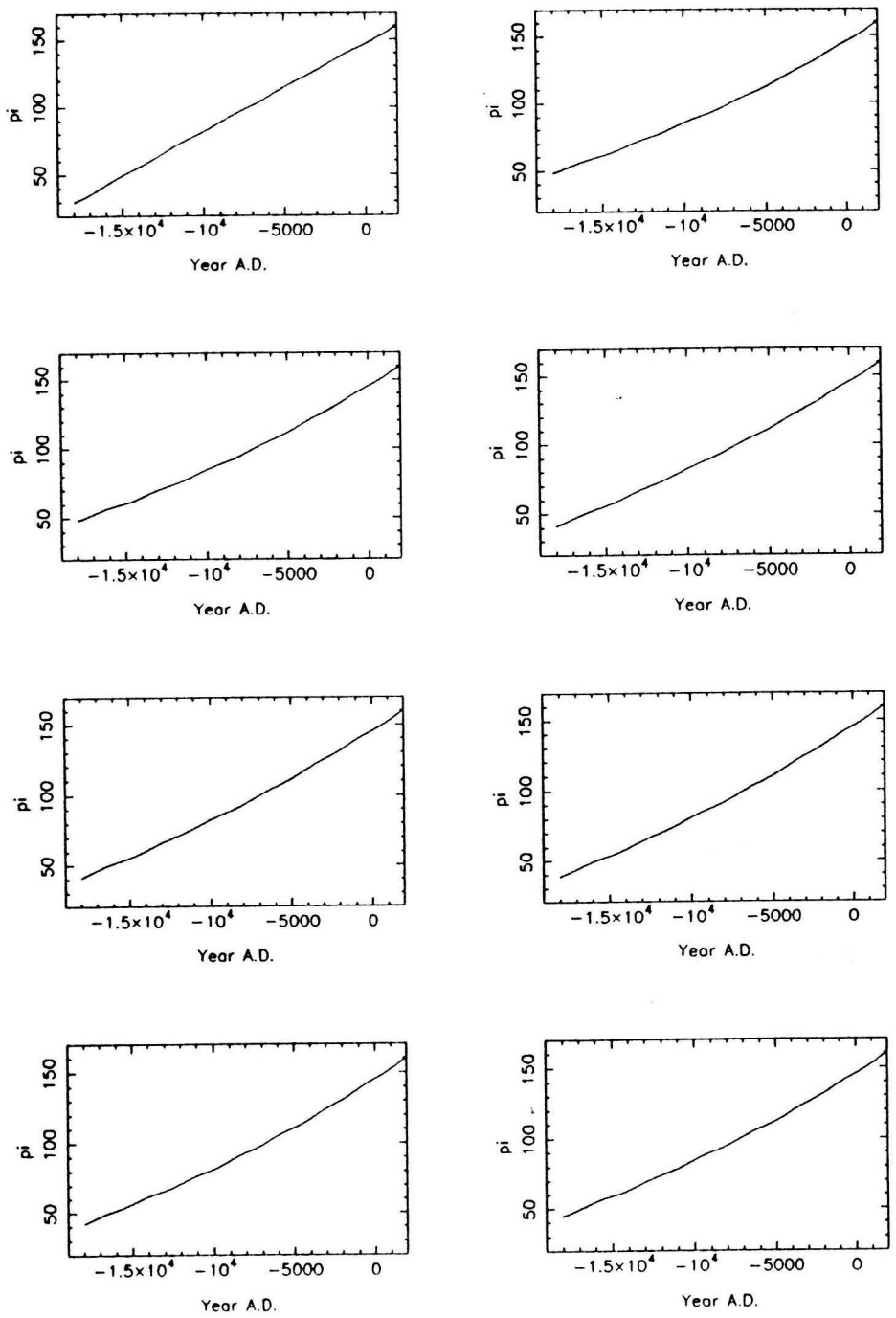

Figure 2.5: Evolution of ϖ over 20 kyr for various planetary models; refer Table 2.2.

in Section 2.2.1. Here we are just interested in the *differences* due to choice of planetary model. Jupiter is by far the dominant effect on both the amplitude of the i-oscillation and the angular precession rate. Parallel comments to those about the behaviour of q can be made. Precession rates are found to be greater when the distance to Jupiter's orbit at the particle's aphelion is less, presumably because

Jupiter can then have an increased perturbing effect. Thus, *e.g.*, we see in Figure 2.5 that ϖ changes at a uniform rate if Jupiter's orbit is circular, but not if it is eccentric since as the particle's longitude changes, so does the distance to Jupiter's orbit at the particle's aphelion. Precession rates can be predicted to 10–20% without allowing for Jupiter's non-zero e. We must allow for Jupiter's eccentricity for greater accuracy; allowing for the change in Jupiter's elements (e in particular) introduces a further small refinement and the fact that there is only a very small difference between results where the elements are updated every 5 kyr and every 500 yr shows that the latter is certainly sufficient. The effect of the inner planets is indirect in that they do not significantly affect the precession rates themselves, but the (fairly random) small changes in a that they induce cause the Jovian effect on angular elements to vary slightly (but unpredictably).

To summarise, the main points are:

1. We can get a broad idea of the evolution of Taurid orbits by allowing for Jupiter only, in a circular orbit.

2. There are nevertheless noticeable differences in the evolution of q, i, ω, ϖ if we allow for Jupiter's non-zero e.

3. The effect of Jupiter's precession is small over the past 5–10 kyr, say, but increases the further back in time we go.

4. Jupiter's precession can be allowed for by updating its elements every few kyr. When we allow for Jovian precession during the work of this thesis, we shall update the elements every 500 yr; this still takes a negligible amount of computer time.

5. The effect of the inner planets is to induce small random perturbations which we can usually neglect. We must be careful in Chapter 3, however, when we regard even small changes in a as significant.

2.2 Comparison with analytic formula

2.2.1 Basic pattern of orbital precession

Most analytical work in Solar System dynamics has concentrated on orbits of small eccentricity (planets and main-belt asteroids), it often being convenient to expand the Hamiltonian in powers of e. For high e, a rare analytical theory was developed by Brouwer (1947), although this is a secular theory and so (as we shall see) subject

to large inaccuracies near mean motion resonances with Jupiter. However, its advantage lies in the fact that it does provide formulae for the behaviour of the orbital elements, and it can be helpful to have formulae rather than always having to discover orbital precession properties empirically by looking at computational results. Consequently we describe it here.

Brouwer's method is designed for low-inclination orbits that are entirely inside Jupiter's orbit, but on which Jupiter is the dominant effect. It is therefore ideally suited to the Taurids. Jupiter is assumed to be in a circular orbit, the other planets are neglected and the disturbing function is limited to secular (*i.e.* non-periodic) terms only. If we follow through Brouwer's working carefully we may present the results of his theory as follows. Using the notation a for semi-major axis, n for mean motion, e for eccentricity, i for inclination, Ω for longitude of ascending node, ω for argument of perihelion, k for the Gaussian constant of gravitation, m for mass, the suffix J for Jupiter and the angle τ related to time t by

$$\tau = \frac{k^2 m_J}{n a^2 a_J}\, t$$

and referring angular elements to Jupiter's orbit, we have:

$$a = \text{constant}$$

$$\omega = \tan^{-1}\left[\sqrt{\frac{A-B}{A+B}}\tan\left(\sqrt{A^2-B^2}\,\tau\right)\right]$$

$$\Omega = \varpi_0 - \omega + C\tau$$

$$i = 2\tan^{-1}\sqrt{\frac{\gamma}{A - B\cos 2\omega}}$$

$$e = \sqrt{1 - \left(\frac{H}{\cos i}\right)^2}$$

with ϖ_0, γ, H, A, B and C constant for any single particle — ϖ_0, γ, and H chosen to fit initial values and A, B and C given by:

$$A = \frac{A_1}{H} - \frac{H A_3}{\sqrt{1-H^2}}$$

$$B = \frac{A_2}{H}$$

$$C = -\frac{H A_3}{\sqrt{1-H^2}}$$

The quantities A_1, A_2 and A_3 are the constant terms in Fourier expansions in mean anomaly M of various quantities and arise because the approach, e not necessarily being low, is to express the disturbing function as a Fourier series rather than

expand it in powers of e. Specifically, A_1, A_2 and A_3 are the constant terms in the Fourier expansions of $\frac{1}{4}\rho c_1$, $\frac{1}{4}\rho c_1 \cos 2M$ and $\frac{1}{2}(a/a_J)\frac{db_0}{d\rho}\cos M$ respectively, with $\rho(M) = r(M)/a_J$, r = heliocentric distance and $c_1(M)$ and $b_0(M)$ we shall define shortly. Therefore the A_i may be expressed as integrals, *e.g.*

$$\frac{1}{4}\rho c_1 = A_1 + \cos jM \text{ terms}$$

gives

$$A_1 = \frac{1}{4\pi}\int_0^\pi \rho(M)c_1(M)dM$$

and similarly

$$A_2 = \frac{1}{4\pi}\int_0^\pi \rho(M)c_1(M)\cos 2M dM$$

$$A_3 = \frac{a}{2\pi a_J}\int_0^\pi \frac{db_0}{d\rho}\cos M dM$$

The quantities $c_1(M) = c_1(\rho(M))$ and $b_0(M) = b_0(\rho(M))$ are Laplace coefficients (Brouwer & Clemence 1961, Chapter XV), defined by the following Fourier series in ϕ (ϕ = angle between particle and Jupiter):

$$(1+\rho^2-2\rho\cos\phi)^{-3/2} = \frac{1}{2}c_0 + \sum_{j=1}^{\infty} c_j \cos j\phi$$

$$(1+\rho^2-2\rho\cos\phi)^{-1/2} = \frac{1}{2}b_0 + \sum_{j=1}^{\infty} b_j \cos j\phi$$

so that

$$c_1 = \frac{2}{\pi}\int_0^\pi (1+\rho^2-2\rho\cos\phi)^{-3/2}\cos\phi d\phi$$

$$\frac{db_0}{d\rho} = \frac{2}{\pi}\int_0^\pi (1+\rho^2-2\rho\cos\phi)^{-3/2}(\cos\phi-\rho)d\phi$$

These integrals may be evaluated easily on a computer. In the past, tables of Laplace coefficients were prepared (*e.g.* Brown & Brouwer 1932), and preparation of the tables as a whole was easier using an infinite series formula (see Brown & Brouwer's paper) rather than evaluating the above integrals numerically. In their work on Encke's Comet and the Taurids, Brouwer (1947) and Whipple & Hamid (1952) used Brown & Brouwer's tables, moderately excruciating but not impossible for just a few meteors. Today the necessary calculations for any orbit can be performed almost instantly on a computer — to derive the long-term formulae for the evolution of the orbital elements there is not much more to be done than evaluate some double integrals. Sufficient information has been given here to enable the theory to be programmed.

An important point is that at one point in his derivation Brouwer restricts terms to lowest powers in i so that the formulae do not represent an exact solution of the secular problem, but are valid for low-i orbits. (He shows that if higher powers of i are included then straightforward formulae for evolution of the orbital elements are not obtainable.) In fact from consideration of Brouwer's equations (2), (3) and (4) we find that we need i (in radians) reasonably small compared to e. In practice (checking results against those of numerical integrations, as described below) the theory seems to work very well if $i \lesssim \frac{1}{2}e$ so that it is excellent for application to the Taurids. One thing to note is that Brouwer's derivation initially proceeds assuming e is constant, with the equation relating e and i (see above) obtained at a later stage. The initial assumption is seen to be reasonable since $\cos i$ hardly varies for small i. During the calculation of the A_i we repeatedly need to evaluate r as a function of a, e and anomaly; we use the initial value of e.

A natural way to check the validity of these formulae is by comparison with secular perturbation methods that have been derived in independent ways. I have checked the derived periods of revolution against those resulting from the theory (Blitzer 1959, Sykes & Greenberg 1986), applicable to low e orbits, described in Section 5.1.3, confirming the results. It also confirms the point that i in radians must be reasonably small compared to e, providing an extra check on Brouwer's derivation. If i is small but e is comparably small then the calculation should be performed for $i \ll e$ and extended to the original i; the Lagrange perturbation equations (see, *e.g.*, Appendix A of Sykes & Greenberg 1986) show that the rates of change of Ω and ω are independent of i for small i.

Thus when the double integrals have been evaluated and the various coefficients calculated, we have formulae for the precession of the orbital elements that are valid for all time. The formulae allow the straightforward calculation (without a lot of work performing numerical integrations) of the time taken for single revolutions in ω and the longitude of perihelion $\varpi \equiv \Omega + \omega$ as functions of a and e only, as well as showing the pattern of orbital evolution within each revolution. A table of the periods of revolution (Table 2.3) enables one to have an immediate idea of the approximate rate at which orbits of different sizes undergo differential orbital precession — the kind of thing of interest in studies of meteor stream evolution.

Brouwer shows what modifications are required to allow for Jupiter's non-zero eccentricity, but if this is done there are no similarly neat formulae. It is interesting to note that Brouwer found a discrepancy between his theory (with Jupiter in a circular orbit) and the theory of Whipple (1940), and it turns out that the true

	e=0.7		e=0.8		e=0.9	
a	ω	ϖ	ω	ϖ	ω	ϖ
1.5	29500	117900	26600	136900	23900	183200
1.6	25400	103000	22700	119100	20200	158400
1.7	21900	90200	19400	103600	17100	136900
1.8	18800	79000	16500	90100	14300	118000
1.9	16200	69100	14000	78200	11900	101400
2.0	13800	60400	11700	67600	9800	86500
2.1	11700	52600	9800	58200	7900	73100
2.2	9900	45600	8000	49600	6200	60900
2.3	8200	39200	6400	41700	4700	49700
2.4	6700	33400	5000	34500	3400	39200
2.5	5300	28000	3700	27800	2200	29200

Table 2.3: Secular periods (in years) of revolution of ω and ϖ for different values of a and e.

precession rates of Comet P/Encke are closer to those derived by Whipple. The two theories provide a useful confirmation of each other in that they derive formulae for angular element precession that are of the same form, but with the derivations having proceeded in entirely different ways. Whipple used the standard equations for the perturbations of the elements (see Sykes & Greenberg 1986, Appendix A) and a model where the Jovian perturbations occur at aphelion and only during the aphelion passages where Jupiter is closest. The discrepancy between the two theories is explained because, having derived the formulae of the correct form, Whipple fitted numerical constants from observed perturbations to Encke's orbit, so that the genuine distance to Jupiter when the particle is at aphelion is taken account of, rather than an inaccuracy being introduced by Jupiter being assumed to be in a circular orbit. In the sense of matching the observed perturbations of Encke, Whipple's theory is superior, but the achievement of a theory is greater the more it can predict results analytically without having to resort to empirical methods — and when applied to meteors, for which no past observations of orbital evolution are available, Whipple's method of estimating precession rates from those of Encke is only very approximate. Brouwer's theory is immediately applicable to Taurid meteoroid orbits for which no measure of recent perturbations is available, since they are only instantaneously observed as meteors.

Some numerical integrations have been done to test how well the formulae derived from Brouwer's theory work. An example of results from this theory superimposed on numerical integration results is shown in Figure 2.6. In the numerical integration,

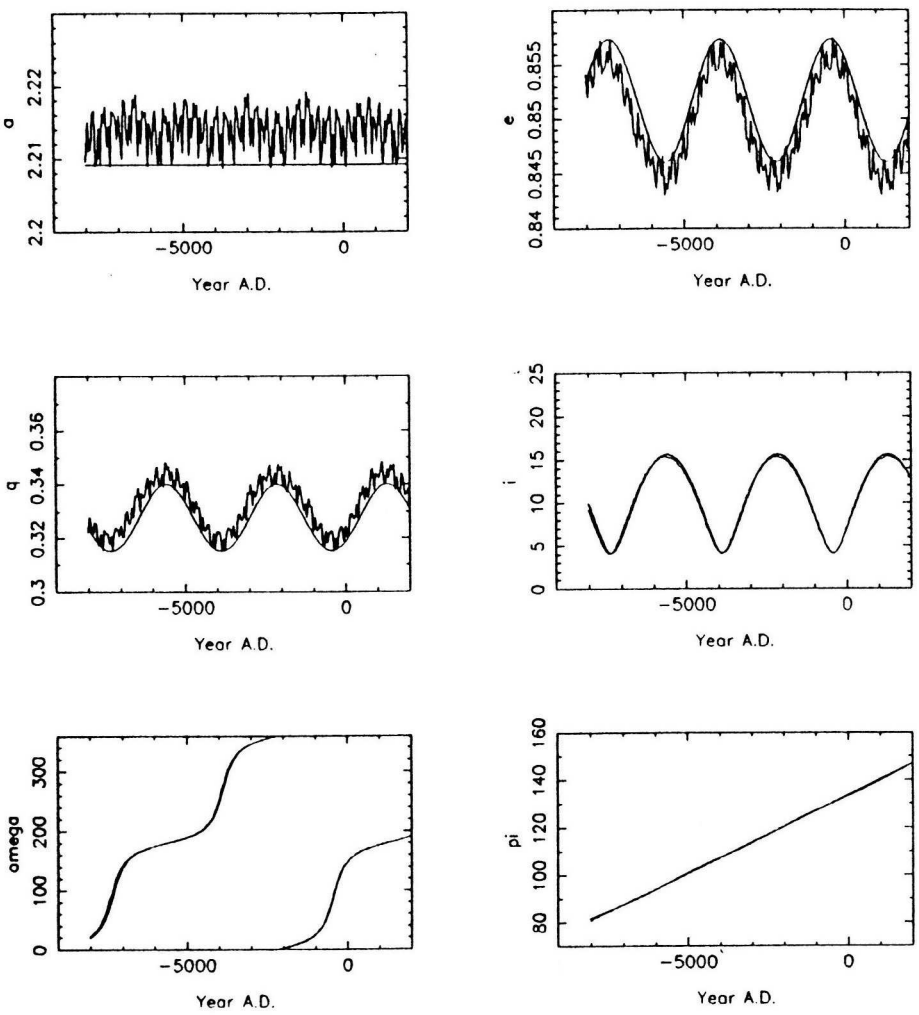

Figure 2.6: Comparison of Brouwer's (1947) secular perturbation theory with numerical integration results — the present-day elements of Comet Encke followed back 10 kyr. Angular elements are referred to Jupiter's orbit.

Jupiter has been taken in a circular orbit so that we can see the effect of using a secular theory rather than the effect of different planetary models, which we have already looked at in Section 2.1.2. We see that although the secular theory cannot reproduce the small, high-frequency variations in a, e, q, the long-term changes in elements are predicted almost perfectly. The results of other integrations show that the secular model usually works just as well as in this example, the exception being near strong Jovian resonances (Section 2.2.2).

We can discover the following fundamental patterns in the evolution of Taurid orbits entirely from the formulae resulting from Brouwer's theory. There is a slight difference between the Jovian and ecliptic frames and we remember that here the angular elements are referred to the plane of Jupiter's orbit:

1. The variations in a and e are small. See below, however, regarding systematic change in e.

2. ϖ increases with time, the variation being roughly constant, and quite a bit smaller than the variation in ω and Ω. Consequently the variations in Ω and ω are comparable but opposite (Ω decreases, ω increases).

3. The orbit spends most time at values of ω near 0 and 180°, *i.e.* with the line of nodes aligned quite close to the line of apsides, and ω precesses most rapidly through 90 and 270°.

4. The variation in i is closely coupled with that in ω, with i taking its minimum value at 90 and 270° and maximum at 0 and 180°. Ω and ω therefore vary most quickly when i is lowest.

Regarding the second point, we mention that this behaviour of Ω and ω is very different from the small-e case, where to a good approximation ω increases at twice the rate at which Ω decreases (see Sykes & Greenberg 1986). Furthermore for low e the rate of change of ω is much more nearly uniform (*cf.* third point). Regarding the fourth point, we note that the variation in i for any one evolving orbit can be a factor of 3–4 but that meteoroids that intersect the Earth's orbit and so can be observed as meteors tend to have values of ω such that i is low (Chapter 4). Whipple (1940) realised this soon after Taurid meteor orbits were first accurately measured, and that it meant that the Taurids and Encke's Comet, with its significantly higher inclination, almost certainly had a common origin.

This i-ω coupling was evident in the plots of Section 2.1.2; also in Figure 2.3 we see the effect of the rotation between Jovian and ecliptic frames — the extremes of the i-oscillation remain fixed in the Jovian frame (Figure 2.6). There is another factor, which can be predicted from the formulae of Brouwer's theory, affecting the amplitude of the i-oscillation in Figure 2.3, namely that when e becomes greater (q smaller), and the proportional short-term variation in $(1 - e^2)$ increases, we have, from Brouwer's formula $(1-e^2)\cos^2 i = H^2 = \text{constant}$, that the range of oscillation in i increases.

Despite its usefulness, there are small effects that this model of secular perturbations due to Jupiter in a circular orbit cannot take into account, which are due to Jupiter's non-zero e and which have been highlighted in Section 2.1.2. From the results of that Section and from trial integrations with other orbits, we find that:

1. The precession of the angular elements, while following the same general pattern, is slightly faster or slower accordingly as the particle's aphelion is near Jupiter's perihelion or aphelion. With present values of Taurid longitudes, the precession is of order 10% faster than given in Table 2.3. If the Taurid stream was in existence ∼20 kyr ago then it would have been at longitudes such that precession rates were >10% slower than given in Table 2.3.

2. The particle's perihelion distance increases (e decreasing, a remaining constant) as its aphelion approaches Jupiter's perihelion.

With regard to the first point, precession rates derived from the above secular model remain useful since the proportional change in precession rate is similar for most Taurid orbits. Therefore the results are still valid when one simply makes a small change in timescale. When we look at orbital elements in Chapter 4, however, the second point is crucial and we cannot simply accept the result of the secular model we have described here which says that there is no long-term change in the perihelion distance of evolving orbits.

2.2.2 The importance of resonances

We have seen that Jupiter's eccentricity causes slight deviations between orbital elements predicted by the theory of Section 2.2.1 and those resulting from actual integrations. Much greater deviations, however, can arise near mean motion resonances with Jupiter. A resonance occurs when the periods of meteoroid and Jupiter are in low integer ratio, *e.g.* P=3.95 yr, a=2.50 AU for the 3:1 resonance (P_J=11.86 yr). Therefore certain periodic terms in the disturbing function, neglected by the secular theory, no longer average to zero.

Despite this failing, the secular results are useful as a reference against which to compare integration results and indeed give a good way to quantify the strength of different resonances. Precession rates could be calculated as smoothly varying functions of a and e (Table 2.3); integrations show there to be significant deviations near certain resonances.

In Chapter 3 where, motivated by observations, we shall be interested in the 7:2 resonance in particular, we shall explain both the mechanism by which a particle can have its period P remain resonant and the details of the behaviour of P, *i.e.* small oscillations about the resonant value. Here we concentrate on the effect that resonances have on orbital element precession; the behaviour of P is only of interest insofar as it affects the precession rate. We first describe effects at a single resonance

and then compare resonances. Jupiter will be assumed to be in a circular orbit; experience with numerical integrations shows that if we allowed for Jupiter's e there would be similar points to be made, except that we should not have the formulae of the secular theory with which to compare integration results. Provided that a particle is never $\lesssim$0.5 AU from Jupiter, when significant and rather unpredictable perturbations to its aphelion are liable to occur, the effect of Jovian perturbations, though strongly affected by certain resonances, remains predictable.

Near certain resonances, it is possible (see Section 3.1.1) for particles to oscillate in longitude about a reference point (the "resonance centre") that:

1. Moves with exactly the resonant period.

2. Best avoids approaches with Jupiter. Since the closest approaches occur (for Taurids) at aphelion, this is probably most easily thought of by considering the distances Jupiter can be at when this reference particle is at aphelion, and maximising the minimum of these distances.

The amplitude of this oscillation, or libration, is small enough so that conjunction with Jupiter never occurs when the meteoroid is at aphelion. For example, for the 4:1 resonance, there will be four possible positions of Jupiter when the resonance centre is at aphelion, the configuration repeating after 4 revolutions (1 revolution of Jupiter), as shown in Figure 2.7; it can be seen that if conjunction is not to occur when the meteoroid is at aphelion, Jupiter's longitude must not differ from what is shown in the Figure by 45° or more so that the maximum permitted amplitude for the particle's longitude libration is $\frac{4}{1}\times 45° = 180°$. For the (p+q):p resonance, the

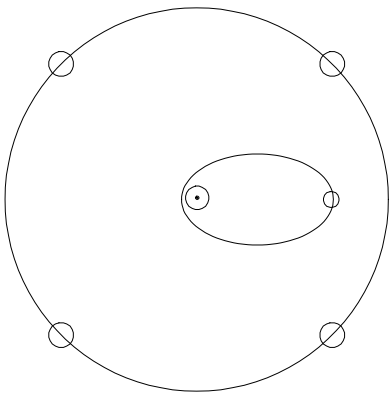

Figure 2.7: Positions of Jupiter when the 4:1 resonance centre passes through aphelion.

maximum permitted amplitude is $\frac{180°}{\mathrm{p}}$.

The effects of this resonant libration may be taken account of, while still eliminating the really short-term fluctuations, along the lines of Schubart (1968), who applied his theory to the Hilda asteroids, by averaging the perturbing force over the number of orbits after which the configuration relative to Jupiter repeats. This would be an approximate procedure since the configuration does not *exactly* repeat except when P goes through the resonant value. In a sense, this would be an approach intermediate between the full secular theory and the straightforward integration of the full equations of motion. Though it would be possible to use this approach to study the effect of resonances on precession rates, I have simply performed full integrations to get results to compare with the secular theory.

In these cases of libration, when the long-term average period is exactly the resonant period (neglecting the very slow change in ϖ; Section 3.1.1), the closest approaches to Jupiter are avoided and we expect the perturbations to be smaller. This is borne out by most integrations, which show a slowing of the precession rate. A few integrations provide exceptions to this rule and show a speeding of the precession rate. These are cases where the amplitude of libration is nearly as great as it can be, and at the extremes of the oscillation, near-conjunctions with Jupiter at aphelion do occur. Because any roughly sinusoidally oscillating function spends most of its time near the extremes of the oscillation (*cf.* dust bands, Section 5.1), the effect of Jupiter ends up being greater than if there were no commensurability. Whether precession is slowed or speeded, the general pattern of precession (*e.g.* i-ω coupling) is maintained quite well, *i.e.* the only difference is a change in timescale.

A particle that is nearly but not quite resonant also has its precession rate affected. Although it goes through times when it repeatedly nearly coincides with Jupiter at aphelion and times when coincidences are repeatedly avoided, it turns out that the perturbations due to the former (*cf.* p. 103 of Öpik 1976) slightly outweigh the latter as far as precession is concerned, *i.e.* there is speeding of precession relative to the secular theory.

As an example, in Figure 2.8, we present integrations relating to the 4:1 resonance at 2.064 AU. The first of the six pairs of plots is for Brouwer's secular theory, the middle four pairs for resonant particles and the final pair, a remaining just below the resonant value at all times, for a near-resonant particle. In the middle four cases, the amplitudes of the longitude oscillation (not shown here, though it is closely linked to the a-oscillation; Section 3.1.1) relative to the resonance centre are $\sim$175° (the theoretical maximum being 180°; see above), 120°, 60° and $\sim$5° respectively. Thus the four cases are in increasing order of avoidance of conjunctions

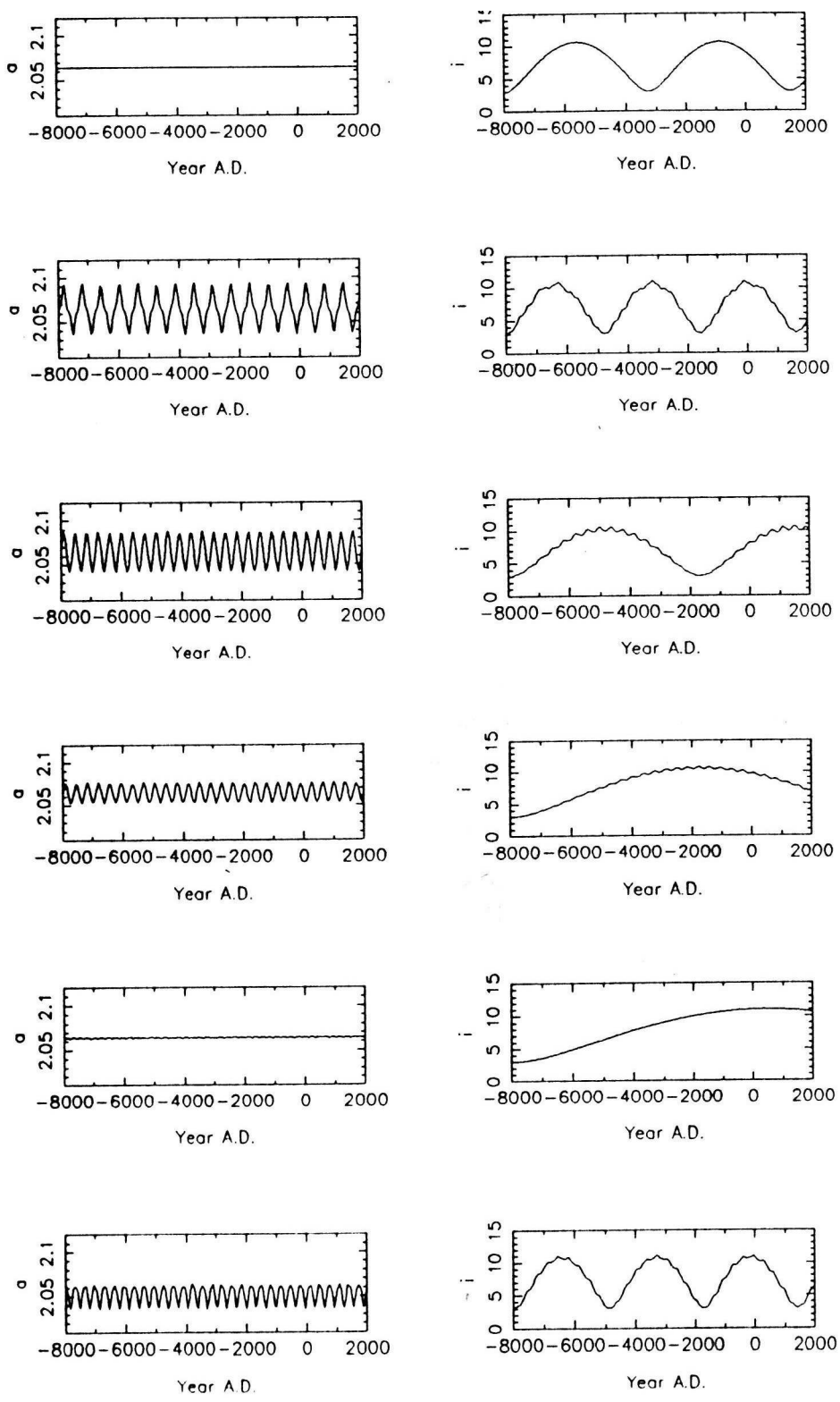

Figure 2.8: Variations in a and i of particles in or near the 4:1 resonance with Jupiter.

with Jupiter at aphelion and, as expected, the last of the four shows the slowest precession in i (also ω and ϖ, though not shown here). Only the first of the four, and also the near-resonant particle, show faster precession than the secular case.

We conclude by comparing the strength of different resonances. Greenberg (1977) contrasts the cases of low and high eccentricity. In the low-e case, writing the resonances as (p+q):p, the strongest resonances are for q=1,[4] when successive conjunctions occur at the same longitude. For moderate or (as for Taurids) high e, the main perturbations occur not at conjunction, but at aphelion (or perihelion if the orbit were outside the perturbing planet) and there can be significant effects for q>1.

In fact the following argument suggest that for Taurids it is (p+q) that is significant. For a particle moving precisely in the (p+q):p resonance, there are (p+q) possible positions of Jupiter when the particle passes through aphelion. The closest of these are displaced in longitude from the particle's aphelion by $\frac{360^\circ}{2(\mathrm{p+q})}$. Thus approaches to Jupiter are most effectively avoided for smaller (p+q). However, the size of the effects due to the resonance will be sensitive to other parameters, *e.g.* the aphelion distance, and so we cannot expect to see the effects simply as a function of (p+q).

We can use rates of ω and ϖ precession to quantify the strength of resonances. Table 2.4 shows the changes in precession rate due to the strongest resonances in the range of Taurids. The numbers will differ slightly if e is altered, *e.g.* for the 3:1

Resonance	a	a-range	$\Delta\omega$		$\Delta\varpi$	
3:1	2.500	2.43–2.57	–95%	+50%	–85%	+50%
10:3	2.331	2.31–2.35	–15%	+10%	$< \pm 2\%$	
7:2	2.256	2.23–2.28	–55%	+20%	–20%	+10%
4:1	2.064	2.03–2.09	–70%	+50%	–80%	+50%
5:1	1.779	1.765–1.79	–40%	+20%	–60%	+20%
6:1	1.575	1.57–1.58	–20%	+5%	–30%	+10%

Table 2.4: Strength of different Jovian resonances for orbits with e=0.85, as measured by the maximum possible change, relative to secular rates, in speed of ω and ϖ precession.

resonance with e=0.75 it becomes possible to have ϖ actually decreasing with time. Also we note that, relatively, smaller orbits have ϖ altered more and larger orbits have ω altered more.

We see that 3:1 and 4:1 are the strongest resonances in the Taurids, with a

[4] q is called the "order" of the resonance.

huge range in possible precession rates at both. Also significant are 7:2 and 5:1. Resonances in the Taurid range that are not listed in Table 2.4 may be classified as weak, having the maximum change in ω or ϖ precession rate $\lesssim$10% (so, *e.g.*, 10:3 is a borderline case whether to classify as weak). Specifically, I ran integrations to check the 13:4, 18:5, 11:3, 15:4, 13:3, 9:2 and 7:1 resonances. While it is possible in the restricted three-body problem for particles to remain in these weak resonances, they cover such a small range in a (note that in Table 2.4 it is the strongest resonance, 3:1, that covers the largest a-range) that the perturbations to a caused by the inner planets (see Section 3.1.2) mean that meteoroids that are Earth- and Venus-crossing are unlikely to stay in one of these resonances continuously for more than $\sim 10^3$ yr so that, even regardless of the fact that their effect on precession is small, these weak resonances are irrelevant for the practical consideration of the long-term evolution of the Taurid stream. We point out that though the a-ranges have been determined from integrations, it is in fact possible to derive them from the theory presented in Section 3.1.1 of the oscillations in a.

As a is increased above the values in Table 2.4, e has to be decreased to keep the particle well ($\gtrsim$0.5 AU) inside Jupiter. Integration results show it to be still possible to have particles trapped in resonances (*e.g.* 5:2 at a=2.824) and precession slowed, but it becomes more difficult to have particles maintained in a single resonant or near-resonant state with precession speeded. This is because unless the particle is protected by a resonance from close approaches to Jupiter at aphelion, it will suffer significant diplacements to its aphelion distance Q, *e.g.* if Jupiter is 0.4 AU away, Q may change by $\sim$0.05 AU during a single aphelion passage. Essentially, Q is likely to undergo a random walk until it is well inside Jupiter or wildly displaced. Thus we cannot predict long-term patterns of orbital evolution, though we can make a general statement that fast precession occurs for these orbits. Particles may in fact move between different resonances on timescales of a few kyr, or even less if they are very near Jupiter's orbit.

Chapter 3

A resonant meteoroidal swarm

In this chapter we consider the evolution of the source object of the Taurid Complex, a giant comet that has already undergone its most active phase and is now substantially devolatilised, most of its material dispersed throughout the Taurid stream and beyond. We use computational modelling to show how various observations may be explained if this source object has been moving in the 7:2 mean motion resonance with Jupiter, giving rise over several millennia to a dense resonant meteoroidal swarm.

A definite knowledge of the precise past orbital evolution of the Taurid progenitor is impossible but a likely evolutionary scheme is the following (see Section 1.2.2). It was captured from a Jupiter-crossing into a sub-Jovian orbit ∼20 kyr ago. During an initial active comet phase lasting ∼10 kyr, its aphelion distance Q progressively decreased owing to non-gravitational forces much as proposed by Sekanina (1972) for Comet Encke, so that its aphelion became decoupled from Jupiter. Q having decreased significantly, the comet was captured into the 7:2 resonance ∼10 kyr ago, since when it has been devolatilised, the cometary non-gravitational force therefore no longer acting. In Chapter 4 we consider meteoroid production during the latter phase especially. We note the possibility that the parent object could have fragmented and now be present as a gravitationally bound cluster of small asteroids (see Section 5.2.4).

The reason for invoking capture of the giant comet into the 7:2 Jovian resonance is because this could produce a resonant meteoroidal swarm, which could explain passages of the Earth through broad meteoroidal swarms happening in some years but not in others. Section 3.2 presents this argument more fully and models the formation and evolution of such a swarm in some detail with a view to comparison with observations (mentioned in Section 1.1.3) that are probably related to the Taurids; it considers whether there are plausible alternative explanations for these

observations.

The existence of the swarm as modelled would be strengthened by independent evidence of the appropriate parent object. In Section 3.3 we address the possibility that this parent is located in, and has given rise to, a bright and broad dust trail discovered by IRAS along the orbit of Comet Encke, but significantly displaced from Encke in anomaly. We consider dynamically the formation of the trail and consider the relative merits of this hypothesis and the previously existing explanation, that the trail is derived from Encke itself.

The resonance 7:2 in particular appears to come out of the modelling, on the one hand by the timing of terrestrial observations explained by the swarm, and on the other hand by its proximity to the period of Comet Encke. Encke is close to, but not exactly in, the 7:2 resonance, being in fact nearer 18:5. We have the proximity to Encke constraint because of the trail observation; this is discussed in Section 3.3, where we also propose that Encke was ejected, shortly before its discovery 200 years ago, from the proposed parent object.

We have, then, a dust *trail* in which the source object is immersed and, ultimately derived from the same source, a broad meteoroidal *swarm* which is centred on the resonance (the "resonance centre" is defined in Section 3.1); the source object oscillates about the resonance centre. There are by implication plenty of meteoroids larger than dust particles in the trail, but the relative importance of smaller particles is greater in what IRAS sees (since surface area is what matters) than in, say, mass influx to Earth. Trail particles are presumed to have separated from the parent object within the past few $\sim 10^2$ yr at most. The swarm is basically all the material that has not yet been perturbed out of the resonance and the relevant timescale is $\sim 10^4$ yr. Dust is not, of course, going to survive on relatively unperturbed orbits for $\sim 10^4$ yr.

A libration period for the source object about the resonance centre of about 400 years will be seen to fit the dust trail observation and the separation of Encke from the source. Passages of the source object and surrounding trail through the densest part of the swarm would then occur every 200 years and the question arises whether a 200 year cyclicity in dust input to the Earth could then occur through an interaction of the trail and meteoroidal swarm producing significant amounts of dust in the inner Solar System. The dust would in sufficient quantities be expected to produce the terrestrial effects described in Section 1.1.4. The phase of these variations in recent centuries is consistent with the core object position inferred from both the dust trail and the first appearance of Encke, and so the idea seems

worth further consideration. In Section 3.4 we investigate the ease with which a 400 year period may be maintained under the influence of perturbing effects other than Jupiter's.

Many of the explanations in this chapter are facilitated by a clear understanding of the behaviour of orbits in the resonance. Section 3.1 will now present the key ideas.

3.1 Orbital evolution of resonant particles

The behaviour of objects in resonance with Jupiter is a huge topic in Solar System dynamics. A lot of work, theoretical and numerical, has been done for small-eccentricity (asteroid belt) orbits (see Froeschlé & Greenberg 1989 for a review). Less attention has been given to the case of higher e, as is relevant for various meteor streams. In work that has been done, a certain amount of theory is possible (*e.g.* Murray 1982) though numerical methods have tended to be favoured (*e.g.* Scholl & Froeschlé 1988). This does not mean that the full equations of motion have to be integrated, since the effect of Jupiter can be allowed for by an averaging procedure, which considerably increases the integration speed (Schubart 1968).

In the present study the full equations of motion are integrated because the effect of the Earth and Venus turns out to be significant on timescales of a few 10^3 yr for 7:2 resonant Taurids. In this description of orbital behaviour some relatively straightforward theory will be presented because it yields simple equations to describe the motion under Jovian influence alone; terrestrial and Venusian gravitational forces can then be considered as a perturbing effect. In Section 2.2.2 we were mainly concerned with precession rates for different resonances. Here we wish to describe the behaviour of single particles in more detail and are interested in the 7:2 resonance in particular.

3.1.1 The case of the restricted three-body problem

For the 1:1 Jovian resonance, the existence of the Trojan asteroids near the L_4 and L_5 Lagrangian points has been known for a long time. For other resonances, we stated in Section 2.2.2 that it is possible for particles to oscillate in longitude about a reference point (the "resonance centre") that moves with exactly the resonant period P_r (neglecting the long-term precession of ϖ) and whose anomaly is such that it best avoids approaches to Jupiter. For the 7:2 resonance, the resonance centre moves with period $P_r = \frac{2}{7}P_J$ and so at instants when the resonance centre passes through aphelion there are 7 possible positions of Jupiter; the sequence of possible positions

repeats every 7 revolutions (2 revolutions of Jupiter). The criterion of best avoiding approaches to Jupiter means that 2 of these 7 Jovian positions are $\pm\frac{1}{14}$ revolution ($\sim$26°) away (Figure 3.1; *cf.* Figure 2.7). For a resonant particle that oscillates

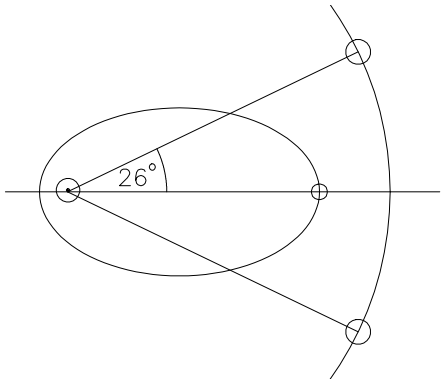

Figure 3.1: Positions of Jupiter on 2 out of 7 passages of the resonance centre through aphelion.

about, rather than comoving with, the resonance centre, the set of 7 positions of Jupiter when the particle is at aphelion varies within a range as shown in Figure 3.2; out of the 7 positions, only that where Jupiter is nearest (*i.e.* within $\pm\frac{1}{14}$ revolution) is shown, this being where Jupiter's perturbing effect is greatest.

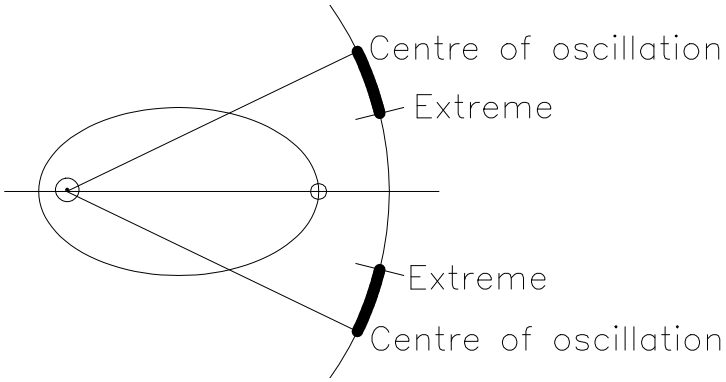

Figure 3.2: The position of Jupiter when a resonant particle is at aphelion is somewhere in the indicated range. Of course, different resonant particles oscillate about the resonance centre with different amplitudes; the range shown is simply representative.

A good qualitative explanation of how objects can be constrained to oscillate about the resonance centre was presented by Cohen & Hubbard (1965) for the case of Pluto being in the 2:3 resonance with Neptune when they discovered by numerical integration that this resonance was maintained for a long period of time ($>10^5$ yr). By considering Pluto's motion in the frame rotating with Neptune, they demonstrated that when Pluto passes its perihelion ahead of Neptune (Pluto

passes close to Neptune's orbit at perihelion; Taurids pass close to Jupiter's orbit at aphelion) the force exerted by Neptune is such that Pluto gains energy, decreasing its mean motion, and vice versa. A similar mechanism operates for resonant Taurids and we may understand it as follows.

We consider the position of Jupiter when the meteoroid is at aphelion and when Jupiter is at the closest of its 7 positions (*i.e.* within $\pm\frac{1}{14}$ revolution). Consider the half of the oscillation (or "libration") when the meteoroid is ahead of Jupiter as it passes aphelion (Figure 3.3). (The other half of the explanation will then

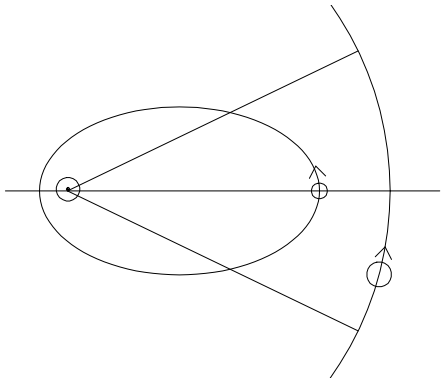

Figure 3.3: A meteoroid is ahead of Jupiter at aphelion.

proceed in an obvious way.) If the instantaneous period P is below P_r then the meteoroid will be even further ahead of Jupiter 7 revolutions later ("instantaneous" is being taken to include timescales of 7 revolutions, this being much less than the libration timescale) and so is moving towards the resonance centre; if $P > P_r$ then it is moving away from the resonance centre. In other words, the first derivative of position in the libration can be positive or negative. Note that although we speak of the *meteoroid* moving towards or away from the resonance centre, the Figures consider the frame where the meteoroid is at aphelion, regarding *Jupiter* as moving towards or away from the resonance centre point. Now, the perturbing force of Jupiter will act to pull the particle back, decreasing its velocity (and energy) and so decreasing P. If $P < P_r$, the meteoroid's period becomes an even greater amount less than P_r and so it moves more rapidly towards the resonance centre. If $P > P_r$, it moves less rapidly away from the resonance centre. Either way, it is accelerated (second derivative) towards the resonance centre. We note that since the condition $P < P_r$ determines whether the meteoroid is moving towards or away from the resonance centre, it reaches the extreme of the libration (and is "reflected") when P goes through the value P_r.

Whether a particle is resonant or only near-resonant depends on whether the P

difference from P_r is so large that it reaches the "breakthrough" point (Figure 3.4) before P reaches P_r; note that Jupiter does perturb P *towards* P_r as the meteoroid moves *towards* the breakthrough point. A meteoroid for which breakthrough occurs

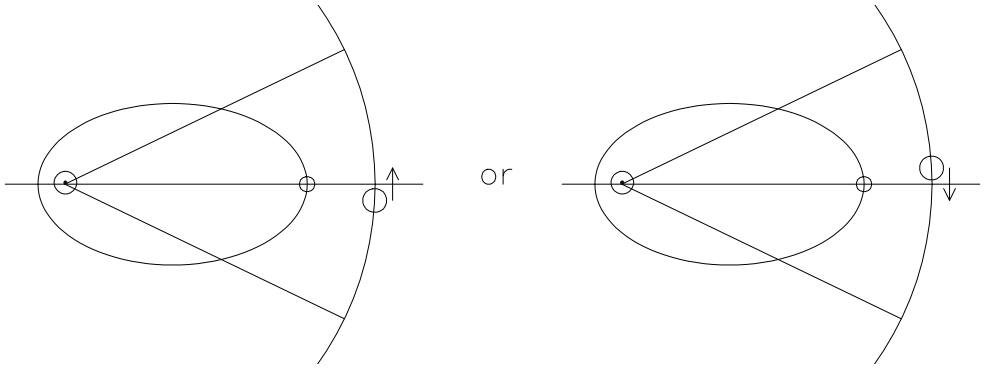

Figure 3.4: A meteoroid breaks through the resonant boundary.

has its long-term average period not equal to $\frac{2}{7}P_J$ since the set of 7 Jovian positions rotates continuously rather than oscillating. An approximate quantitative theory to predict when "reflection" back into the resonant zone and "breakthrough" occur is described in Öpik (1976).

To study the variations of P about or near P_r it is useful to consider the slowly varying parameter $7\lambda_J$–2λ (λ = mean longitude). The variation of this parameter is closely coupled with the variation of P, increasing when $P > P_r$ and decreasing when $P < P_r$. The parameter librates (oscillates) for resonant particles and circulates for near-resonant particles. From the above discussion it is clear that the centre of resonant oscillations depends on the aphelion and following, *e.g.*, Yoshikawa (1989) we introduce the critical argument

$$\sigma = 7\lambda_J - 2\lambda - 5\varpi$$

(ϖ = longitude of perihelion). A little thought shows that for resonant particles σ librates about 0. In general, for the (p+q):p resonance, it librates about 0 for odd q and about 180° for even q (though these are not the exact values; see next paragraph). The amplitude of the σ-libration can be anything up to 180°; otherwise breakthrough occurs. A low-amplitude libration corresponds to reflection occurring well inside the resonant boundary and the meteoroid being strongly trapped in the resonance.

Jupiter's eccentricity e_J is negligible compared to Taurid eccentricities and variations in Jupiter's heliocentric distance during one revolution are irrelevant — it is the meteoroid's radial distance that determines when approaches to Jupiter occur.

However, e_J does have an effect through the difference it induces between Jupiter's true and mean longitudes, which can differ by $>5°$ for the present-day value of e_J. It is Jupiter's *true* longitude near the particle's aphelion that determines resonant behaviour. The midpoint of the σ oscillations is displaced from 0 by 7 times the difference between the two Jovian longitudes (this is borne out by the results of all the integrations I have done). For present values of Taurid longitudes the libration centre is $\sim 20°$. The libration centre is exactly 0 only when $\varpi = \varpi_J$ or $\varpi_J + 180°$. Thus the σ oscillations due to P variations are imposed on very much slower oscillations due to the gradual rotation of ϖ. Schubart (1968) in his Hilda asteroid studies, uses the terminology "period of libration" imposed on "period of perihelion". However the relevant timescale for the evolution of the resonant Taurid swarm ($\sim 10^4$ yr) is several times smaller than the timescale for ϖ to undergo one revolution.

We have given a description of resonant oscillations and a qualitative description of why they occur, but it would be useful if we could derive quantitative expressions for how P (equivalently semi-major axis a) and σ vary (the variations, as we have seen, being closely coupled). We may proceed by considering the Hamiltonian. For a particle under the influence of Jupiter, it is

$$H = H_0 + H_1$$

where H_0 is the particle's energy for unperturbed Kepler motion around the Sun and H_1 is the perturbing Hamiltonian, due to the force exerted on the particle by Jupiter. The perturbing force is $-\frac{\partial H_1}{\partial \mathbf{r}}$. Thus

$$H_0 = -\frac{Gm}{2a}$$

$$H_1 = -\frac{Gm_J}{\mid \mathbf{r} - \mathbf{r}_J \mid} + \frac{Gm_J \mathbf{r}.\mathbf{r}_J}{r_J^3}$$

The second term in the expression for H_1 (the "indirect term") arises because $\mathbf{r}$ and $\mathbf{r}_J$ are in heliocentric coordinates, meaning that we must allow for the force of Jupiter on the Sun. The ideas of Hamiltonian mechanics, including Delaunay variables, canonical transformations and generating functions, all of which are required below, are explained, *e.g.*, by Goldstein (1980).

When a particle is trapped in a resonance, the variation in a is tightly controlled by Jupiter. In this chapter the amplitudes and periods of oscillations in a are of great interest. It is extremely useful for us to be able to consider idealised, instantaneous values of the amplitude and period. In the following approach, we neglect variations in e, i, Ω and ω. We shall learn these variations from full numerical

integrations, but at any instant the a-variations can be calculated theoretically. Including precession of e, i, Ω and ω in the theory complicates the algebra in a way that is unnecessary when what we are interested in is the behaviour of a and its consequent effect on mean anomaly. The following, as well as neglecting the e, i, Ω and ω precession, describes the behaviour in a neglecting variations of very short period. It is possible to calculate (numerically) the evolution of *all* the elements for resonant particles neglecting the shortest-period terms and consequently not having to integrate the full equations of motion, using Schubart's averaging method mentioned above. However to investigate the resonant Taurid swarm we shall want to perform full integrations in any case, in order to discover the effect of the inner planets.

One purpose of presenting this theory rather than using only integrations to study orbital behaviour is, as with the secular perturbation theory in Section 2.1, to simplify and to be descriptive, *i.e.* we can describe the orbital evolution by using simple, precise formulae (though whilst the formulae may be precise, certain approximations will have been made to obtain them). The theoretical approach both explains and confirms integration results. The theory can be applied to give a rough idea of libration periods, and also facilitates consideration of the effects of perturbations to a (Section 3.1.2).

The problem having been simplified so that there are just two phase space variables, the Hamiltonian (the particle's energy) is a function of a, of mean longitude λ and, through Jupiter's coordinates, of time t. In the restricted three-body problem, which we are considering, Jupiter's mean longitude λ_J is a linear function of t. Because H_1 is periodic in λ and λ_J, it can be expressed as a Fourier series:

$$H_1 = h_0 + \sum_j \sum_k h_{j,k;c} \cos(j\lambda_J + k\lambda) + h_{j,k;s} \sin(j\lambda_J + k\lambda)$$

where (j, k) ranges over all possible pairs of integers, except that we exclude $(-j, -k)$ when we include (j, k) since the terms are not independent. The range may be taken as $\sum_{k=-\infty}^{k=\infty} \sum_{j=1}^{j=\infty} + \sum_{k=1,j=0}^{k=\infty}$. The Fourier coefficients h are given by

$$h_0 = \frac{1}{4\pi^2} \int_0^{2\pi} \int_0^{2\pi} H_1 \, d\lambda d\lambda_J$$

$$h_{j,k;c} = \frac{1}{2\pi^2} \int_0^{2\pi} \int_0^{2\pi} H_1 \cos(j\lambda_J + k\lambda) \, d\lambda d\lambda_J$$

and $h_{j,k;s}$ similarly.

For the (p+q):p resonance, if we are interested only in terms that do not average to zero in the long-term, we keep only the constant term h_0 and terms with $\frac{j}{k} =$

$-\frac{\mathrm{p+q}}{\mathrm{p}}$. Writing ψ for $(\mathrm{p+q})\lambda_J - \mathrm{p}\lambda$, we have

$$H_1 = h_0 + h_{1;c}\cos\psi + h_{1;s}\sin\psi + h_{2;c}\cos 2\psi + h_{2;s}\sin 2\psi + \ldots$$

We begin by considering the case where H_1 is even and so the sin terms are zero — this basically means that there is no asymmetry, either in orbital plane or in direction of perihelion, in the relative alignment of the orbits of Jupiter and resonant particle. Also, the derived equations are simpler if all h's after h_1 are small compared to h_1; we shall check whether this is the case when we apply the theory to 7:2 resonant Taurids.

With these two assumptions,

$$H = H_0 + h_0 + h_{1;c}\cos\psi$$

We have $H = H(L, \lambda, t)$ where the Delaunay variable $L = \sqrt{Gma}$ and the variables L, λ are canonical. We wish to have equations of motion involving ψ and so want a canonical transformation from (L, λ) to (A, ψ) where A is the appropriate action variable. The generating function $S(\lambda, A, t)$ for the transformation must satisfy

$$\psi = \frac{\partial S}{\partial A}$$

and so is

$$S(\lambda, A, t) = ((\mathrm{p} + \mathrm{q})\nu_J t - \mathrm{p}\lambda)A$$

with ν_J = angular velocity of Jupiter and the origin of t chosen appropriately. A is given by

$$\begin{aligned} L &= \frac{\partial S}{\partial \lambda} \\ &= -\mathrm{p}A \\ \Rightarrow \quad A &= -L/\mathrm{p} \\ &= -\frac{1}{\mathrm{p}}\sqrt{Gma} \end{aligned}$$

The transformed Hamiltonian is

$$H(A, \psi) = H(L, \lambda, t) + \frac{\partial S}{\partial t} = H_0(A) + h_0(A) + h_{1;c}\cos\psi + (\mathrm{p} + \mathrm{q})\nu_J A$$

Because A and ψ are canonical coordinates, we have Hamilton's equations

$$\dot{A} = -\frac{\partial H}{\partial \psi} \quad \text{and} \quad \dot{\psi} = \frac{\partial H}{\partial A}$$

Therefore one equation of motion is

$$\dot{A} = h_{1;c}\sin\psi$$

where $h_{1;c} = h_{1;c}(A)$ but since A takes values only near the resonant value A_0, we take $h_{1;c} = h_{1;c}(A_0)$ with the desirable consequence that we need only evaluate the Fourier coefficient once. For the other equation of motion, we are interested in the A-dependence of H. We note that Jupiter's mass is much less than the Sun's and so just consider the term H_0 in H. Also we observe that $\dot{\psi} = 0$ when $A = A_0$, *i.e.* $\frac{\partial H}{\partial A} = 0$ and, Taylor expanding H,

$$H \approx -\frac{Gm}{2a} = -\frac{G^2m^2}{2\mathrm{p}^2A^2} \approx -\frac{G^2m^2}{2\mathrm{p}^2A_0^2} + \frac{1}{2}B(A - A_0)^2$$

where

$$B = \frac{\partial^2}{\partial A^2}\left(-\frac{G^2m^2}{2\mathrm{p}^2A^2}\right)\bigg|_{A_0} = -\frac{3G^2m^2}{\mathrm{p}^2A_0^4}$$

whence

$$\dot{\psi} = B(A - A_0) = -\frac{3G^2m^2}{\mathrm{p}^2A_0^4}(A - A_0)$$

In terms of the original variable a, noting that

$$A = -\frac{1}{\mathrm{p}}\sqrt{Gma} \quad \Rightarrow \quad (A - A_0) \approx -\frac{1}{2\mathrm{p}}\sqrt{\frac{Gm}{a_0}}(a - a_0) \text{ near } a_0$$

we have

$$\dot{\psi} = \frac{3}{2}\mathrm{p}\sqrt{Gm}\, a_0^{-5/2}(a - a_0)$$

This expression for $\dot{\psi}$ could in fact have been derived without using Hamiltonians since $\dot{\lambda}$ (and so $\dot{\psi}$) is a simple function of period and thus, by Kepler's third law, of a. Thus $\dot{\lambda} = \sqrt{Gm}\, a^{-3/2}$ and since $\dot{\lambda}_J = \frac{\mathrm{p}}{(\mathrm{p}+\mathrm{q})}\dot{\lambda}_0$ (where $\dot{\lambda}_0$ is the angular motion of a precisely resonant particle) we have

$$\dot{\psi} = \mathrm{p}(\dot{\lambda}_0 - \dot{\lambda}) = \mathrm{p}\sqrt{Gm}(a_0^{-3/2} - a^{-3/2}) \approx \frac{3}{2}\mathrm{p}\sqrt{Gm}\, a_0^{-5/2}(a - a_0)$$

for a near a_0.

Eliminating A gives

$$\ddot{\psi} = Bh_{1;c}\sin\psi$$

which is the equation of motion of a pendulum. That a resonance configuration leads to a pendulum equation has been known for a long time and discussed by many authors, *e.g.* Brown & Shook (1933). For this investigation of the resonant Taurid swarm I am using a comparatively simple application of this idea and have just derived as much theory as the application requires.

The next stage is to assume the orbits of Jupiter and the resonant particle are not aligned, *i.e.* the sin term is non-zero. This simply corresponds to a phase shift since

$$h_{1;c}\cos\psi + h_{1;s}\sin\psi = h_1\cos(\psi - \psi^*)$$

provided $h_1 = \sqrt{h_{1;c}^2 + h_{1;s}^2}$ and ψ^* is chosen to satisfy $h_{1;c} = h_1 \cos\psi^*, h_{1;s} = h_1 \sin\psi^*$. Thus we still have a pendulum equation, with h_1 replacing $h_{1;c}$ and the centre of the oscillation shifted from 0 to ψ^*. The angle ψ^* will allow firstly for ϖ (effectively replacing ψ by the critical argument σ) and also for the difference, mentioned earlier, between Jupiter's true longitude and mean longitude at the resonant particle's aphelion, *i.e.* $\psi - \psi^*$ differs from σ by the difference between Jupiter's longitudes.

Thus the pendulum equation is

$$\ddot{\psi} = Bh_1 \sin(\psi - \psi^*)$$

where $B < 0$ and $h_1 > 0$. Setting $\phi = \psi - \psi^*$ we have the first integral (basically an energy equation)

$$-\frac{1}{2B}\dot{\phi}^2 - h_1 \cos\phi = E \tag{3.1}$$

where E is a constant given by ϕ and $\dot{\phi}$ at some starting time. Therefore the extremes of the libration are given by

$$\phi_e = \cos^{-1}\left(-\frac{E}{h_1}\right)$$

and the period by the elliptic integral

$$\frac{4}{\sqrt{-2B}} \int_0^{\phi_e} \frac{\mathrm{d}\phi}{\sqrt{E + h_1 \cos\phi}}$$

We have now derived a convenient expression for an instantaneous value for the libration period. Its validity will depend on whether the assumption that $h_2, h_3, \ldots$ were zero was justified. This assumption appears reasonable for main-belt asteroids that are a long way inside Jupiter's orbit. For Taurids in the 7:2 resonance it turns out that the h's are negligible from h_3 onwards but that h_2 is of order 10% of h_1. It is very easy for a computer to calculate both amplitude and period of the libration allowing for h_2 and this seems worth doing. The new idealised resonant motion, then, is very slightly different from a simple pendulum equation. The equation of motion for $\dot{A}$ becomes

$$\dot{A} = h_1 \sin\phi - 2h_2 \sin 2\phi$$

and instead of (3.1) above we use

$$-\frac{1}{2B}\dot{\phi}^2 - h_1 \cos\phi + h_2 \cos 2\phi = E \tag{3.2}$$

with libration amplitude and period easily calculated numerically; the solution of

$$h_1 \cos\phi_e - h_2 \cos 2\phi_e + E = 0 \tag{3.3}$$

defines the amplitude ϕ_e (the libration centre being 0 when the angular variable is ϕ), and

$$\frac{4}{\sqrt{-2B}} \int_0^{\phi_e} \frac{\mathrm{d}\phi}{\sqrt{E + h_1 \cos\phi - h_2 \cos 2\phi}}$$

giving the period. If $E > h_1 + h_2$ then (3.3) has no solution and the particle is non-resonant. The amplitude can be seen to be uniquely determined if $h_1 > 4h_2$ since $h_1 \cos\phi - h_2 \cos 2\phi$ is then a decreasing function on (0,π) (derivative = $(-h_1 + 4h_2 \cos\phi) \sin\phi < 0$).

On evaluation of the Fourier coefficients, the phase of the h_2 term is found to be almost exactly 180° different from that of the h_1 term (*i.e.* $2\psi_1^* = \psi_2^* - 180°$, where ψ_1^* and ψ_2^* are the phase shifts calculated when evaluating h_1, h_2 respectively), as expected since they refer to the same resonance (meaning that, for the centre of oscillations, positions of Jupiter when the resonant particle is at aphelion will be the same). The 180° shift is simply because in the expression (p+q):p, q is even for 14:4 but odd for 7:2 (see earlier). Both h_1 and h_2 are positive and the phase is allowed for by the appropriate signs before h_1 and h_2 in (3.2).

Whether this theory is any use depends on whether it accurately reproduces the (a, σ) behaviour of real meteoroids. We present an example of the evolution of a in Figure 3.5, where we show analytic results superimposed on those from full integrations. We note that the coupled differential equations for $\dot{A}$ and $\dot{\phi}$ must be solved numerically, but this is orders of magnitude quicker than the numerical solution of the full equations of motion. All 3 particles were started at the resonance centre (ϕ=0) with $e = 0.85$, $i = 12°$, $\Omega = 334°$, $\omega = 186°$ (these are in fact the present values for Comet Encke). For the 7:2 resonance at $a = 2.256$ AU, the numerical coefficients work out as $B = -2.357$ and $\dot{\phi} = 2.47(a - a_0)$ (in units of years and AU, where $Gm = 4\pi^2$), and the above e, i, Ω, ω give the Fourier coefficients $h_1 = 0.000403$ and $h_2 = 0.000038$, with $\psi^* = 102°$ ($5\varpi = 80°$ and the remaining 22° is, to a very good approximation, due to the difference between Jupiter's longitudes). The 3 integrated particles started with $a = 2.237$, 2.257, 2.277 AU, but one immediately apparent thing from Figure 3.5 is that in the short term, a deviates from a smoothed average value by up to $\sim\pm 0.005$ AU. Since the analytic solution derived in this Section is in terms of smoothed values, the starting values of a were not taken as the same instantaneous values used for the integrations but were 2.238, 2.261 and 2.280 respectively. When this is done, there is seen to be an excellent fit to the integrations (Figure 3.5) and so we have a good demonstration that the behaviour of (a, σ) when orbital evolution is dominated by a resonance can be predicted to a large degree theoretically.

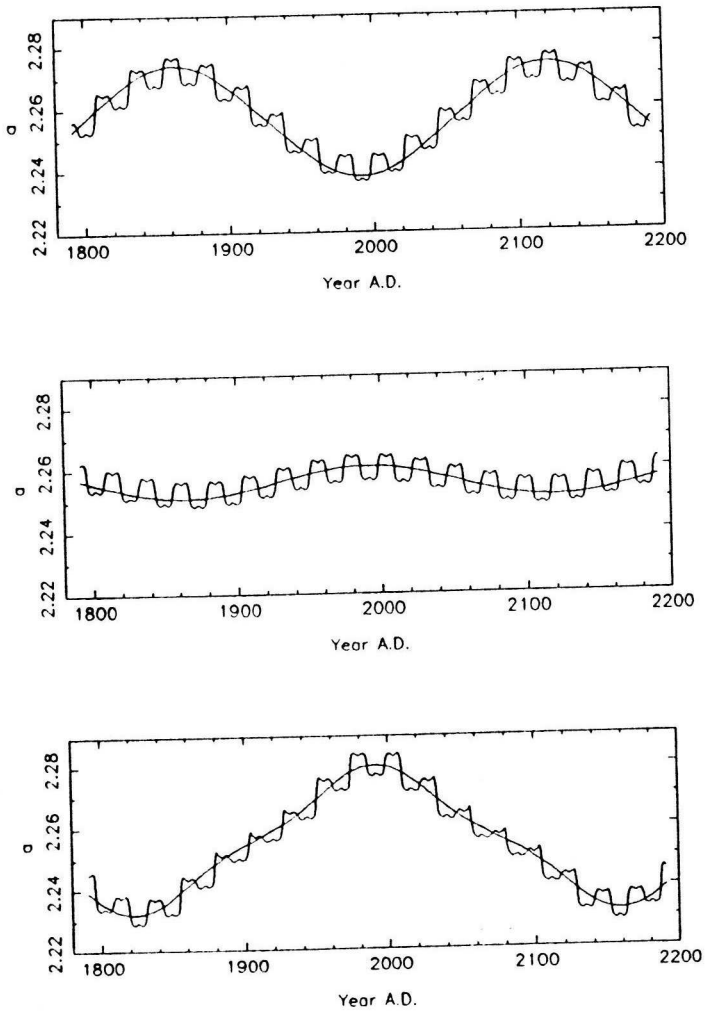

Figure 3.5: Behaviour of a, from numerical integration (irregular lines), and smoothed a, from analytic theory, of 3 particles.

The short-term effects are due to Jovian perturbations during individual aphelion passages. It is possible to follow the opposite approach (*i.e.* discrete rather than smoothed) — *e.g.* see Öpik (1976) for the Neptune-Pluto resonance. An advantage of the approach we have used is that it immediately yields numbers for libration periods, and ranges in oscillation of a and σ (see below) so that these do not have to be derived from detailed inspection of integration results (*cf.* secular theory in Section 2.2, which yielded numbers for ω and ϖ precession rates).

Thus given an actual orbit with an instantaneous value of a, this theory does not know what the smoothed value of a is (though it must be within $\sim$0.005). Nevertheless, the theory, and the use of smoothed a-values, provides a good way to describe and gain an understanding of (a, σ) behaviour. Essentially, the expressions for $\dot{A}$ and $\dot{\phi}$ mean that the oscillations of a and σ are $\frac{1}{4}$ of a cycle out of phase, with

a taking its central value ($\frac{2}{7}$ of Jupiter's period) at either extreme of the libration about the resonance centre, its minimum value when the particle is at the resonance centre (ϕ=0; we recall that ϕ librates about 0 but σ about a value slightly displaced from 0) travelling forwards through the resonance (σ decreasing) and its maximum value when the particle is at the resonance centre travelling backwards. Therefore at extreme values of ϕ, a must be very near $\frac{2}{7}P_J$ if the particle is to be resonant, but when ϕ=0, a wide range (about $\sim\pm$0.025 AU) is permitted. This is really just because all resonant particles pass through the resonance centre during their libration, but only ones with high amplitudes reach the extremes of the resonant zone.

We now turn to a discussion of how libration amplitudes and periods relate to values of ϕ (equivalently σ) and smoothed a. Table 3.1 shows such quantities; the values of h_1 and h_2 from the above example have been used. We list the value of

ϕ=0°			
$\mid \Delta a \mid$	E	Ampl.	P/yr
0.000	–0.000365	0°	-
0.001	–0.000364	6°	274
0.005	–0.000333	29°	258
0.010	–0.000236	57°	251
0.015	–0.000075	85°	250
0.020	0.000151	116°	265
0.021	0.000204	123°	272
0.022	0.000259	131°	283
0.023	0.000317	140°	299
0.024	0.000378	152°	331
0.025	0.000441	179°	653

ϕ=120°			
$\mid \Delta a \mid$	E	Ampl.	P/yr
0.000	0.000183	120°	269
0.002	0.000188	121°	270
0.004	0.000203	123°	272
0.006	0.000229	127°	276
0.008	0.000265	132°	284
0.010	0.000311	139°	297
0.012	0.000368	150°	324
0.014	0.000435	172°	453

Table 3.1: Period, and amplitude in ϕ, of libration for particles which have the stated value of a when ϕ=0 (left) or ϕ=120° (right); Δa is the difference in a from the 7:2 resonant value (2.256 AU).

the constant E (defined earlier), which is a function of the instantaneous values of a and ϕ, and uniquely determines the amplitude and period (for given h_1 and h_2). Values have been listed for a range of a-values for each of two ϕ-values; if two (a, ϕ) combinations give the same value of E then they refer to the same particle but at a different point in its oscillation. We note that there is a minimum permitted period of $\sim$250 yr (*cf.* for a simple pendulum the period is independent of the amplitude for small oscillations) and also that values of 250–300 yr for the libration period are preferred, in that for values which are rather higher, a small perturbation to a (of the kind induced by the inner planets; Section 3.1.2) causes a significant change in the

libration period. These periods are typical of 7:2 resonant Taurids, *e.g.* repeating the calculations with e=0.8 instead of 0.85 (details not shown here) only increases periods by ∼10 yr. Rotating the longitude ϖ also affects periods slightly; see below.

High libration amplitudes are associated with longer periods, then. This is demonstrated with numerical examples in figure 3.6. We also point out that high amplitudes are associated with faster precession rates (*cf.* Section 2.2.2); for the 9 examples shown here the changes in ϖ over the timescale of the integration (nearly 10 kyr) are 80, 69, 67, 65, 65, 66, 67, 69 and 74° respectively.

Figure 3.6 also shows that there is a tendency for the libration period to decrease slightly with time. This is a result of Jupiter's non-zero eccentricity, and periods predicted by the analytical theory confirm this point, *e.g.* reducing the longitude by 50° causes predicted libration periods to be ∼30 yr higher. Thus for 7:2 resonant Taurids, which for the past ≫10 kyr have been precessing so that their aphelion has been approaching Jupiter's perihelion, there has been a systematic tendency for the effects of the resonance to make them become gradually more strongly trapped in the resonance as time progresses. Indeed it is possible to run integrations back in time for particles that have high libration amplitude and see them leave the resonance. However, in practice this systematic effect is negligible compared to that due to changes in a caused by approaches to the inner planets.

3.1.2 The effect of the inner planets

We have, then, a set of rules giving us quite a precise description of the behaviour of Taurid orbits that are in the 7:2 resonance with Jupiter, in particular the way the anomaly is constrained by resonant effects. The next question is whether this provides a true picture of how meteoroids behave, or whether there are other effects that we must allow for. Though Jupiter's effect is certainly dominant, we now consider the other planets.

Saturn has a slight effect on the precession rate, but its effect on the amplitude and phase of the resonant libration is negligible, as shown by a comparison of Figure 3.7 with Figure 3.6. The change in σ is hardly detectable, even after 10 kyr. We saw in Section 3.1.1 that a sudden displacement to a can have a significant effect on libration amplitude and phase; however, particles never go near enough to Saturn for the planet to induce a change in a (*i.e.* an energy change) that is not completely negligible.

The same is not true of the 4 inner planets. Figures 3.8 to 3.11 present integration results for the same starting conditions as with Figure 3.6 but with Mercury, Venus,

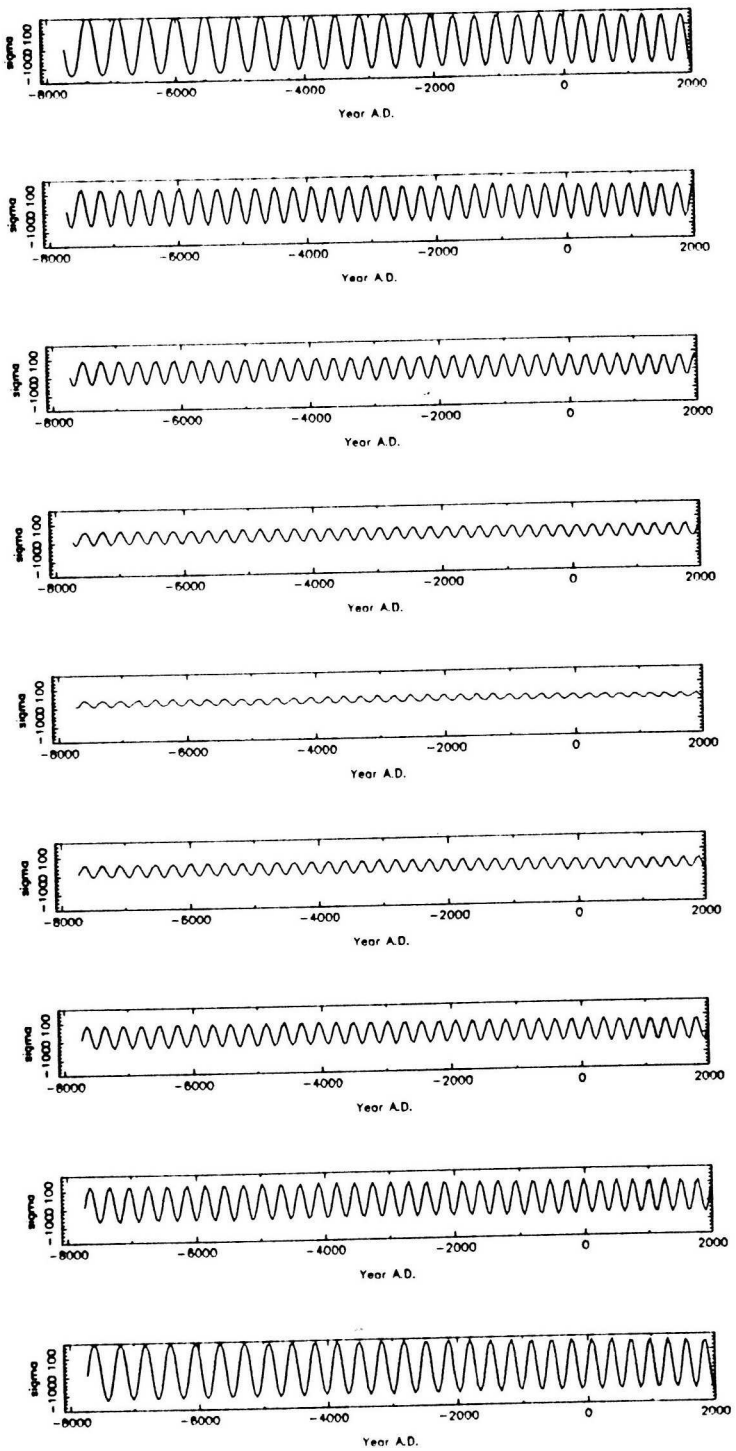

Figure 3.6: Evolution of σ forward in time $\sim$10 kyr, taking account of Jupiter only, of 9 particles starting at the resonance centre with values of a from 2.240 to 2.280 AU, spaced by 0.005 AU. The particles with more central initial a-values have both amplitude and period of libration smaller.

Earth and Mars included (with Jupiter) in turn. The effect of Mars is small, though not quite as difficult to detect as the effect of Saturn. That of Mercury is

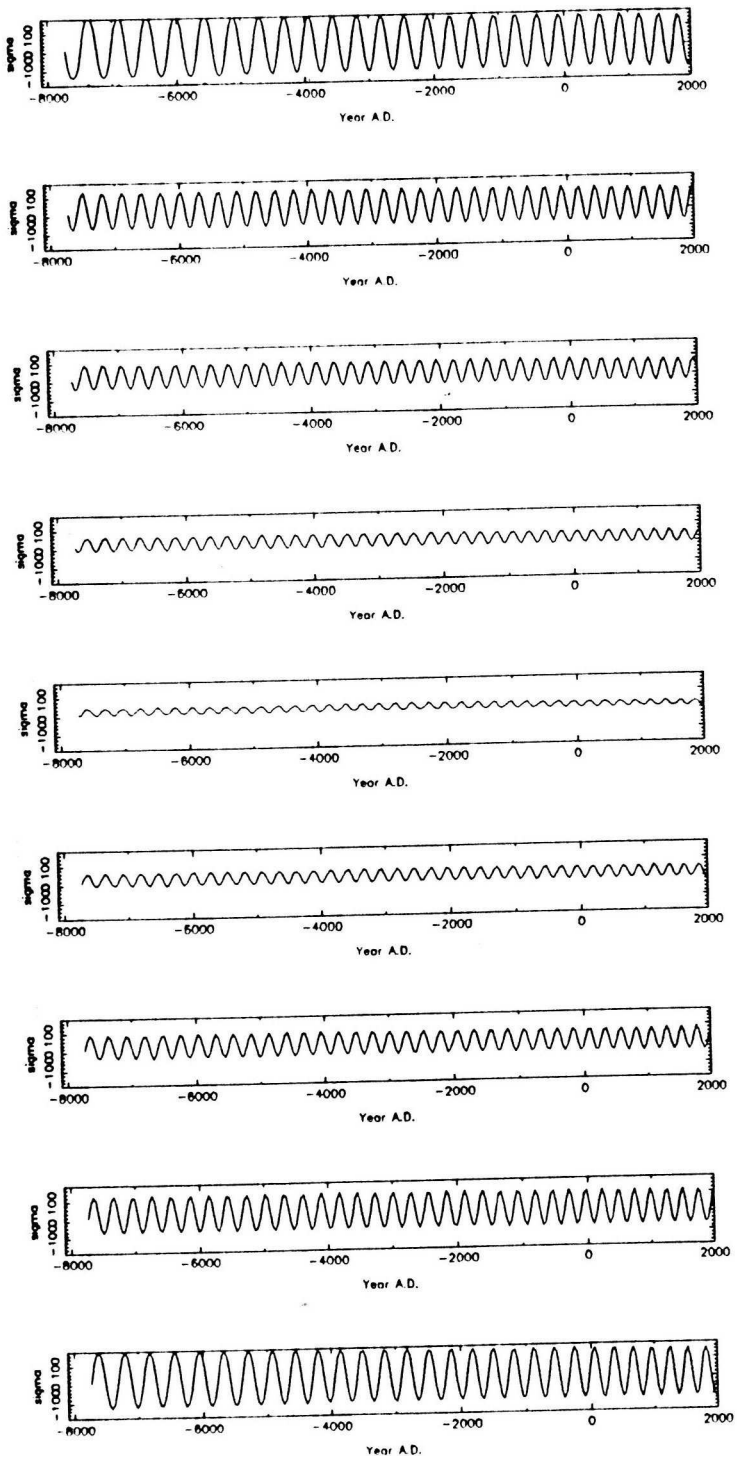

Figure 3.7: As figure 3.6, but with Saturn included in integrations.

slightly greater and indeed it perturbs one particle (which was not strongly trapped in the resonance, having a high libration amplitude) out of the resonance. The Earth and Venus can be seen to have severe effects on libration amplitude and phase (and consequently precession rate) in many cases.

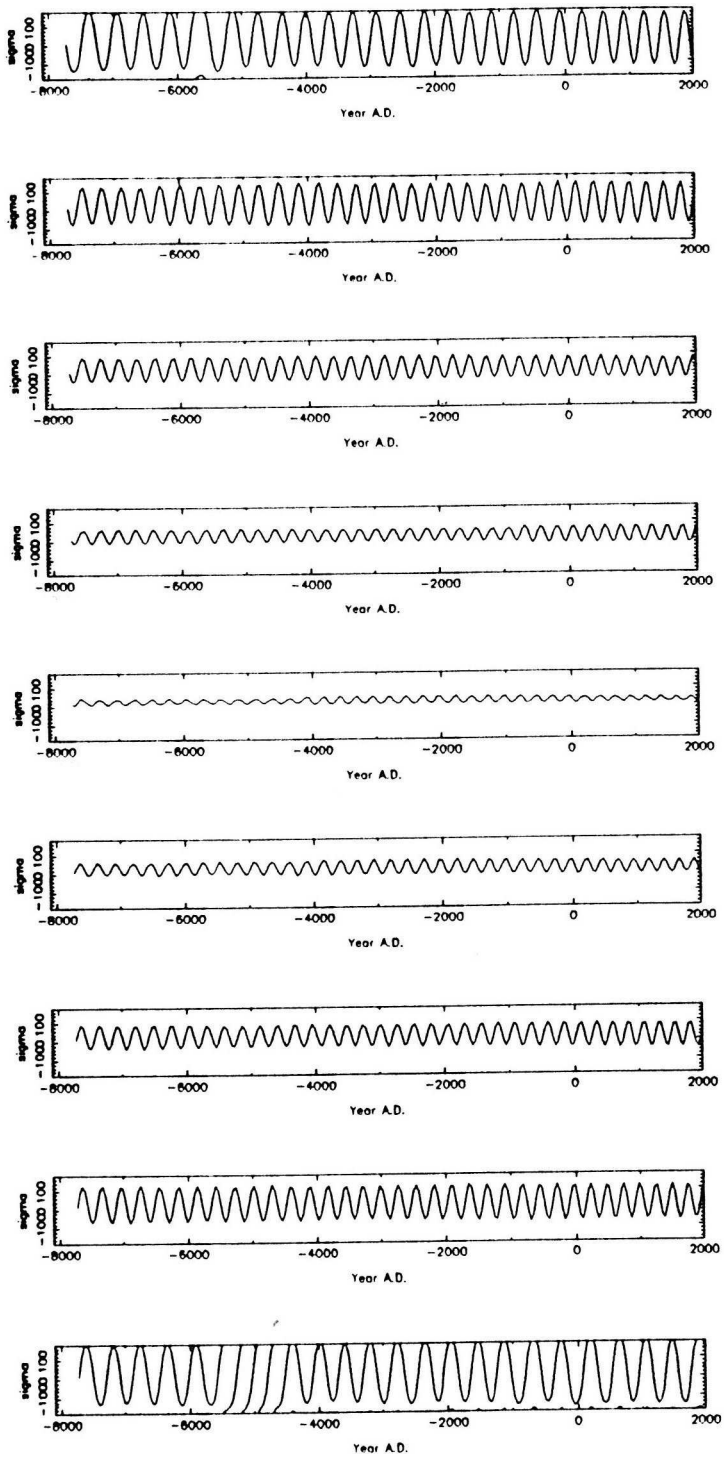

Figure 3.8: As figure 3.6, but with Mercury included in integrations.

On the basis of the empirical evidence of these integrations it would now be reasonable to proceed with dynamical modelling including the Earth and Venus in addition to Jupiter. However, it seems worth briefly investigating some of circumstances under which the inner planets induce changes in a. One important fact will

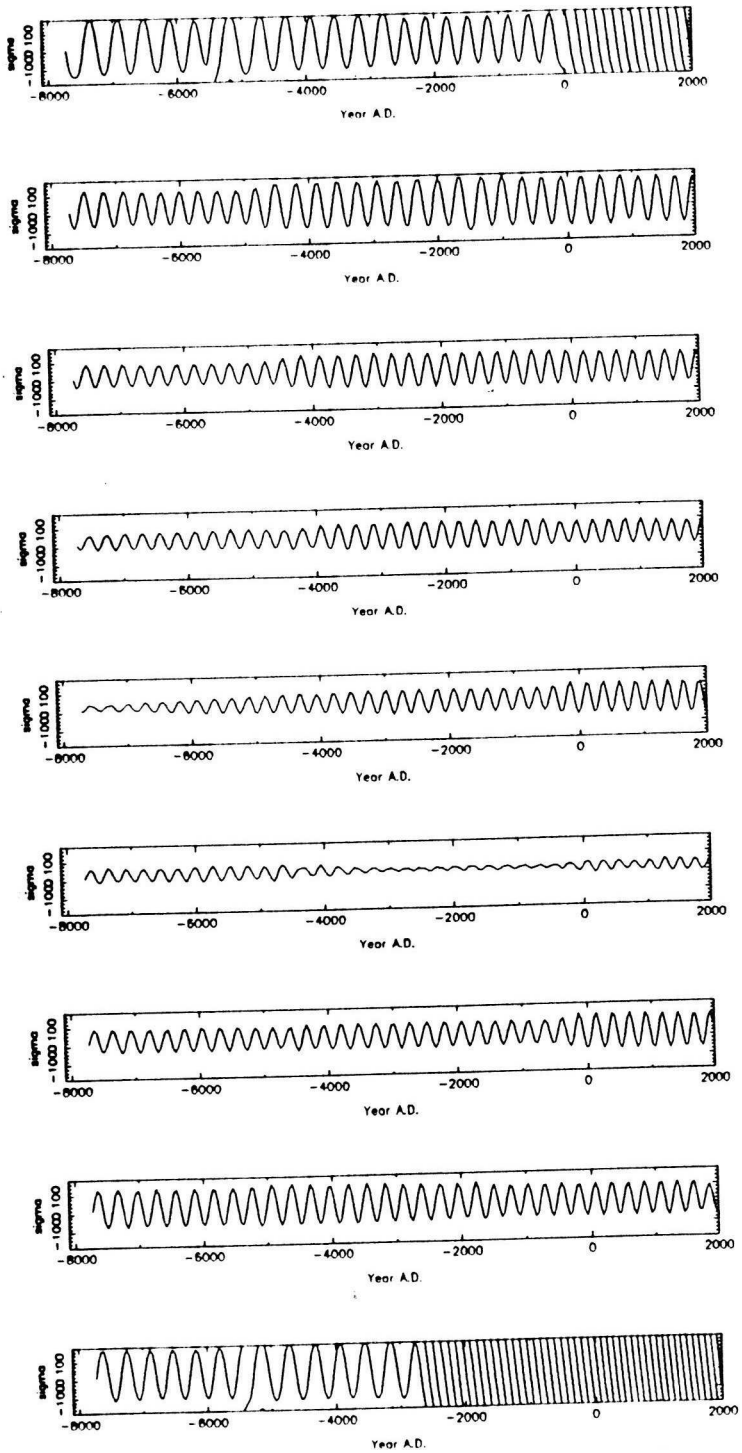

Figure 3.9: As figure 3.6, but with Venus included in integrations.

be that there is a tendency for the greatest perturbations to occur at particular epochs, *viz.* when the meteoroid's orbit has precessed so as to take it close to the orbit of Earth or Venus.

The importance of an inner planet depends on the number of times a meteoroid

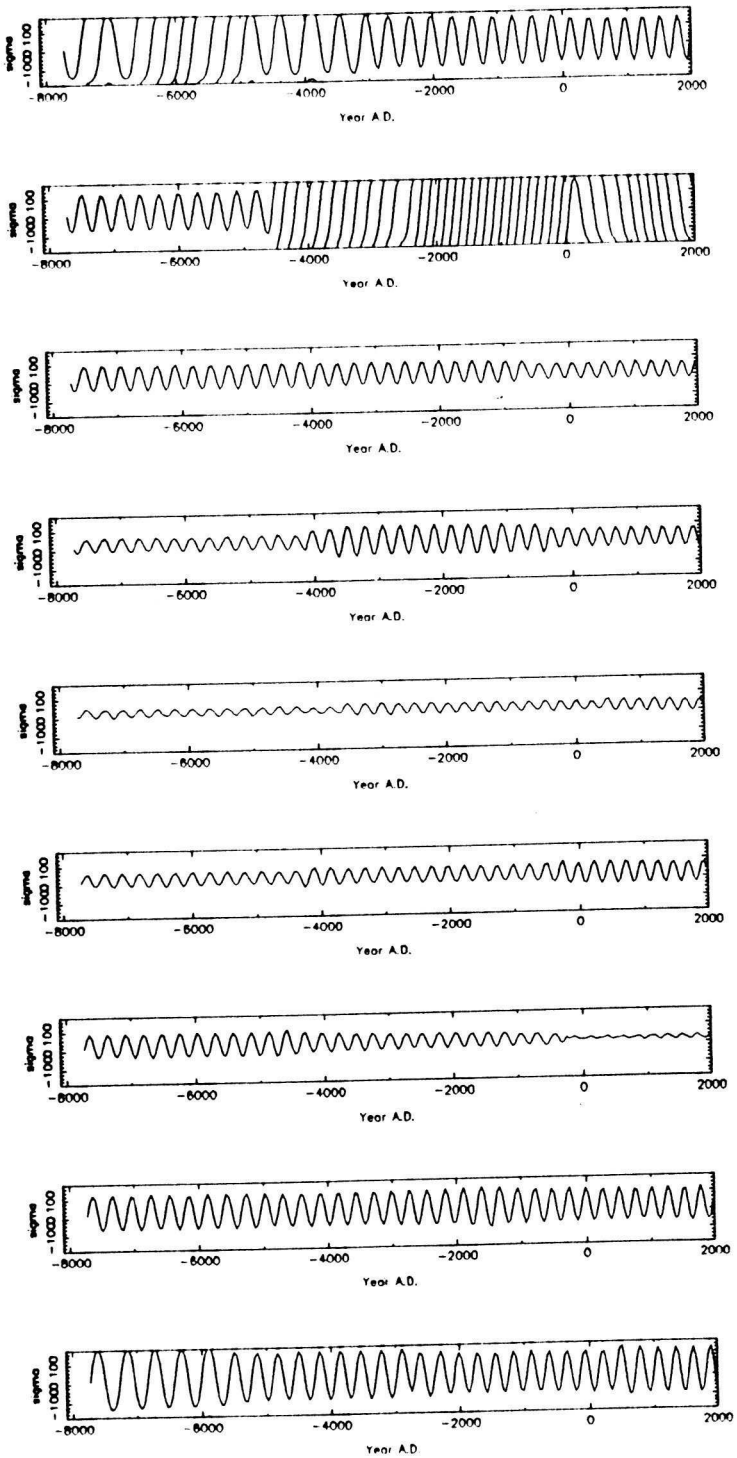

Figure 3.10: As figure 3.6, but with Earth included in integrations.

is expected to pass within a certain distance of it, and the size of the perturbation to a when this happens. Perturbations to elements due to an impulse depend on the direction of the impulse (see, *e.g.*, p. 184 of Roy 1978); thus if the Taurid particle passes above or below the planet then i is affected more than a, but vice versa if it

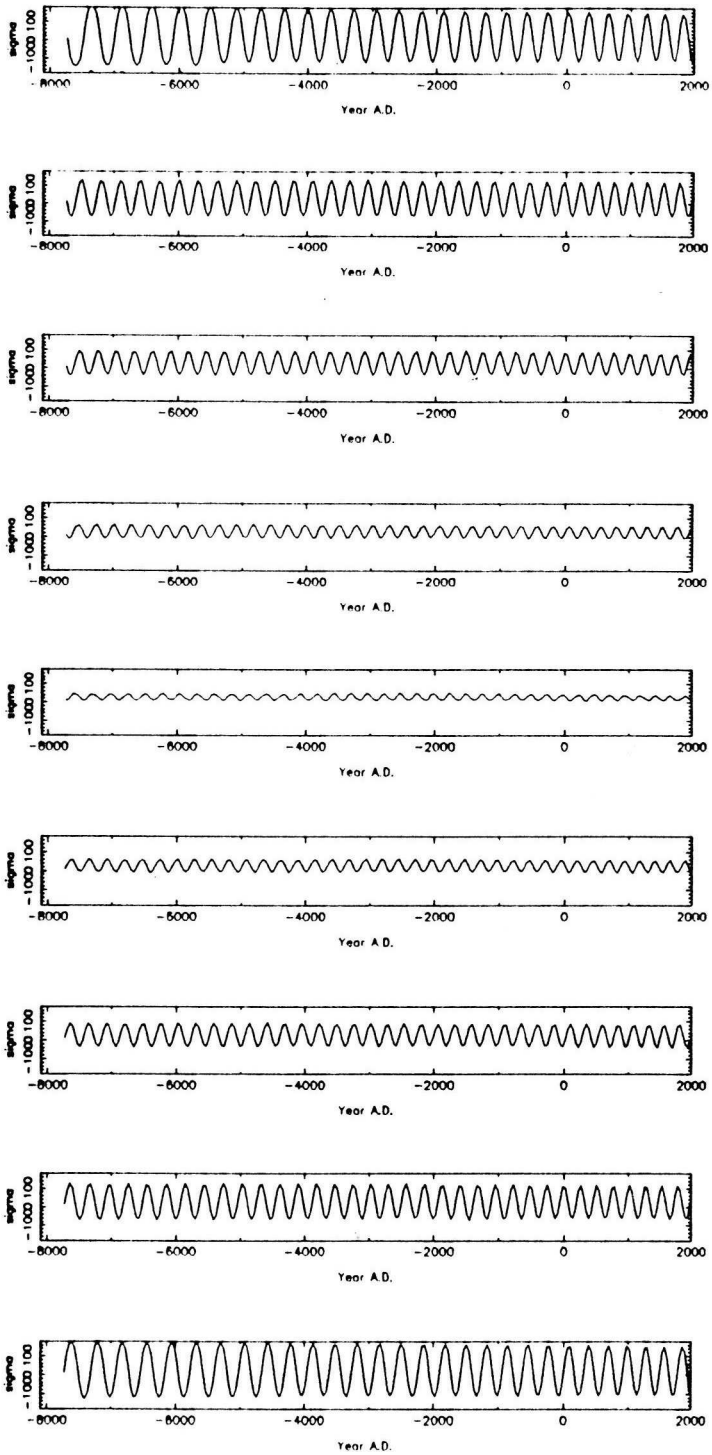

Figure 3.11: As figure 3.6, but with Mars included in integrations.

passes by the side of the planet. Integrations I have done confirm that for approaches to within a fixed distance of a particular planet, a comparatively large change in i is associated with a small change in a and conversely. As well as regarding the occurrence of an approach to within a certain distance of a planet as a random

event, we can also regard it as random as to whether a or i is affected more. A change in i does not affect the amplitude and phase of the resonant libration.

Integrations of 25 particles over 10 kyr (*i.e.* 250 kyr of integrations) with Jupiter and the 4 inner planets (in contrast to the above integrations, where only one inner planet was included at a time) have yielded the statistics for approaches shown in Table 3.2. This broadly seems to show that for any one planet, the number of

D (AU)	.005	.010	.015	.020	.025	.030	.035	.040	.045	.050
Mercury	23	83	224	381						
Venus	4	16	34	63	96	130	177	225	290	346
Earth	2	9	16	29	46	71	88	129	160	197
Mars	1	2	7	14	23	31	44	63	84	113

Table 3.2: Number of approaches to within distance D of the inner planets in 250 kyr. For Mercury, only approaches within 0.020 AU were recorded.

approaches to within distance D is proportional to D^2, as expected, and that the ratio for the 4 planets, in order, is about 25-4-2-1. It is possible to derive encounter probabilities theoretically, and we note that these numbers seem in good agreement with the figures on p. 42 of Öpik (1976) for collision probabilites of Comet Encke with the 4 planets (after we allow for the cross-sectional areas of the planets).

We can perform some rough calculations on the expected perturbation to a for an approach to within distance D of a planet. The impulse applied to the particle is approximately proportional to m/Dv where m is the planet's mass and v the particle's planetocentric velocity. For a given impulse, a greater change to a is possible at smaller heliocentric distance r (see Roy 1978, p. 184), so that the distance D at which we can get a given change in a is roughly proportional to m/vr. The velocities are similar for approaches to all 4 planets and so the relative distances D work out to be in a ratio of about 2-15-15-1 (for Mercury-Venus-Earth-Mars). Now, the number of approaches to within D is proportional to D^2 so that if the 7:2 resonant particle approached each planet equally often then perturbations to a would occur in the ratio 4-200-200-1. Combining this with the ratio for relative number of approaches from the previous paragraph we obtain 100-800-400-1. These calculations make no claim to be anything other than approximate but they confirm theoretically what we found numerically, namely that we may allow for the effect of the inner planets by including just the Earth and Venus, though Mercury's effect is not completely insignificant.

We shall not attempt to link the frequency distribution of approaches to within

D of each planet quantitatively to the long-term effect on libration amplitude and phase (due to a number of perturbations to a over several kyr), rather discovering the latter empirically when we come to the dynamical models (Section 3.2.3). The most useful thing here has been to discover the relative effects of the inner planets. We just mention that a *single* perturbation to a that is enough instantly to transform a particle from being strongly trapped in the resonance, *i.e.* with very low libration amplitude, to being non-resonant probably occurs every 1–2$\times 10^5$ yr.

In the long term, we understand these inner planet perturbations to 7:2 resonant particles probabilistically so that (from the results of the simulations described in Section 3.2.3) we can talk of a half-life of a particle in the resonance of $\sim$20 kyr. The perturbations to a are, however, not constant on timescales of a kyr, but are greater during epochs of nodal intersection with the orbits of the Earth and Venus. The geometry of the orbit in fact means that ascending and descending node intersections with both planets occur within a few centuries with a gap of $\sim$3 kyr before the next set of intersections. Thus approaches to the Earth and Venus, which are primarily responsible for perturbing the amplitude and phase of the resonant libration, occur in bunches, as shown in Figure 3.12. In the last of the three plots, the particle is precessing slightly more quickly than the other two so that it goes through an extra epoch of nodal intersection during the same timescale.

This Section is an appropriate place briefly to make the important point that when the inner planets are included, the evolution of Taurid orbits becomes chaotic. When Jupiter only is included, as we improve the integration accuracy (by reducing the parameter ε defined in Section 2.1.1), we converge towards a well-defined solution. Also, we may run an integration in the reverse time direction and recover the initial conditions. The perturbations induced by single approaches to inner planets cause two initially almost identical orbits to diverge rapidly. It turns out that with a Fortran double precision program, we can neither obtain a convergent solution by improving integration accuracy nor reverse time and recover the initial conditions over a timescale of more than, say, 2 kyr. This timescale, though, varies from orbit to orbit; in particular, it is more difficult to follow orbital evolution predictably through epochs of nodal intersection with the Earth and Venus.

The effect of the inner planets on resonant behaviour, then, is best thought of as essentially random perturbations to a. No integrations have produced any suggestion that a resonance with an inner planet is important. In their integrations of Earth-crossing asteroids, Milani *et al.* (1989) found an example of an orbit that was in the Jovian 7:2 resonance but which spent an appreciable period in the 5:17

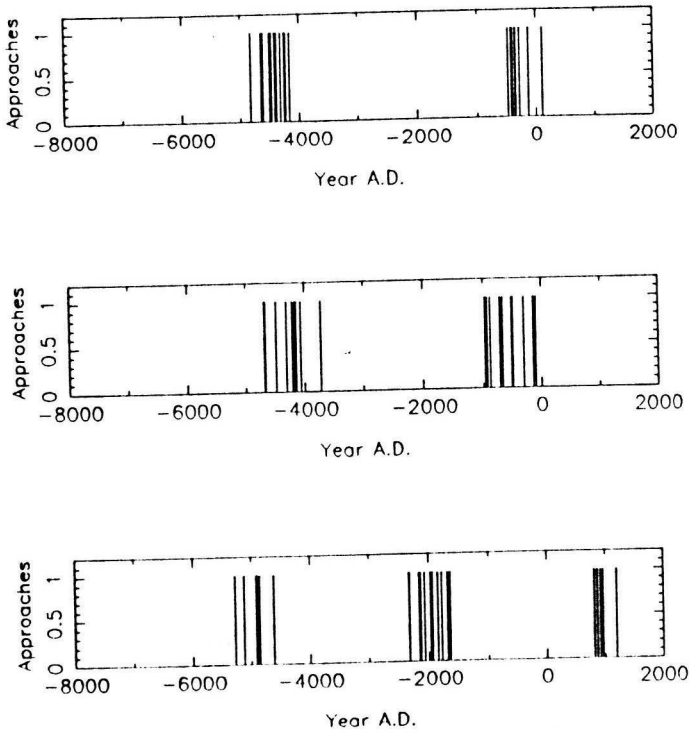

Figure 3.12: Times of approaches within 0.05 AU of the Earth or Venus (not shown separately) for three 7:2 resonant Taurid particles.

resonance with the Earth. The a-value associated with the latter resonance is 2.261 AU, within the range of typical oscillations of the former. However, Taurid orbits are unlikely to be captured into the 5:17 Earth resonance because they are sufficiently close to Jupiter at aphelion that the influence of the 7:2 Jovian resonance is simply too strong. The example of Milani *et al.* had e around 0.55. I have run a few trial integrations with this value of e and found that resonant behaviour, *i.e.* avoiding close approaches to the Earth, occurs in an analogous way to behaviour at the 7:2 Jovian resonance, provided that aphelion is roughly aligned with Jupiter's aphelion. If the aphelion is moved near Jupiter's perihelion (reducing the distance from Jupiter's orbit), let alone e changed to higher values typical of Taurids, then it does not appear to be possible to have particles trapped in the 5:17 Earth resonance.

3.2 Evolution of the swarm

Usually when meteor streams form, material spreads all the way *around* the orbit before dispersing to any significant degree *across* the orbit. However, we have seen that the presence of a resonance with a major perturber can lead to a meteoroid being constrained to librate about a centre of oscillation that has *precisely* the

resonant period, *e.g.* $\frac{2}{7}$ the period of Jupiter. Meteoroids ejected from a resonant parent object will themselves be in the resonance (provided they are ejected with sufficiently low velocity) and thus the population of meteoroids as a whole will be concentrated in just part of the orbit for a long time, quite possibly long enough for a substantial dispersion across the orbit to occur.

In this Section we see whether this idea can be applied to various Taurid Complex meteoroidal swarm detections in the Earth-Moon system. We describe the observations, then consider why we should invoke the explanation of a resonance at all, and the 7:2 resonance in particular, and then proceed to detailed modelling of the swarm's evolution.

3.2.1 Observations and non-observations

Various detections near the Earth of meteoroidal material believed to be associated with the Taurid Complex were reviewed in Section 1.1.3. The critical observations as regards the existence of a broad meteoroidal swarm are those which firstly are of groups of meteoroids as opposed to single objects; thus, *e.g.*, we consider the Tunguska object as less significant for the present purpose. Furthermore, we are looking for observations which last, say, a week — meteoroids observed within a very short time are likely to be products of quite a recent break-up. A final requirement is that the meteoroids concerned are large enough that gravitational forces dominate their orbital evolution — on timescales of several 10^3 yr, dust, and even very small meteoroids, will be completely dispersed.

We are thus left with the lunar meteoroid detections in 1975, the swarm of very bright Taurid meteors in 1951 and the meteoroids causing obscuration at points in the Earth's dayglow in 1981. We consider each of these in turn, remembering that in addition to the observations we are interested in times when the phenomenon could have been detected but was not. No results were sought only relating to a specific year during which the resonant swarm was expected, nor have I found any reports of week-long swarms occurring at either of the appropriate times of year other than those mentioned below. Such reports would be an invaluable future test of the model.

The week-long meteoroid swarm that has frequently been associated with the Taurid Complex (*e.g.* Dorman *et al.* (1978) suggested that it could be a rare enhancement of the β-Taurids) is that detected by lunar seismometers in 1975. Instruments which could detect vibrations of the lunar surface were left at four sites on the Moon by Apollo missions between late 1969 and April 1972; results were recorded until

September 1977. Signals due to impacts are very different from those due to the internal geological activity of the Moon. A recent study of the impacts detected is by Oberst & Nakamura (1991). Distances of the order of 1000 km separate the sites, but they are all on the near side of the Moon; events are more likely to be detected when meteoroids land nearer the instruments.

By far the most significant clustering of impacts occurred in late June 1975. The statistical analysis of Oberst & Nakamura (1991) gives a mean date for the encounter of 22 June and the significance level of the detection as being above the background level is maximised by taking the duration as 9–10 days. Oberst & Nakamura found a minor enhancement (significance level 99.93% in what they classify as large impacts, but not listed in small impacts) of the lunar impact detection rate lasting 9 days centred on 2 July 1974 and suggested it could have been caused by the swarm detected in 1975, though this cannot be the case under the scenario we model here. We briefly mention that mid-1974 matches the anomaly of the proposed trail parent of Section 3.3 so that this small 1974 swarm could be due to a recent violent ejection of material from the parent object (recent so that meteoroids have not had time to spread round the orbit, violent so that they were immediately well dispersed across the orbit). In Section 3.2.2 we discuss why we do not wish to appeal to a recent violent fragmentation to explain the large 1975 swarm.

A plot in Hartung (1991) suggests that lunar seismic detections at the end of June 1972 were slightly above the background rate, *e.g.* 7 impacts from 27–30 June against an expected background, that may be calculated from Oberst & Nakamura (1991), of $\sim$0.5 impacts/day. Oberst & Nakamura do not mention it because they only list clusterings with significance level $>$99.9%.

Evidence that the 1975 storm was detected at another time during the lunar seismic experiment does not seem conclusive. Non-detections can be because the swarm did not intersect the Earth or because the detectors were not preferentially orientated; in the latter case only very large impacts would register. Only masses $\gtrsim$10 kg are likely to register wherever they land (Dorman *et al.* 1978). Very roughly, the efficiency of the detector varies as the cosine of the angle between the Earth-Moon line and the meteoroid arrival direction, falling to zero when the angle exceeds 90° (Hartung 1991). Hartung also points out that in late June 1972, detecting conditions (*i.e.* the phase of the Moon) were only a couple of days different from those in 1975. With advance knowledge of dates we shall regard as important in Section 3.2.2, it seems worth noting that in the first week of November 1971 the seismic stations were on the opposite side of the Moon to that facing the Taurid radiant, and the

fourth station had not been set up. The lunar phase in early November 1974 was almost as unfavourable.

Very low frequency (VLF) radio waves propagate in an Earth-ionosphere waveguide, the upper boundary of which is set by a certain electron density. The fact that the ionisation caused by incoming meteoroids produces detectable changes in VLF transmissions led Kaufmann *et al.* (1989) to search data for a corresponding effect on Earth during the lunar swarm encounter. This they found, with an electron production rate apparently several times larger than during the spectacular 1946 Giacobinid shower. They argued in favour of a southern hemisphere radiant (which, since the equator is well below the ecliptic at this longitude, would preclude very low-inclination meteoroids in the Taurid Complex) because effects were greater on paths with greater lengths in that hemisphere. However, this interpretation seems far from unique and it appears plausible that if one could model the expected effects of a low-inclination swarm with, for example, lower end heights for meteors incident on the Earth at lower latitudes then a Taurid swarm would not be excluded. Kaufmann *et al.* also quoted a right ascension of 105–120° for the storm radiant (from studying diurnal patterns in the effects); this is not quite in agreement with an expected Taurid resonant swarm apparent radiant of ∼80°, but the Taurid association probably cannot be excluded given uncertainties (in, *e.g.*, ion recombination times) in calculating how long the effects on the ionosphere are expected to last.

We turn now to the pre-perihelion intersection with the Earth and consider firstly Taurid meteors and fireballs. Observations of bright meteors by Dutch observers between 1947 and the beginning of 1954 are described by van Diggelen & de Jager (1955). There would naturally not have been uniform coverage during this time; nevertheless over 50 very bright meteors (magnitude 0 to –5, corresponding to meteoroids of mass 1–100 g), for 26 of which apparent paths could be drawn, were observed in a swarm in 1951. The range of dates is 28 October – 11 November (Fonk 1951) and the radiants appear to be just north of the ecliptic.

Bone's (1991) analysis of British Taurid observations from 1981 to 1988 suggests no detection of any great variability from year to year. This probably means that the rates of the Taurids as a whole show little annual variation. However, Bone (1989, 1991) describes a report of several bright Taurids in early November 1988 and this may lead us to believe that if we searched for Taurids that were firstly bright and secondly localised during a period of a few days during the shower (which lasts for many weeks), we may discover interesting observations which would tend to be disguised when the year's Taurids are considered in their entirety. It could be that

meteoroids in a resonant swarm that has been formed over several kyr are likely to be large (producing meteors brighter than magnitude 0, say) if for smaller objects over such a timescale the decrease in semi-major axis a due to the Poynting-Robertson effect were comparable to the a-range that defines the resonance.

I have looked through available issues of *The Astronomer* back to 1967 and found that the exact dates of observation in 1988 were the nights of 2 and 4 November; one observer (N. White) saw many Taurids between magnitudes –2 and –4 at the rate of about one an hour. Several observers in Tenerife spent several hours in good conditions in 1989 (nights of 27 and 31 October and 3 November) and saw no Taurids brighter than magnitude –1 [*The Astronomer* **26,** 200 (1990)]. They noted the "very low level of Taurid activity after the good 1988 display". Some observers in Finland found a disappointing Taurid display on the night of 3 November 1979 and compared it to 1 November 1978, when several Taurids brighter than magnitude 0 were seen [*The Astronomer* **16,** 163 (1979)].

A very useful detection of the swarm at its pre-perihelion encounter with the Earth, obtained by a completely different method from visual meteor observations, is apparently provided by results of Frank *et al.* (1987), who found "atmospheric holes", or temporary localised decreases in the Earth's ultra-violet dayglow emissions as seen by satellite. For discussion of the physical cause see Section 1.1.3, and Steel & Clube (1991), who also address various important considerations relating to radar meteor detections, not discussed by Frank *et al.*. To demonstrate an extraterrestrial origin for the phenomenon, Frank *et al.* presented the occurrence rate from 1 November 1981 until 21 January 1982 and compared it to radar meteor rates. Extremely noticeable was a major decline in the atmospheric hole rate between about 8 and 12 November. Frank *et al.* interpret it as corresponding to the sporadic meteor rate and say that the hole rate is not correlated with shower meteor rates. Yet their plot does seem to provide a little evidence for a small increase during showers, and in the context of the meteoroidal swarm we are postulating, the fact that the time of enhancement of the atmospheric holes corresponds so closely to the time of the Dutch fireball swarm observation in 1951 is certainly suggestive of a connection between the two.

For reference, we give the area of the Earth to which the hole counts refer; the three-month period was chosen because the satellite was able to image the same area continuously. The area is bounded by ecliptic latitudes 30 and 90° and longitudes (measured from the Sun) 285 and 315°. Meteors from a Taurid radiant would have passed over the top of the Earth and been observable there.

3.2.2 The 7:2 resonance as an explanation

Brecher (1984) invoked a swarm in an Encke-like orbit to explain the lunar event of 1178 reported by Gervase, the Tunguska meteoroid of 1908 and the lunar impacts of 1975 (these events all occurring in late June), showing that a mean orbital period of 3.349 yr gives an extremely good fit to these three dates, with the next exact commensurability of swarm with Earth being in June 2042. The actual size of variations in period due to Jovian perturbations is not mentioned; also there is a presumption that the swarm's range in anomaly is small so that actual encounters with the Earth are rare, but in fact given the figure of $\sim$0.1 AU for the swarm's width, a much larger range in anomaly is to be expected. Clube & Asher (1990) found that the period 3.35 yr fitted Tunguska, the 1975 swarm and the 1951 Taurid fireball swarm, and discussed various possible effects of a centrally concentrated swarm of highly friable meteoroids derived from the Taurid core object. They noted that the proposed period was near the 7:2 resonance. The possibility of a resonant mechanism to explain the lunar swarm is mentioned in the paper by Oberst & Nakamura (1991), but the argument leading to a meteoroidal swarm at the heart of the Taurid Complex formed through the mechanism of the 7:2 Jovian resonance appears to be new, as does a detailed description of the spatial properties of such a swarm.

On the assumption that a resonant swarm has not formed only in the last few centuries (in which case meteoroids would concentrate towards the parent object), the swarm centre, as measured by spatial density of meteoroids, is at the resonance centre. To calculate the position of the resonance centre we need to have a value of the longitude of perihelion ϖ (Section 3.1). There will be a non-zero (though small) range of ϖ within the swarm, but we can use a central representative value. The central date of the swarm passage as calculated from lunar observations by Oberst & Nakamura (1991) is sensitive to the orientation of the Moon. However, a comparison with the VLF propagation data of Kaufmann *et al.* (1989) suggests that we may reasonably take 23 June 1975 as the central point in the cross-section of the swarm. The Dutch meteor and satellite ultra-violet observations suggest that roughly 4 November is the central point at the other intersection with the Earth. As well as defining an average eccentricity of around 0.845, these two dates lead us to adopt $\varpi = 156.5°$. An error of 1° would cause an error in calculated mean anomalies below of about $3\frac{1}{2}°$, for the 7:2 resonance. We have been considering longitudes of the central date of the swarm; we note that the width of the swarm is also an important observational constraint and shall return to it when modelling

the swarm.

Using $\varpi = 156.5°$, we may calculate displacements in mean anomaly M of the resonance centre from the Earth-Moon system at the times of the 3 main swarm detections; see Table 3.3, where ΔM is also listed for other swarm encounters that may be of interest (*e.g.* some relating to the lunar seismic experiment). The three

Encounter with Earth Moon system	ΔM
Mid-1975 lunar swarm	0°
Late-1951 Taurid fireball swarm	+35°
Late-1981 meteoroid swarm	–20°
1988 Taurids	+5°
1974 Taurids	–45°
1971 Taurids	0°
1954 Taurids	–5°
June 1972 lunar encounter	+40°
June 1992 encounter	+5°

Table 3.3: Mean anomaly displacements of resonance centre from point of encounter with Earth.

ΔM fits are good; in Section 3.2.3 we shall model the expected M distribution of the swarm. We note that for the 7:2 resonance there are two resonant zones, each covering half the orbit, so these good fits mean that fits for the other resonance centre would be bad (ΔM near 180°).

In Table 3.4 values of ΔM are shown for other resonances within the range of Taurids; fits are shown for all 3 resonance centres for 10:3 and 11:3. The 3:1

Date	3:1	4:1	$10{:}3^{(1)}$	$10{:}3^{(2)}$	$10{:}3^{(3)}$	$11{:}3^{(1)}$	$11{:}3^{(2)}$	$11{:}3^{(3)}$
Mid-1975	+75°	+105°	–35°	+85°	–155°	–25°	+95°	–145°
Late-1951	+110°	+140°	+120°	–120°	0°	–110°	+10°	+130°
Late-1981	–40°	–175°	–85°	+35°	+155°	–10°	+110°	–130°

Table 3.4: ΔM values for other possible resonances; *cf.* Table 3.3.

and 4:1 would have the advantage of being stronger resonances, so that it would be more difficult for particles to be perturbed out of them, but the resonant zone extends around the whole orbit and swarm meteoroids may be expected to occupy a significant fraction of this. For 10:3 and 11:3, in contrast, meteoroids could concentrate within <120° of the orbit (probably rather less than 120°, if there is similar behaviour to the M distributions we shall model for the 7:2), but they may get perturbed into non-resonant orbits on timescales that are too short. It may be that 7:2 represents the best compromise, though the timings of the terrestrial encounters

and not this handwavy argument are of course the main reason for favouring 7:2.

To explain why some phenomena have been observed in some years only, one must invoke a meteoroidal swarm. An alternative to a resonant swarm is a recent fragmentation (it must be recent or else the fragments will have spread out in mean anomaly). Obviously the immediate spread of the swarm at the actual point of fragmentation is zero, but provided that the fragmentation is violent enough (*i.e.* ejection velocities are large enough), it is possible that the width of the swarm where it crosses the Earth's orbit can be ∼0.1 AU. However, the formation of a swarm covering a restricted part of the orbit is a natural consequence of the parent body moving in a reasonably strong mean motion resonance, and the resonant explanation has the power to predict years of interaction with the Earth. Thus the timing of the various Taurid Complex detections, while not providing direct evidence against the recent fragmentation hypothesis, is a strong reason to favour the mechanism of the 7:2 resonance. In the later sections of this chapter we look for further reasons to believe that the Taurid parent object is in the 7:2 resonance (in particular in the Encke dust trail discovered by IRAS), but at this stage we attempt to deduce the swarm's existence from swarm observations alone, and not from possible detections of the parent object.

3.2.3 Computer modelling of swarm

Meteoroids librating in the 7:2 resonance will have various amplitudes and phases. The first purpose of this swarm modelling is to see the overall distribution in mean anomaly M produced by an ensemble of particles with these different amplitudes and phases. Precession rate is strongly correlated with amplitude (Section 3.1.1) and the second purpose of the modelling is to see how large a spread in the swarm's cross-section occurs over several kyr as a result of the differential precession.

All meteoroids in the 7:2 resonance with Jupiter have their semi-major axis a within a range of about 2.23–2.28 AU. When we model the swarm, we clearly do not want meteoroids to have a-values immediately after ejection covering a range hugely greater than this. For the ejection velocities that give a within this range, the variations in other elements — in particular M, or equivalently the critical argument σ — will be small. Now, the instantaneous values (a, σ) define the amplitude and phase of the libration (Section 3.1.1). Thus at a single instant of ejection the only significant difference in orbital elements of ejected particles is that in a. We sample the whole possible range in σ also (provided that the parent object itself has a large amplitude) if ejection occurs over the timescale for the parent to oscillate through

all values of σ (a few 10^2 yr).

Rather than generating ejection velocities and calculating orbital elements from them, we shall set perihelion distance q and angular elements i, Ω, ω equal to the values of the parent object at a particular epoch and generate ranges of a and M directly. Thus we assume that the ejection velocities are whatever gives the appropriate range in a, *e.g.* if ejection takes place at perihelion, relative velocities of $\sim$50 m/s are sufficient to cover all resonant values. We also assume that ejection occurs over a timescale that is long enough (*i.e.* not instantaneously) that the range in M-values is permitted, but short enough that it is acceptable to use constant values of q, i, Ω, ω. To allow for ejection over several kyr, during which q, i, Ω, ω will change significantly, we use a new epoch of ejection, with updated elements for the parent object, every 2 kyr.

The results presented here were obtained using an integration accuracy of $\varepsilon = 10^{-9}$ (Section 2.1.1) and Jupiter, Earth and Venus following approximate Kepler motion and with their elements updated every 500 yr (Section 2.1.2). An earlier set of integrations had been done using Jupiter, Saturn and all 4 inner planets and $\varepsilon = 10^{-8}$ with very similar results; thus the additional rate at which particles are removed from the resonance because of either integration error (*i.e.* the orbit not being calculated accurately enough) or the presence of Mercury and Mars is very small.

As discussed above, orbital elements for the parent object were required over the timescale being integrated. The parent was chosen to lie in the IRAS trail; see Section 3.3, where the question of whether it genuinely is located there will be addressed. Here we shall indicate which aspects of the results are dependent on the choice of parent. Various trail orbits were integrated back in time, and one that remained resonant for over 16 kyr was selected. This had $a = 2.255$ AU, $M = 213°$ and other elements equal to Comet Encke's at the time of the IRAS observation. Its past behaviour of a is shown in Figure 3.13.

In one model for which results will be presented here, particles are ejected at various epochs (multiples of 2 kyr in the past, up to 16 kyr BP; BP = before the present day) to fill the resonance, *i.e.* to have all possible (a, M) values. Thus at each epoch we use a from 2.230 to 2.280, spaced by 0.005 AU, and M, measured relative to the resonance centre, from –75 to 75, spaced by 15°. As the particles are integrated forward in time to the present day, their a-value is checked periodically and the integration is stopped if a is either above or below the resonant value for more than 300 yr continuously, because we only wish to consider resonant particles

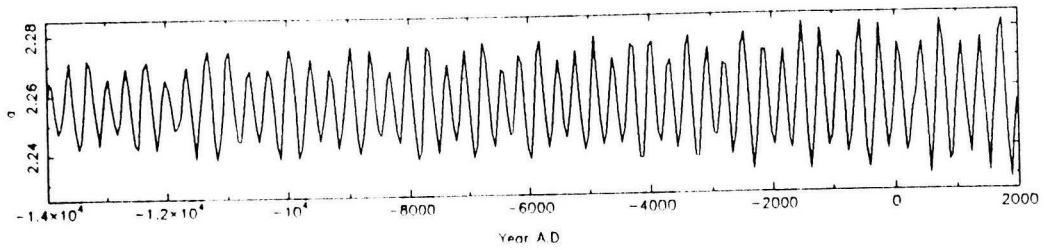

Figure 3.13: Evolution of a over the past 16 kyr for the orbit used as the parent object for the swarm modelling.

rather than those that are dispersed into the background Taurid Complex.

What if rather than filling the resonance, ejection has concentrated orbits near that of the parent? If the starting elements are all exceedingly close to the parent then it will be a long time before the particles have spread out to be centred on the resonance centre rather than on the parent. If at the present day orbits still cluster near the parent, this rather defeats the point of considering a resonant model since the observations cannot relate to the resonance centre. Nevertheless, it proves instructive to perform integrations for a second model as follows, in order to see the timescale on which the swarm eventually spreads out in mean anomaly. We use the same epochs as in the first model (16 to 2 kyr BP spaced by 2 kyr) and at each epoch, a from 2.250 to 2.262 spaced by 0.002 AU and M (relative to the resonance centre) from –15 to 15 spaced by 5°. This would basically imply firstly that the parent is moving with a low-amplitude libration (though for simplicity we take q, i, Ω, ω from the parent in the first model) and secondly that the ejection velocities are quite low. Nearly as many orbits end up being integrated as in the first model since in the first model about half the (a, M) values correspond to orbits that are immediately not resonant (as can be roughly determined from Section 3.1.1).

Figure 3.14 illustrates the tendency for the libration amplitudes to increase in the second model. The evolution of the critical argument σ is plotted for the 49 particles ejected 12 kyr BP. At the time of ejection the highest libration amplitudes are $\sim\frac{1}{3}$ of the maximum, so that all particles must be within $\sim$30° of the resonance centre. As time passes, higher amplitudes become possible owing to the presence of the Earth and Venus. The sharpest amplitude changes tend to happen during epochs when the precessing orbit crosses the Earth's and Venus' orbit.

We shall discuss first the resultant mean anomaly distributions of the models, and then the cross-sectional distributions. Figure 3.15 shows the evolution of M for the first model. Meteoroids were generated every 2 kyr, leading to the overall increase in the number of particles, though particles were gradually lost from the

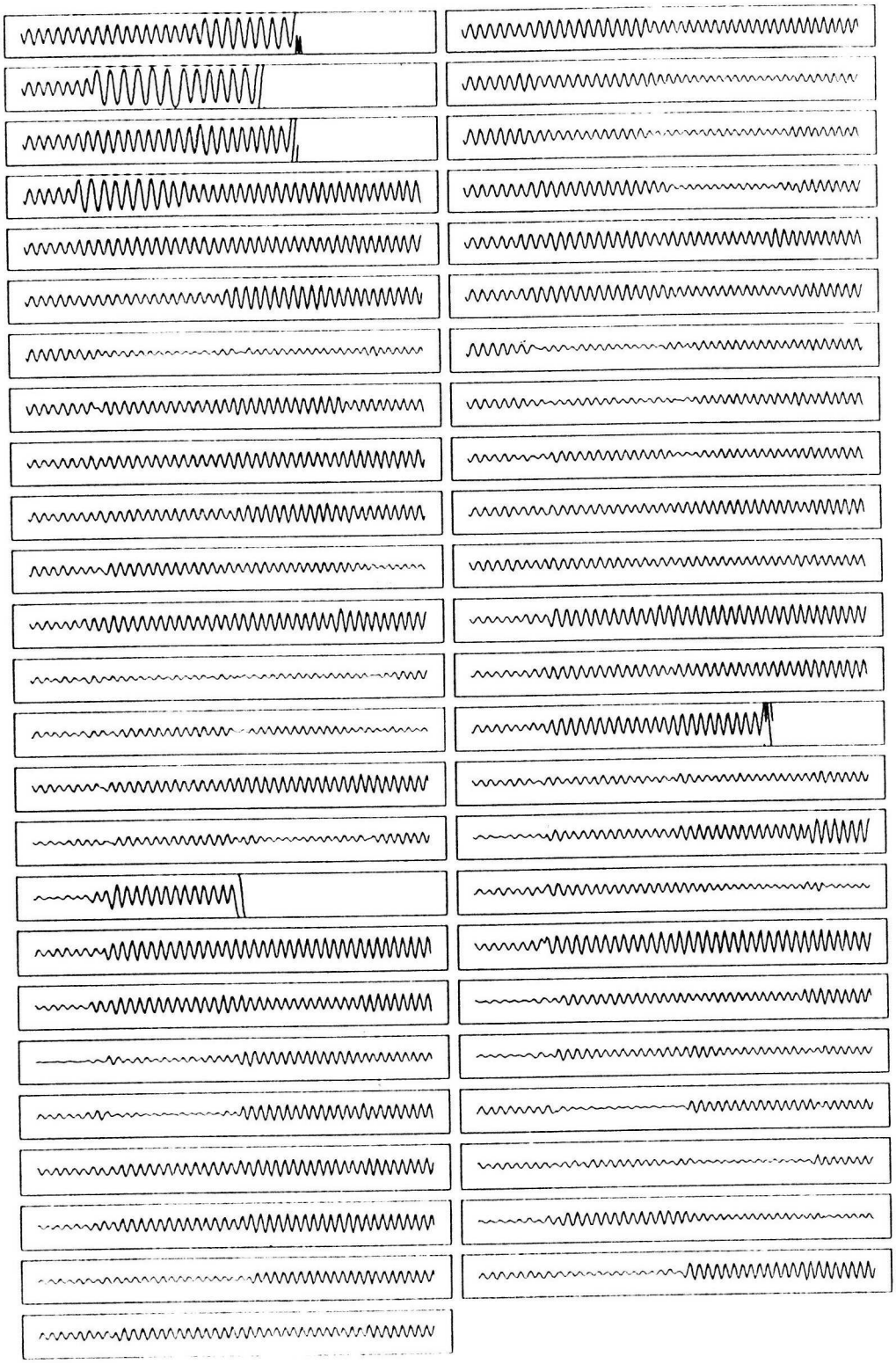

Figure 3.14: Evolution of σ (defined in Section 3.1.1) until the present day for particles ejected near the resonance centre 12 kyr BP.

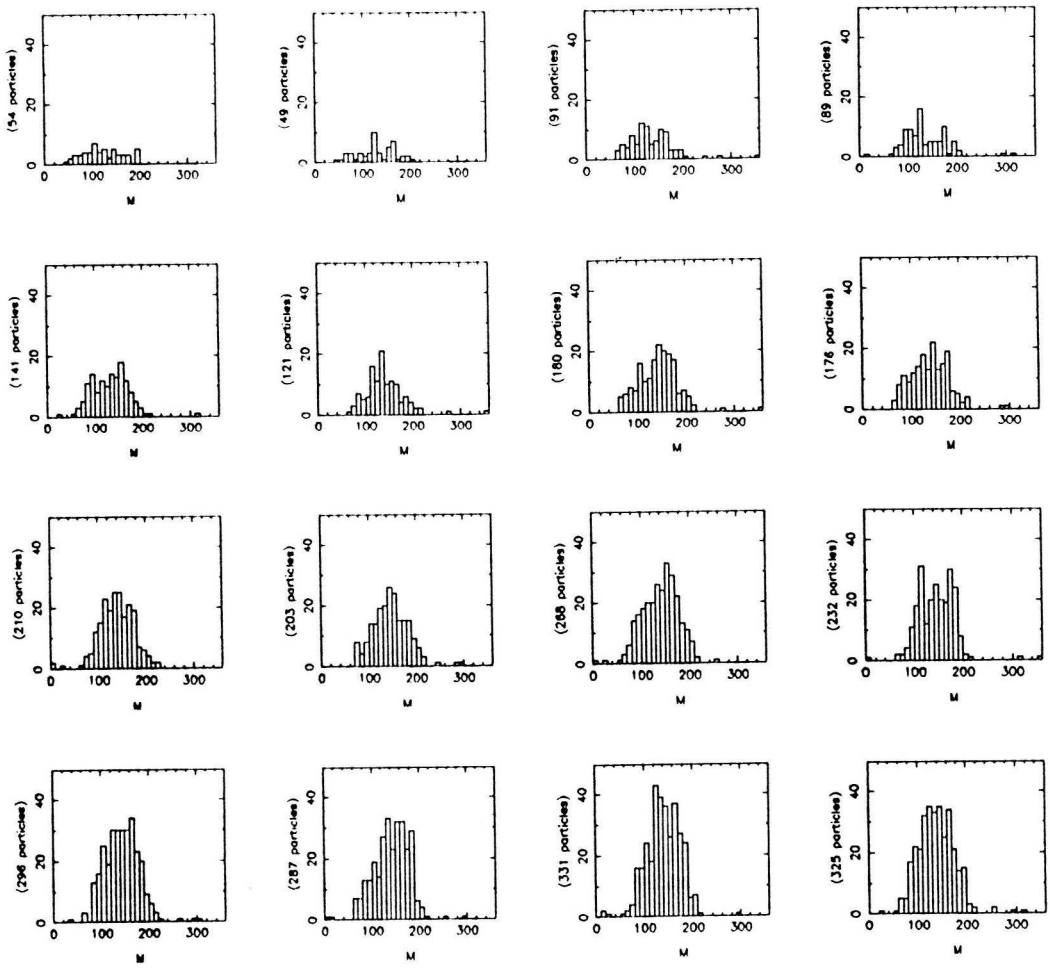

Figure 3.15: Mean anomaly distributions at intervals of 1 kyr from 15 kyr BP to the present day (1st row is 15, 14, 13, 12 kyr BP, *etc.*) for the model where particles are generated to fill the resonance every 2 kyr.

resonance under the perturbing influence of the Earth and Venus (see later). The early plots show quite a flat distribution over most of the resonant zone (which has a range of 180° in M). As time progresses and a smaller proportion of the particles are those generated recently, the tails of the distribution tend to disappear and we have perhaps 80–90% of the particles within the central 90° in M. This therefore represents a sort of equilibrium state which is not quite represented by the initial distribution which fills the resonance. The meaning of the "equilibrium state" is that under inner planet perturbations there is a long-term distribution of libration amplitudes (with phases well mixed), implying a long-term distribution in M.

The equivalent M-plot for the second model is shown in Figure 3.16. There is a gradual spreading out of particles but by the present day they are still more concentrated than in the first model. This is probably because when ejected particles

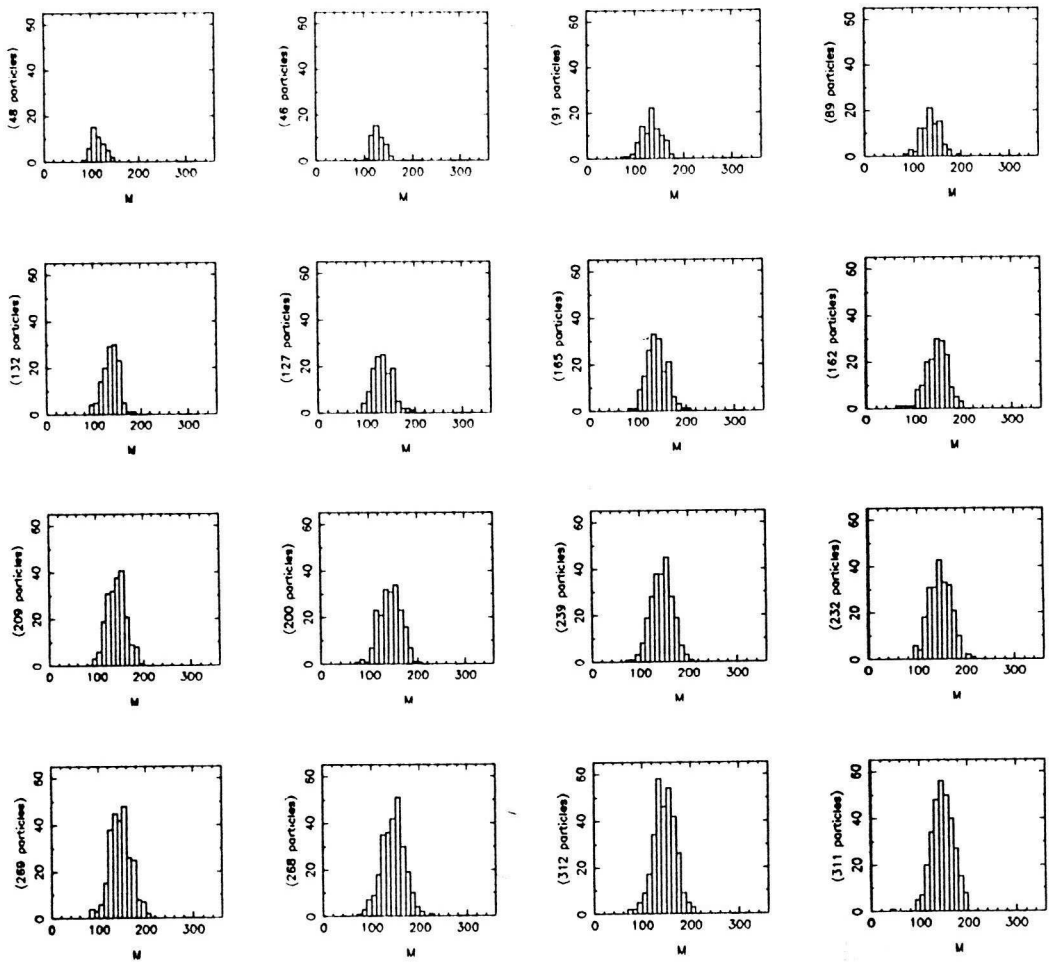

Figure 3.16: Mean anomaly distributions at intervals of 1 kyr from 15 kyr BP to the present day (1st row is 15, 14, 13, 12 kyr BP, *etc.*) for the model where particles are generated to be near the resonance centre every 2 kyr.

are quite so concentrated towards the resonance centre, this represents a state that is very different from the equilibrium state, in the sense that the timescale for the perturbations of Earth and Venus to cause the equilibrium state to be reached is quite long. The fact that there nevertheless is a tendency towards the equilibrium is illustrated by Figure 3.17 where particles generated from 10–2 kyr BP are omitted and so only those generated from 16–12 kyr BP are included. At the present day there is clearly much less of a peak than in Figure 3.16, now that the particles that have not had enough time to reach the equilibrium state have been excluded. The present-day distribution is very similar to the equivalent one generated from the first model, *i.e.* where only particles generated from 16–12 kyr BP are included (Figure 3.18). It appears that the evolution of the M distribution in an equilibrium state, *i.e.* with no new particles generated, is characterised by an unchanging shape, with

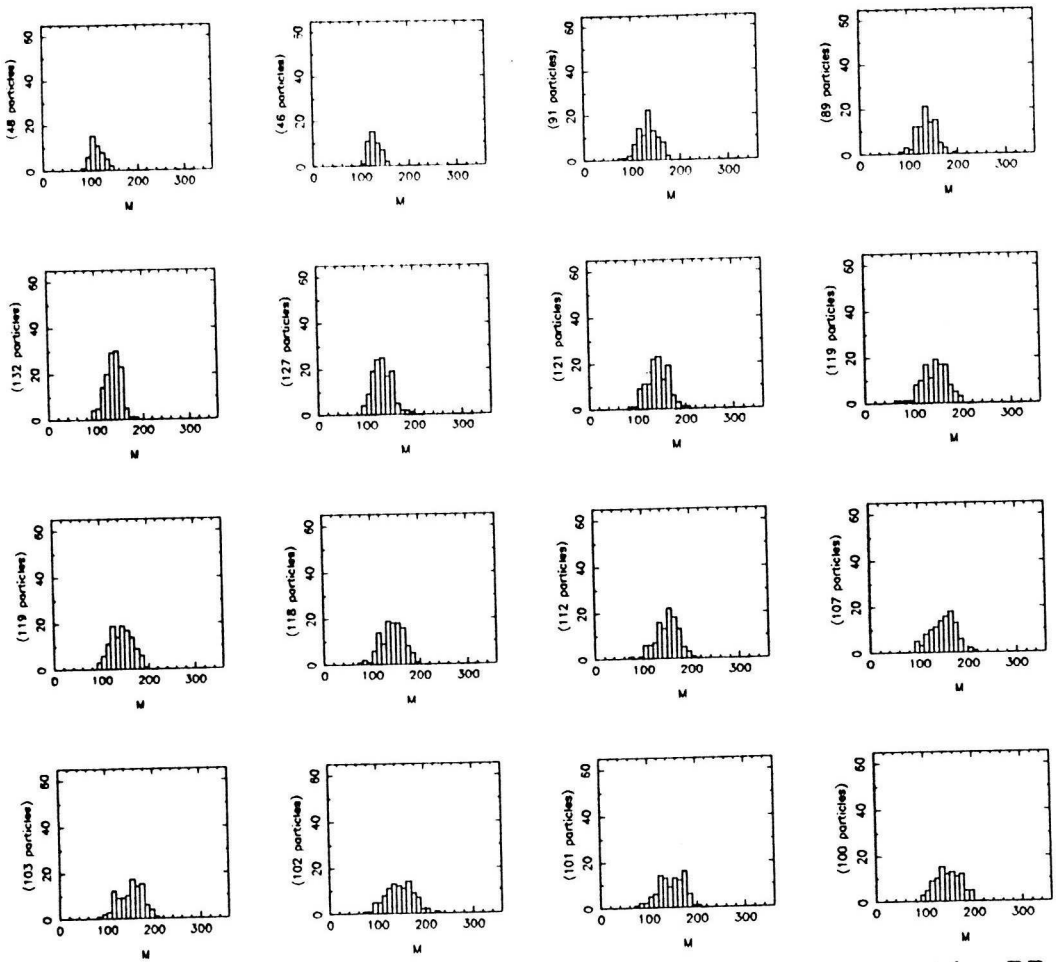

Figure 3.17: Mean anomaly distributions at intervals of 1 kyr from 15 kyr BP to the present day (1st row is 15, 14, 13, 12 kyr BP, *etc.*), including only particles generated from 16–12 kyr BP from the model where particles are generated to be near the resonance centre every 2 kyr.

only a gradual reduction in the total number as particles are lost from the resonance.

It can take ∼10 kyr for approximate equilibrium to be reached, from certain distributions, such as the one with particles heavily concentrated towards the resonance centre, so that we need not necessarily expect the resonant swarm to be exactly in the equilibrium state, given that it is possible that the timescale of formation of the swarm is under 10 kyr. We cannot be sure if there is currently an equilibrium state as we do not know the precise orbital history of the parent object. In theory, a detailed knowledge of the swarm structure could shed light on the history of the parent, but further observations would probably be needed to pursue this line to maximum benefit. We point out that a high-amplitude librator such as that considered in Sections 3.3 and 3.4 could only give rise to the second model if it had had a

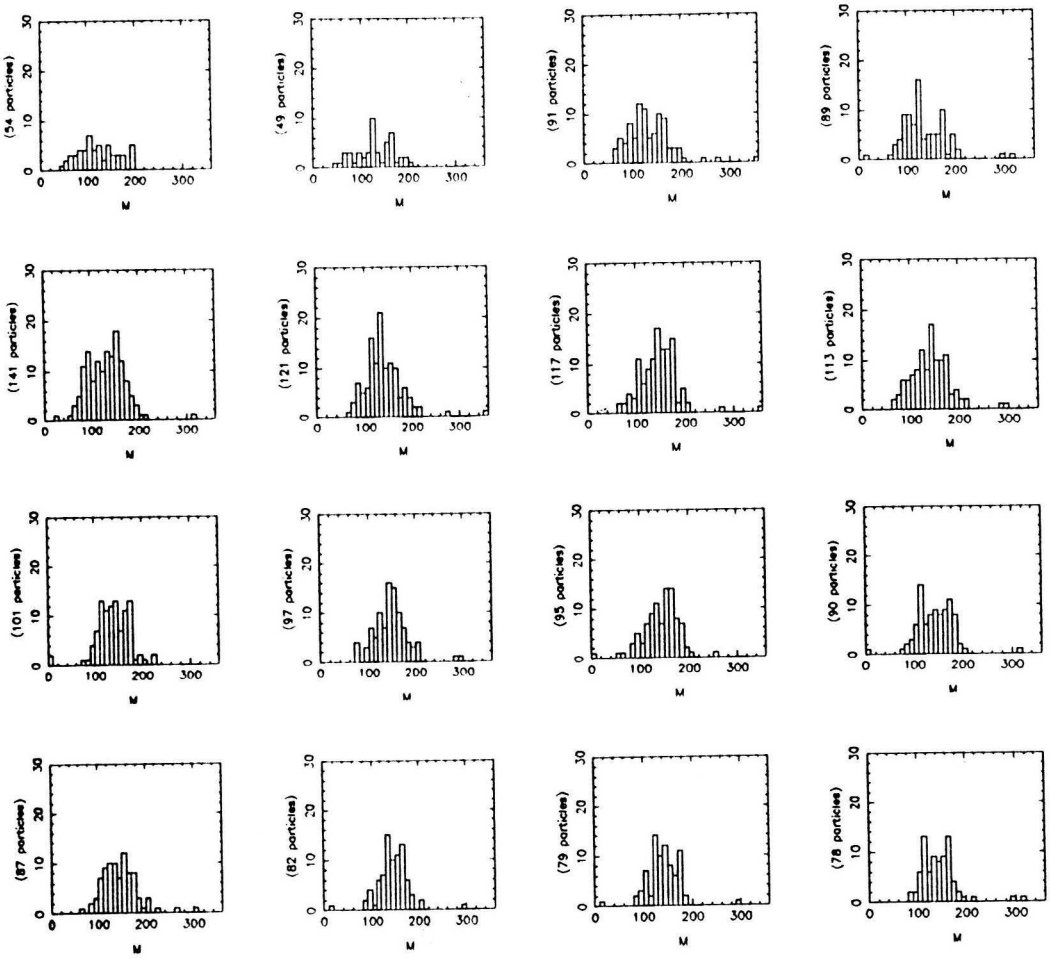

Figure 3.18: Mean anomaly distributions at intervals of 1 kyr from 15 kyr BP to the present day (1st row is 15, 14, 13, 12 kyr BP, *etc.*), including only particles generated from 16–12 kyr BP from the model where particles are generated to fill the resonance every 2 kyr.

much lower amplitude in the past.

At any rate, on the grounds that an equilibrium state is reached eventually and that it is in some sense more similar to a greater family of distributions, we shall now assume equilibrium and compare it to observations. For this purpose we shall add together the particles in the last plots in Figures 3.17 and 3.18. In Figure 3.19 the 178 particles turn out to have an average longitude of perihelion ϖ of $\sim$156.5°, which leads to the resonance centre in Figure 3.19 being at $M \approx 142°$ (the date being 1983.48). On this scale of M, the 1975 lunar swarm is at $M = 142°$, the 1951 bright Taurid meteors at 107° and the 1981 dayglow detections at 162°. The most significant constraint on the model would seem to be that the 1972 lunar encounter, when no large swarm was detected, lies only 7° to the left of the 1951

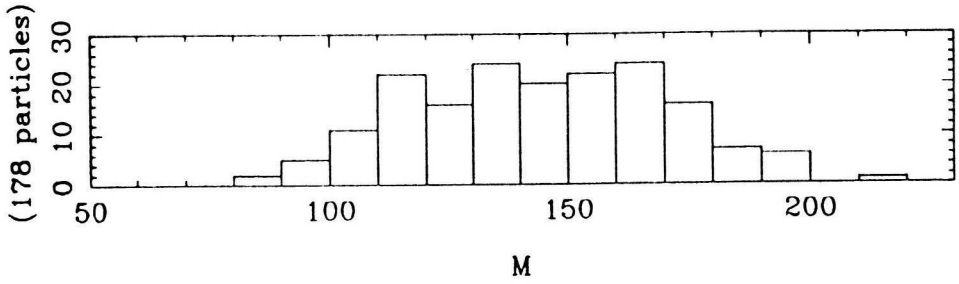

Figure 3.19: The swarm's present day M distribution, assuming it has reached an equilibrum state. (2 of the 178 particles are off the ends of the scale.)

Taurid observation (and this differential remains even if there were a different value of ϖ). This need not render the model impossible since it seems that if we were to draw a smooth curve through the M distribution then the curve may decrease quite a bit between 107 and 100°. Essentially, then, an M distribution starting to fall off significantly at around $\pm 30°$ of the resonance centre both fits the observations and comes naturally out of the model.

We turn now to the cross-sectional distribution. Heliocentric ecliptic latitude plotted against longitude when each particle is at a heliocentric distance $r = 1$ is shown in Figures 3.20 and 3.21 for the pre-perihelion (night-time) and post-perihelion (daytime) intersections with the Earth respectively. At times during the first few kyr when the swarm crosses the ecliptic, the swarm width is only a few degrees, but after $\sim$10 kyr a width of $\sim$10°, corresponding to a crossing time of 10 days, is achieved.

For comparison, Figure 3.22 shows the post-perihelion cross-section for the second model (particles generated near resonance centre), including only particles generated from 16–12 kyr BP. We see that a width corresponding to a crossing time of, say, a week can be achieved in $\sim$10 kyr even though the particles are on much more similar orbits when ejected. This demonstrates the effectiveness of the combined mechanism of, firstly, the Earth and Venus perturbing particles into different amplitude librations and, secondly, the differing precession of ω and ϖ due to Jupiter when particles have different libration amplitudes.

The swarm width is broadly reproducible by the modelling. As regards the actual longitudes, from the dates considered in Section 3.2.2, we expect the daytime intersection to be at longitudes $\sim$265–275° and night-time at $\sim$40–50°. In Figure 3.20 the longitude of the model particles is $\sim$10° too small and in Figure 3.21 $\sim$10° too large. We happen to have ϖ correct but e a little too large. Noting that ejected particles' initial elements depended on those of the parent at the time, this means

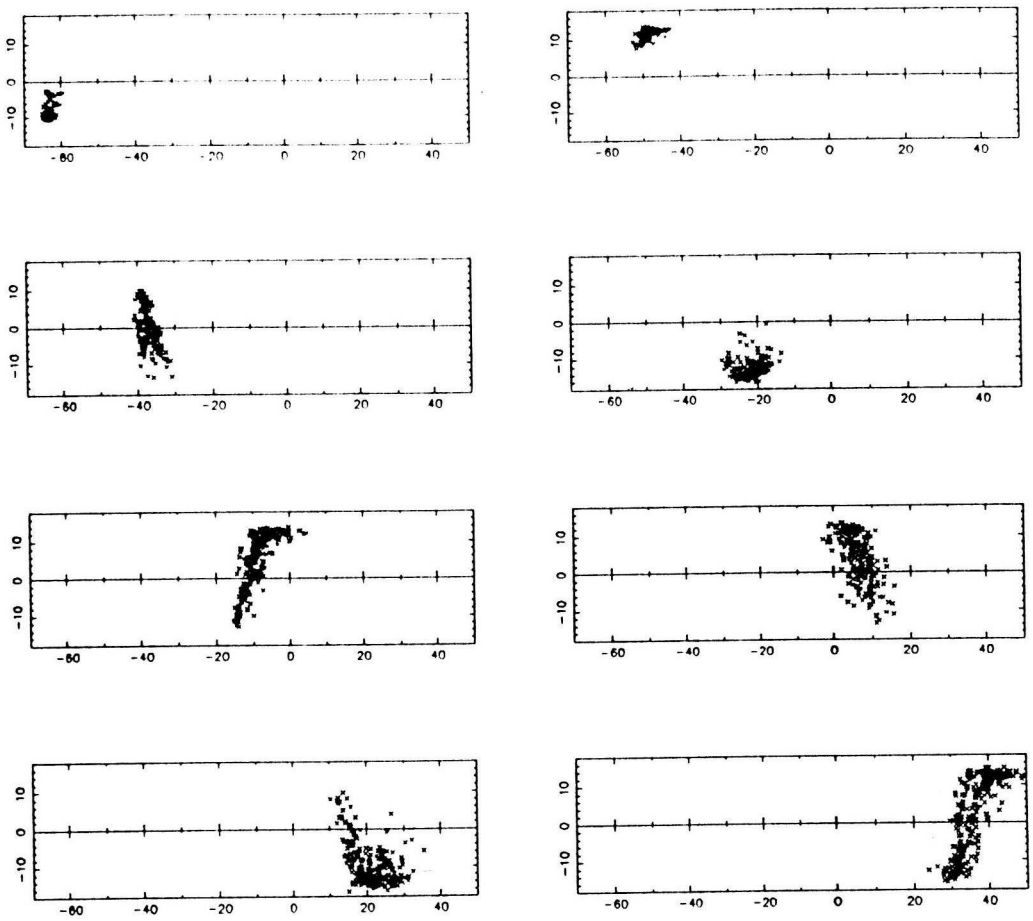

Figure 3.20: Swarm cross section at r=1, pre-perihelion, at intervals of 2 kyr from 14 kyr BP to the present day (1st row is 14, 12 kyr BP, *etc.*) for the model where particles are generated to fill the resonance every 2 kyr.

that the genuine parent's orbit has evolved differently from the way it has been modelled for at least some of the time over which integrations have been done. The adjustment would be a fine tuning of the results which would allow an excellent fit to the observations. The swarm M distribution and cross-sectional dispersion can be reasonably expected to be very similar if we repeated the modelling using a parent with a slightly modified orbital history.

At the present day, the parent object we have used has angular elements equal to those of Comet Encke, so that it is above the ecliptic at r=1 pre-perihelion and below at at r=1 post-perihelion. Particles can be seen to concentrate near the parent to some extent in Figures 3.20 and 3.21. As the parent has tended to have quite a high amplitude libration, most of the particles that are not concentrated near it are behind rather than ahead of it in precession. The maximum amount of differential precession that has occurred is just over half a revolution in ω. In the

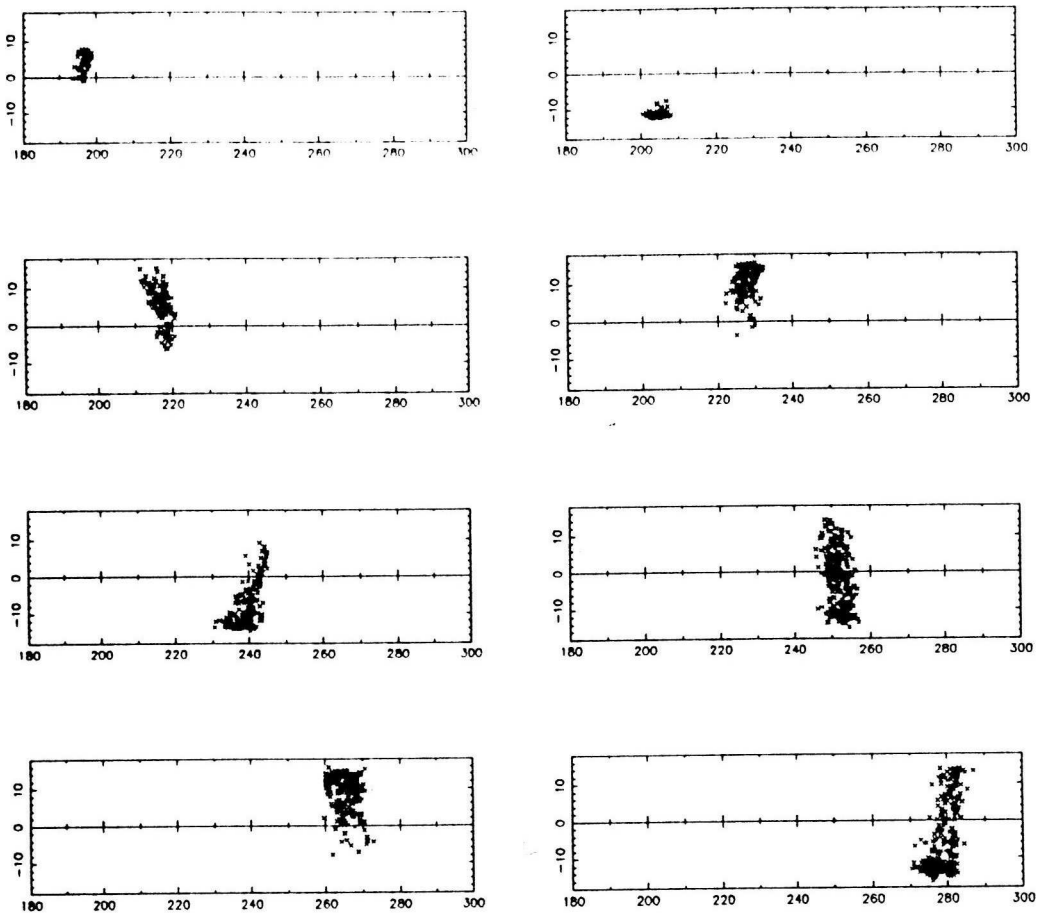

Figure 3.21: Swarm cross-section at r=1, post-perihelion, at intervals of 2 kyr from 14 kyr BP to the present day (1st row is 14, 12 kyr BP, *etc.*) for the model where particles are generated to fill the resonance every 2 kyr.

Taurid Complex as a whole (Chapter 4) the spread in ω is greater than this, but there is a much wider range in a. The reason significant differential precession can occur with a only in the range 2.23–2.28 is because the 7:2 resonance is quite strong.

At either intersection with the Earth, meteoroids crossing the ecliptic can be at either their ascending or descending node (corresponding to radiants south and north of the ecliptic respectively; see discussion of Taurid branches in Chapter 4). The fact that differential precession in ω is only a little over half a revolution means that only occasionally in Figure 3.20 and, as it happens, at none of the instants sampled in figure 3.21 are both kinds of radiant present simultaneously, and then not at the same longitudes. Therefore unless the timescale of formation of a resonant swarm were ∼30 kyr — and then it would be much more spread out in longitude, even neglecting the problem that most particles would be lost from the resonance due to inner planet perturbations — we should not expect significant numbers of swarm

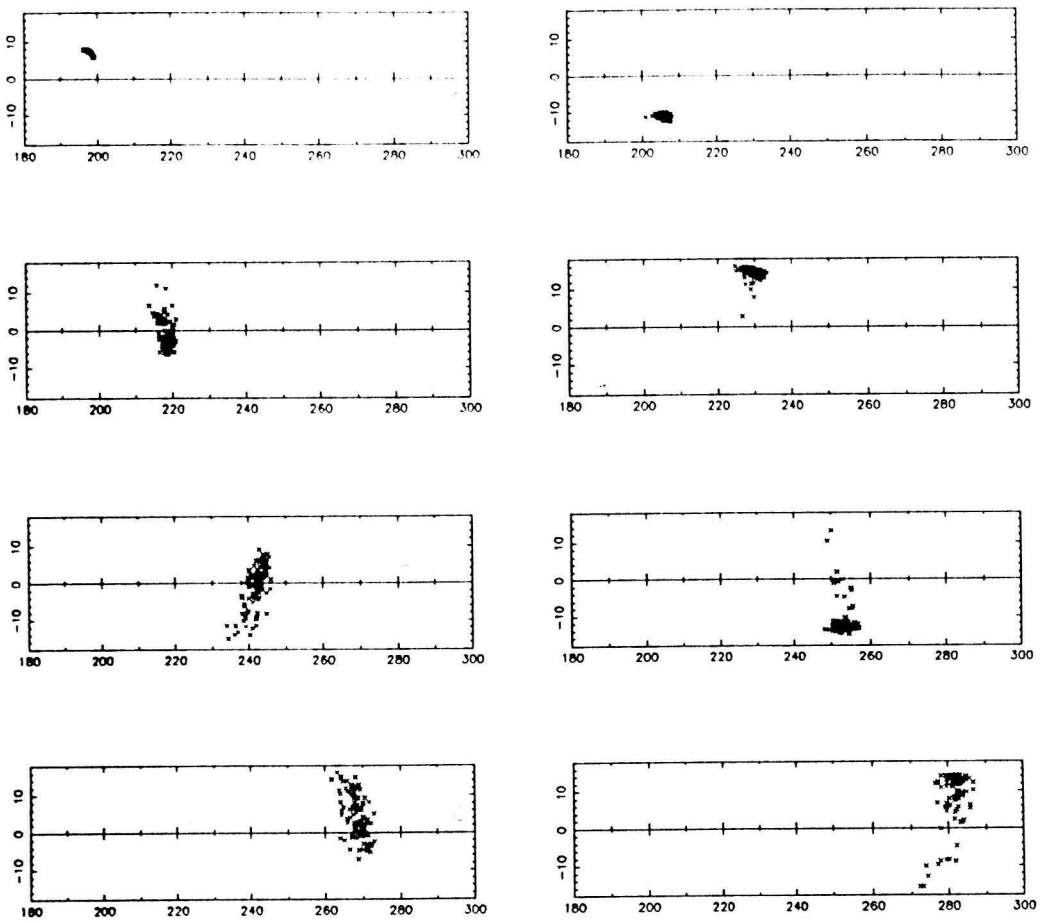

Figure 3.22: Swarm cross-section at r=1, post-perihelion, at intervals of 14 kyr from 2 kyr BP to the present day (1st row is 14, 12 kyr BP, *etc.*), including only particles generated from 16–12 kyr BP from the model where particles are generated to be near the resonance centre every 2 kyr.

particles at both radiants. The fact that most particles are falling behind the parent in precession means that, though this cannot be seen immediately from the Figures, the above models have produced a northern branch at the daytime intersection and a southern branch at the night-time intersection at the present epoch. From the observations (Section 3.2.1) we conclude tentatively that the opposite is the case. If future observations confirmed this then, again, refinement of the model would be needed using a parent that had at least some of its orbital history different, though this would not affect the broad properties of swarm M distribution and cross-section.

We briefly consider whether the cross-sectional distribution varies at different M-values in the swarm. In Figure 3.23 the particles at the present epoch from the model where ejected particles fill the resonance are divided on the basis of M and plotted at the daytime intersection. We recall that the parent is well below the ecliptic. The particles above the ecliptic are lagging the parent and we see a slight

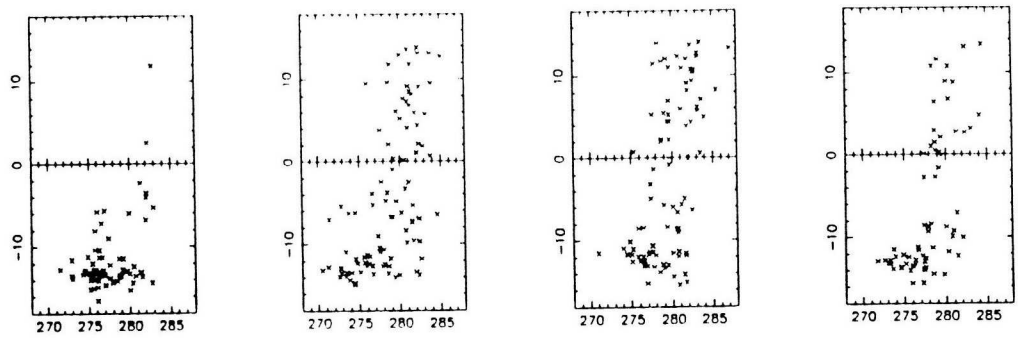

Figure 3.23: Swarm cross-section at r=1, post-perihelion, with the particles from the last plot in Figure 3.21 separated into 4 groups, with ΔM<–30°, –30°<ΔM<0, 0<ΔM<30° and 30°<ΔM, where ΔM is the difference in mean anomaly from the resonance centre.

tendency for those particles to be towards the resonance centre. This is because slow precession is correlated with low libration amplitude. However, there is much variation in the libration amplitude over the millennia and so we expect the effect to be quite small. Though it is reasonably small, this still shows that there can be some detailed structure in the swarm, though at this stage it is probably not worth modelling it with a view to precise comparison with observations as there would really be too may free parameters in the model (*i.e.* a very wide choice of in which epochs the parent had which libration period, and in which epochs ejection occurred and with what velocities).

A check would confirm that loss of particles from the resonance occurs continuously but that the rate is greatly enhanced during times of intersection with the orbits of Earth and Venus; two nodal crossings, (pre- and post-perihelion) with each planet take place within a few centuries followed by a few kyr with no crossing, *e.g.* between 11 and 10 kyr BP in the first model 20 out of 141 particles are lost, and during this time most of the particles move from north to south of the ecliptic at the pre-perihelion intersection and vice versa at post-perihelion. Overall, the loss rate from an equilibrium M distribution is $\sim\frac{1}{3}$ in 10 kyr. Meteoroids that are perturbed out of the resonant swarm will still have a quite near the resonant value and so the differential precession in longitude will not be large. Therefore the meteoroids will continue for some time to cross the Earth's orbit at similar longitudes. Since we detect the swarm in some years but not in others, we certainly believe that larger meteoroids at these longitudes are quite concentrated in mean anomaly, and the above loss rate into orbits with near-resonant a-values seems to provide a good dynamical reason for believing that much of the swarm was formed at some time during the past ∼10 kyr. Also, it is extremely unlikely that the observed concen-

tration in anomaly could occur through meteoroids randomly being perturbed into the resonance; it does seem that their source (the presumed defunct giant comet) is itself in a resonant orbit. Besides, meteoroids perturbed into the resonance would also be perturbed into the other 7:2 resonant zone.

The idea of a dense resonant meteoroidal swarm in the Taurid Complex, through which the complex as a whole is quite possibly fed to a great extent, seems to be quite well supported by this modelling. Mean anomaly and cross-sectional distributions apparently in good agreement with available observational data are both naturally produced by the theory. Significant production of swarm meteoroids ∼10 kyr ago seems to be implied but it is difficult to distinguish between the scenario where meteoroids have been produced continuously since then and that where they were mainly generated at that earlier epoch. In both cases similar dispersion of the swarm would occur. There is probably little to be gained from any further detailed attempts at modelling the evolution of a 7:2 resonant meteoroidal swarm until further confirmation of the theory is forthcoming from observations. For example, an encounter with the swarm is predicted for June 1992 (Table 3.3) during which it may be possible to observe bright meteors using radar methods. Accurate orbital data would be invaluable. One would also want to repeat the experiment in 1993 in the hope of finding fewer detections. It may not yet be possible to distinguish between this model and the comparatively *ad hoc* alternative in which the swarm has a period near 3.35 yr, since the resonant period of 3.39 yr means that the difference in mean anomaly between the two alternatives is only ∼25° since 1975, but given sufficient enthusiasm next century the answer should be obtainable.

3.2.4 Estimation of swarm mass

Finally, we derive an estimate of the mass of the swarm from the lunar observations. Duennebier *et al.* (1976) showed that if the impacts were due to a spherical meteoroid cloud of diameter ∼0.1 AU then the total mass in the cloud of meteoroids with masses between 50 g and 50 kg was 10^{13-14} g; the lower limit of the mass function corresponding to the mass below which a meteoroid would hardly ever be detected by the seismic network and the upper limit being the largest swarm meteoroid detected. The resonant swarm model developed here permits its own calculation of the total swarm mass based on the lunar data. We recognise of course that the conversion of amplitudes of seismic oscillations to masses of impacting meteoroids is a little uncertain.

Taking Duennebier *et al.*'s figure of 1800 kg for the total mass (within the limits

50 g and 50 kg) that landed on the Moon during the meteoroid storm (of which an estimated 320 kg was detected, the smaller meteoroids only being recorded if they landed near one of the seismic instruments) we have a flux of 1800 kg per 10 days over the Moon's cross-sectional area, 4.2×10^{-10} AU^2. From the model swarm cross-section diagrams (*e.g.* Figure 3.21), we may adopt, say, 0.1 AU^2 as the cross-sectional area of the swarm. The apparent radiant is near enough to 90° from the direction of the Earth's apex that we need not allow for the angle of incidence on the Moon. Thus the flux is 1800 kg × 0.1 / 4.2×10^{-10} per 10 days $\approx 5\times10^{14}$ g per 10 days. The duration, ∼10 days, of the storm corresponds to about 3° in mean anomaly. From the model swarm M distribution diagrams (*e.g.* Figure 3.19), we have that, say, $\frac{1}{20}$ of the swarm is in the central 3° in mean anomaly, leading to a swarm mass of 10^{16} g (between meteoroid masses of 50 g and 50 kg alone). We saw in the cross-section diagrams a tendency for meteoroids to concentrate around the parent. The chances are against the parent's orbit at r=1 being very close to the ecliptic at the present epoch (since any single orbit spends most of its time with the argument of perihelion ω near 0 or 180°; Section 2.2.1) and so probably the Earth-Moon system does not currently pass through the densest part of the cross-section. The swarm mass is therefore expected to be several 10^{16} g (from 50 g – 50 kg).

The total mass of the swarm is very sensitive to the mass function. Duennebier *et al.*'s adopted slope of the cumulative mass distribution curve is –1.23 so that the differential mass index (*cf.* Section 4.3) is 2.23, slightly bottom-heavy. If we extrapolated this mass distribution down 3 orders of magnitude to 0.05 g the mass would be multiplied by 5. The resonant swarm is unlikely to extend below this mass as smaller particles are too easily dispersed (*cf.* Section 4.2.3) and observations suggest it may not even extend this low, *e.g.* the swarm meteor observations of 1951 went down to a mass of ∼1 g. Indeed these 1 g meteoroids may themselves be concentrated in much larger objects (*cf.* Bigg & Thompson's (1969) observation of a disintegrating large meteoroid). The question of whether there is a lot of mass in >50 kg objects is also uncertain. The Taurid stream as a whole certainly seems to contain a lot of mass in larger objects (Section 4.3) and although the Tunguska object was almost certainly not a resonant swarm member (Section 3.5), nor are there any known km-sized asteroids in the swarm, these large bodies may be characteristic of swarm members produced. Despite the uncertainties, we may speculate that the swarm mass is as high as 10^{18} g. We note that between 50 g and 50 kg, the figures of Section 4.3 suggest that the mass of the Taurid stream is $<10^{16}$ g so that at these intermediate meteoroid sizes, the swarm dominates the stream.

3.3 Trail formation

3.3.1 Encke dust trail observed by IRAS

The Infra-Red Astronomical Satellite (IRAS) observed most of the sky in broad wavelength bands centred on 12, 25, 60 and 100 μm and discovered about 100 cometary dust trails (Sykes *et al.* 1986a), although only a few were along the orbits of known comets. The brightest was associated with Comet P/Tempel 2, seen near perihelion ($q \approx 1.4$ AU). Possibly the next brightest was along the orbit of Comet P/Encke, seen just after aphelion at 3–4 AU, this heliocentric distance being consistent with the fact that the thermal emission was most clearly detectable at 60μm. The projected angular length as seen from Earth was about 10°, corresponding to ∼2 AU; the trail was first reported as extending from around 16–80° in mean anomaly behind Encke (Sykes *et al.* 1986a), since this was where it was most clearly visible, but Sykes (1988) found a faint extension through Encke to around 20° in front of the comet. At the other end of the trail, it would become difficult to distinguish if it stretched to ∼100° behind the comet as it would start to become confused with the central Solar System dust bands (see Section 5.1). However, on examination of an IRAS picture the trail appears to stop being visible strictly before one reaches the dust band (and corresponding rather sudden change in intensity of the zodiacal emission). The trail intensity thus genuinely appears to decrease very significantly at ∼80° behind Encke rather than becoming obscured by other infra-red emission. The width of the trail as seen from Earth is about 10′.

The orbit of the trail particles is not uniquely determined by the projection of a limited part of the orbit on the sky as seen from Earth, but since it would be unsatisfactory to invoke a coincidence as resulting in the same projection on the sky as the projection of Encke's orbit, we must look for a near-Encke orbit. It is possible to measure the trail on IRAS maps of the sky and compare it with calculated projections to see what is the permitted variation in any one orbital element that is consistent with the observations. Doing this with a picture constructed from IRAS scans made in late June 1983 yields the following maximum deviations (relative to Encke):

$$\Delta a \lesssim 0.1 \quad \Delta e \lesssim 0.03 \quad \Delta i \lesssim 0.2^\circ \quad \Delta\Omega \lesssim 0.5^\circ \quad \Delta\varpi \lesssim 1^\circ$$

Fairly elaborate processing of IRAS images was done by Sykes *et al.* (1990) for the dust trail of Comet P/Tempel 2. Such an analysis for the Encke trail would go beyond what is required for the present purpose, which is to get a broad idea of whether the proposed resonant Taurid parent object, rather than Encke itself,

could have given rise to the trail. There would be too many free parameters in the modelling to make an exceedingly detailed attempt to fit IRAS photometric data worthwhile — the obvious extra free parameter compared to the case of Tempel 2 (or a model with Encke producing dust) is the exact orbit of the comet itself.

3.3.2 Comet Encke as the trail source

Sykes *et al.* (1986b) modelled the formation of IRAS cometary dust trails as due to the two factors ejection velocity and particle size (different sizes of particle being subject to different radiation pressure). The width of the trail sets an upper limit on the (presumed isotropic) ejection velocities. These velocties yield a difference $\Delta a_{\rm ej}$ in semi-major axis. Combined with an a-difference $\Delta a_{\rm rp}$ due to radiation pressure, this difference being taken as a function of particle size only, the rate of increase of mean anomaly deviation from the comet is derived. Thus a size distribution of particles in the trail can be derived, though this is not unique, depending on the timescale over which particles were ejected.

This theory does not predict the particle size distribution; rather it provides a means of determining it. A considerable range of size distributions is permitted by theory, making this model of the trail rather difficult to disprove. On the other hand, when dust is observed along the orbit of a known comet, the comet itself is in a sense the most natural source and in the absence of strong reasons in favour of other ideas, it would be reasonable to accept Sykes *et al.*'s model. Indeed, it could be useful, for example, in constraining over what proportion of the orbit ejection takes place.

This interpretation cannot therefore be excluded, and P/Encke's small perihelion distance is indicative of rapid dust production relative to other comets. Against this, the comparatively small size of Encke's nucleus, the fact that Encke is not a very dusty comet — Newburn & Spinrad (1985) found that the dust to gas ratio fell to $\sim$0.004 inside 1 AU, an order of magnitude below that of any of the other comets they observed — and the observation of the trail at >3 AU from the Sun make the detection of such a bright trail a little surprising, inviting any alternative model that can provide good reasons in support of itself.

3.3.3 An unseen resonant source for the trail

We now address the possibility that the object that has given rise to the IRAS trail is actually within the trail. Given the known existence of Comet Encke and the lack of a direct identification of this hypothetical alternative object, some further

reason for invoking the alternative is required. We consider the idea that the object that has given rise to the resonant meteoroidal swarm is immersed in the dust trail. Thus in the argument being developed, this follows on from the inferred existence of the swarm, without which there would be little justification for pursuing this trail model. In contrast, the swarm's existence was deduced independently of the trail's existence (though the trail model if successful would be a useful confirmation of the swarm model).

Sykes' (1988) analysis of IRAS dust trails distinguished narrow trails associated with known active comets from broad trails with no visible source. Clube & Asher (1990) suggested that the broad trails could be due to the gradual release of material, over longer timescales than those associated with the narrow trails, from clouds of meteoroids and dust gravitationally bound to defunct comets, which may be present in the trails as exceptionally dark asteroids (*i.e.* the stage that comets physically evolve to; Sections 1.2.1, 1.2.2). Clube (1991) noted that the proposed greater age of the broad trails coupled with their restricted length could be due to the source being in resonance with a major planet. Though this line seems quite promising, we do not follow it here because we are seeing if we can demonstrate a direct connection between the Encke trail and the 7:2 resonant swarm, and the trail is not situated around the resonance centre.

Any model of the trail that does not have Comet Encke as the source of the dust must provide a reason for the IRAS observation being closely aligned to Encke's orbit. We suggest here that Encke was ejected from the proposed resonant Taurid progenitor shortly before the former's discovery in 1786 and that the two objects will therefore be on very similar orbits. The question of whether they are similar enough to be consistent with the IRAS observation will be considered below.

On the one hand, then, this model has the merit of explaining Encke's discovery. On the other hand, bringing Encke into the model introduces a useful constraint when selecting parameters for the modelling. The question is whether material ejected at the time of the proposed splitting off of Encke with orbital parameters concentrated around those of the parent can reproduce the IRAS trail.

We therefore try to construct a model of trail formation due to a resonant, librating parent object that is subject to the constraints firstly that it gave rise to the swarm detected on the Moon in 1975 and secondly that Comet Encke separated from it shortly before Encke's discovery. Regarding the Encke discovery, Kronk (1984) defines a favourable northern hemisphere apparition as when perihelion passage occurs from November to February, noting that the first three (independent)

discoveries of Encke, in 1786, 1795 and 1805, were all made at such times. It is simple to calculate that the previous favourable northern hemisphere apparition would have been in late November 1772, when there would have been a reasonable chance of the comet's discovery; several observers were in the habit of searching the sky for comets. The comet has usually been believed to have undergone a gradual decline in brightness over the past two centuries, though Kamél (1991) has suggested that the perceived fading is due to a change in the time of maximum brightness, perhaps caused by precession of the spin axis re-orienting the active parts of the nucleus.

On relating Encke to the resonant source object, we find that Encke entered the 7:2 resonant zone (*i.e.* was 90° behind the resonance centre) during the revolution preceding the 1772 perihelion passage and gradually moved forward, being ∼50° behind the resonance centre at the 1786 discovery apparition. We recall that there are two resonant zones, each covering half the orbit; naturally the one we refer to corresponds to the proposed meteoroid swarm. A position for the source object near the back of the resonance in the late 18th century corresponds well to it being in the IRAS trail, at the front of the resonance, two centuries later, 200 yr being a typical time for a resonant object to move from end to end of the 7:2 resonant zone. Encke's orbital period being below the resonant value, it will in fact already have overtaken the resonant object once (early in the present century). The simultaneous fit of IRAS trail position and origin of Encke may of course be coincidence, but it is encouraging at this stage that the discovery circumstances of Encke should fit when we relate the positions of Encke and the resonance. The model of Kamél (1991) could explain why Encke was generally less easy for northern observers to see during the couple of centuries preceding its discovery (being less well placed for these observers at its time of maximum brightness). However, the IRAS trail model we are considering gives a much more precise prediction of when Encke should have first been discovered.

We introduce the following numerical values, of mean anomalies at the time of IRAS observation, to clarify the picture. The brightest part of the trail, as found by Sykes *et al.* (1986a), is between about M=200 and M=260°, the resonance boundary at about 220° and Encke at about 280°. The exact M values depend on the exact orbital periods, but these figures give a rough idea. We see that the trail has actually extended further into the other resonant zone than the one containing the swarm (M=200–220° corresponding to the front of the resonance). Though the scenario of the source object recently having left the resonance is possible, it would weaken the theory if we had to appeal to this explanation. Thus the parent object of the trail

has $M < 220°$ and so is not located at the centre of the trail, but nearer the back. The key question, then, is whether there is a reason for the apparent asymmetrical spread of the trail.

By allowing ourselves to choose any ejection velocity distribution we wanted, we could guarantee to fit any possible trail observation, but this would be parameter-fiddling of such a level that we could hardly regard the modelling as lending weight to the idea of a resonant parent object in the trail. Therefore let us impose the condition of isotropic ejection velocities, which implies that ΔP, the (small) difference in orbital period from that of the source object, is symmetrically distributed about zero; P is the parameter that will determine the gradual spread in anomaly. As stated above, we wish the source object still to be resonant and so we also have the constraint on the P distribution that the central value (corresponding to the source object) must correspond to a resonant orbit.

With a symmetrical ΔP distribution, can we produce an asymmetrical mean anomaly distribution? The answer is no, for the first few decades, when there is a gradual spread of particles outwards symmetrically from the source object, but the following argument shows how the asymmetry could be possible after a slightly longer timescale, during which the effects of the 7:2 resonance can modulate the behaviour of P to a significant degree. Consider particles ejected when the source object is near the back of the resonant zone and so has $P \approx P_r = \frac{2}{7}P_J$. Some particles will be resonant, some will be non-resonant with $P > P_r$ and some non-resonant with $P < P_r$. As the resonant particles move forward through the swarm, their period decreases and then increases again towards P_r. Thus their average period, over the time during which they move forward through the resonance, is nearer that of the particles that had $P < P_r$, and those particles spread only gradually away from (in front of) the source. The particles that had $P > P_r$ become spread well away from the main part of the trail. The fact that this mechanism for producing asymmetry needs enough time to work is a strong reason for favouring a timescale >100 yr or so in this trail model. Furthermore, a timescale much in excess of 200 yr is excluded as the resonant particles start to move backward through the resonance, having a higher than average period and so starting to separate from the low-period particles much more quickly. Again, the time of origin of Encke is interesting.

To check how this mechanism works in practice, we consider first an example in which Jupiter, but not the inner planets, is included. In Figure 3.24 mean anomaly distributions of particles are plotted at the time of ejection and after approximately 50, 100 and 200 yr, for a simulation involving Jupiter only. All 4 plots are shifted

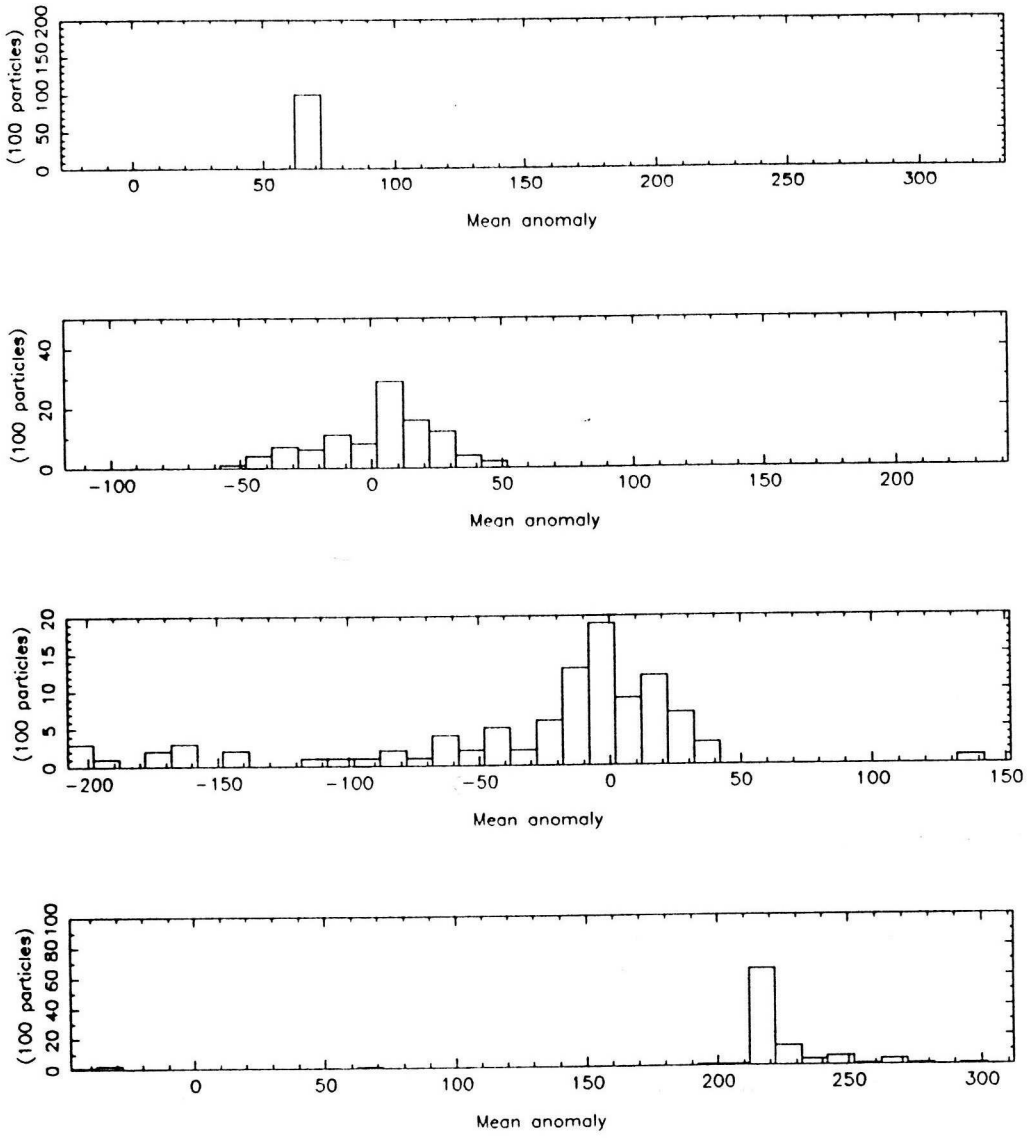

Figure 3.24: Mean anomaly distributions at the time of ejection and after 50, 100 & 200 yr, for a simulation involving Jupiter only.

so that the resonance centre is at the midpoint, the resonance boundaries therefore being at $\pm 90°$ from the central point. The motion of the trail forward through the resonance is clear. In the second plot, the source object has $M \approx 5°$ and particles have spread a similar amount in front of and behind it. In the third plot, the source object has $M \approx 350°$ and particles have spread well behind but less so in front.

In the fourth plot, where the source object has $M \approx 215°$, bunching has occurred as the orbits are mostly near the extreme point of their libration at the front of the resonance. The particles with higher periods have performed almost exactly one revolution less than the others and so have become mixed up with them, but a

check (not shown here) demonstrates that the small diffusion of particles forward of the resonant zone is indeed mainly due to particles that have just gone forward of the resonant zone and not to ones that have fortuitously ended up there having performed one whole orbital revolution less. (In fact the source object's initial period was marginally below the resonant value and so slightly more low-period particles were generated.) It turns out that the effects of Earth and Venus do over 200 yr affect the M distribution by significant amounts compared to the length of the IRAS trail and so we now proceed with a rather fuller investigation including them.

Various possibilities were tried systematically, the important free parameter being the time of ejection (equivalently the position in the resonance, defined by the position of Encke). Permitted dates were roughly 1772–1785. The source object needed its initial P value chosen so that it ended up in the observed trail at the time of the IRAS observation, since although an asymmetry in particle spread was possible, the complete separation of source and trail would not be. Ejection velocites were isotropic (directions randomly generated). There is freedom to choose the exact form of the distribution; both ejection velocities uniformly distributed in one-dimensional velocity space, so that in three-dimensional velocity space orbits would be concentrated near that of the parent, and velocities uniformly distributed in three-dimensional space were tried. The choice between these was found to affect the results only slightly; the more important parameter was the maximum ejection velocity, since this critically affected the extent of the trail 200 yr later. The computer program calculated ejection velocities at perihelion, but this is not significant for this investigation into resultant M distributions 200 yr later — the crucial quantity that affects the M spread for these resonant and near-resonant orbits is the initial range of P, and we could generate this at any point in the orbit simply by choosing a different limiting ejection velocity.

A common problem, illustrated in Figure 3.25, was an excess of particles at $180^\circ \lesssim M \lesssim 200^\circ$, not present in the IRAS trail. This tended to happen when ejection occurred too far inside the resonance (even just 15° being too far), resulting in too many particles with slightly lower libration amplitudes and periods so that they were too far inside the front of the resonant zone in 1983. Reducing this problem by narrowing the ejection velocity range also caused too much of a decrease in the particle density in the front half of the trail.

The best fits were obtained when the starting point was quite near the back of the resonance, *i.e.* at a date before, say, 1776. Figure 3.26 demonstrates such a model. The simulation with Jupiter only displayed in Figure 3.24 in fact used

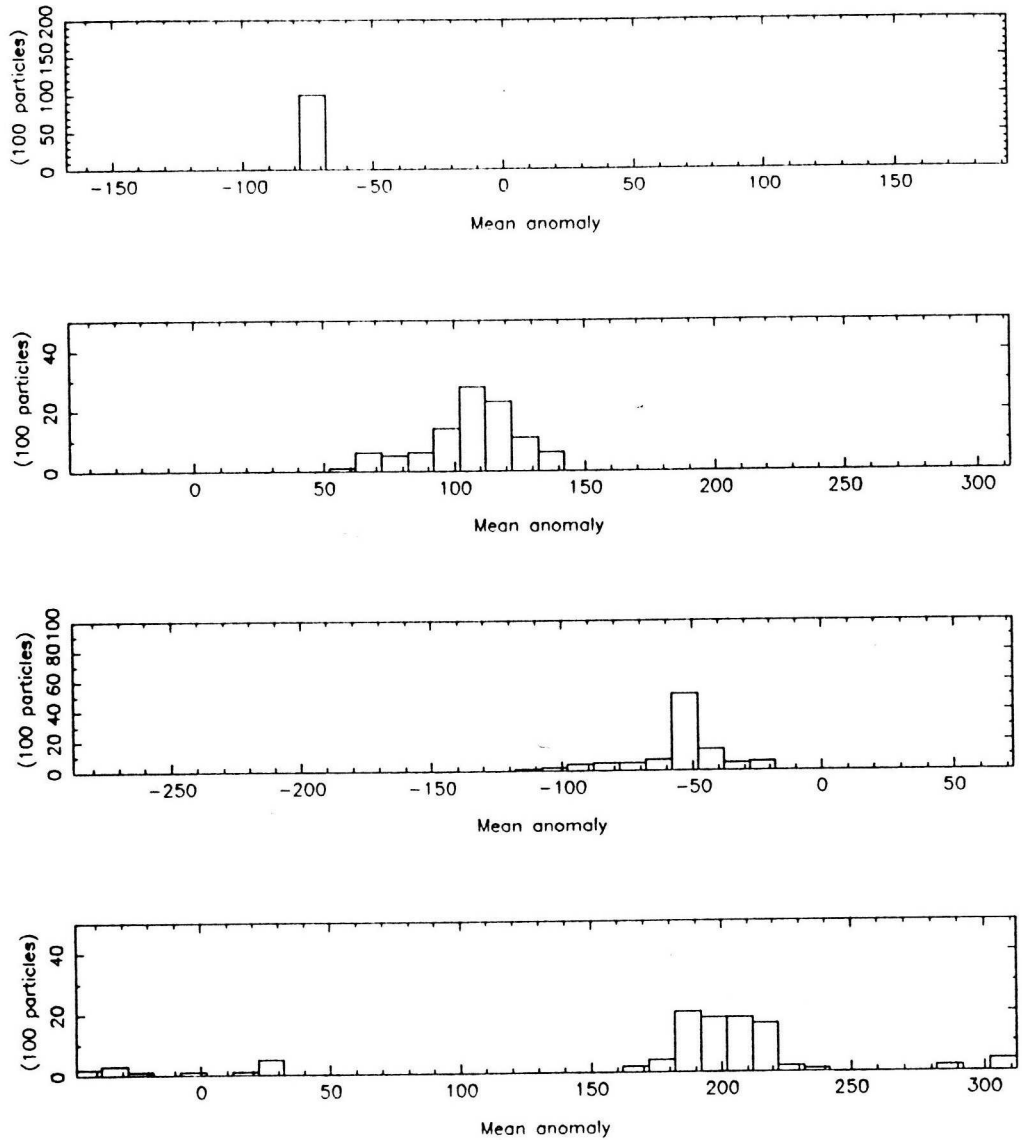

Figure 3.25: Mean anomaly distributions at the time of ejection and after 50, 100 & 200 yr, for a simulation involving Jupiter and the 4 inner planets. At time of ejection, parent has $a = 2.250$ AU and is 15° inside resonant boundary. Isotropic ejection velocities uniformly distributed up to 15 m/s in one-dimensional velocity space.

the same starting elements for the particles, so the effect of the inner planets in spreading out mean anomalies from the very sharp peak near the parent at the front of the resonance in the IRAS trail in 1983 is illustrated.

The fit of the fourth plot in Figure 3.26 to the IRAS observations is quite good, but not perfect — it would be desirable to have a few more particles between $M =$ 240 and 260°. No simulation was much more successful, and all possibilities consistent with the position of Encke at the time were apparently tried. M distributions

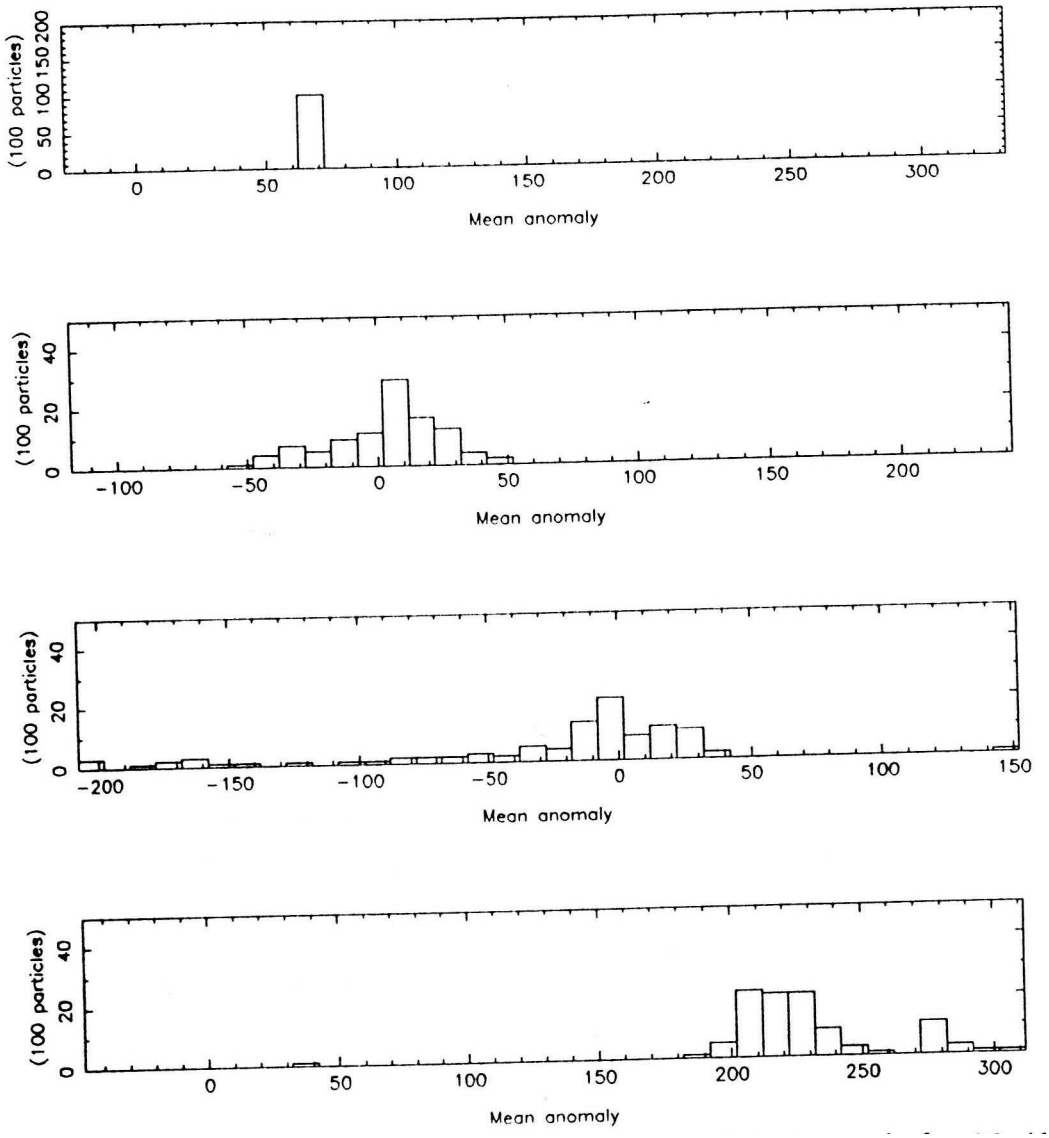

Figure 3.26: Mean anomaly distributions at the time of ejection and after 50, 100 & 200 yr, for a simulation involving Jupiter and the 4 inner planets. At time of ejection, parent has $a = 2.253$ AU and is 7° inside resonant boundary. Isotropic ejection velocities uniformly distributed up to 15 m/s in one-dimensional velocity space.

in the few decades preceding and following 1983 were checked for the general possibility of a more even spread into the 40° forward of the resonant zone while only filling the front 20° of the resonance itself but nothing clearly better was found. Of course, while the extent of the spread in M can be asymmetrical, it is probably not reasonable to expect the total number of particles in front of and behind the parent to be substantially different.

The modelling has probably had sufficient success that it would be unfair to

exclude the idea. Nevertheless, the problems may be summarised as follows.

1. More model particles between $M = 240$ and 260° would be desirable.

2. Radiation pressure has been neglected. Its importance depends on the (unknown) size distribution of the particles, and also on various properties such as their density. It acts in a direction opposite to the Sun's gravity and so effectively simply reduces the mean motion. Thus it tends to spread particles backward rather than forward of the source object (*cf.* Sykes *et al.* 1986b), but the actual extent of this is difficult to determine. In a first investigation it would seem useful to study the trail model under gravitational forces only, as has been done.

3. The following point, which we make about i but which also applies to the other angular elements, is slightly unsatisfactory. The fact that the proposed source object has a high-amplitude libration means that it precesses comparatively quickly. In fact over 200 yr the differential precession in i between it and Encke is ∼0.5°. Since the present-day difference is <0.2° (Section 3.3.1), we are forced to hypothesise that Encke was ejected with i different by at least 0.3° but that the two orbits have just happened to converge. This is quite acceptable though a little contrived.

Continuous ejection of meteoroids over 200 yr or so has not been modelled above. In this case, as there is no single time specified, there is no particular reason to include Encke in the model, but the possibility remains that a resonant source object has given rise to the swarm over the past several kyr, while producing a visible trail of material that has simply not had time to disperse further. Under this scenario, the source object, being in the resonant zone containing the swarm, is still in the back part of the trail and asymmetrical spreading is still required. A timescale of over ∼100 yr would still be demanded, material ejected over the most recent decades being symmetrically distributed, assuming isotropic ejection velocities (as stated above). It seems probable that the mechanism giving the asymmetry would work in a very similar way to that modelled above for a single ejection time.

While any model explaining Encke's origin has this point in its favour, it may be that for most of the eighteenth century Encke remained undiscovered by chance, or that it suddenly brightened, perhaps owing to the release of a previously covered active part of its surface. An old observation of Encke may one day be found in historical records, though no identification has yet been made (see Whipple & Hamid 1972). Furthermore such an identification if made could relate to the source object

on a similar orbit. Napier (1984) pointed out that the progenitor could be expected to be recorded as an object much more spectacular than usual comets.

We cannot conclude, then, that the modelling has firmly demonstrated the proposed origin of the IRAS trail (and Encke). It is still possible that the trail is derived from Encke (Section 3.3.2), and also that there is a separate trail source in the middle of the brightest part of the trail. This latter idea is less powerful in the sense that it is not testable, there being no independent constraints on the source object. In contrast the above model, with the trail due to the still-resonant swarm source, predicts source position and trail particle distribution.

It may be worth developing the particle simulations at a later date if future trail observations, *e.g.* by the Infra-red Space Observatory in a couple of years time, lent further evidence to the suggested model. In the present epoch, Encke and the resonance-based trail are separating; in the ten years since the IRAS mission, Encke will have moved a further 30° ahead of the trail.

3.4 Maintaining a 400 year libration period

I regard it as a little more likely that the swarm model of Section 3.2 is the genuine explanation for various meteoroid detections than that the model of Section 3.3 describes the genuine model for the formation of the trail. Nevertheless, just as the primary motivation for the trail model was to provide independent evidence for the existence of the swarm parent somewhere in the swarm resonant zone, we turn now to possible independent evidence for the parent object being located in the IRAS trail.

3.4.1 A dust-producing machine

In Section 1.1.4 we discussed the way in which meteoroidal input to the Earth may modulate terrestrial effects. There is now known to be a ∼200 yr periodicity going back several kyr in both isotopic and climate data (Oeschger & Beer 1990, Sonett & Suess 1984) and the question arises as to whether there is any appropriate mechanism that could produce this. Clube & Napier (1984) pointed out that if the Earth repeatedly underwent passage through each of two swarms with slightly differing periods then the 200 yr cyclicity could be caused by a beat period, an interesting suggestion that is quite possibly correct but that we do not pursue here in the absence of any independent evidence for a second dense swarm (existing observations apparently being adequately explained by the 7:2 swarm at a=2.256

AU; a ∼200 year beat period corresponds to Δa of only ∼0.025 which does not represent another strong Jovian resonance). The possibility we consider instead suggests itself as a result of the swarm and IRAS trail modelling, as follows.

In this chapter we have developed a model of a dense, massive meteoroidal swarm due to the Taurid progenitor, and envisage a possible picture whereby the defunct cometary source object is in a resonant orbit, with high libration amplitude so that it was located in the dust trail when IRAS observed it. The librating source object will periodically pass through the central, densest part of the swarm. Thus we have a naturally occurring cyclicity, and we now consider the idea that meteoroidal impacts on the fragile core object generate new meteoroids and dust, periods of meteoroid production reaching a maximum every 200 yr if the libration period of the defunct giant comet is 400 yr. If material can reach the Earth on timescales of under, say, 100 yr (see below) then we have a mechanism for explaining the patterns in the various observations. In any case, though, this can act as a periodic replenishing source for the zodiacal complex.

This model has the immediate advantage that, independently of the climatic and isotopic data, period and phase are both predicted by the IRAS trail modelling, and at least seems worth further investigation. We recall that the reason that the period must be at the high end of those typical for 7:2 resonant objects is because the proposed trail parent is near an extreme of the resonant zone; the phase (with the extreme of the libration at the present day) is broadly in agreement with presumed maxima (from climate records) in the dust input at 1900, 1700, *etc.*.

Given the apparent broad fit of present-day period and phase, an obvious next stage is to test the stability, under inner planet perturbations (Section 3.1.2), of a ∼400 yr libration period. The philosophy at this point will be simply to test the orbital evolution of the presumed source object, rather than developing the physical model in any detail. Thus whether the appropriate periodicity falls naturally out of the orbital evolution studies is itself a useful test of the likelihood of the theory. Regarding the physical model, we just consider two questions briefly.

The first question is the meteoroid-producing mechanism. The general picture we have been constructing of the defunct giant comet implies that it is presently devolatilised and highly fragile. Quantitative calculations of the amount of material lost during meteoroidal impacts, though, are difficult and highly sensitive to the exact physical nature of the comet. A few simple calculations concerning the volume of space swept out by the comet, based on estimates of the size of the swarm in Section 3.2.4, with reasonable extrapolations of the mass function do, however,

suggest that if this model of meteoroidal input to the Earth is correct, then most of the material must be fragmented from the comet itself rather than deriving from the impacting meteoroids. If there is material concentrated with orbital elements, including anomaly, similar to the parent (*cf.* trail) then this will pass through the swarm at the same time and there could be a contribution from these collisions also. We draw attention to a recent paper by Babadzhanov *et al.* (1991), who investigated the possibility that the splitting of Comet Biela last century was caused by the comet's passage through the densest region of the Leonid meteor stream.

The second point is the transfer of material to Earth on timescales short enough that a 200 yr cyclicity in its production rate can be maintained in its arrival pattern at the Earth. Given the presumed orbit of the parent object (well away from intersecting the Earth's orbit at the present epoch), either material must be ejected at high enough velocities to put it on to Earth-crossing orbits almost immediately, or there must be forces other than gravity that can disperse it widely over short timescales. For dust, radiative forces would do. However, there is known to be a substantial proportion of 10^2–10^6 g friable meteoroids incident on the Earth (Fechtig 1982); perhaps non-gravitational forces could have a significant effect on these on short enough timescales.

It could well be that investigations into the two subjects of past atmospheric variations, plausibly due to an astronomical dust input, and past evolution of dominant bodies in the inner Solar System will prove very helpful to each other in the future. Here we concentrate on just one aspect of this, which follows on naturally from the work on the resonant meteoroid swarm and its proposed parent, *viz.* testing whether the 400 yr libration period can be maintained over quite a few kyr, rendering at least possible this particular model of dust and meteoroid production from the giant comet.

3.4.2 Orbital stability

The numerical studies here are done considering gravitational forces only. Any additional perturbing force would be likely to decrease the stability (and since we shall in fact be seeing that the resonant orbit is rather unstable, this would simply strengthen the conclusion). In any case, though, since the giant comet is presumed extinct over the last several kyr, there will not be a cometary non-gravitational force due to momentum of evaporating mass.

The theory of Section 3.1 showed that when a libration period is ∼400 yr the orbit is in a rather unstable part of the resonance, in the sense that a small energy

perturbation from an inner planet has a large effect on the libration period. Indeed, it takes a comparatively small inner planet Δa perturbation to perturb the orbit out of the 7:2 resonance completely. Thus even before commencing a numerical study we have reason to believe that, for example, a 300 yr period would most likely be maintained for a longer time than a 400 yr period. This notwithstanding, it is still worth checking whether a 400 yr period can last for a few kyr.

Initial orbits for the giant comet are selected according to the constraints that it is in the 7:2 resonant zone that includes the meteoroid swarm we have modelled (and not in the resonant zone defined by the other half of the orbit), that it is in the IRAS trail and that its present-day libration period is 400 yr ($\pm$20 yr, say). Since the IRAS trail is very near Encke's orbit, the e, i, Ω, ω values are taken as Encke's current values. Some brief integrations involving Jupiter only are done to find, for each value of semi-major axis a, the appropriate value of mean anomaly M that gives the 400 yr period. Thus all the selected orbits behave as required, if the inner planets' forces are neglected.

When the inner planets (Earth and Venus especially) are included, the basic result is that the libration periods are not very stable, the orbits either being perturbed to lower periods, or to higher, in which case they often proceed to be thrown out of the resonance entirely. Essentially, orbits with 400 yr periods are too near the boundary of the resonant zone. The perturbations to values more than, say, 40 yr displaced from 400 yr often occur within a century or two and usually within under 1 kyr. These results are consistent with the fact that in the simulations of large numbers of swarm particles, periods in the range 250–350 yr were apparently present more frequently.

The effect of the inner planets is most simply thought of as random perturbations to a (Section 3.1.2) which cause changes in libration period as expected from the theory of Section 3.1.1. Of course, the perturbations are not random in the sense that the equations of motion are deterministic. It was decided to continue the investigation a little further, searching the initial (a, M) space for regions of stability, as there is at least some pattern to be discerned if one looks hard enough. In the event of the source object one day being discovered in the trail, if it turned out to be in a region of higher stability, it would lend weight to the theory we are testing here.

It was decided to integrate the whole planetary system (using Newtonian point masses with initial conditions from the DE200 ephemeris of the Jet Propulsion

Laboratory) at high accuracy ($\varepsilon = 10^{-11}$ in the notation of Section 2.1.1[1]) to give a good chance of conditions resembling those of the genuine Solar System for as long as possible (though, given the chaotic nature of the orbits, one has to accept a lack of predictability at some level).

A hundred or so orbits that spanned the whole permitted range of (a, M) values were integrated. A representative sample are shown in Figure 3.27. Plotted is the critical argument σ; we recall that it circulates for non-resonant particles and oscillates for resonant ones, maxima and minima corresponding to reaching back and front of libration respectively. We see that a lot of the orbits cease to be resonant, and several more soon take on periods that are more typically, say, 360 yr. There was found to be little discernible pattern with the (a, M) values spaced by the amounts selected (typically 0.002 AU, 1°), *i.e.* the significant inner planet perturbations are different for every orbit.

There were nevertheless a few orbits that looked more promising (*e.g.* the 6th one down in the left-hand column in Figure 3.27). Thus very restricted regions could be chosen where particles did not immediately get perturbed on to undesirable orbits, so that they would have a higher chance of being what was sought. In other words, a fine grid was imposed on a few areas of (a, M) space. Some examples are shown in Figure 3.28. With initial values so close, patterns do become detectable, at least over the last few centuries, *i.e.* it is a few centuries before the cumulative effect of inner planet perturbations causes the orbits to diverge appreciably. The general result now is that there are a few examples that survive 1.5 kyr or so (*e.g.* the 9th one in Figure 3.28), but in no case out of over 200 integrations did a 400 yr period (±30 yr say) last beyond 2 kyr ago. This timescale beyond which the 400 yr libration periods apparently do not survive is explicable in terms of the times of nodal crossings. Precession rates being closely linked to libration periods, nodal crossings occur at similar times for these orbits, and in fact both ascending and descending node crossings of Earth and Venus orbits occur in the space of a few centuries around 1.5 kyr ago. As discussed in Section 3.1.2, during these epochs there are likely to be more severe perturbations to a and consequently to the libration period. We also note that not only do the periodicities not survive through the nodal crossings, but initially adjacent orbits are not perturbed on to the same new orbit, *i.e.* the motion is chaotic.

Unfortunately, then, though a currently high libration period is implied if the

[1]This value of ε means that Mercury's orbit, which suffers from the greatest integration error, is calculated sufficiently accurately that a comparable error is likely to occur owing to the fact that the equations of motion are an idealisation.

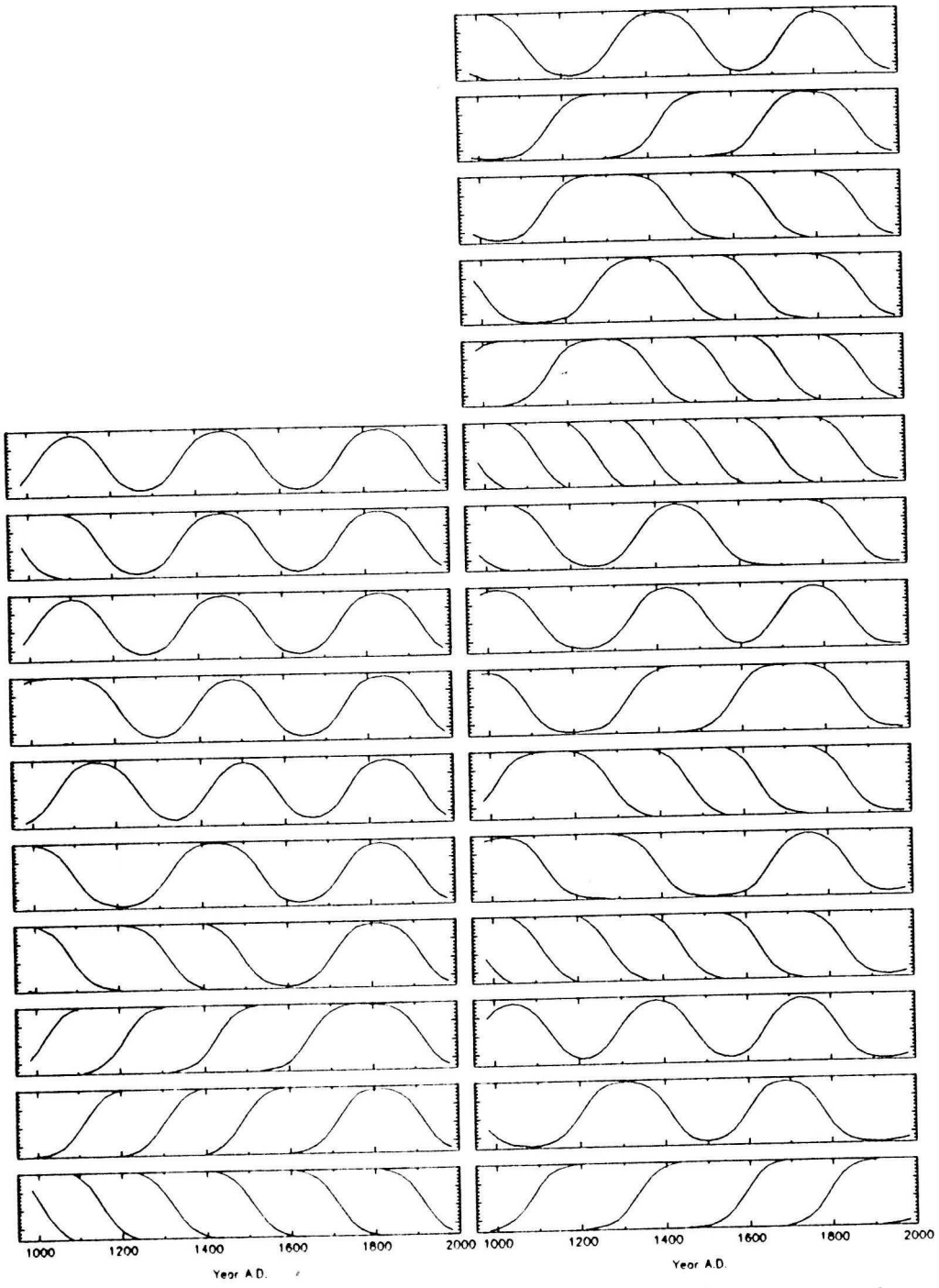

Figure 3.27: Behaviour of σ for orbits initially with 400 yr libration periods over the last 1 kyr. 5 initial a-values, 5 particles of each a. Left column is $a = 2.244$ (first 5 plots) then 2.248 (last 5 plots). Right is 2.252, 2.256, 2.260. For each a, 5 M values are chosen, spaced by 1°, such that the libration period is near 400 yr when unperturbed by inner planets. For different a's the M's can differ by up to $\sim$10° though all M's are within IRAS trail.

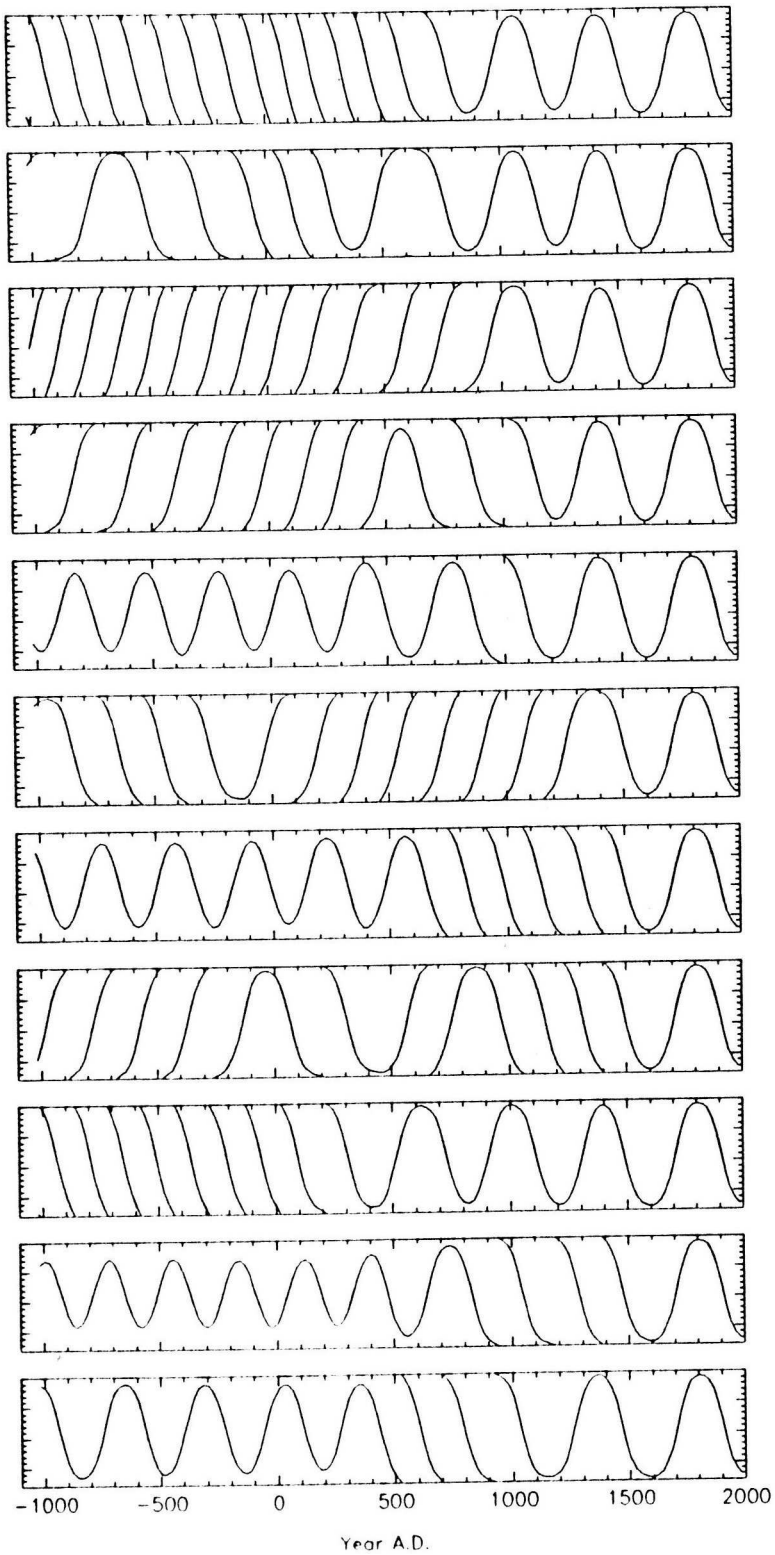

Figure 3.28: Behaviour of orbits initially with 400 yr libration periods over the last 3 kyr. These examples have initial $a = 2.2501$, M from 212.94 to 212.95° spaced by 0.001°.

IRAS trail model is correct, long-lasting 400 yr periods do not come naturally out of this scenario. It is periods roughly in the range 250–350 yr that can sometimes survive for several kyr (though they can also be perturbed, especially during epochs of nodal crossing). What this kind of model predicts, in fact, is reasonably constant periods in the range 250–350 yr, undergoing rather sudden changes every few kyr. In this context the evidence presented by Neftel *et al.* (1981) for a ∼150 yr cyclicity in ^{14}C data (which would correspond to a ∼300 yr libration period) in the millennia preceding 4 kyr ago appears interesting, but there is certainly no way to predict a resonant orbit's definite evolution back that far.

For the time being, therefore, one is not inclined to support this explanation for any ∼200 yr cyclicity in terrestrial data. Furthermore the integrations have demonstrated that the stability of a 400 yr libration period is not predictable over timescales greater than centuries, no matter how accurately we knew planetary positions and the initial resonant orbit, meaning that even if the comet were discovered, it would be impossible to demonstrate its stability over a long timescale. The timescale of predictability would be expected to be longer if one wanted to demonstrate the constancy of an orbit with smaller libration period.

It is conceivable that there is some special configuration involving near commensurabilities with the Earth and Venus which allows serious perturbations from those planets to be avoided over a few kyr. However, no particle in the integrations has accidentally been perturbed into such a configuration. The interpretation of inner planet random perturbations to a causing displacements within the resonance (*i.e.* affecting the libration period) and sometimes actually into or out of the resonance still seems the best way to understand this dynamical problem, and indeed this idea is applicable to various other Solar System orbits, not just 7:2 resonant Taurids. However, even if this model is not the explanation of the terrestrial 200 yr cyclicity, the presence of the mechanism as described (with possibly a different, or less regular, period) is certainly not excluded as a major source of meteoroids and dust to the inner Solar System, material that indeed could be the dominant input to the broad zodiacal dust cloud, given enough time to disperse.

3.5 The Tunguska object

Many authors have proposed that the Tunguska meteoroid of 30 June 1908 is associated with the Taurids. This is extremely likely both because the radiant direction constructed from eyewitness reports closely matches typical radiants of the daytime β-Taurids and because the object apparently had a rather low density and friable na-

ture (Kresák 1978). The question arises whether it closely fits into the evolutionary model of the resonant source described in this chapter.

There is quite a close similarity in mean anomaly to Comet Encke, which passed r=1 post-perihelion only about 3 weeks before Tunguska. Such a small difference would occur by chance with a probability of only 4%, but the lack of any mechanism for keeping the two objects quite that close in anomaly while differential precession of 60° in Ω occurs means that it must be regarded as a coincidence, as stated by Kresák (1978).

However, an association with Encke and not just with the Taurid Complex in general has been proposed (Kresák 1978) on the grounds that the point of intersection with the Earth's orbit (provided the node of Encke is rotated by ∼60°; Encke actually passes ∼0.18 AU below the end-of-June part of the Earth's orbit) is very similar (within ∼1°). Is this alignment, too, a coincidence? The Tunguska object has an Earth-intersecting orbit and therefore node differing from Encke's by 60°. The separation could have occurred by differential gravitational perturbations over millennia (as suggested by Kresák) or they could have separated more recently (*e.g.* at the proposed event which produced Encke and the dust trail; Section 3.3) but with large enough ejection velocities to be placed immediately on to very different orbits. The former possibility can be tested by performing a few integrations, the latter by simply calculating orbital elements from positions and velocities. Either way, we find that, for a difference in Ω of 60°, the expected difference in ϖ is several degrees, meaning that the alignment in longitude is something of a coincidence even if the two objects do have a common origin. A common origin is quite possible; alternatively they are just two objects which are located in the core of the Taurid Complex and happen to be at the same longitude.

As far as the meteoroidal swarm as a whole is concerned, the date 1908.5 is displaced from the calculated resonance centre by ∼0.7 yr, placing the Tunguska object at the back of, and well away from the densest part of, the swarm. In Section 3.2, Tunguska was given little weight because it was a single observation as opposed to a broad swarm passage producing several meteoroid detections over many days. Therefore while the Tunguska meteoroid almost certainly originally came from the Taurid progenitor, there does not seem to be any special reason to assume that it has followed a resonant or near-resonant evolution, of the sort considered in this chapter, in the recent past.

3.6 Gegenschein dust

Roosen's (1970) interpretation of a decreased brightness on 21 February 1969 in the centre of the Gegenschein (not normally observed in scans of the Gegenschein) was that there was a dust cloud sufficiently near to the Earth that enough of it would be in the Earth's shadow to produce both the width ($\sim 3^\circ$) and intensity decrease of the relevant region. (The location, at the antisolar point, was indicative of an extraterrestrial cause.) Observations on 21 February 1971 failed to reproduce the 1969 event (Roosen *et al.* 1973). The point on the Earth's orbit corresponding to this date is close to the Earth's passage through the node of both Comet Encke and the presumed Taurid parent on a similar but resonant orbit. The dust cloud had been predicted to occur in 1971 because that was only six weeks after the passage of Encke itself through the node, a plausible timescale for dust, blown off the comet nucleus and away from the Sun by radiation pressure, to reach the Earth. The event, then, certainly seems unconnected with Encke.

Neither does the Taurid parent, if located in the IRAS dust trail, have the correct anomaly to explain the 1969 observation, and the reason for considering the IRAS trail rather than the broad meteoroidal swarm is because the orbital plane of Encke (and the trail) appears to be relevant. On the other hand, the models of Section 3.2.3 suggest concentrations of particles near the orbital plane of the parent object so that a central core of the swarm may be expected to produce dust that could cause the Gegenschein observation. In 1969, the date of the observation was ~ 0.6 yr behind the passage of the resonance centre through the node, a reasonable timescale thus being allowed for dust to reach the Earth.

We note also evidence for continuous production of small particles by the swarm as evidenced by detections at an actual intersection of the swarm orbits with the Earth (as opposed to at a nodal longitude). Singer & Stanley's (1980) report of $<10^{-15}$ g particles centred on 4 November 1974 related to material ~ 0.4 yr ahead of the resonance centre.

Chapter 4

The Taurid meteoroid stream

In this chapter we investigate the history of the Taurid Complex by looking for dynamical models that yield present-day orbital distributions in accord with observations. The nature of the data is quite different from the swarm detections, when (Section 3.2) we tried to fit dates and years of observation rather than orbital elements. Most of the orbital data we have relate to accurately measured meteors, though the chapter's final section looks at the population of Earth-crossing asteroids. The main section of the chapter concerns dynamical modelling with the aim of matching meteor observations, but an essential preliminary is to select the orbits from the wide database available.

Reference will occasionally be made to work that has been done on other streams to illustrate the points being made. Some comments apply to all streams but some are rather specific, *e.g.* the fact that the Taurid stream is so broad distinguishes it from many other streams when the cross-section at the Earth is being considered.

After the first accurate meteor orbits had been measured, studies of the orbital evolution of meteor streams became possible. The past relationship between Comet Encke and the Taurids was first investigated by Whipple (1940). The subject of the Taurids has been looked at by various authors since then, most recently Steel *et al.* (1991a,b). Sections 4.1 and 4.2 describe the study of Steel *et al.* (1991a), but with several opportunities taken to discuss further aspects of the work and results of a few extra computational simulations included. In places the reader is simply referred to the published papers.

4.1 Observed Taurid orbits

4.1.1 Available orbital data

Many meteor orbits have been determined over the past fifty years in programmes that have used various observational techniques. Nearly 70,000 orbits are available through the IAU Meteor Data Center in Lund (Lindblad 1987) and these represent the most valuable resource for determining the evolution of the giant comet that has given rise to the Taurids. The first task is to select those meteors that are actually part of the Taurid Complex. This cannot be done with absolute certainty but even if a few meteors that do not originate from the Taurid progenitor are accidentally selected it should still be possible to extract a data-set that provides useful information on trends and concentrations in the Taurid stream.

We shall see later that it is a crucial question whether scatter in the orbital elements is genuine or simply due to observational errors. Therefore only the most accurate data were used, the appropriate surveys being listed in Table 4.1. We have a total of over 18,000 orbits from which to select Taurids. The numbers of

Survey	Total	Nn	Sn	Nd	Sd	Total Taurids
Harvard (precise reduction)	1244	24	52			76
Harvard (graphical reduction)	1799	13	34			47
MORP & Prairie Network fireballs	554	5	8			13
Soviet photographic	1111	6	21			27
Canadian TV meteors	531	5	2			7
Total visual	5239	53	117			170
Obninsk	9358	9	0	14	0	23
Adelaide	3759	16	62	32	10	120
Total radar	13117	25	62	46	10	143
Total	18356	78	179	46	10	313

Table 4.1: Number of orbits in each of the meteor surveys used, and the number of orbits selected in Section 4.1.2 as being Taurids. The branches Nn, Sn, Nd and Sd Taurids are described in Section 4.1.3.

orbits chosen as Taurids in Section 4.1.2 are also shown in this Table. Naturally the daytime shower (Nd and Sd in the Table being the northern and southern daytime branches) is only detectable by radar methods. In the Obninsk survey only meteors with radiants north of the ecliptic were recorded.

The original references for the various surveys may be found in Lindblad (1987) and Steel & Lindblad (1992). In these we find that errors of a few 0.1 AU in semi-major axis a are not uncommon in some of the surveys. However, we draw attention to the precisely reduced orbits measured at Harvard, in which errors in a are often

as low as ∼1%. Indeed Lindblad (1973), using a sizable fraction of these orbits, was able to demonstrate the existence of the Kirkwood gaps in meteor orbit distributions. The Harvard (precise reduction) data-set will be considered individually below to emphasise that a significant amount of scatter in the element distributions is real. The original references explain the computational short-cuts that distinguish the graphical from the precise reduction method.

4.1.2 Selection of Taurids

Given the set of meteor data from which to select Taurids, we first impose restrictions on the months of observation so that night-time meteors are separated from daytime ones; thus September – December for the pre-perihelion intersection with the Earth and May – July for post-perihelion. We then plot radiants to show where Taurids are most concentrated. This is best done from the photographic meteors because radar meteors are smaller and so disperse more quickly; also the radar surveys tended to have less uniform coverage. Indeed it is even better done from the most accurate photographic orbits; the first plot in Figure 4.1 shows bands of radiants both north and south of the ecliptic, but the structure in the radiant plot is even clearer in the second plot, where only radiants from the Harvard (precise reduction) data-set are plotted. The different symbols correspond to meteors of different veloc-

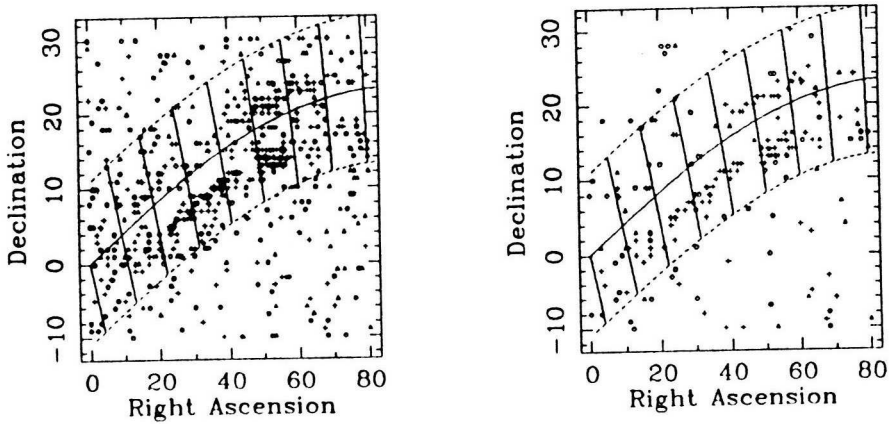

Figure 4.1: Radiants of photographic meteors observed from September to December. The first plot includes all the photographic surveys, the second plot only meteors from the Harvard (precise reduction) data-set. Lines represent 10° spacings in ecliptic latitude and longitude.

ities; the vertical crosses represent the range 26–34 km/s typical of Taurids (circles representing lower velocities, triangles higher). Thus the concentrations of Taurid radiants are highlighted even better when velocities are considered.

The two bands of radiants are not symmetrical about the ecliptic as Jupiter's

orbit is $\sim 1^\circ$ below the ecliptic at those longitudes. For the night-time Taurids, limits of 10 to 70° in ecliptic longitude and 1 to 6° (Northern Taurids) and –8 to –3° (Southern Taurids) were regarded by Steel *et al.* (1991a) as fairly representing the radiant concentrations and therefore the core of the complex. For the daytime radiants, for which only radar observations are available, the same ecliptic latitude limits were used as Jupiter's orbit is at about the same latitude as for the night-time meteors. There was no obvious choice of longitude limits owing to the non-uniform coverage of the observations and so 30 to 90° was used to match the width of the night-time shower.

Though the radiant plots have shown clear concentrations of Taurids, it is highly desirable to impose further conditions regarding similarity to typical Taurid orbits. Simply considering velocities (shown in Figure 4.1) would be one approach but there are better methods, which involve consideration of the individual orbital elements. Southworth & Hawkins (1963) devised a criterion of orbital similarity. They defined the quantity D by

$$D^2 = (q_1 - q_2)^2 + (e_1 - e_2)^2 + \left(2 \sin \frac{I}{2}\right)^2 + \left(\left[\frac{e_1 + e_2}{2}\right] 2 \sin \frac{\Pi}{2}\right)^2$$

where the subscripts refer to the two orbits being compared, I is the angle between the orbital planes and Π is the difference between the longitudes of perihelion measured from the intersection of the orbits. The semi-major axis a is not included in the expression because it is less accurately determined from observations than the perihelion distance q. The Π term is scaled by the sum of the eccentricities since clearly two near-circular orbits are more similar than two highly eccentric orbits separated by the same difference in longitude of perihelion. By considering the change in orbital elements for various perturbations to velocity, Southworth & Hawkins showed that this orbital discriminant could be thought of roughly as the amount of perturbation needed to transform one orbit to the other and that including more precise numerical coefficients before the various terms was unnecessarily complicated. Southworth & Hawkins used this "D-criterion" to identify photographic meteors that were members of streams. Drummond (1981) defined a slightly modified D-criterion, in which each of the terms was normalised to be dimensionless and to have a maximum possible value of 1. In practice, it seems to matter little which D-criterion is used.

Both Southworth & Hawkins and Drummond found that typical values of D between pairs of meteors were quite a bit higher for Taurids than for the other best known streams. This is not surprising given that the Taurid shower lasts for

months (Jupiter has dispersed Taurid longitudes by several tens of degrees), but, as discussed by Štohl & Porubčan (1987), it means that it is quite easy to impose too small a value of D when testing for associations of meteors with the Taurid Complex and to reject meteors that are clearly part of the stream. In fact Porubčan (1968) showed that significant numbers of Taurids (numbers being measured relative to the sporadic background flux) were found with a cut-off of the Southworth & Hawkins D as high as 0.40 (compared with the frequently used cut-off value of 0.20).

For a reference orbit to which meteor orbits could be compared using the D-criterion, Štohl & Porubčan (1990) used an earlier determination (Porubčan & Štohl 1987) of a mean Taurid orbit, which varied with longitude. The meteors thus selected, with quite a tight restriction on D, then defined a varying (elements varying linearly with date) mean orbit of greater reliability, to which orbits could be compared and selected on the basis of a less restrictive cut-off in D.

Steel *et al.* (1991a) decided to use the Southworth & Hawkins D-criterion with the longitude dependence removed, *i.e.*

$$D^2 = (q_1 - q_2)^2 + (e_1 - e_2)^2 + \left(2 \sin \frac{i_1 - i_2}{2}\right)^2$$

so that trends with date would not actually be used in the selection of Taurids but only noted on inspection of the orbital element plots. It would be expected that similar trends would be apparent as those found by Štohl & Porubčan (1990). Based on previous studies of observed Taurid elements, Steel *et al.* adopted $q_1 = 0.375$ AU, $e_1 = 0.82$ and $i_1 = 4^\circ$ as the reference orbit, with a limit of $D < 0.15$. A possible crucial selection effect induced by the use of this D-criterion will be discussed when we consider the dynamical models. The limiting value of D is naturally expected to be lower than those quoted above since this new expression for D^2 involves less terms. Nevertheless values slightly above 0.15 would be expected to yield further Taurids. However Steel *et al.* wanted to be reasonably restrictive in the selection of meteor orbits because their intention was to model the core of the Taurid Complex rather than the component that has dispersed into the sporadic background (though of course there is no sharp dividing line between the two; Section 1.1.1). This latter component has probably formed over a longer timescale and dynamical models of it will inevitably be less precise. The present investigation is aimed at explaining the structured component of the Taurid Complex. The value of 0.15 was chosen after various possible limits had been tried; higher values tended to add widely dispersed meteors and obscure patterns in the data whereas values much lower would simply reduce any patterns to being the results of selection effects. With the extraction of

the Taurid core in mind, Steel *et al.* chose only orbits with aphelion distance below 4.8 AU as larger orbits undergo very rapid precession due to Jupiter and so their present distribution in space is less predictable by a computational simulation. As Štohl & Porubčan noted, such orbits cannot represent the relatively stable core of the complex.

Thus meteors were selected on the basis of month of observation, radiant, simplified D-criterion and aphelion distance. The numbers of meteors to be considered as representing the Taurid Complex core in this investigation were listed in Table 4.1. The radiants are shown in figure 4.2.

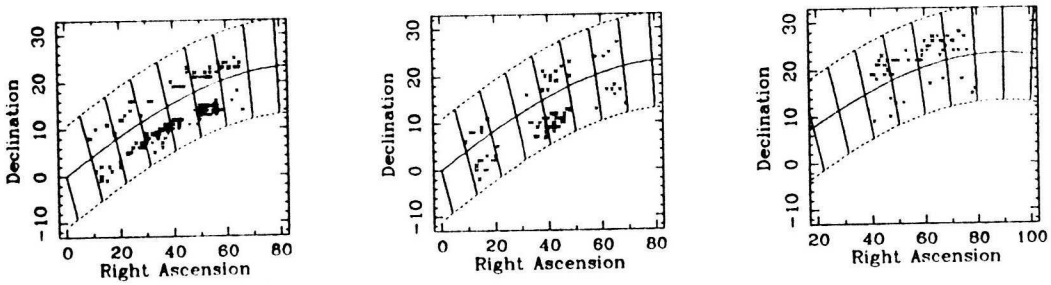

Figure 4.2: Radiants of Taurid meteors. Visual and then radar night-time meteors observed from September to December and then (radar) daytime meteors from May to July. Lines represent 10° spacings in ecliptic latitude and longitude.

The numbers of meteors selected in the different branches suggest that at the pre-perihelion (night-time) intersection with the Earth, the branch with radiants south of the ecliptic is more active than the northern branch, whilst at the daytime intersection the northern branch produces more meteors. This fact is borne out by studies considering just radiant counts (as opposed to just meteors for which accurate orbits have been determined); see Steel *et al.* (1991a). These relative numbers may give useful constraints in models of how meteoroids have spread out from the Taurid progenitor over past millennia. A survey (Bone 1991) of visual meteor observations in the past decade suggests that the Northern (night-time) Taurids are more active than the Southern, and it may be that when one includes more widely dispersed meteors rather than those with quite a narrow distribution of radiants, then the relative proportions do change. This may be indicative of evolution over different timescales.

4.1.3 The four branches of the Taurid stream

It is important that we give a clear idea of the spatial orientation of Taurid orbits. The orbits are of low inclination i and high eccentricity, and have aphelion reasonably

near Jupiter's orbit. Whipple (1940) realised, from orbits of night-time Taurids only, that a family of such low-i orbits would be likely to produce meteors incident on the Earth at the post-perihelion (daytime) intersection with the Earth's orbit. Sekanina (1973) used the term "twin showers" to describe two such showers occurring at very different times of year but nevertheless due to the same family of orbits. A well known example is the pair of showers associated with Comet P/Halley, the Orionids occurring pre-perihelion and η-Aquarids post-perihelion. (Though having a daytime true radiant the η-Aquarids *can* be observed visually, shortly before sunrise.)

At each of the two encounters with the Earth, meteors may come from a direction north or south of the ecliptic, according as they are at their descending or ascending node. Provided that all the orbits are inclined to the ecliptic by a significantly non-zero (albeit low) amount, there is a discontinuity in the latitude distribution of the radiants and we have separate northern and southern branches. Therefore there are four possible branches altogether. If the semi-major axis a and eccentricity e are specified, and if i is non-zero, then there are just four possible values for the argument of perihelion ω that permit intersection with the Earth's orbit, given by

$$\pm \cos \omega = \frac{a(1-e^2)-1}{e}$$

(assuming a circular orbit for the Earth). In the case of the Halleyids, not all possible values of ω are present in the stream and though the space occupied by the set of orbits is quite dispersed vertically (McIntosh & Hajduk 1983), the orbits all have their ascending node before perihelion and descending node after. Thus Orionids all have radiants south of the ecliptic and η-Aquarids north. In contrast, in the Taurid stream, where meteoroids spend a larger proportion of their time nearer Jupiter, precession in ω occurs fairly rapidly and all four values of ω are present.

A discussion of the formation of branches in meteoroid streams is provided by Babadzhanov & Obrubov (1987), including the possibility of 8 rather than 4 related branches for certain families of orbits (which undergo considerable variations in e as they precess), though the Taurids are not such a case and we shall not consider that further here. Restricting ourselves to the more straightforward case where there are just 4 possible branches, we briefly mention one more example, that of the Geminids. Babadzhanov & Obrubov calculated secular perturbations and showed that $\sim$20 kyr was sufficient for the formation of the 4 branches. This is much longer than the equivalent timescale for the Taurids (the Geminids being much further inside the orbit of Jupiter) and it is not surprising that the distribution of meteors is much more even (though there are still variations in the numbers) amongst the 4

Taurid branches. With the Geminid stream, it is just the one branch, the Geminids themselves, that produce a spectacular shower, since meteoroids are concentrated near the orbit of the parent, Asteroid 3200 Phaethon.

Representative values of ω for the Taurids are listed in Table 4.2, with a range of about $\pm 20^\circ$ allowed because of the range of (a, e) values present. Values of

Branch	Abbreviation	Name	No. of meteors	Ω	ω
Northern night-time	Nn	Northern Taurids	78	205	295
Southern night-time	Sn	Southern Taurids	179	25	115
Northern daytime	Nd	ζ-Perseids	46	75	65
Southern daytime	Sd	β-Taurids	10	255	245

Table 4.2: Names, abbrevations and values of Ω and ω of the four Taurid branches, and (from Table 4.1) the numbers of meteors with accurate orbits used in this study.

the longitude of ascending node Ω are also given, assuming that the longitude of perihelion ϖ is 140°, though again, a range of a few tens of degrees in ϖ is permitted. We also list abbreviations that we shall use henceforth for the branches, and the commonly used names for the showers (though there are names for other showers which form part of the continuous complex). The four branches are illustrated in Figure 4.3.

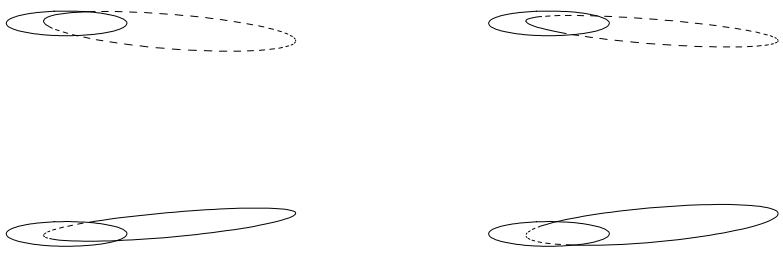

Figure 4.3: Orbits from each of the four branches of the Taurid stream; Sn and Nd branches, then Nn and Sd. Dotted part of orbit is below ecliptic, solid part above; the Earth's orbit is also drawn in each diagram.

The β-Taurids are the "twin" of the Northern night-time Taurids, in the sense that a comparatively small change in ω rotates one orbit into the other (similarly the ζ-Perseids are the twin of the Southern night-time shower). Indeed measured in terms of time to precess rather than difference in angle, the difference is extremely small since at these values of ω (near 90 and 270°) the rate of change of ω is at its fastest, as described in Chapter 2 (we are here neglecting the difference between ω referred to the ecliptic, which defines whether meteoroid orbits intersect the Earth's

orbit, and ω referred to Jupiter's orbit, in terms of which we considered precession rates). We note, then, that nodal intersections of a precessing Taurid orbit occur in pairs with the two intersections separated by just a few centuries, but with millennia separating each successive pair.

We saw in Chapter 2 how (with angles relative to Jupiter's orbit) the variation of i for an orbit is at a minimum when ω is at 90 or 270° and at a maximum when ω is at 0 or 180°. Therefore the above constraint on ω means that the meteors we sample will have low values of i as against the complex as a whole. Also in Chapter 2 we saw that the range of variation of i for a single orbit was a factor of 3–4. It seems that the low end of this range is significantly displaced from an inclination of exactly zero for the vast majority of Taurid meteors, perhaps because the range of variation in i for all Taurids is comparable to that for a single parent object, explaining why a discontinuity of observed radiants is apparent between northern and southern branches.

It may be expected that, although only a restricted range of ω-values can be sampled as meteors, if we were to plot i against ω (both angles referred to Jupiter's orbit), the relationship, just discussed, between the two elements would be clear. However, the conversion of i and ω between ecliptic and Jovian coordinates varies somewhat with longitude (Jupiter's inclination is 1.3°) and plots by Steel *et al.* (1991a) of (i, ω) distributions of, firstly, observed meteors and, secondly, all Taurid-like orbits that could possibly be observed show that this effect of conversion between frames dominates the i-ω coupling to the extent that minima in i (Jovian frame) are not seen near $\omega = 90$ or 270° so that unfortunately the observed (i, ω) distribution cannot be used as a check on the theory of Chapter 2.

Dynamical models will tend to produce meteors over the whole range of ω and it can be seen that, because of the selection effect that is due to our observational point being restricted to being on Earth, care must be taken when comparing the results with observations. Inclination plots should certainly be done separately for the different branches, and in fact in this investigation we shall plot the semi-major axis and perihelion distance for separate branches also. Apart from the clear effect on angular elements due to the constraints on ω there may be differences between branches because of the precise history of the Taurid Complex. Thus although differential precession in ω has dispersed meteors into all four branches, there do appear to different numbers of meteors in each branch. It may also be that trends with longitude and overall values of, say, the semi-major axis a vary from branch to branch owing to overall relationships between a, the precession rate of ω and the

precession rate of longitude.

We conclude this section by emphasising that the separation of the Taurids into branches is nothing to do with a physical segregation in space. It is simply due to the fact that our observational platform on Earth means that only four discrete values of ω can be observed, for a given (a, e).

4.1.4 Orbital distribution of Taurids

In the night-time and daytime Taurid meteor showers on Earth, then, we essentially see just four cross-sections through a continuous broad meteoroidal complex. Meteor measurements give us no information on the remainder of the stream. We now plot orbital element distributions for the four branches. When we produce computational models whose results are to be compared with these plots, we shall have to impose the restriction that the orbits intersect that of the Earth in the present epoch.

We shall plot distributions of semi-major axis a, perihelion distance q and inclination i against the longitude of ascending node Ω. The inclination will be referred to Jupiter's orbit; there can be a difference of up to $\sim 1^\circ$ in the conversion of i between ecliptic and Jovian frames over the Ω-range in each branch. Converting Ω to the Jovian frame would make little difference; it will be left in ecliptic coordinates and will therefore correspond precisely to the date of observation (with there being a 180° difference in Ω between northern and southern branches of a shower at a particular date). Finally in this section we shall plot a against the eccentricity e.

The variations in a and q and the (a, e) distribution are probably best understood as being due to the stream's orbital evolution and can be expected to be highly dependent on the dynamical model being constructed. The i-variations are probably due to the selection effect that meteors can only be observed if their orbit intersects that of the Earth. We shall hope that the i-values produced by our various models automatically fit the observations; as far as i is concerned the important observational parameter will be the scatter (see later).

Figure 4.4 shows the a, q and i distributions for the optical meteors. A general increase in a and q as one progresses through the >2 month duration of the shower is evident. In the case of a, this provides an immediate demonstration of the effect of Jupiter in inducing faster precession of larger orbits. Another point to note is the existence of clusters of orbits in both (a, Ω) and (q, Ω) space. Apparent clusters around $a \approx 2.25$ AU in both branches could well be related to the existence of a parent object as hypothesised in Chapter 3. In the Sn branch there is a further grouping around $a \approx 2.0$ AU at an earlier longitude, and the two Sn branch groupings in a are

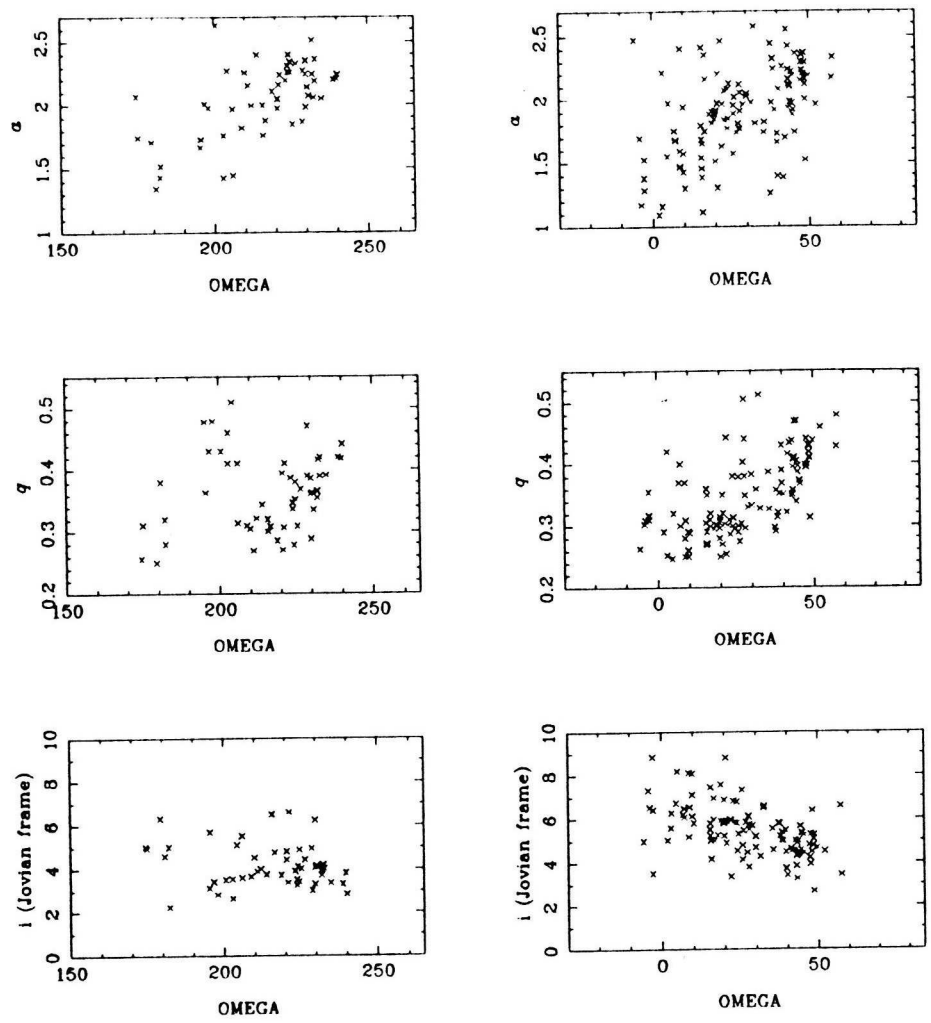

Figure 4.4: Plots of a, q & i against Ω for meteors detected optically in the northern (left) and southern (right) night-time branches of the Taurid stream.

also apparent in the q-plot, *i.e.* clusters at ($q = 0.3$ AU, $\Omega = 20°$) and ($q = 0.4$ AU, $\Omega = 45°$). This structure within the overall stream has led to separate names for sub-showers, with the left-hand grouping being called the Southern Arietids, though the fact that the showers are related was realised soon after accurate meteor orbits were measured (*e.g.* Wright & Whipple 1950). Possible explanations include the left-hand cluster being a whole cycle in ω-precession behind the right-hand cluster, so that although the intermediate values may exist in the stream, they do not intersect the Earth's orbit as Southern Taurids. Alternatively the existence of the left-hand grouping may be indicative of a secondary object of sizable mass.

With regard to the q-plot for the Nn branch, we draw attention to a possible division into two groups, below and above $\Omega = 205°$, with each group separately showing a marked increase of q with Ω. Though this could conceivably be due to

small-number statistics, it is still quite striking and we shall demonstrate a model in Section 4.2 that can reproduce the phenomenon. It further seems that many meteors in the q-plot for the Sn branch would fit into the gap in the Nn plot, at least at the lower Ω-values, provided that the appropriate 180° is added to Ω, and our observational point on the Earth may be sampling meteoroids that have undergone amounts of ω-precession spaced by half-revolutions; the orbits that have precessed more do appear to have larger a-values.

When we come to model the Taurid Complex, it will turn out to be a key feature of these plots of observed meteors that there is quite a large amount of scatter. Lest it should be thought that all the scatter is due to observational error, Figure 4.5 repeats Figure 4.4 but with points plotted restricted to those meteors from the Harvard precisely-reduced data-set. It can now be seen that nearly all the scatter is genuine. For example in i, typical observational errors for the precisely-reduced meteors are well under 1° (Hawkins & Southworth 1961).

Figure 4.6 repeats the last two Figures but this time for the meteors detected by radar. There are gaps at some values of Ω because the instruments were not operated continuously. Though trends are apparent, they are not as obvious as those for the optical meteors. This can be both because errors are greater, and for physical reasons, *i.e.* radar can detect fainter meteors than photographic methods, and very small meteors are subject to greater dispersion due to radiative forces. Nevertheless, one very clear thing about the radar meteor plots is that the a-values tend to be smaller than for the (brighter) photographic meteors, supporting the notion that this particle size range suffers significant orbital degradation under the Poynting-Robertson effect over the appropriate timescale of evolution. The possible effect of radiative forces on the Taurid stream will be discussed in Section 4.2.3.

In Figure 4.7 we plot the same orbital elements but this time for the two branches of the daytime shower. There is less useful information in these plots than in those for the optical meteors, but we hope that the results of dynamical simulations will broadly fit them.

Plots of eccentricity e against Ω are not shown here but may be found in Steel *et al.* (1991a). Much of the information in them is effectively contained in the a and q plots. We simply emphasise that there is a considerable amount of scatter in them too, but little discernible overall trend.

The distribution of a against e will turn out to be important, however, and it is shown in Figure 4.8. There is a clear trend of increasing a with e. Before accepting it as genuine, though, we must ask whether we have caused it artificially by using the

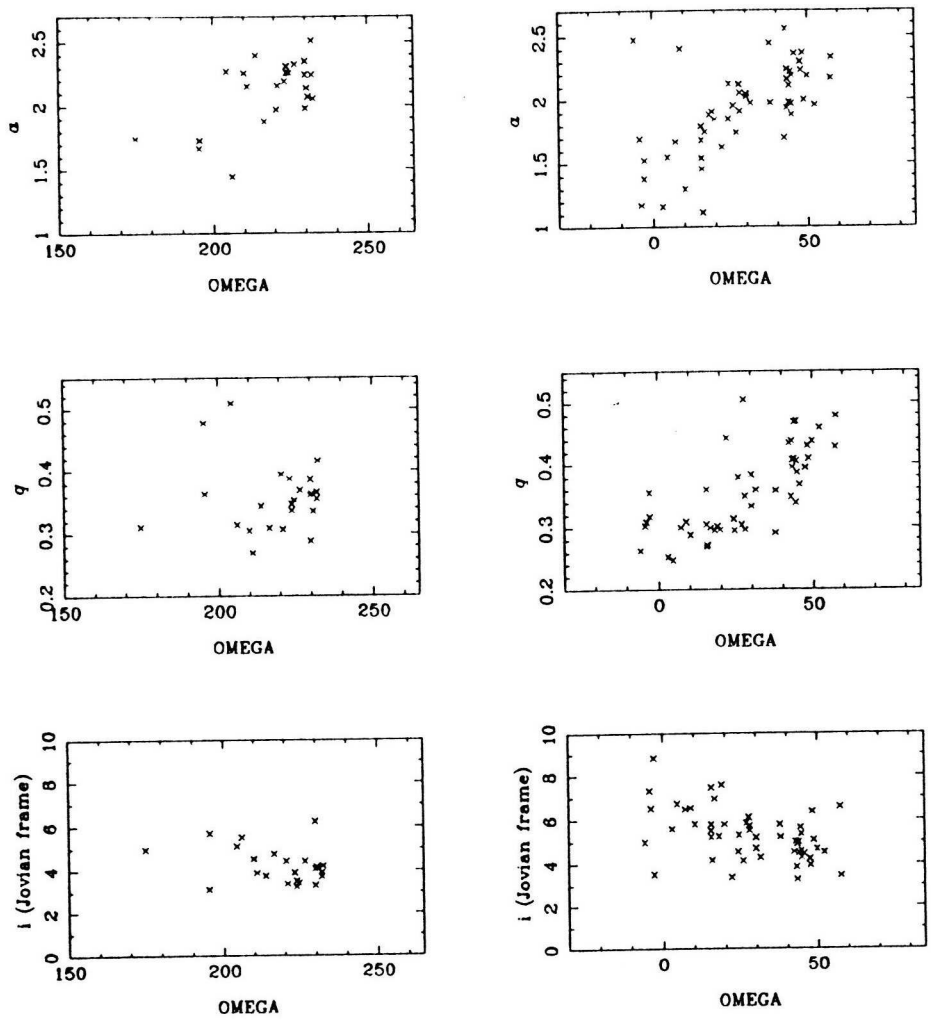

Figure 4.5: Plots of a, q & i against Ω for precisely-reduced meteor orbits from the Harvard survey in the northern (left) and southern (right) night-time branches of the Taurid stream.

(simplified) D-criterion to select Taurids — in particular by referring to a fixed value of q (0.375 AU), noting that a increases with e for constant q. Steel *et al.* (1991a) therefore repeated the (a, e) plots after reselecting the meteors without using the D-criterion and found that the trend, though accentuated slightly by the use of the D-criterion, was still clear.

4.2 Modelling the core of the Taurid Complex

4.2.1 Previous work

Soon after photographic meteor orbits were first accurately measured, Whipple (1940) noted that the orbital elements a, e and ϖ were very similar for the Taurids

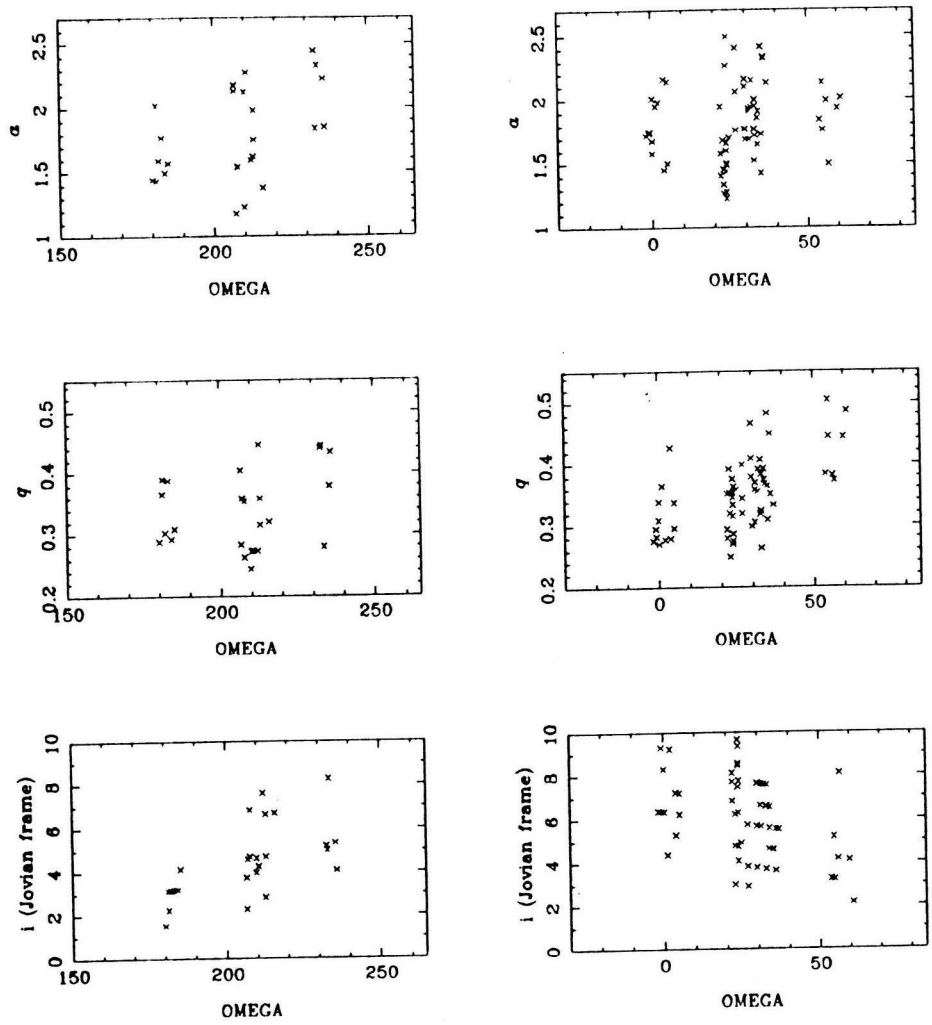

Figure 4.6: Plots of a, q & i against Ω for meteors detected by radar in the northern (left) and southern (right) night-time branches of the Taurid stream.

as for Encke's Comet, suggestive of a common origin. Realising the discrepancy in the elements i and ω, he developed an approximate theory of Jovian perturbations on Taurid-like orbits to see how the orbital plane precessed over millennia. In this way he showed that the orbits of meteors and comet could have coincided in the past and suggested 14 kyr as a rough age for the stream. Furthermore he demonstrated the reason why Taurid meteors have a significantly lower i than Encke (the i-ω coupling discussed in Section 4.1.3).

Whipple & Hamid (1952) used orbital data for 9 Taurid-Arietid meteors and Comet Encke and traced the orbits back in time using Brouwer's (1947) secular perturbation theory (described in Section 2.2.1), searching for convergences of orbital planes and alignments in longitude. Gustafson (1989) has used a similar approach to investigate the Geminids over the past 3 kyr, looking for points of orbital inter-

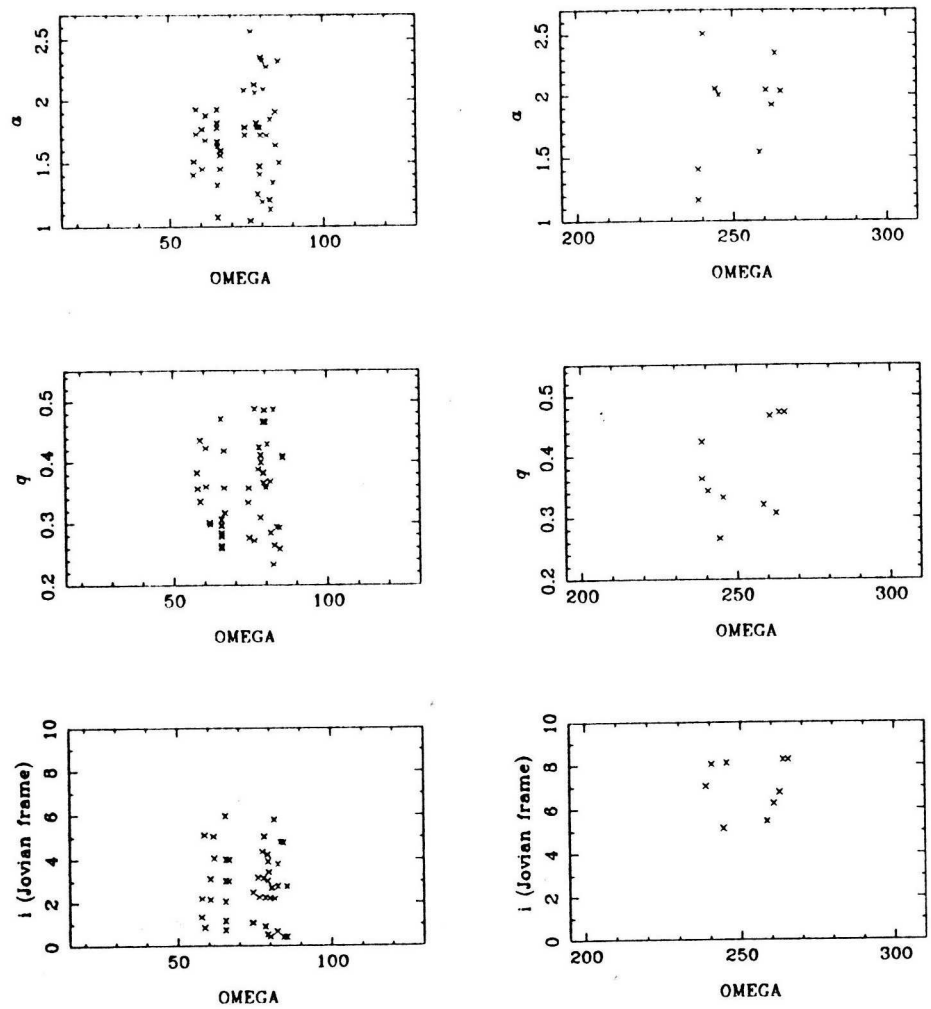

Figure 4.7: Plots of a, q & i against Ω for meteors detected by radar in the northern (left) and southern (right) daytime branches of the Taurid stream.

section. Whipple and Hamid found that most of the orbits could be explained as originating in one of two fragmentations in the asteroid belt, 1.5 and 4.7 kyr ago. In the absence of the large volume of data that subsequently became available (allowing patterns in orbital element distributions to be discovered, *e.g.* Štohl & Porubčan 1990, and the present study), this is a reasonable approach and one would certainly hope to demonstrate a general convergence in longitude for orbits of different sizes, since we can be confident that the theory of Jupiter causing differential orbital precession on orbits of different sizes is sound. However, although in principle by tracing meteoroid orbits back in time we could recover the entire history of the complex, in practice the uncertainties in starting elements, the lack of knowledge of the precise magnitude of radiative forces and the fact that the orbits, crossing the inner planets, suffer unpredictable perturbations in any case, means that the possible error in the

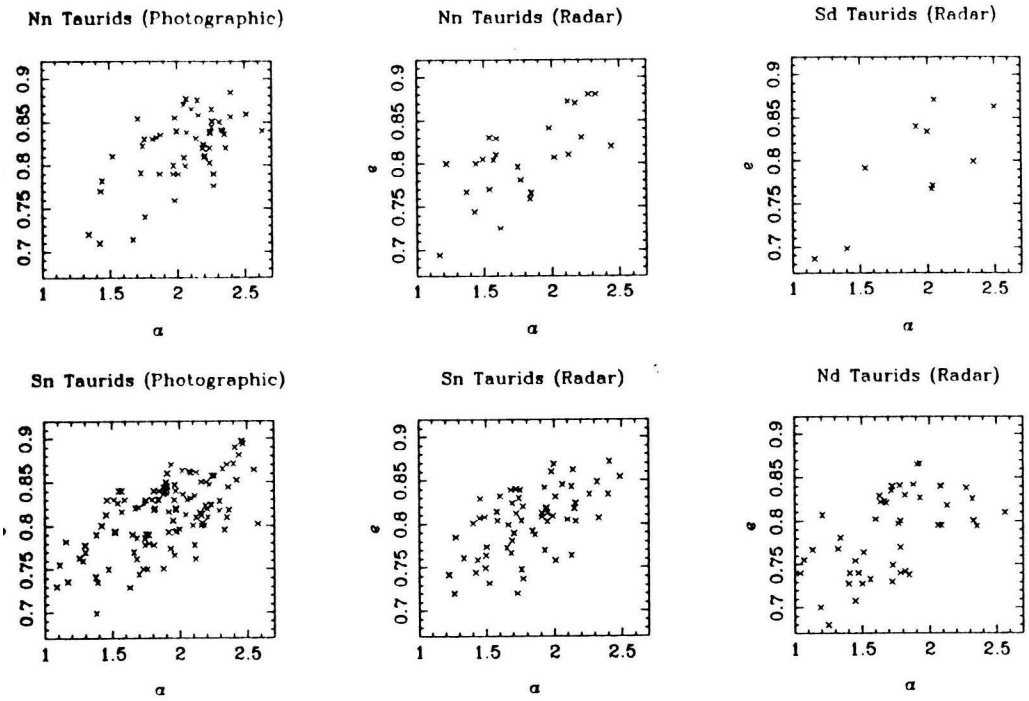

Figure 4.8: Plots of a against e for meteors in various branches of the Taurid stream.

inclination of an orbit even a few kyr ago becomes quite large, since i fluctuates between its maximum and minimum values on timescales of 1–2 kyr.

Jones (1986) integrated particles spaced around the orbit of Comet Encke and showed that 100 kyr was necessary for the separation into Northern and Southern Taurid branches. He predicted that the timescale would be greatly shortened if a range in initial a-values was used, and this has been confirmed by more recent studies of the Taurids.

Babadzhanov *et al.* (1990) used a secular perturbation method — the Halphen-Goryachev method, *i.e.* not the method used by Whipple & Hamid (1952) — and worked forward in time to demonstrate, for a given range in a observed in the Taurid shower, the timescales required firstly for the formation of different branches (by differential precession in ω) and secondly for the overall differences in longitude observed. They found that the four branches could form in under 5 kyr and, assuming a range in a of 1.5–2.6 AU, that a range in ϖ of 110–185° could be achieved in 8 kyr. This shows that by using values from a secular perturbation theory, such as those given in Section 2.2.1, we can predict timescales for dispersion of orbits; this provides a useful check on integration models. If integration results fail to match these timescales then we should have to search for possible explanations, *e.g.* the effect of resonances.

Here, as in Steel *et al.* (1991a), we hope to confirm the above timescales, but also try to go beyond this and see if some of the patterns present in the various orbital element plots of Section 4.1.1 can help to discriminate amongst various models for the ejection of meteoroids over the past several millennia. This we do by letting various computational models evolve forward in time and discovering which aspects of them reproduce which features of the observed distributions. The reverse approach, following orbits of observed meteors back in time, suffers from the danger of allowing too much significance to be attached to the detailed orbital histories of individual objects, which are inevitably rather uncertain, and is unlikely to produce general rules for discriminating between different physical models of meteoroid ejection on the basis of observed orbital distributions. Today's computers allow the preferable approach of working forward in time and comparing different models. It has been used with some success in the case of the Geminid meteor stream (see below).

4.2.2 Stream evolution under gravitational perturbations

The computer modelling described here will involve gravitational forces only. We do not exclude the significance of other perturbing forces, but the approach will be to generate distributions of orbits at the time of ejection from the parent object and to look at the subsequent spreading of the stream under differential gravitational perturbations. Essentially we envisage a scenario in which, *given* a range in a (and e), differential Jovian perturbations disperse the stream, but a mechanism other than gravitational forces is needed to cause the range in a. In Section 4.2.3 we discuss whether the initial distribution mechanisms are realistic (in particular whether the sizes of the ejection velocities are realistic) and consider other possibilities to explain the range in a that we know, from meteor data, to be present in the Taurids.

Regarding the initial orbital element distributions produced by various physical models, we shall essentially be considering two possibilities, ejection near perihelion and ejection due to fragmentation in the asteroid belt. Similar procedures have been followed in order to explain various features of the activity profile of the Geminid meteor shower. Fox *et al.* (1983) developed a model in which particle ejection took place predominantly near the Sun according to Whipple's (1951) model of cometary activity whereby solid particles are swept away from the nucleus with the subliming gases, and found that various aspects of the activity profile, including the skewness, could be explained. Starting with the cometary ejection process described by Fox *et al.*, Jones & Hawkes (1986) modelled the additional dispersion due to subsequent planetary perturbations. Hunt *et al.* (1986) considered the alternative of

an impact on the parent body in the asteroid belt and found that this resulted in an acceptable cross-section but the wrong distribution of aphelion distances.

Whichever part of the orbits meteoroids are generated at in this section's Taurid models, the ejection velocities must be chosen to give a range in a comparable to that observed because gravitational perturbations will not change a significantly. (Perturbations due to random encounters with the inner planets will typically change a by $\ll$0.1 AU over the timescales considered.) We then see whether both the distributions of orbital elements against Ω and the (a, e) distribution that result after thousands of years evolution under gravitational perturbations are in accord with the observed meteor data.

We saw in Section 4.1.4 that there is a range of 0.3 AU in q amongst Taurids. Whipple & Hamid (1952) noted that this spread could not be the result of normal cometary ejection processes since they occur predominantly near perihelion so that ejected meteoroids must all have similar q to the parent. Since according to Brouwer's (1947) secular perturbation model, q remained approximately constant, there was good reason to favour ejection at rather greater heliocentric distances, plausibly caused by violent collisions with asteroidal bodies in the general region of the asteroid belt.

However, the results of numerical integrations show that, because of Jupiter's non-zero eccentricity, q does not remain constant as Taurid orbits precess; rather, q increases as the particle's aphelion approaches Jupiter's perihelion (Section 2.2.1). Thus *absolute* changes in q for individual orbits certainly occur, and we must at least consider the possibility that *differential* changes in q could occur to give the observed range in the meteor data.

Therefore we cannot exclude the scenario where ejection occurs predominantly near perihelion. In fact, we can put forward the following argument which *does* exclude a single asteroid belt collision as the main event that generated the Taurid Complex. Thus we now describe our first physical model for which we perform integrations.

All the simulations in this section use values of the integrator's error control parameter ε (defined in Section 2.1.1) of 10^{-8} or 10^{-9}. All of Steel *et al.*'s (1991a) simulations considered Jupiter only, in a non-precessing orbit. They said that preliminary trials they had done suggested that the neglect of both Jupiter's precession and the other planets did not alter their conclusions. We shall present many of their results here, but in a few places also display results generated using other planetary models, to support their claim.

Over the past 30 kyr (much longer than the timescale of evolution of the Taurid Complex core), Jupiter's longitude of perihelion has remained within $\sim 10^\circ$ of its present-day value. Its eccentricity reached a minimum of just below 0.03 about 15 kyr ago, since when it has risen to its present value of 0.048 (the value Steel *et al.* used in all their integrations). It thus turns out that this variation in Jupiter's eccentricity has had little effect on the dispersal of the Taurid stream and the orbital distribution of Taurids in general, though of course it has been important to check this by including Jupiter's precession in some trials. To update Jupiter's orbital elements every 500 yr, as described in Section 2.1.2, allows for Jupiter's varying e without increasing the integration time.

We consider a model where a fragmentation 10 kyr ago at r=2.6 AU gives rise to isotropic ejection velocities up to 5 km/s, centred on a parent with a=1.85 AU, e=0.85; this gives a roughly comparable range in a to that observed in Taurid meteors. We integrate 123 particles forward to the present day. The initial and final (a, e) distributions are shown in Figure 4.9. Though Steel *et al.*'s (1991a) equivalent

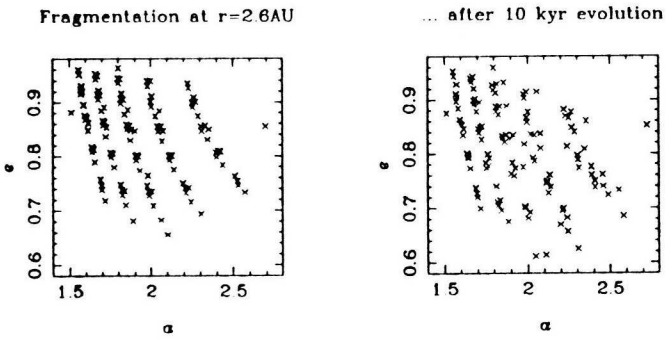

Figure 4.9: (a, e) plots, at time of ejection and after 10 kyr evolution, of particles generated in a model where the parent undergoes a single fragmentation at r=2.6 AU. Jupiter's precession has been included in the evolutionary model.

plot was of results neglecting Jupiter's precession, while for the model here Jupiter's precession was included, the results are almost identical. We see that immediately after ejection, there is no positive correlation of e with a such as there would be if ejection took place near perihelion. After 10 kyr evolution, e and a are negatively correlated, contradicting Figure 4.8. There are two steps in the reason for this. Firstly, orbits with large a precess more quickly. Secondly, Taurid orbits are at longitudes such that as they precess, their aphelion approaches Jupiter's perihelion and, as discussed above, this causes an increase in q (equivalently decrease in e). This result shows that although Jupiter's precession is relatively unimportant, its

non-zero eccentricity is crucial.

This therefore excludes a model involving the disruption of the Taurid progenitor in a single asteroid belt collision, especially as the presumed isotropic ejection velocities generate a range of inclinations (5 to nearly 50°) greatly in excess of those between which Taurid meteoroids usually oscillate. We are led to requiring an ejection process at perihelion to produce the positive (a, e) correlation, and this is what we shall consider henceforth. As we have said, we must assume the necessary ejection velocities; we shall consider in due course what physical process could give rise to them. A collision near perihelion would be a good way of explaining the large relative velocities required, but there is no known population of potential objects for the Taurid parent to collide with in this innermost region of the Solar System.

Thus we now proceed to model ejection at perihelion. If we have isotropic ejection velocities, it turns out that subsequent precession is similar for orbits of similar (a, e). We shall therefore consider ejection only along the direction of motion at perihelion, this corresponding to the component of ejection velocity that changes a. We shall be imposing the sizes of ejection velocities in order to try to get (a, e) values roughly to match those of Taurids. This approach, where we do not, for example, make any attempt to concentrate the orbits of ejected meteoroids near the orbit of the parent, means that we shall not be hoping to reproduce clusterings in the meteor data plots which may well be indicative of large objects in the Taurid Complex. We simply wish to generate meteoroids that, after orbital evolution, fill the appropriate areas of the orbital element plots, but not necessarily at the correct density. It is acceptable to assert that the ejection of several meteoroids on similar orbits would concentrate points in the plots, without performing a large number of almost identical integrations.

The models we construct require a parent object. The fact that we are being selective in our choice of ejection velocities rather than necessarily concentrating meteoroids around the parent means that the main purpose of defining a source object is to define an orbital history for its q, i, Ω, ω values, around which ejected particles *will* be clustered. The parent's a value is not so important. When we look at the results we shall point out which features of them are dependent on the angular elements of the parent. For the rest of this section we shall make a single choice of parent, working with the proposed object that we showed in Chapter 3 may have given rise to a resonant meteoroidal swarm, and possibly to the Encke dust trail discovered by IRAS. Its present-day elements are a=2.24 AU, e=0.85, i=12°, Ω=334°, ω=186° and anomaly such as to locate it in the IRAS trail. This seems a

reasonable choice for the source object given that the elements are typical of known Taurid Complex asteroids and also because of the apparent concentrations in orbital element plots (Figure 4.4), quite apart from the evidence that was presented for its existence in Chapter 3.

In the next model, then, 165 particles were integrated forward to the present day, 11 starting at each multiple of 1 kyr ago up to 15 kyr ago. Ejection velocities were –2.0 to +0.25 km/s (not uniformly spaced), larger positive velocities giving larger orbits that are rapidly dispersed by Jupiter. Figures 4.10 and 4.11 present the (a, e) distributions, the only difference being that Figure 4.11 is from integrations that take account of Jupiter's precession. As well as the entire set of particles, we plot two subsets relating to more limited periods of ejection; this may suggest a preferred timescale of evolution of the Taurid Complex core. Thus the left-hand plots are for the whole set of 165 particles, the middle plots correspond only to particles ejected from 10–1 kyr ago and the right-hand plots to particles ejected from 15–6 kyr ago.

The tendency for orbits with larger a to show a greater decrease in e as they

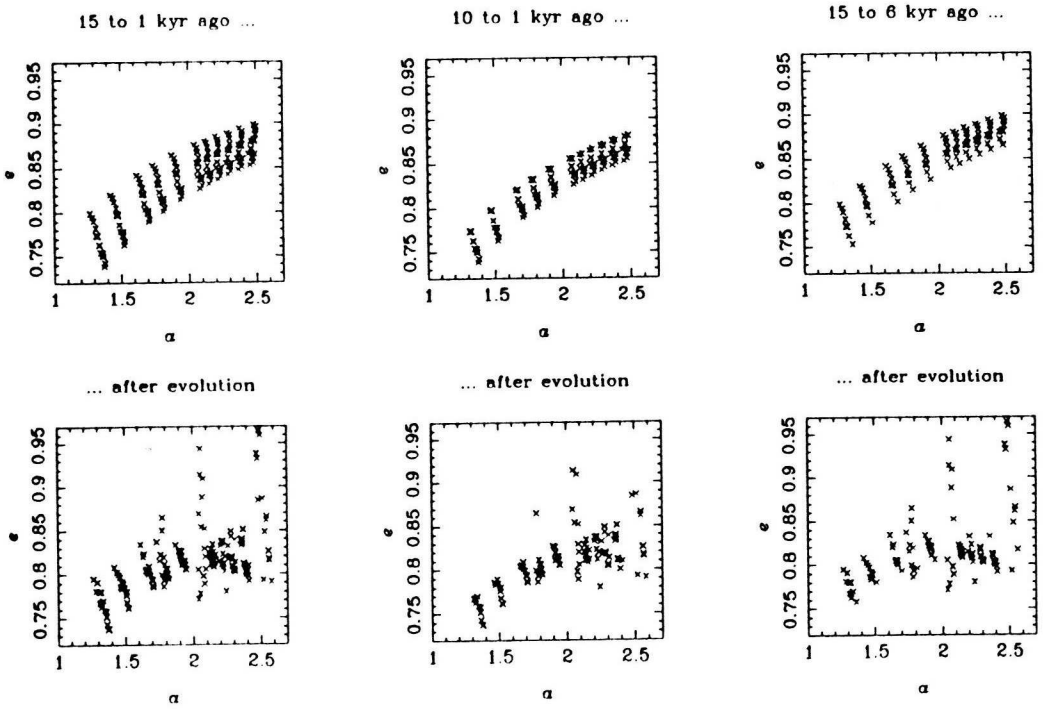

Figure 4.10: (a, e) distributions of Taurid meteoroids, from the model in which particles are continuously generated at perihelion; *cf.* Figure 4.8. The 3 pairs of plots correspond to 3 different periods during which particles are ejected. The particles included in the bottom row of plots are all at the present day, while each of the plots in the top row does not relate to a single time but rather a period of several kyr over which ejection has occurred. From Steel *et al.* (1991a).

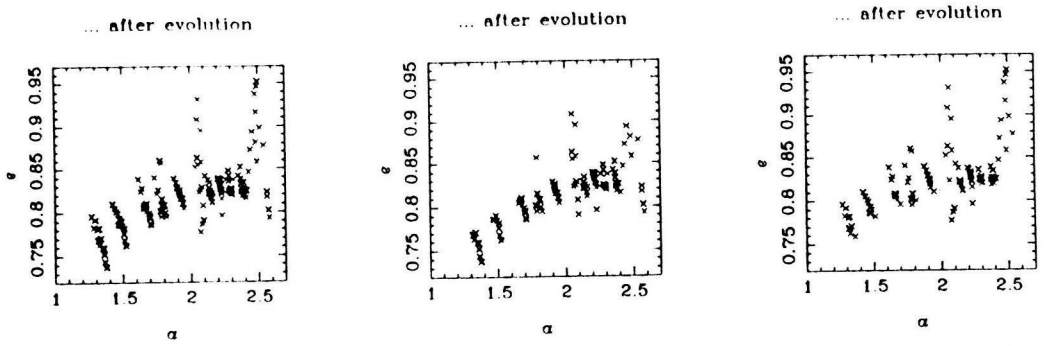

Figure 4.11: The 3 "after evolution" plots as in Figure 4.10 except that Jupiter's precession has been included in the evolutionary model.

precess is again evident, except for some particles in the strong 3:1 and 4:1 Jovian resonances at 2.5 and 2.06 AU respectively. Thus immediately after ejection we have the positive (a, e) correlation as desired (Figure 4.8). The more time passes, the greater tendency there is for particles having larger a but smaller e to be produced. Thus the (a, e) distributions lead us to favour a more recent period of production of Taurid meteors, *e.g.* we slightly favour the period 10–1 kyr ago over 15–6 kyr ago. We may prefer, *e.g.*, 5–1 kyr ago even more, but this is not permitted when we consider the range in Ω, as follows.

Figure 4.12 shows the distributions of a, q & i (referred to Jupiter's orbit) against Ω for the two branches of the night-time shower and Figure 4.13 for the daytime shower; from now on we are restricting the timescale for the model to the past 10 kyr, *i.e.* particles from the middle plots in Figures 4.10 and 4.11. When plotting (a, e), we plotted all integrated particles and not just those intersecting Earth's orbit. This intersection condition (Sections 4.1.3 & 4.1.4) is unlikely to affect the (a, e) distribution but likely to affect the angular elements. Therefore, unlike in the (a, e) plots, points are only shown if the meteoroid orbits intersect the Earth's orbit at the present day so that meteors in one of the four branches could be produced. The condition of orbital intersection is calculated by checking the heliocentric distances r of ascending and descending nodes every year during the several kyr of evolution and seeing when either node switches from below to above 1 AU or vice versa. Ideally by "present day" we should mean, say, just the present century, but in order to obtain a sufficient number of points we include all orbital intersections of the last 2 kyr. It may reasonably be expected that over the several kyr evolution of the stream, the cross sections stay sufficiently unchanged over just 2 kyr. As with the observational data in Section 4.1.4, we refer the reader to Steel *et al.* (1991a) for the (e, Ω) plots.

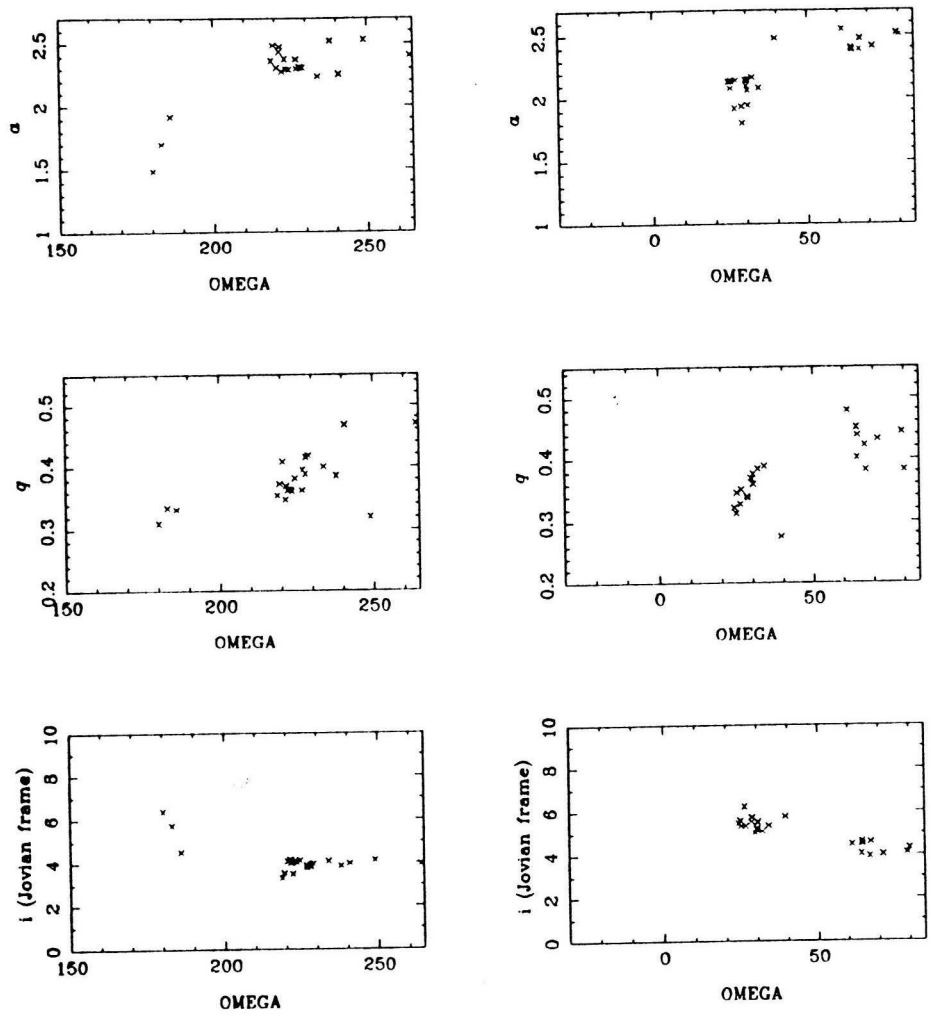

Figure 4.12: Plots of a, q & i against Ω for meteors in the northern and southern night-time branches of the Taurid stream, from the model in which particles are continuously generated at perihelion; *cf.* Figures 4.4, 4.5 & 4.6.

Figure 4.12 gives an important constraint on timescale because the 3 points at the left of the Nn branch all correspond to particles ejected $\geq$7 kyr ago. Therefore if we reduced the timescale of evolution to within the past 7 kyr, we should fail to reproduce the longitude range evident in Figure 4.4. We note that although a sufficient range in Ω has been produced, there are gaps in both night-time branches (Figure 4.12). Significant differential precession in ω has occurred over 10 kyr; model meteors to the left of the gap (in either the Nn or Sn branch) are one cycle in ω precession behind those to the right. Precession of ω of meteoroids relative to each other and to the parent object will be discussed again later.

The Ω-values for the model Sn branch (right-hand plots of Figure 4.12) are a little larger than those of observed meteors (Figure 4.4). It may be that a slightly different

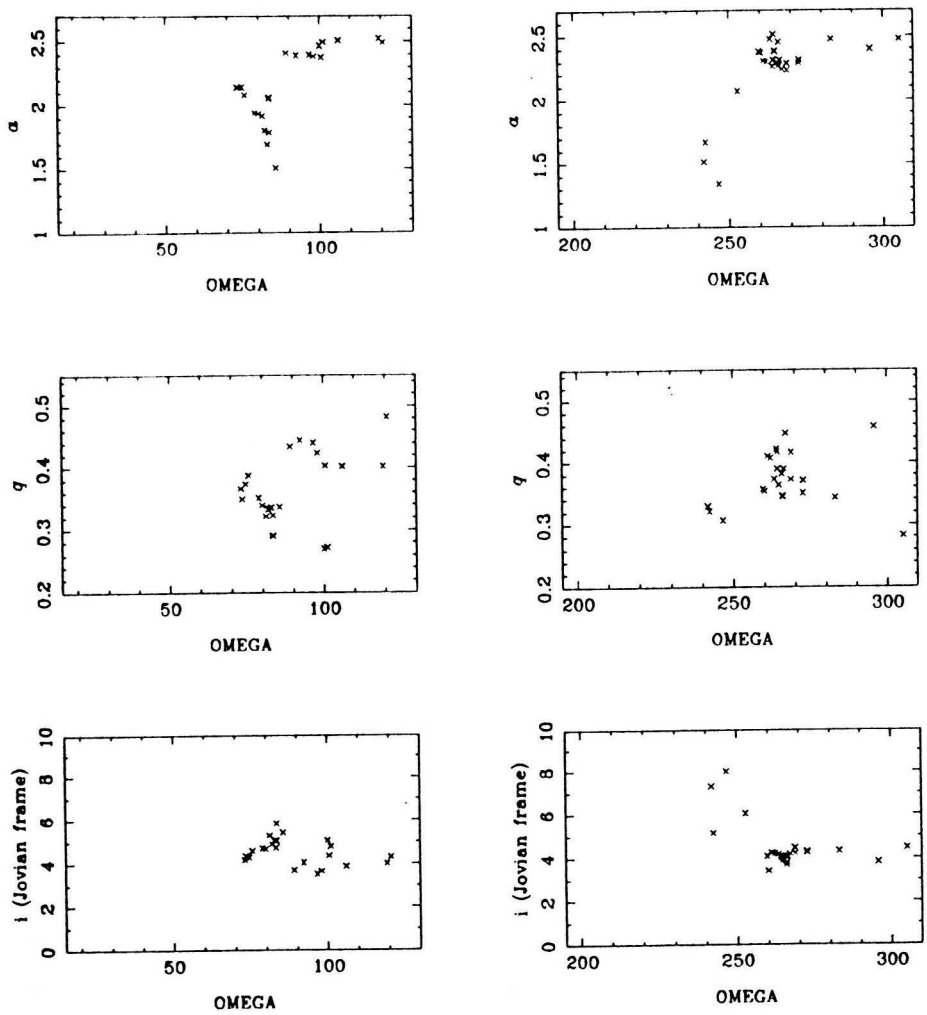

Figure 4.13: Plots of a, q & i against Ω for meteors in the northern and southern daytime branches of the Taurid stream, from the model in which particles are continuously generated at perihelion; *cf.* Figure 4.7.

choice of e or ϖ for the parent would be preferable; this would be fine tuning of the model. Essentially, we may conclude that ejection at perihelion during the past 10 kyr is able to produce the correct (a, e) trend, range in Ω and trends of various orbital elements with Ω. It is encouraging that the Farmington meteorite, which fell near the end of June 1890 and is possibly a Taurid Complex member, has an exposure age of this order (very low for meteorites), providing an estimate of the age of the Taurid Complex independent of the dynamical modelling, as well as supporting the model (which we are about to discuss) in which Taurid stream material may become contaminated with pieces from fragmenting main-belt asteroids (Clube & Asher 1990). For further discussion of Farmington see Steel *et al.* (1991a).

The main failing of this model is that it fails to reproduce the scatter seen in

all the plots of observed meteors. At this point we present two further Figures as further justification for the statement that Jupiter's precession and the non-Jovian planets do not affect the conclusions. We just present Figures for the night-time showers. For Figure 4.14, Jupiter's precession was included in the integrations and for Figure 4.15, Saturn (but no precession) was included along with Jupiter. It can

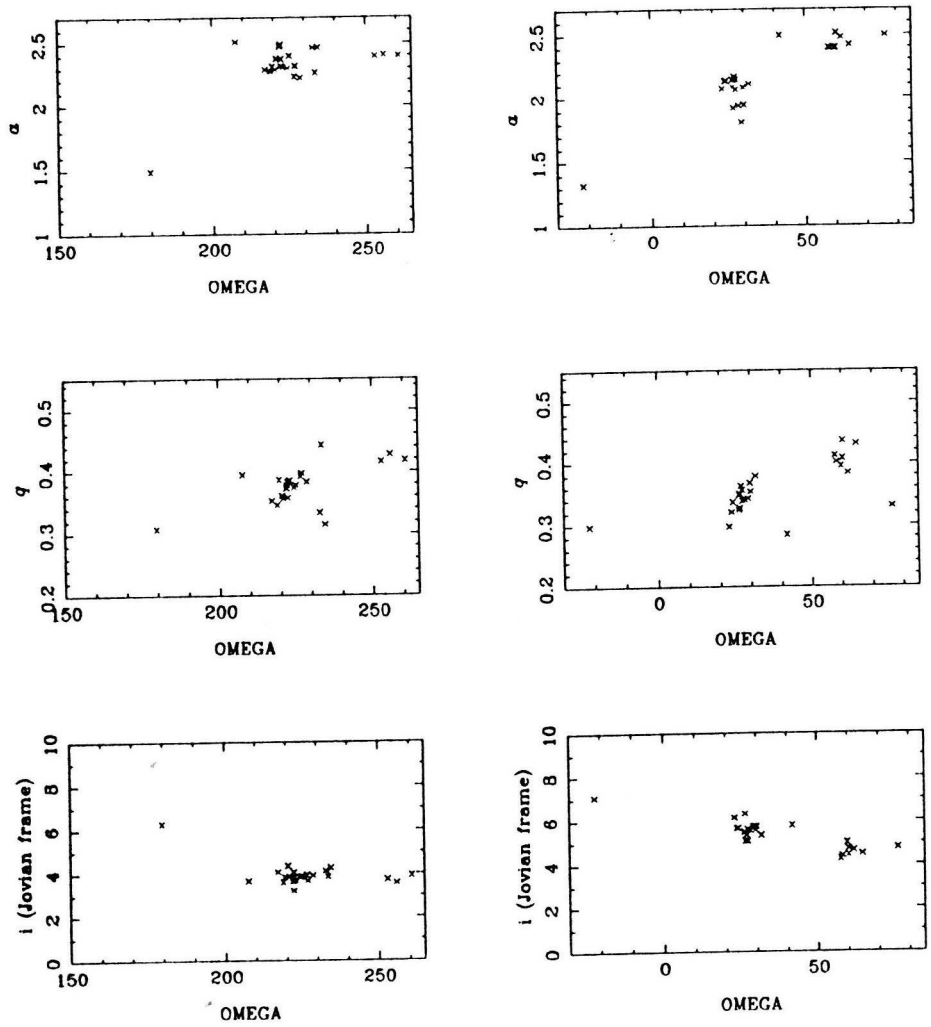

Figure 4.14: As Figure 4.12 except that Jupiter's precession has been included in the evolutionary model.

be seen that Jupiter's precession, and Saturn, make little difference to the spread in longitude or the scatter in the other elements. Neither does the inclusion of the Earth and Venus as well affect the results much; see Steel *et al.* (1991b). Indeed Jones (1986), in his integrations of Encke-like orbits found (using the precession of ϖ as a measure of the effect of different planets) not only that the effect of Jupiter was over 30 times that of its nearest rival Saturn, but that the Earth and Venus combined

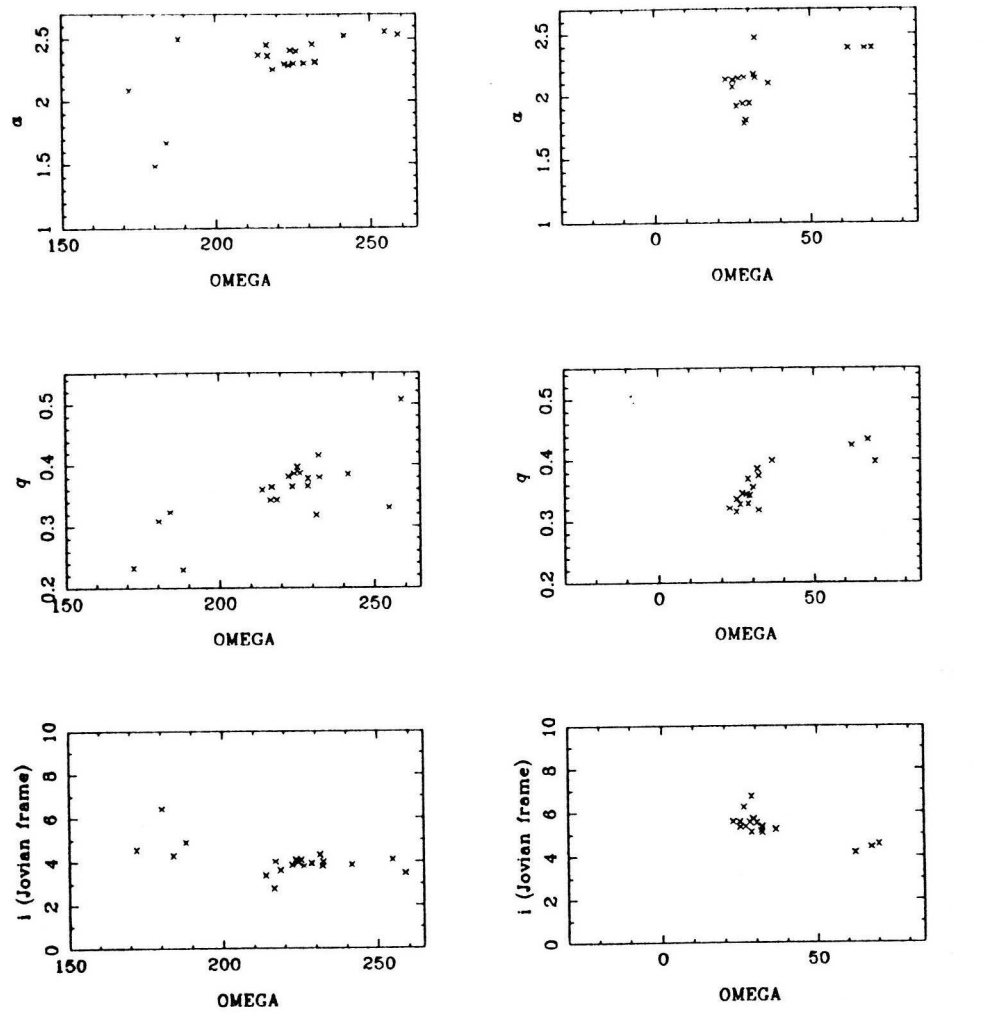

Figure 4.15: As Figure 4.12 except that Saturn has been included in the evolutionary model.

roughly cancelled the effect of Saturn. Thus for studies of the general dispersal under gravitational forces of the Taurid stream, Jupiter is all that matters. This is in contrast to the situation in Chapter 3 where we studied the resonant swarm — in that case we were interested in very small changes to a induced by the Earth and Venus. Such small changes to a are irrelevant in the present chapter.

We now move on to the final model of this section, for which we use the integrations done by Steel *et al.* (1991a), which used Jupiter only, in a non-precessing orbit — we can be confident that this is acceptable as the timescale is the past 10 kyr only. We have seen that in order to produce the (a, e) trend, we require an ejection process near perihelion, but that the last model we tried failed to produce the scatter observed in the meteor data. We consider whether splitting at perihelion

could be the dominant cause of the ranges in a and e with subsequent disintegration of large cometary fragments at larger heliocentric (asteroid belt) distances inducing the appropriate scatter in orbital elements. This is therefore distinguished from the last model by the fact that previously the ejection process near perihelion gave rise to small meteoroids which tended to undergo orbital evolution without producing any further significant meteoroids whereas now large secondary parent objects split from the original comet near perihelion and many of these later fragment to produce further meteoroids in a range of different orbits.

We include all the particles from the previous (perihelion) model. We then select some of these to undergo fragmentation in the asteroid belt. Five fragmentations have been adopted, happening from 9–3 kyr ago at heliocentric distances from 2–3 AU, with isotropic ejection velocities up to 1.5 km/s. Bodies to fragment were in fact chosen because their angular elements were such that they were likely to produce many ejected meteoroids that would intersect the Earth's orbit in the present epoch; we assume that many other fragmentations would have occurred but there is less point in integrating such particles as they will not generate many points for the plots. Isotropic ejection velocities appear reasonable if the cometary fragments disintegrate totally (*cf.* Hunt *et al.*'s (1986) asteroidal collision model for the Geminids which considered an asteroidal impact that did not totally destroy the Geminid parent so that ejection velocities had to be above the horizon at the point of impact on the parent). Our scenario whereby catastrophic fragmentation tends to take place even when the impacting objects are comparatively small is perhaps understood if the Taurid giant comet ended its most active phase ∼10 kyr ago and has since been substantially devolatilised so that fragments which split from it are highly fragile; we discuss asteroid belt collisions further in Section 4.2.3.

The results for this model are shown in Figures 4.16, 4.17 and 4.18, with points plotted if the particles have intersected the Earth's orbit within the past 2 kyr. We remember not to read any significance into particularly localised areas of high concentration in these plots; we are interested in whether the trends and the ranges in elements produced match observations. We see that both the trend and the scatter in the (a, e) distribution (Figure 4.16) give a good fit to the observed data; the positive correlation is present because the fragmenting objects split from the main object at perihelion, with the asteroid belt events generating merely a little extra dispersion rather than the overall pattern.

Although the fit to observations of the plots of elements against Ω is not yet perfect, there is certainly a much improved agreement in the overall scatter. Fur-

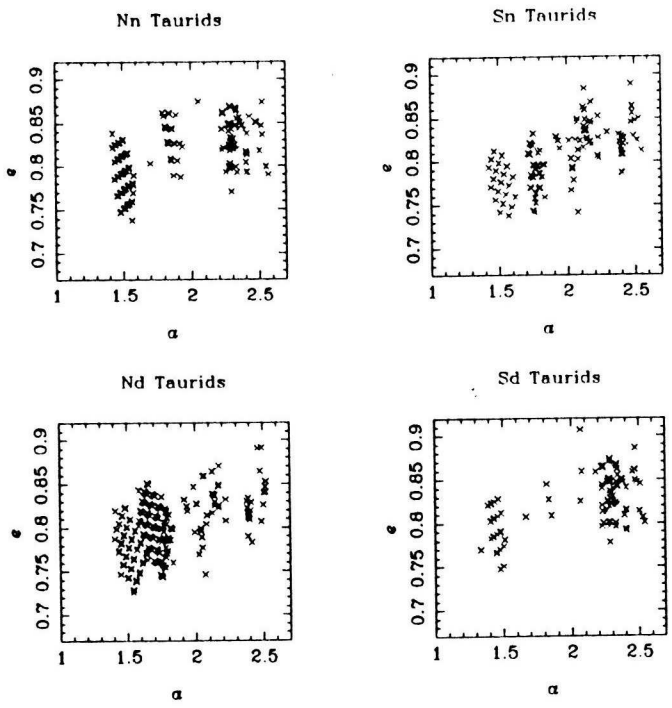

Figure 4.16: (a, e) distributions of Taurid meteoroids, from the model in which particles are generated at asteroid belt fragmentations of large components that have split from the parent object at perihelion; *cf.* Figures 4.8 & 4.10.

thermore, there is a clear double slope in the (q, Ω) plot for the Nn branch (Figure 4.17; *cf.* Figure 4.4). The slopes are generated mainly at the times of fragmentation (as opposed to when ejection takes place at perihelion, when particles initially have the same q), the particles in the left-hand group being generated at earlier fragmentations than those in the right-hand group. In the left group, the particles centred on $a \approx 1.5$ AU were generated at a fragmentation 7 kyr ago and those centred on $a \approx 1.9$ were generated 9 kyr ago. The parent object had the appropriate value of ω to be in the Nn branch 5–6 kyr ago but these ejected particles, having small a, have fallen behind the parent in ω precession and only intersect the Earth's orbit as the Nn Taurid branch in the present epoch. On the other hand, the particles in the right-hand group have large a and are ahead of the parent in ω precession, already intersecting the Earth as the Nn branch in the present epoch whereas the parent will not do so again until 1–2 kyr in the future. Although we were not completely sure that the double slope in (q, Ω) space displayed in Figure 4.4 was a real feature, we have demonstrated how such a pattern could be produced, by returning to Whipple & Hamid's (1952) idea of violent collisions in the asteroid belt. While the perihelion model could produce differential precession in q, it did not produce q-variations over

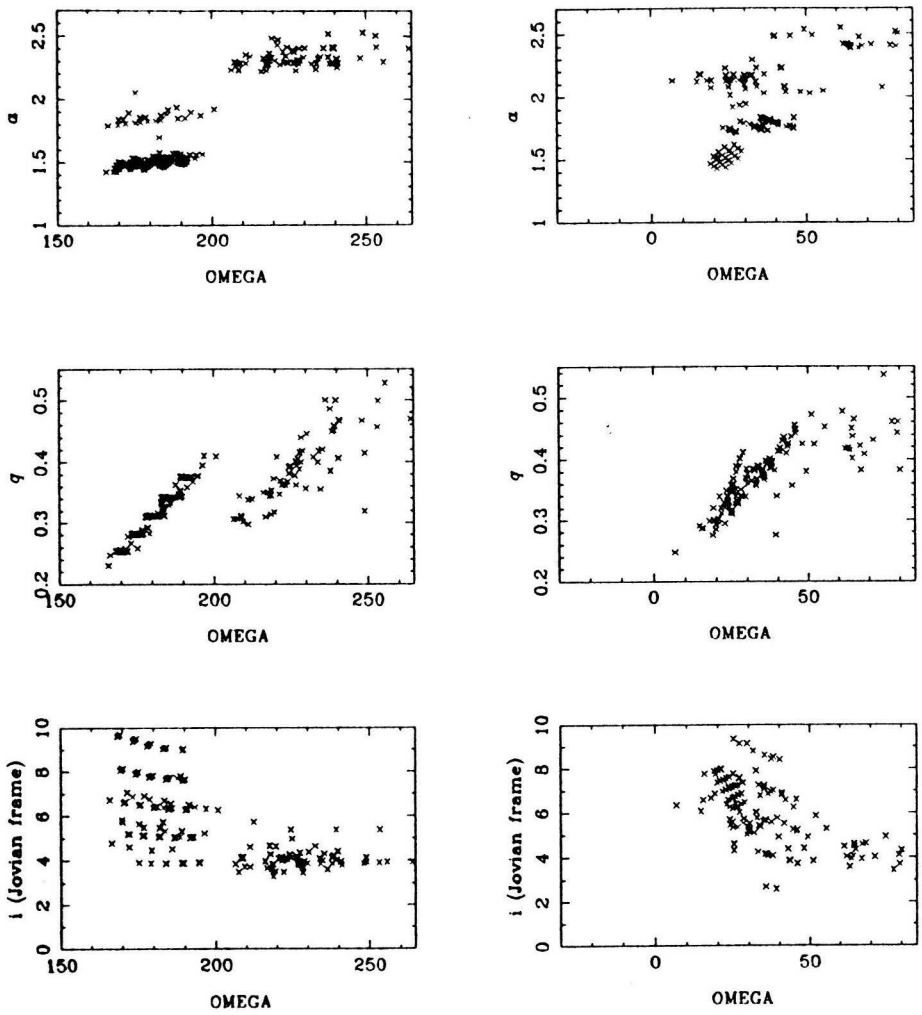

Figure 4.17: Plots of a, q & i against Ω for meteors in the northern and southern night-time branches of the Taurid stream, from the model in which particles are generated at asteroid belt fragmentations of large components that have split from the parent object at perihelion; *cf.* Figures 4.4, 4.5, 4.6 & 4.12.

such a small Ω-range as to give a double slope.

Though the discussion of ω precession in the last paragraph was directed towards a discussion of the double (q, Ω) slope in the Nn branch, it is an important general consideration for the evolution of the Taurid Complex. Taurid meteors are observed over a sufficiently wide range in Ω that in any one branch there are certainly some meteors that are at least one whole cycle ahead of others in ω precession. It is the differential ω precession of meteoroids relative to the parent object that determines at what epoch their orbits will intersect that of the Earth, and the present-day value of ω for the parent, and the rate at which it has changed in the past, are clearly important parameters of any dynamical model, though we have only considered one

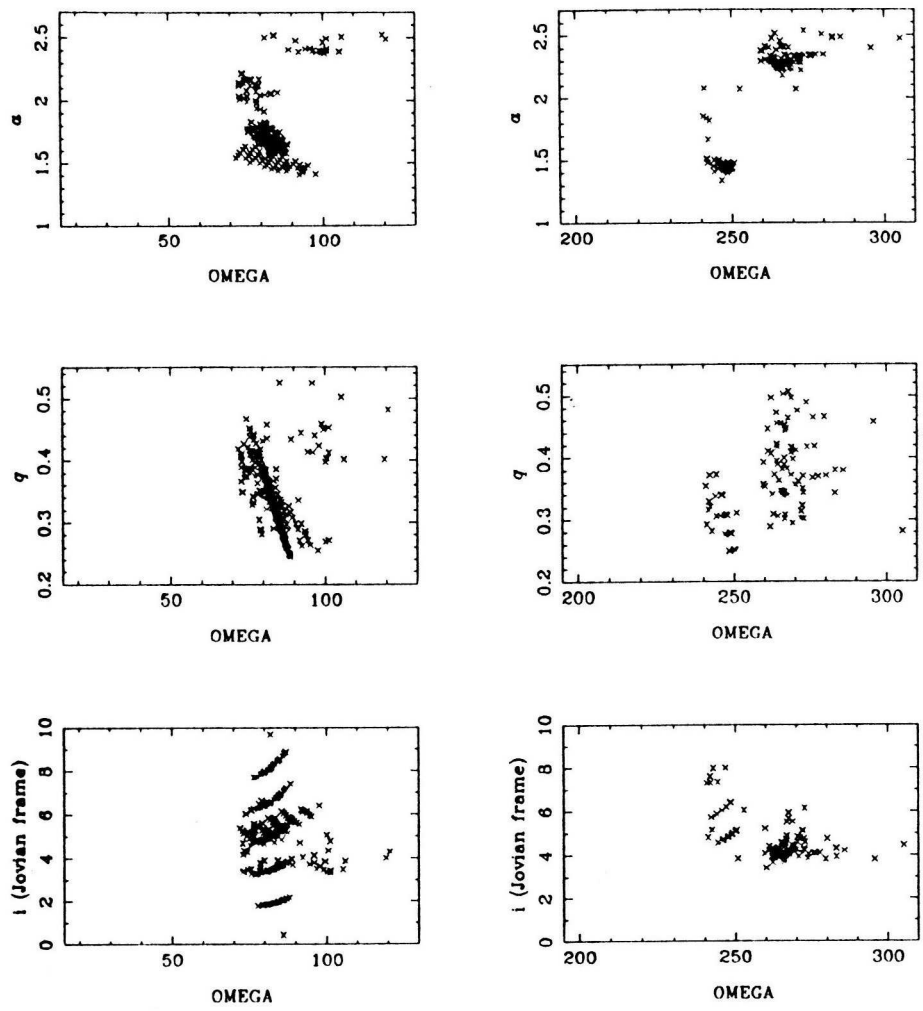

Figure 4.18: Plots of a, q & i against Ω for meteors in the northern and southern daytime branches of the Taurid stream, from the model in which particles are generated at asteroid belt fragmentations of large components that have split from the parent object at perihelion; *cf.* Figures 4.7 & 4.13.

possible parent in this study.

We briefly mention the fact that various meteoroids were generated in the models that precessed very quickly so that at the present epoch they did not have longitudes that would place them in the Taurid Complex core. This was despite the cut-off in ejection velocity that had been imposed to stop particles with $a \gtrsim 2.5$ AU being produced. In a possible future investigation we could search the meteor data for meteoroids that have been dispersed into the broad sporadic stream (Štohl 1986), and although patterns in orbital elements would be less clear than in the more structured Taurid stream, we may still hope to draw conclusions from dynamical modelling. The existence of the broad sporadic stream (and the background zodiacal

cloud beyond) could be due both to a longer timescale of formation and to orbits that precess rapidly. This would be a valuable future study, given the importance of the broad sporadic stream, derived from the Taurid progenitor, in the inner Solar System.

To summarise, the observed (a, e) distribution leads us to favour a mechanism of ejection near perihelion, and also a timescale that is not so long that large-a orbits decrease too much in e owing to Jovian perturbations. The observed range in Ω, though, imposes a lower limit on the timescale of formation of the core of the Taurid Complex, and the past $\sim$10 kyr seems the best estimate for this timescale. However, a model in which meteoroids are produced exclusively at perihelion, while essentially producing the correct range and broad trends in elements, fails to give sufficient scatter. A further dispersive mechanism is required and this is plausibly the catastrophic fragmentation in the asteroid belt of large cometary fragments that have originally split from the parent object near perihelion. We move now to a discussion of whether regular splitting followed by collisional fragmentation is realistic, and also consider other possible mechanisms for dispersing the stream.

4.2.3 Causes for velocity dispersion

The range in a present in observed Taurid meteors corresponds to a velocity dispersion at perihelion of up to $\sim$3 km/s. The question is how relative speeds of this magnitude arise, both for photographic meteors (corresponding to particles $\sim$1 cm across) and radar meteors (corresponding to $\sim$1 mm meteoroids). It cannot be due to normal cometary activity near perihelion as modelled by Whipple (1951); even for a giant comet nucleus ($\sim$100 km across) with a very small perihelion distance ($<$0.1 AU) the expected ejection velocities are under 0.1 km/s for these sizes of meteoroid. The jet effect due to mass loss from meteoroids soon after they are ejected could produce a certain amount of velocity dispersion (see Steel *et al.* 1991a), though this would happen mainly near perihelion. Our investigation has shown that some dispersive mechanism is required that does not act exclusively near perihelion.

In fact, we have shown that many aspects of the orbital element distributions of Taurids are well explained provided that two processes regularly occur — the splitting of large fragments from the parent body near perihelion, and disruption of many of these large fragments in the asteroid belt. With regard to each process, two questions arise — that of the frequency with which we may expect such events to occur, and whether, if they do occur, they are likely to produce the required velocity dispersion amongst the resultant meteoroids.

A sizable fraction of known comets have been observed to split and the heliocentric distances at which this happens are indicative of solar radiation or the tidal action of the Sun being the cause (Pittich 1972). (The tidal action of Jupiter may also be significant but this is less relevant for the Taurid progenitor since it does not pass within the Jovian sphere of influence.) Although the splitting takes place near perihelion, it could be that it is sometimes brought on as a result of recent (non-catastrophic) collisions with small objects in the asteroid belt, through a mechanism of cratering revealing new volatile material and the consequent localised increase in cometary activity during the next perihelion passage causing large pieces to split from the very fragile comet (see Babadzhanov *et al.*'s (1991) discussion of Comet P/Biela).

Frequent splitting at perihelion of large fragments from the giant comet Taurid parent therefore seems plausible, but relative velocities of 1–2 km/s for large (discussion of the actual size follows shortly) fragments are not realistic. It is preferable to appeal to a cometary non-gravitational force acting on each of the fragments, or, if the volatiles present cannot be responsible for the entire change in orbit, one may appeal to "hierarchical fragmentation" whereby splitting does not occur from the parent object during a single perihelion passage but rather large fragments themselves split and give rise to new fragments during further perihelion passages.

Turning to processes in the asteroid belt, we used ejection velocities from the cometary body in each collision up to 1.5 km/s, comparable to those invoked by Whipple & Hamid (1952). We need velocities of this order to produce the observed scatter in Taurid meteor orbital elements. Current estimates of velocities to be expected as the result of collisions tend to rely on extrapolations of laboratory experiments by many orders of magnitude in the mass of the objects involved, and while scaling-law predictions can be compared (Fujiwara *et al.* 1989) with size distributions and orbital elements in asteroid families, which are believed to be collision products, the results of impacts on much more weakly constituted cometary bodies cannot be known for certain. Values as great as 1.5 km/s for the highest speed ejecta could no doubt occur if the impacting body were large enough. We can certainly derive one straightforward constraint on ejection velocities, depending on the mass of the impactor, from kinetic energy considerations; an impact speed of $\sim$30 km/s in the frame of the cometary fragment is expected. An rms ejection velocity of 1 km/s would then require the impacting body to have mass 10^{-3} that of the cometary fragment so that, *e.g.*, we require a 1 km object to have an encounter with a 100 m object. Let us assume that catastrophic disruption of the cometary body

will occur (this seems likely for fragments of the highly evolved and fragile Taurid progenitor) and furthermore that the desired ejection speeds can be achieved, and proceed to a few simple calculations of how often we expect one of the proposed cometary fragments to encounter an asteroid of $\frac{1}{1000}$ its mass. The best estimates of energy partitioning suggest that the proportion of impact kinetic energy going into motion of ejecta may be an order of magnitude down on the upper limit we have assumed (see Fujiwara *et al.* 1989), but these calculations are very rough and in any case it may be that slightly lower speeds (several hundred m/s, say) are just sufficient to fit the meteor data.

The question, then, is whether the large cometary fragments that we consider to be products of splitting can undergo total disruption, due to impacts with sufficiently large asteroidal objects, on short enough timescales, *i.e.* whether the expected lifetime is at most a few 10^4 yr, so that a significant proportion will undergo such disintegration during the timescale of evolution of the Taurid Complex. Calculations of paths of objects through space show that the timescale for a 1 km object with a, e and i typical of Taurids to hit a smaller object moving on a typical asteroid belt orbit is of the order of 10^{17} yr (Wetherill 1967). Next, we need to know how many asteroids of size, say, 100 m (mass $\sim 10^9$ kg) there are. The collisional lifetime of the few largest asteroids is of the order of the age of the Solar System, but the remainder of the asteroid belt is probably in collisional equilibrium. We use the following expression from the collisional model of Dohnanyi (1969):

$$N(m)\,dm \approx 2.6 \times 10^{16}\, m^{-1.837}\, dm$$

for the number N of asteroids with mass in the interval $(m, m + dm)$; m is in kg. Therefore the total number of asteroids with mass greater than m is about $3{\times}10^{16} m^{-0.837}$, *i.e.* $\sim 10^9$ asteroids with $m > 10^9$ kg, leading to a collision time for a Taurid fragment of $\sim 10^8$ yr. This is much too large. Reducing the size of the Taurid fragment to 1 m and the asteroidal body to 10 cm, we have $\sim 10^{7.5}$ as many asteroids but the cross-section for impact down by 10^6 so that the timescale is reduced by $10^{1.5}$.

The discrepancy in required timescale is still one or two orders of magnitude, but my attitude to this is that at least it is not the age of the Universe, and the various approximations probably allow the true answer to differ by quite a large factor. For example Ishida *et al.* (1984) showed observationally that the size distribution of main-belt asteroids is bottom-heavy at sizes of $\sim$1 km and we really cannot be sure of the number of, say, 10 cm or 1 m asteroids. Also, explosive energy arising

from compression due to the impactors would lead to a smaller impactor for a given size parent inducing velocities ∼1 km/s. It is further worth considering the possibility that the orbital element dispersion is not introduced during *single* asteroid belt fragmentations of perihelion splitting products but that there are significant contributions, which individually provide a smaller velocity dispersion, from *successive* impacts (*cf.* discussion of hierarchical splitting above); this could well reconcile the requirements of the modelling with the theoretical considerations. The intention here has not been to prove that we definitely expect the various processes to occur as desired, since there have been quite a few assumptions made. Rather, we have shown that perihelion splitting and asteroid belt destruction of the resulting fragments of the fragile, evolved giant comet are not unrealistic expectations within the constraints of the theoretical uncertainties. The positive evidence for these processes is the conclusion of Section 4.2.2 that catastrophic disruption of fragments of the Taurid parent provides a good explanation for the observed meteor data. It does appear that asteroidal impacts on cometary bodies with dramatic effects are not exceedingly rare, *e.g.* the recent outburst of Comet P/Halley was quite possibly due to such an event (Hughes 1991).

Our physical model appears plausible, but it is now worth discussing another important matter, that of radiative forces. This may be particularly relevant given that we saw a difference between orbital elements of optical and radar meteors, which correspond to meteoroids of different sizes.

Mass segregration has been observed in various meteor streams. It can be due to radiative forces, to larger ejection velocities during normal cometary activity for smaller particles and perhaps to the mass distribution of ejected particles changing as the comet nucleus evolves physically, during which time the comet's orbit may change (see Hughes *et al.*'s (1981) investigation into the Quadrantids). Fox *et al.*'s (1983) model in which meteoroids of different sizes had differing ejection velocities went some way to explaining the rate profile of the Geminids, though as we have noted a model involving only normal cometary activity (as modelled quantitatively by Whipple 1951) followed by differential gravitational perturbations cannot reproduce the characteristics of the Taurids since the velocity dispersion required is much too high.

Considering the Taurids, for the night-time meteors we selected in Section 4.1.4, we have the following mean values of a: 2.05 and 1.90 AU for the optical Nn and Sn branches, 1.78 and 1.81 for the radar. The single main concentration at a=2.25 in the optical Nn branch leads to the mean a being higher than in the optical Sn

branch. There may be significant selection effects for the radar detections relating to when the instruments were operated, but for the moment it seems reasonable to accept a typical difference in a of $\sim$0.1 AU between meteors of the two size ranges. It is encouraging that if we solve (numerically) the expressions, given by Wyatt & Whipple (1950), for the rates of change of a and e for particles whose motion is altered by the Poynting-Robertson effect, then we do find that timescales of the order of 10 kyr cause a decrease in a of 0.1 AU for particles 1 mm across with density 0.5 g/cm^3 moving on Taurid orbits.

Olsson-Steel (1987c) explained the dispersion of the Geminids by a combination of radiative effects, most importantly the Yarkovsky-Radzievskii effect on rapidly spinning meteoroids. Similar forces could well act on the Taurids and would certainly help to produce the substantial velocity dispersion required at perihelion, but these effects change the aphelion distance much more than the perihelion distance. It does seem that some process at larger heliocentric distances is required in the Taurids, and the most likely explanation remains catastrophic disruption in the asteroid belt.

4.3 Mass of the Taurid Complex from meteor observations

In calculating meteoroid stream masses, Hughes & McBride (1989) regard the mass influx (in the form of meteors) to the Earth as the most difficult quantity to estimate, the uncertainty possibly being as much as a factor of 10, owing to problems in determining both the ionisation efficiency (needed to derive the meteoroid mass from a meteor observation) and the mass distribution. The major remaining uncertainty is the stream cross-section; for this parameter the dynamical models we have been constructing of the Taurid stream are of use. Of course, while an improvement on existing estimates will be possible because of the more detailed knowledge of the stream cross-section, we shall still have to accept a considerable possible remaining error.

The mass of the proposed resonant swarm in the Taurid stream was estimated (from the influx to the Moon as measured by lunar seismometers) in Section 3.2.4. One significant difference from that calculation is that here we assume that meteoroids are evenly spread around the orbit (as opposed to being concentrated for the most part in $<\frac{1}{4}$ of the orbit). The other difference is in the extent of the cross-section. Figure 4.19 shows the pre-perihelion cross-section for the Taurid stream as studied in this chapter. We use the model from Section 4.2.2 where particles were

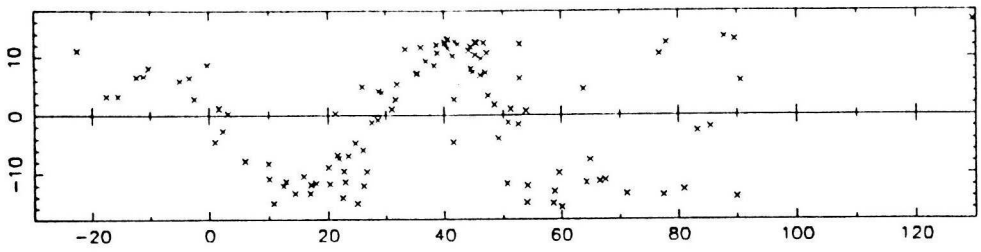

Figure 4.19: Cross-section (at r=1 AU) of the night-time Taurids, from the model (see Section 4.2.2; we are here using the set of integrations where Jupiter precessed) where particles are ejected at perihelion over the past 10 kyr. The x-axis is degrees longitude, the y-axis latitude.

ejected at perihelion over the past 10 kyr. We do not include the particles generated at asteroid belt fragmentations as the fragmentations were specifically to produce meteoroids that intersected the Earth's orbit in the present epoch — this would give rise to false concentrations in the cross-sectional plot.

All values of ω are present in our model Taurid stream; indeed differential precession of well over one revolution has occurred. In contrast, in the swarm model of Chapter 3, little over half a cycle of possible ω-values was present. There are even more restricted ranges of ω in the Quadrantids (Murray *et al.* 1980) and the Geminids (Fox *et al.* 1983), for although these streams may be sufficiently dispersed in ω to give rise to more than one shower (Babadzhanov & Obrubov 1987), there is no question that meteoroids are highly concentrated in orbits similar to that of the parent object (Asteroid 3200 Phaethon for the Geminids, but not known with absolute certainty in the case of the Quadrantids). This has limited the cross-section so that the streams were only first detected as highly active showers last century, as the streams began to be swept across the Earth's orbit. A further example is the Halleyids, where substantial ω-mixing has taken place, but where the majority of meteoroids are quite possibly on orbits that librate in ω between limited values (McIntosh & Hajduk 1983).

Considering the estimation of cross-sections, on the one hand there is an advantage with the Geminids and Quadrantids in that the dates of the first recorded observations of the showers give a measurement of an edge of the cross-section. On the other hand, in the Halleyids and the Taurids there is the advantage that we definitely have more than one cross-section through the stream and good dynamical models should be able to tell us what is to be expected at the intermediate values of ω, which cannot be observed from the Earth. Of course, we cannot be absolutely sure of the strength of the concentration of meteoroids near the parent object if the

parent is well displaced from having a nodal intersection with the Earth's orbit.

Conventionally, one defines the equivalent transit width of a stream as the time for which it would have to last at maximum activity for the Earth to pass through it and collect the same amount of meteoroidal influx that the Earth actually does collect, but during a longer time and with a varying activity profile. One then assumes a cross-section for the stream which is symmetric above and below the ecliptic and circular across the stream orbit, but through which the Earth will in general pass at an angle, the length of the Earth's path being taken as equal to the transit width. Štohl (1987) found an equivalent transit width for the Taurids of 25 days and thence estimated the mass of the Taurid stream, doubling it because of the broad sporadic stream into which the Taurids gradually disperse. He reached figures for the more structured stream of 1.6×10^{16} g and for the whole complex of 3×10^{16} g (between limiting masses of 10^{-6} and 10^{6} g). We shall use his calculation of the mass influx; however, we shall see if our dynamical model leads to a different result through its prediction of the likely cross-section.

Figure 4.19 can be used to estimate the cross-section. Alternatively the secular perturbation theory of Brouwer (1947) that we described in Chapter 2 gives a neat way of performing certain calculations provided that it is acceptable to assume that the stream is sufficiently old that complete randomisation of ω has occurred. We proceed for the moment along these lines. We accept Štohl's calculation from observations of the mass influx (4.7×10^{8} g per passage; this corresponds to 25 days at maximum activity) each year for the Earth's October–November passage through the structured Taurid stream, *i.e.* we accept the calculation of the transit width from the *horizontal* distribution of points in the cross-section (which corresponds to the meteor activity profile). We consider the *vertical* distribution of points in the cross-section; we note in Figure 4.19 a tendency for the density of points to be greater away from than near the ecliptic. This is because precessing orbits spend most of their time at values of ω that keep them away from the ecliptic at r=1 AU (see Section 4.1.3). Brouwer's theory may be employed to quantify the proportion of time for which the points in the r=1 cross-section are near the ecliptic.

For time t scaled suitably, we have

$$t = \tan^{-1}\left(\sqrt{\frac{A+B}{A-B}}\tan\omega\right)$$

where A and B are functions of a, e and i (the i-dependence is not strong) as described in Chapter 2. As ω varies between $-\frac{\pi}{2}$ and $\frac{\pi}{2}$ radians, t also varies between $-\frac{\pi}{2}$ and $\frac{\pi}{2}$ so that the average rate of change of ω with t is 1 (with t in these units).

Instantaneously, the rate of change of ω with t is

$$\frac{d\omega}{dt} = \left(\frac{dt}{d\omega}\right)^{-1} = \sqrt{\frac{A-B}{A+B}}\cos^2\omega\left(1+\frac{A+B}{A-B}\tan^2\omega\right)$$

We are interested in $\frac{d\omega}{dt}$ when ω takes the values that correspond to the orbit intersecting the Earth's orbit, *viz.* $\cos^{-1}([a(1-e^2)-1]/e)$ (Section 4.1.3). Performing the numerical calculations, we find that at these values of ω, the rate of change of ω with time is a factor of 2–4 above the long-term average (2 for smaller Taurid orbits, 4 for larger). We shall adopt a factor of 3, noting that the approximations here no doubt make it valid to neglect the rotation between ecliptic and Jovian coordinates, the Earth-intersecting values of ω being calculated in the former frame and Brouwer's theory applying in the latter.

When we displace ω by a small amount $\Delta\omega$ from its Earth-intersecting value, we induce a small change in vertical displacement from the ecliptic at r=1 given by

$$\Delta z = \Delta\omega \sin i$$

so that if the stream was spread out vertically at r=1 with its density uniform and equal to the density at z=0, the vertical spread would be $3\pi\sin i$, the factor π appearing because the points maximally displaced above and below the ecliptic have ω differing by π radians and the factor 3 appearing since we have just shown that the density of points at z=0 is $\frac{1}{3}$ what it would be if all values of ω were equally likely. Taking $\sin i = 0.1$, the vertical spread is $\sim$1 AU ($\frac{1}{2}$ AU above and below the ecliptic). The spread is $\pm\frac{1}{6}$ AU or so assuming the circular cross-section and so, based on the variation of density of points in the cross-section with vertical distance, Štohl's mass estimates should be multiplied by 3. Thus we obtain the values $\sim 5\times10^{16}$ g for the core of the stream and $\sim 10^{17}$ g for the Štohl (1984, 1986) sporadic stream. If there are concentrations near the parent away from the ecliptic (*e.g.* see above the ecliptic at longitude 40° in Figure 4.19) then perhaps doubling these quantities would be reasonable, giving $\sim 10^{17}$ g and $\sim 2\times10^{17}$ g.

For reference we quote Hughes & McBride's (1989) values of 1.3×10^{15} g for the Quadrantid stream, 3.1×10^{17} g for the Perseids, 3.3×10^{16} g for the Halleyids and 1.6×10^{16} g for the Geminids. Each of these increased the answer by a factor of 10 (*cf.* the factor of 3, plausibly doubled to 6, that we have just used for the Taurids) to allow for the fact that to assume that the Earth passes through the centre of a circular cross-section is probably not entirely realistic. Factors of $\sim$10 have been shown, from dynamical modelling, to be reasonable in particular for the Halleyids,

with a cross-section elongated in a direction roughly perpendicular to the ecliptic (McIntosh & Hajduk 1983), and Geminids (Fox *et al.* 1983).

Štohl's (1987) calculation was between limits of 10^{-6} and 10^{6} g in the mass function, this reaching a peak at particles of size $8{\times}10^{-3}$ g, the differential mass indices being 1.9 and 2.2 respectively below and above this particle size. Štohl's mass function is in general accord with those expected for meteor streams, with the mass concentrated in the intermediate sized particles (Hughes 1978). The contribution from smaller particles is unlikely to be significant; we need only go a few orders of magnitude below 10^{-6} g before meteoroids will be quickly removed from the stream by radiation pressure. On the other hand, it could be that the nature of the Taurid progenitor causes many large masses (frequent perihelion-splitting fragments, as opposed to only smaller meteoroids lost during normal cometary activity) to be present in the Taurid Complex. The presence of large objects in the Taurid/sporadic complex is supported by the orbital distribution of sporadic fireballs, which tend to have semi-major axes and aphelia typical of Taurid orbits (see Dohnanyi 1978).

In fact the above mass function, for meteor-sized particles, definitely does not extend to larger objects in the Taurid Complex. Using the above values, and normalising to a total mass of 10^{17} g between 10^{-6} and 10^{6} g, some straightforward algebra leads to a figure of just 10^{15} g in masses $>10^{6}$ g, and no km-sized asteroids, even though some are known, and no doubt many remain to be discovered. Clearly, further considerations are necessary.

The timescale for a single object to strike the Earth is $\sim 10^{8}$ yr (either from theory — see Öpik 1976 — or from the mass influx of Taurids to the Earth as a fraction of the total calculated mass in the stream) so that number counts of incoming large meteoroids can in theory yield information on the total number in the stream. However, the single-number statistics of the Tunguska object ($\sim 10^{11}$ g) and the Bruno crater object ($\sim 10^{15}$ g; Clube & Napier 1990, Chapter 11) make this difficult in practice. Statistically useful numbers may be derived from cratering data and one Tunguska event per century is consistent with the long-term cratering flux (Shoemaker 1983). However, there is reason to believe that the present rate, due to the Taurid progenitor, is substantially above the average (Clube & Napier 1990); overall there may be well over 10^{6} objects of mass $>10^{11}$ g in the Taurid stream. There are probably under 10^{2} asteroids of mass $>10^{15}$ g (Section 4.4) so that at larger masses the distribution may be bottom heavy, with $\lesssim 10^{17}$ g per logarithmic mass interval for km-sized asteroids, but substantially more at Tunguska levels. As a reasonable estimate, in the Taurid stream we expect a few 10^{18} g in km-sized

asteroids and below, with a parent object (or cluster of objects; Section 5.2.4) of mass 10^{19} g perhaps still present at the core of the stream (Clube & Napier 1984). A devolatilised parent of this size having supplied meteoroids to the zodiacal complex for the past 10 kyr is consistent with the 10^{14-15} g/yr required by Grün *et al.*'s (1985) steady-state collisional model. The rate of meteoroid production need not have been constant throughout, *e.g.* it could have varied cyclically with period 200 yr, say, through the mechanism described in Section 3.4.

In Section 3.2.4 we estimated the mass of the proposed resonant Taurid swarm to be possibly something approaching 10^{18} g and a somewhat larger figure for the Taurid/sporadic stream as a whole now appears plausible. We envisage a picture of the now devolatilised Taurid parent feeding both the resonant swarm (low-velocity ejecta) and the core part of the Taurid stream. Loss of particles from the swarm also feeds the stream. The next stage in the dynamical evolution is for the structured Taurid stream (which broadly speaking produces meteors classified as Taurids) to disperse into the broad sporadic stream surrounding the Taurids and then for the sporadic stream to disperse into the background zodiacal cloud when collisions, and radiative forces on the resultant smaller particles, start to have a significant effect. The mass of the zodiacal cloud (Section 1.1.2) is probably several 10^{19} g in masses up to 10^{6} g (of course this is unlikely to extend to larger masses in the same way as for the Taurid stream since it is smaller meteoroids that are more easily dispersed dynamically), most of the mass of the original giant comet probably being lost in its initial active comet phase and these meteoroids now being dispersed into the zodiacal cloud. An original giant comet size of 100 km, as suggested by Clube & Napier (1984) seems possible, if one allows for the loss from the Solar System altogether of the smallest particles under radiation pressure (collisions gradually reducing the meteoroidal sizes present).

4.4 Taurid Apollos

We have investigated the structure of the Taurid Complex as determined from meteor observations. It is interesting to consider whether, in the population of Earth-crossing asteroids, there is a statistically significant number aligned with the Taurid stream. These would be expected to be "cometary" asteroids (Sections 1.2.1, 1.2.2).

Drummond (1991), using both the D-criterion as defined by Southworth & Hawkins (1963) and as modified by himself (1981), analysed orbital similarities amongst 139 asteroids with perihelion distance q below 1.3 AU that were discovered

before mid-1990. He demonstrated the existence of three "asteroid streams" containing 5, 5 and 4 asteroids respectively, all three of which had $q \approx 1$, eccentricity $\approx$ 0.5 and low inclination but which had widely differing longitudes of perihelion. No stream on a Taurid-like orbit was identified. One reason for this is that the Taurids are dispersed by several tens of degrees in longitude, *i.e.* assuming the D-criterion includes a longitude-dependent term, a significantly higher value of D would be required to identify a related set of Taurid orbits than to find many other asteroid streams (*cf.* discussion of meteors in Section 4.1.2).

I have investigated the orbits of 181 asteroids with q up to 1.33 AU (available from E. Helin), discovered before August 1991. If we selected asteroids on the basis of some kind of D-criterion similarity to Taurid meteors, but with longitude not being included in the basis for selection, the question arises as to whether there would be a tendency for the resultant longitudes to be aligned with the Taurids.

Therefore let us calculate the quantity D for all the asteroids, defined by

$$D^2 = (q_1 - q_2)^2 + (e_1 - e_2)^2 + \left(2 \sin \frac{i_1 - i_2}{2}\right)^2$$

with the reference values $q_1 = 0.375$ AU, $e_1 = 0.82$ and $i_1 = 4°$, as in Section 4.1.2 with Taurid meteors. However, unlike with the meteors, whose angular elements satisfy the condition such that the orbits intersect that of the Earth, we shall not take i as the present-day value of i, since we are looking for groups of asteroids that are related but that have nevertheless undergone separate orbital evolution for several kyr, so that they may all be anywhere within their overall range of oscillation in i. We shall use Brouwer's (1947) secular perturbation theory (Section 2.2.1), which describes how angular elements evolve over time, and convert i to its long-term minimum value, referred to the plane of Jupiter's orbit. This secular theory breaks down for Jupiter-crossing orbits and so we shall exclude 4 asteroids, leaving 177.

The 20 asteroids with the smallest values of D are shown in Table 4.3. $\Delta\varpi$ is the difference between the asteroid's longitude of perihelion and 140°, the approximate value at the centre of the Taurid stream as defined by meteors. We may calculate probabilities that, out of the n asteroids with the smallest values of D, m of them would by chance be within a certain angle of 140°. Assuming a uniform distribution in ϖ, various probabilities are shown in Table 4.4. We see, *e.g.*, that the probability that 6 of the first 10 asteroids would by chance be within ±40° of ϖ=140° is only 1%. Interestingly, ±40° fairly well covers the range of the Taurid stream as defined by meteors.

Of the 6 asteroids, 1984 KB, 1982 TA and Oljato have been previously recognised

	a	e	i	Ω	ω	$\mid \Delta\varpi \mid$	i_J	D
2212 Hephaistos	2.16	0.84	12	28	208	96.1	7.0	0.058
2101 Adonis	1.87	0.76	1	351	42	107.7	2.1	0.094
1991 AQ	2.16	0.77	3	342	240	81.7	3.9	0.134
1984 KB	2.22	0.76	5	169	336	5.7	3.2	0.159
1990 SM	2.16	0.78	12	137	106	103.2	10.4	0.163
4197 1982 TA	2.30	0.77	12	10	119	11.3	10.3	0.189
1566 Icarus	1.08	0.83	23	87	31	21.3	13.3	0.249
4341 Poseidon	1.84	0.68	12	108	15	17.0	5.7	0.258
1990 UO	1.23	0.76	29	205	333	38.0	18.5	0.271
2201 Oljato	2.18	0.71	3	76	96	32.2	1.3	0.280
1991 AM	1.70	0.70	30	125	153	137.5	18.3	0.312
1937 UB Hermes	1.64	0.62	6	35	91	14.0	5.7	0.313
3200 Phaethon	1.27	0.89	22	265	322	86.7	15.6	0.319
4450 Pan	1.44	0.59	6	312	291	102.9	6.2	0.324
1987 OA	1.50	0.60	9	180	235	84.9	7.5	0.328
1991 GO	1.96	0.66	10	24	89	27.1	9.4	0.341
1991 CB1	1.69	0.62	16	317	347	164.0	9.8	0.344
1989 VA	0.73	0.59	29	625	3	127.8	18.4	0.346
1864 Daedalus	1.46	0.61	22	6	325	168.5	15.9	0.347
1991 BA	2.24	0.68	2	118	71	48.9	0.6	0.370

Table 4.3: Asteroids with similar q, e and i to Taurid meteors. i_J is the minimum value of the inclination during the asteroid's long-term precession, referred to Jupiter's orbit.

	n=5		n=10		n=15		n=20		n=25		n=30	
$\mid \Delta\varpi \mid$	m	p	m	p	m	p	m	p	m	p	m	p
20.0	1	0.445	3	0.091	4	0.076	4	0.175	4	0.300	4	0.431
40.0	1	0.715	6	0.011	7	0.031	8	0.057	9	0.083	10	0.110
60.0	1	0.868	6	0.077	7	0.203	9	0.191	10	0.304	12	0.276
80.0	1	0.947	6	0.250	7	0.530	9	0.566	10	0.740	13	0.618
100.0	3	0.603	8	0.106	11	0.129	13	0.268	14	0.565	17	0.527

Table 4.4: Out of the n asteroids with smallest D-values, the number m with $\mid \Delta\varpi \mid$ within the limit shown, and the probability p that m or more out of n would be within this range of ϖ by chance.

as being members of the Taurid Complex (Clube & Napier 1984). The case for Poseidon also appears strong, but the orbits of Icarus and 1990 UO are rather small. The association of such small asteroid orbits with the Taurid Complex is uncertain and we shall exclude them for the moment. We then have a probability of 8% that 4 out of 8 asteroids would by chance be within $\pm 40^\circ$ of ϖ=140°. However, we point out that the alignment of Hephaistos, 1991 AQ and 1990 SM appears quite

remarkable, and these 3 asteroids could well be related to each other, even if not to the Taurid Complex. If they constitute an independent asteroid stream, perhaps derived from the previous giant comet (see below), then we have 4 out of 5 asteroids aligned with the Taurid Complex within $\pm 40^\circ$ and the probability of this happening by chance is only 1%.

The evidence for the Taurid Complex contributing to the population of Earth-crossing asteroids appears compelling, especially when we realise that Asteroid 5025 P-L is probably associated with the Taurids (Olsson-Steel 1987a), though it was not included in the above calculations because it is Jupiter-crossing. Furthermore, another asteroid associated with the Taurid Complex, 1991 TB2, has very recently been discovered (Steel 1992).

Since there are several known Taurid asteroids, the question arises whether it is possible to find any trends in the orbital elements, in particular whether the orbits that we expect to precess more rapidly are found at larger longitudes. We shall consider the asteroids we have already mentioned, and also from Table 4.3 we shall select Hermes, 1991 GO and 1991 BA since they are the best aligned with the Taurid stream. Given Hermes' low e of 0.62, its association with the Taurid Complex is perhaps more questionable than that of the remaining asteroids, but we shall leave it in for the time being. The full list of asteroids is in Table 4.5. Their orbits projected on to the ecliptic were illustrated in Section 1.1.1.

	a	e	q	i	Ω	ω	ϖ	H	Relative $\dot{\varpi}$
1991 GO	1.96	0.66	0.66	10	24	89	113	19.0	5.6
Poseidon	1.84	0.68	0.59	12	108	15	123	15.7	4.7
Hermes	1.64	0.62	0.62	6	35	91	126	19.0	3.9
1982 TA	2.30	0.77	0.52	12	10	119	129	14.9	8.5
1991 TB2	2.40	0.84	0.39	9	296	196	132	$\sim$19.5	9.9
1984 KB	2.22	0.76	0.53	5	169	336	146	15.5	7.8
5025 P-L	4.20	0.90	0.44	6	356	150	146	15.9	-
Oljato	2.18	0.71	0.63	3	76	96	172	15.4	7.6
1991 BA	2.24	0.68	0.71	2	118	71	189	28.5	8.5

Table 4.5: Asteroids probably derived from the Taurid progenitor.

One or two trial integrations of 5025 P-L, taking account of Jupiter and Saturn, show the orbit to undergo fairly drastic perturbations on timescales of several kyr, and indeed perturbations to a of several tenths of an AU even on much shorter timescales. Its value of ϖ appears to increase going back in time, contrary to the usual behaviour of Taurid orbits, though there is no reason for it to obey rules

of orbital evolution for Taurids given its Jupiter-crossing nature. At any rate, it cannot be included in a general discussion of patterns in ϖ precession, but its very good alignment with the Taurids and small value of q relative to most of the other asteroids in Table 4.5 do suggest that it could have recently (in the past few kyr) split near perihelion from the Taurid progenitor. (The Taurid progenitor, to judge from the modelling of Chapter 3, has a smaller q than most of the asteroids in Table 4.5.)

Unknown changes to a through the action both of non-gravitational forces (the asteroids presumably being cometary in the past) and of the essentially random perturbations of the inner planets mean that the relative precession rates of the asteroids could have differed in the past (especially if any were captured into a strong Jovian resonance), so that we cannot expect an exact correlation of precession rate with present-day longitude. Nevertheless, for the 8 asteroids (not including 5025 P-L) the secular precession rates of ϖ calculated from Brouwer's (1947) theory are shown in the last column of Table 4.5, in units of degrees/kyr. The a-values in the Table suggest that the only asteroid on which there may be a non-negligible effect from a resonance is 1991 BA, from the 7:2 resonance; however, its orbit is uncertain (a in error by up to 2%) as, being one of the smallest asteroids ever observed, with a diameter of 5–10 m, it was only observed over an arc of a few hours, as it came to within a few hundred thousand km of the Earth (Scotti *et al.* 1991).

It is noticeable that the 3 asteroids at lowest ϖ have significantly lower precession rates than the remainder and although no pattern is apparent in the final 5 asteroids, the precession rates seem to add a little extra evidence to the already convincing picture of km-sized asteroids being a component of the Taurid Complex. Dispersion of the asteroids listed in Table 4.5 has probably taken place within the last $\sim$10 kyr.

Just as there appear to be meteors with Taurid-like elements observed at all longitudes (though obviously strongly concentrated towards the Taurid stream), it is possible that there are Apollo asteroids at widely dispersed longitudes that perhaps separated from the Taurid progenitor $\sim$20 kyr ago, but it is more difficult to identify these than the asteroids aligned with the more structured Taurid stream. We mention that Hephaistos, 1991 AQ and 1990 SM have ϖ precession rates of $\sim 7^\circ$/kyr, similar to those of the asteroids in Table 4.5, so that with their current (a, e) values it is difficult to associate them with the Taurid Complex, since they have ϖ-values $\sim 90^\circ$ greater than the central value for the Taurids. The suggestion of Clube & Napier (1984) that just as likely as a Taurid association was that Hephaistos was the remnant of a previous giant comet, despite its similarity in a, e, i to Comet Encke,

is supported by these precession rate figures. For reference, Encke has ϖ=160° and secular $\dot{\varpi}$=6.8°/kyr.

It is worth briefly considering the likely total number of Taurid asteroids of a given size. The diameters of Oljato, 1982 TA and 1984 KB are in the range 1–2 km (see McFadden *et al.* 1989) and the list of absolute visual magnitudes H in Table 4.5 suggests that Poseidon and 5025 P-L are comparable, with Hermes (though perhaps it is not a Taurid Complex member), 1991 GO and 1991 TB2 a few hundred metres across. The number still to be discovered is uncertain but there could be several times as many as the 5 listed here with diameter over 1 km, and perhaps even several hundred with diameter >500 m (see Helin & Shoemaker 1979, Steel 1992).

Note added in revision: I have recently found out (Marsden 1991, personal communication to D.I. Steel) that the orbit of 5025 P-L, being determined from a very short arc, is highly uncertain. It is therefore possible that its orbit is more similar than previously believed to those of other Taurid asteroids. Its aphelion distance could be as low as 3 AU.

Chapter 5

Miscellany

This chapter covers topics that did not fit anywhere else.

5.1 Dust bands

The high-frequency components of zodiacal dust detected by IRAS (the Infra-Red Astronomical Satellite) were dust trails and dust bands (Sykes 1988). The bands appear in pairs above and below the ecliptic and each pair is understood as being due to a family of orbits with similar inclinations, since a particle moving on an inclined orbit spends more of its time nearer the extreme latitudes than nearer the ecliptic (this is illustrated in Sykes & Greenberg 1986). The bands stretch around all longitudes because, though the family of orbits giving rise to them have similar inclinations, their nodal longitudes are well dispersed.

The bands have been understood as being due to material associated with asteroid families (Dermott *et al.* 1984), or debris from single random collisions between large asteroids (Sykes & Greenberg 1986). Alternatively, dust band latitudes being similar to inclinations typical of short-period comets, they could be the debris from a comet or family of comets with perihelion distance in the asteroid belt (Sykes *et al.* 1989), the thermal emission being dominated by the material that is closest to the Sun.

The dominant contribution to the zodiacal cloud of the Taurid progenitor giant comet has been one of the main points of this thesis and in this context we are bound to ask the question whether the bands can be understood as being associated with the Taurid Complex. This possibility was put forward by Clube & Asher (1990) and will be considered here.

Dispersed though Taurid orbits are, there is nevertheless a concentration towards preferred longitudes. I therefore thought it would be worth obtaining some IRAS

data to see what, if any, variations in longitude were detectable. We shall discuss firstly the IRAS data and then predicted spatial patterns of dust due to Taurid Complex material.

5.1.1 IRAS data

IRAS scans were done perpendicular to the ecliptic and the data I obtained from the Rutherford Appleton Laboratory have the infra-red flux added in half-degree bins in ecliptic latitude. The bulk of the emission at the 12, 25 and 60 μm wavelengths is due to the background zodiacal cloud and a method is needed to isolate the high-frequency (dust band) components. It can be done by subtracting flux from a background zodiacal emission model (*e.g.* Gautier *et al.* 1986) or by using Fourier methods (*e.g.* Dermott *et al.* 1986).

Trials with various techniques (especially trying various filters) showed the following to be a good method of isolating the bands, in particular the prominent band pair at about $\pm 10^\circ$ latitude — the γ-bands in the notation of Sykes (1988). It was not possible to isolate the α and β-bands (see Table 5.1) with the resolution of data available, but it is useful to concentrate on just the one band pair to see if there is any possibility of determining variation in longitude that could possibly be a signature of the Taurid Complex. In Figure 5.1 we see an IRAS scan, which then has

Band	Geocentric ecliptic latitude
α	$\pm$(0 to 2.5)
β	$\pm$(1 to 3.5)
γ	$\pm$(8.5 to 11.5)

Table 5.1: Latitudes of the brightest zodiacal bands, and notation used to label them (see Sykes 1988).

a cosine bell applied to it in order to diminish the emission due to a galactic dust component, seen especially in this particular scan at the higher latitudes, and also in order to eliminate the discontinuity between one edge of the scan and the other (noting that a function is effectively regarded as periodic when its discrete Fourier transform is calculated). Thus the cosine bell (by which the original scan is multiplied) falls to zero at the extremes of the scan but takes values close to unity near the centre, so that the zodiacal dust band components are not seriously affected. Next, the Fourier transform of the scan (with cosine bell applied) is calculated, and low frequencies are removed so that the band components are highlighted when the frequency function that has been high-pass filtered is transformed back into original

space. The effects of two filters are shown in Figure 5.1. The first filter removes

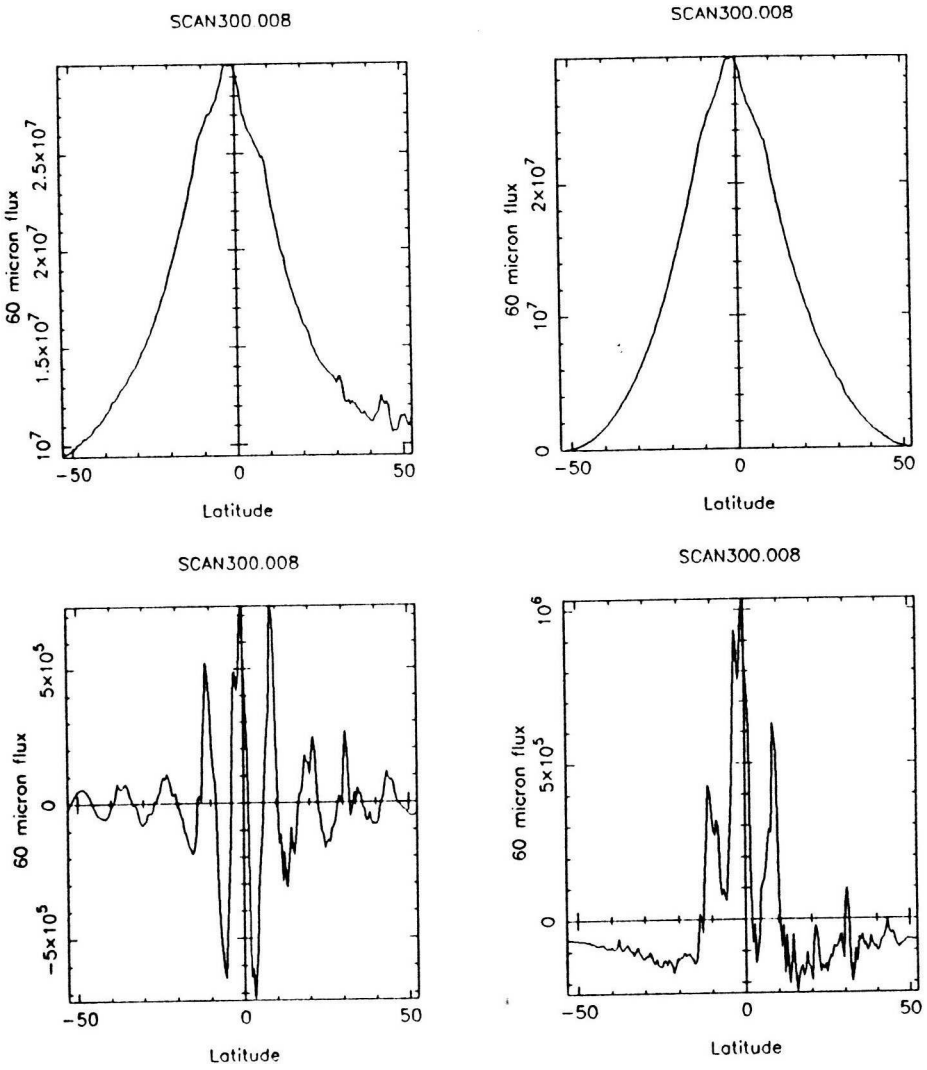

Figure 5.1: An IRAS scan — firstly the entire flux, then with a cosine bell applied. Then the residual flux after the scan has been high-pass filtered in transform space, firstly using a top-hat filter and then a Butterworth filter.

completely all frequencies up to a particular value (in this case the 8th frequency out of the ∼100 frequencies present in transform space, there being just over 200 points in the scan) and leaves all higher frequencies unaffected. This produces the rather unsatisfactory result shown, with the side-lobes being due to the sharp cut-off in the frequency domain (see, *e.g.*, Brigham 1974) and thus being an artefact of the filtering. The second filter illustrated here is the Butterworth filter (Gonzalez & Wintz 1977), where the Dth frequency is multiplied by

$$\frac{1}{1+(D_0/D)^2}$$

(in this example using D_0=9) and gives a preferable filtered scan, without the sidelobes.

The Butterworth filter was used to look at various scans, slight adjustments to D_0 being tried to see which value best isolated the γ-bands (the exact value is expected to depend on the band width, typically a few degrees). Experiments with artificially constructed scans, adding imaginary bands to a smooth background component, showed that, using these filtering methods, it was easier to make an accurate determination of band latitudes than amplitudes, as stated by Dermott *et al.* (1986).

The dust bands are in fact fairly uniform at all longitudes, with apparent differences in latitude only arising because of small variations in the viewing angle (solar elongation) of IRAS. Measurements of band latitudes in scans that I examined are listed in Table 5.2. I have only estimated the band latitudes to the nearest $\frac{1}{2}^\circ$, but

Date (1983)	Longitude	Solar elongation	Band latitudes	
5 May	130	86	10	–8
24 Jun	1	91	9	–11
10 Jul	200	92	$10\frac{1}{2}$	–9
10 Aug	40	$96\frac{1}{2}$	$8\frac{1}{2}$	–11
15 Nov	322	90	$8\frac{1}{2}$	$-10\frac{1}{2}$
15 Nov	151	$81\frac{1}{2}$	10	–8

Table 5.2: Dust band latitudes in various IRAS scans.

the decreased separation when the solar elongation decreases, even by these comparatively small amounts, is evident (the distance from observation point to bands increasing when the solar elongation angle of the viewing direction decreases). Overall shifts in the band latitudes by over a degree are because Jupiter's orbit is inclined at $\sim$1.3° to the ecliptic, and the band particles' dynamics is controlled by Jupiter.

It is possible to derive a heliocentric distance of the material that dominates the band emission based on the parallactic effect as the viewing angle changes. Gautier *et al.* (1986) give the distance as 2.3 AU. The important conclusion so far is that, a selection of scans at different longitudes having been examined, it appears difficult to find evidence for significant variation of derived heliocentric distance with longitude. Therefore although the low inclination of the Taurid stream suggested that the possibility of its association with the dust bands should certainly be considered, it may be that the uniformity with longitude of the bands precludes a direct Taurid Complex association. However, we shall now check this.

5.1.2 Expected dust emission

We generate model scans at fixed geocentric longitude (with solar elongations near 90° since this matches the IRAS observations) by spacing particles evenly in mean anomaly round families of orbits and adding the thermal infra-red flux emitted by all of them. For simplicity we use a Planck function, and the black-body temperature at the appropriate heliocentric distance. We let the family of orbits cover different (a, e) values. For each (a, e), we assume sufficient mixing of the argument of perihelion ω has taken place that we can use Brouwer's (1947) secular theory (see Chapter 2) to generate (i, ω) values covering the whole possible range; it is necessary to specify a single (i, ω) value and then all the other possible values follow. That is, we are assuming that the particles in the family of orbits have a common origin and will therefore have a common (i, ω) relationship. We here neglect the difference between Jupiter's orbit and the ecliptic; the present purpose is to get a general idea of under what circumstances latitude peaks in the emission arise. For the longitude of perihelion ϖ, in the case of the Taurid stream we clearly do not let it vary over the whole 360°. However, we first display an example of lower-eccentricity orbits — which, it is usually presumed, give rise to the bands — and we assume that all possible values of ϖ are possible. Therefore, since there is no preferred value of ϖ, the scan at 90° elongation angle will be the same at all times of year. Figure 5.2 shows such an example, where i has been chosen to give rough correspondence to the γ-bands.

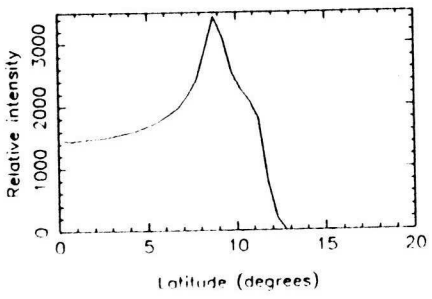

Figure 5.2: Model 25 μm flux, seen at solar elongation angle of 90°, due to particles with a from 3.1–3.4 AU and e=0.3, uniformly spread in longitude.

The free parameter of the proper inclination ("proper" means that long-term variation due to secular precession in ω has been taken account of; see, *e.g.*, Dermott *et al.* 1984) makes it easy to fit a north-south band pair at any latitude. We shall not go into modelling of fluxes in any more detail for the low-e case as it has received a lot of attention in the literature. Suffice to say that the most prominent

bands, which stretch around all longitudes, can be fitted by a family of orbits with the appropriate proper inclination, and perihelion distance of $\sim$2.3 AU, provided that they have had long enough for differential precession to spread Ω around all longitudes (Sykes & Greenberg 1986, and we discuss timescale in Section 5.1.3). An interesting question in the context of this work on the Taurids is what emission distribution may be expected to arise from a set of orbits that firstly has high e and secondly is concentrated towards preferred longitudes.

Thus we now see what patterns in thermal emission the Taurid stream is likely to give rise to. We use (a, e) values of (2.2,0.84), (2.0,0.81) and (1.8,0.78) with a minimum i of 4° (so that i ranges up to 11–14°). We take ϖ to be uniformly spaced between 80 & 200°, a reasonable choice for the broad sporadic stream surrounding the Taurids. (100 values of ϖ have been used for the results shown here, and, for both the Taurids and the low-e example above, we are using 100–200 (i, ω) values and 100–200 particles per orbit.) The elongation angle is held at 90°, to match IRAS (particles are in fact added between 87 & 93° in order to obtain a reasonable quantity). Figure 5.3 shows model scans for 8 observation points spaced equally round the Earth's orbit. For quite a significant proportion of the year the Taurid Complex is not within the field of view, looking at 90° elongation angle. During much of the remaining time, there is seen to be a peak at 4–5° in latitude above and below the plane of Jupiter's orbit. Though it cannot be seen from this Figure, this peak is in fact due to particles at larger heliocentric distance, *i.e.* for these high-eccentricity orbits the fact that particles spend so much time nearer aphelion overcomes the fact that they are at a lower temperature. This is in contrast to the case of low e, with all particles well outside the Earth's orbit, conventionally associated with the bands, where the combined effect of proximity to Earth and Sun more than compensates for the lower particle density (Dermott *et al.* 1984). Of course, the precise effect depends on the emission model for the particles, the one used here being a simplification.

The longitudes where this peak in emission due to the Taurid stream may be expected to appear range from a little below 300° through to somewhat above 0°. We cannot be sure whether infra-red flux due to the the Taurids was detectable in IRAS data, but the band pair labelled E & F by Sykes (1988) seems interesting; Sykes reports it as being at geocentric latitudes of $\sim$4–6° above and below the ecliptic, and best resolved between longitudes of 270 and 360°. It will be interesting if this band pair shows up in a future infra-red survey. However, we accept that the most prominent bands cannot be associated with the high-e, aligned orbits.

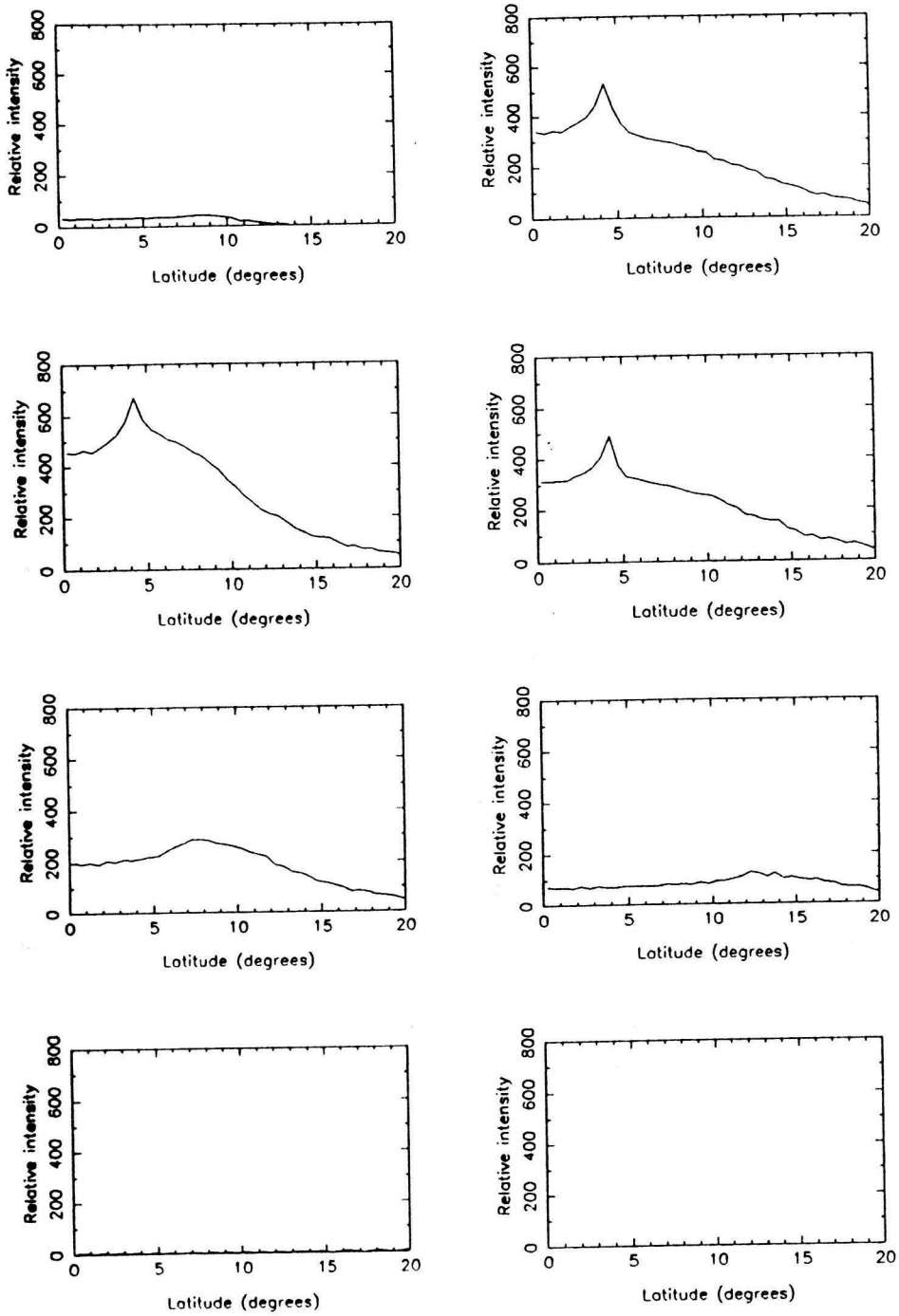

Figure 5.3: Model 25 μm flux, seen at solar elongation angle of 90° (looking in the apex direction), due to Taurid stream particles. The heliocentric longitudes of the Earth at the times of observation are 162.5, 207.5, 252.5, 297.5, 342.5, 27.5, 72.5, 117.5° (1st row is 162.5, 207.5, *etc.*) so that the longitudes of the viewing direction are 252.5, 297.5, 342.5, 27.5, 72.5, 117.5, 162.5, 207.5°.

5.1.3 A lower-eccentricity solution

The possibility that the bands could be due to the Taurid Complex essentially reduces to a question of timescale. There are mechanisms whereby material from

the Taurid progenitor could end up on lower-e orbits. Given the proposed history of the Taurid progenitor, with frequent collisions of large cometary fragments with asteroidal bodies in the main belt (Chapter 4), there is a possibility (Clube & Asher 1990) that when the complete disintegration of the cometary fragment occurs, some of the cometary material is ejected on to low-e orbits similar to that of the incident asteroid. Alternatively we can consider the question in terms of short-period comets in general since single giant comets may well be expected to give rise to many smaller comets (Section 1.2.1); that the dust bands could be associated with comets has often been mentioned in the literature but detailed attention has tended to focus on an asteroid belt origin. Either way, the timescale of evolution of the Taurid Complex being ∼20 kyr (Chapters 1, 4), the requirement is that nodal dispersion of the low-e orbits over all longitudes must occur within this time. The longitude dispersion is caused by the differential effect of Jovian perturbations on orbits of different sizes.

Sykes & Greenberg (1986) considered the mechanisms of ejection velocities during a collision between two asteroids, and differential Poynting-Robertson drag on particles of different sizes, causing a range in semi-major axis a within a family of orbits, and then used a secular perturbation method to calculate the timescales for resultant dispersion around all values of Ω. For example, for ejection velocities of 0.5 km/s, they calculated that the timescale for a band pair to spread around all longitudes is 10^5 yr if $a \sim 3.5$ and $\sim 4 \times 10^5$ yr if $a \sim 2.2$ AU. Naturally if there is to be any chance of reducing the timescale near that associated with the Taurids, we must concentrate consideration on the higher a-values.

Sykes & Greenberg's method of calculating differential Ω-precession follows the approach of Blitzer (1959), where the mass of the perturbing body is spread out in the appropriate way over its orbit. The approximations introduced because e and i are small are valid, but it turns out that if insufficient terms in powers of a are kept then the derived equations become invalid for a-values typical of the outer asteroid belt. Some tedious though straightforward algebra shows that the first 3 terms in the expression for the long-term average rate of change of Ω are

$$\overline{\dot{\Omega}} = -\frac{3}{4}\frac{GM_J a^{3/2}}{R_J^3\sqrt{GM_S}}\left(1 + \frac{15}{8}\frac{a^2}{R_J^2} + \frac{175}{64}\frac{a^4}{R_J^4} + \cdots\right)$$

with the differential $\overline{\dot{\Omega}}$ due to the difference in a being

$$\Delta\overline{\dot{\Omega}} = -\frac{9}{8}\frac{GM_J a^{3/2}}{R_J^3\sqrt{GM_S}}\left(1 + \frac{35}{8}\frac{a^2}{R_J^2} + \frac{5775}{576}\frac{a^4}{R_J^4} + \cdots\right)\frac{\Delta a}{a}$$

but the expression used in Sykes & Greenberg's calculations terminates after only 2 terms. Thus the larger is a, the more important it becomes to keep extra terms

if these expressions for secular perturbations are being used. I have checked results against those of Brouwer's (1947) theory (see Chapter 2) and found that inclusion of the third term increases the range of a over which agreement between the two theories is good, though it becomes clear that even more terms are needed as a is increased further. The two theories do in fact provide a good independent check on each other (at low eccentricities; only the Brouwer theory extends to high e).

Therefore for a-values typical of the outer asteroid belt the timescales, calculated from secular perturbations, for band formation quoted by Sykes & Greenberg are an overestimate by a factor of two, say. This still does not bring the timescale down to the level required if an association with the Taurids is to be possible, but there are certain families of orbits for which much faster differential precession can occur. For example, there is the possibility of substantial effects on precession rates near the 2:1 Jovian resonance at a=3.28 AU. Figure 5.4 shows the results of integrations of particles forward 10 kyr with initial elements a from 3.16 to 3.40 AU (corresponding to a range of velocities of $\sim\frac{1}{2}$ km/s), e=0.3, i=10, Ω=0, ω=90 and M=180, *i.e.* a mean longitude of 270°; Jupiter starts at mean longitude 0. These (a, e) values

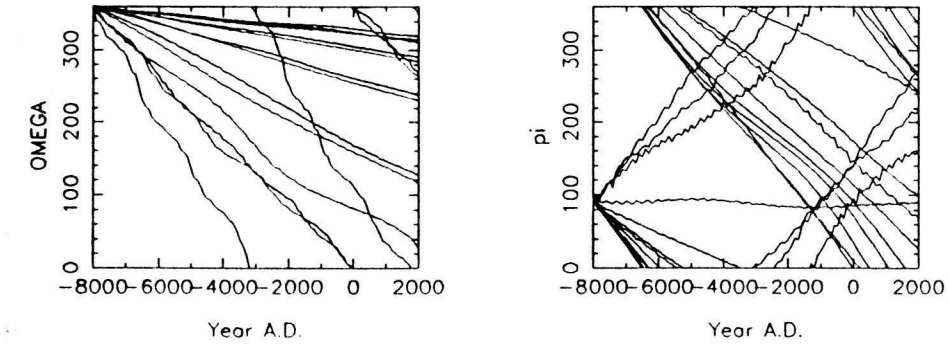

Figure 5.4: Evolution of Ω and ϖ over 10 kyr for particles in the 2:1 resonance with Jupiter.

yield a perihelion distance consistent with the observed bands. The secular periods of revolution for the same range of a, calculated from Brouwer's theory, cover ∼5–8 kyr for Ω and ∼9–13 kyr for ϖ so that the necessary time for differential precession of one revolution is ∼13 kyr for Ω and ∼30 kyr for ϖ. We see in Figure 5.4 that because of the resonance, differential precession of an entire revolution can occur on a timescale of several 10^3 kyr only. Therefore on a timescale less than that of the evolution of the Taurid Complex it is possible for Ω precession to occur so that the band pair is present at all longitudes and for ϖ precession to occur so that the heliocentric apparent distance of the bands is similar at different longitudes. Of course, the variations in Ω and ϖ precession rates are correlated for particles in the

2:1 resonance so that although the band pair is quickly formed at all longitudes, a longer timescale is required for the heliocentric distance to become uniform (*cf.* discussion in Section II B of Sykes & Greenberg 1986); however, the correlation is not completely precise and besides, the relationship between Ω and ϖ precession will be different for particles with slightly different e-values, and for particles that are not quite moving in the 2:1 resonance.

We have demonstrated that for families of orbits with appropriately chosen orbits, timescales for band formation can be well over an order of magnitude below those derived by Sykes & Greenberg (1986). Of course, a resonance is not the only way to bring this about, *e.g.* increasing the velocity dispersion to a few km/s would probably have the desired effect. Thus the theory that the bands are due to cometary material from the giant comet Taurid parent cannot be excluded.

The theories that associate the bands entirely with the asteroid belt are subject to various constraints, which are evaluated in a recent study by Sykes (1990). The fact that some of the most prominent bands have similar latitudes as the three largest asteroid families is an argument in favour of such an association, though the best estimates of band brightnesses tend to disprove an equilibrium model of gradual erosion of family members continuously feeding the dust component, since under this scenario the amount of dust would be proportional to the total mass of asteroids in the family. Sykes therefore argues that asteroid families and band pairs are due to single random collisional events and that bands gradually fade away because of comminution and subsequent susceptibility to radiative forces (some asteroid families have no detectable band association and these would be presumed to have formed long ago).

The reasons against an asteroid belt explanation for the bands, and an asteroidal origin for the zodiacal dust complex in general, include the failure of spacecraft to find any dust enhancement on passage through the asteroid belt, and also collisional models (see Section 1.1.2, and Fechtig 1984). On the other hand a cometary (Taurid) explanation for the bands could really only have been convincingly demonstrated if the aligned Taurid/sporadic stream could have reproduced the IRAS observations; we saw in Section 5.1.2 that the most prominent IRAS bands could not be modelled in this way. Thus although we have demonstrated timescales comparable to that of the evolution of the Taurid Complex, it is unfortunate to have to allow a free orbital parameter that has no connection with the structured Taurid stream, but if that is the nature of the bands then it has to be accepted.

Even if the bands are primarily due to asteroid belt processes (perhaps they are

just a small perturbation on the background zodiacal dust), there is no reason to doubt that the dominant input to the present zodiacal dust cloud has been a recent giant comet. That is, given that we know that a very large parent object must have given rise to the huge sporadic meteoroid complex surrounding the Taurids and given that the expected evolution of the material (under collisional evolution and subsequent dispersion) is into the background zodiacal cloud, there is no need to invoke a substantial asteroid-belt contribution.

5.2 Asteroids on Schmidt plates

This section represents the closest I have come to doing observational work during the course of this thesis. Large objects (asteroids) in the Taurid Complex may by chance have appeared on photographic plates taken with the 48 inch U.K. Schmidt telescope in Australia. A large library of plates taken since 1973 is available at the Royal Observatory, Edinburgh. The plate search described here was aimed at looking for possible asteroids both in the resonant swarm and in the Encke dust trail[1] (Chapter 3) rather than the stream in general since by concentrating on part of the orbit, it is easier to narrow down the set of plates to choose the appropriate ones to look at.

If the theory developed in Section 3.3 is correct and the Taurid parent is located in the Encke trail, then the Encke trail is probably the best place to be looking in this plate search. Finding significant numbers of swarm asteroids on particular plates would of course be a convincing way of demonstrating the existence of the swarm in addition to providing information on its mass function, but it may be that the swarm is nearly entirely meteoroidal. As it happened, no obviously Taurid asteroids were found and so we simply derive upper limits on the number of asteroids of the relevant sizes, a useful, if less exciting, result. In Section 5.2.4 we address the possibility that the Taurid parent is no longer a single object but has broken up into a gravitationally bound cluster of slightly smaller bodies. We discuss whether this could hide it on a Schmidt plate.

Many main-belt asteroids appear on these plates (over 100 in some cases). There is no possibility of demonstrating the existence of Taurid asteroids simply by number counts and so plates must be selected where trailed images on the plates (typically a few tenths of 1 mm in length) due to main-belt asteroids (the telescope tracks

[1]There is a danger of ambiguity in the word "trail" in this Section. We shall try to avoid confusion between trailed images on the Schmidt plates and the dust trail along Encke's orbit discovered by IRAS.

the stars) are distinguishable from trailed images of objects moving on the orbits of interest.

The first stage is to decide which plates give the best chance of having asteroids we are interested in. We then check the populations of main-belt asteroids found, since although studying them is not the purpose of this investigation, there is no avoiding the fact that they dominate the set of asteroidal images on the plates. We finally see whether any images were found that are plausibly due to Taurid Complex asteroids.

5.2.1 Plate catalogue search

The catalogue of plates was searched firstly for orbits relating to the Encke dust trail (Section 3.3) and secondly relating to the resonant meteoroidal swarm (Section 3.2). For the former, plates were considered if they contained part of the trail orbit from –100 to +18° in mean anomaly relative to Comet Encke. Out of these, plates were preferred that contained part of the orbit at nearer distances. It was also a condition that moving object images would have different expected orientations and lengths for main-belt asteroids as for asteroids in the Encke trail. Only plates taken in blue were selected as they went down to a faint limiting magnitude. For the swarm, similar selection rules applied, but more possible orbits were considered, the angular elements being allowed to vary — a few degrees in ϖ, and ω was allowed to vary through all values with i taking appropriate values given the value of ω (the long-term precession of i and ω being closely connected; Chapter 2). The part of the orbit corresponding to the central 40° of the resonant swarm was considered. Some plates were chosen because they contained comparatively wide ranges of swarm orbits; some were chosen specifically in mid-1975, the time of the lunar meteoroid swarm detections. The 7 plates selected, 2 relating to the Encke trail and 5 to the swarm, are listed in Table 5.3. There were some further suitable plates, but constraints on time and effort limited the selection to these 7, which probably represented the best guesses for plates on which Encke trail and swarm asteroids may have fortuitously appeared.

Table 5.3 also lists expected angular motions. For the main belt, they are derived from calculations of the actual motions of the first ∼3000 numbered asteroids observed looking in the same direction and the same date but added over a few years to get a reasonable sample size (typically ∼20 for each plate); the standard deviation, due to dispersion of elements within the main belt, on each plate is 5–10″/hr. The figures for the Taurid asteroids are merely representative since they vary sig-

		Plate centre		Main-belt		Taurid	
Plate	Date	α	δ	$\dot{\alpha}$	$\dot{\delta}$	$\dot{\alpha}$	$\dot{\delta}$
4393	29 Jul 1978	21^h16^m	–25°	–35	–9	–79	–15
10265	15 Jun 1985	22^h24^m	–20°	19	–1	–34	–15
1559	7 Jun 1975	23^h0^m	–30°	47	–4	–30	–20
1633	7 Jul 1975	21^h56^m	–45°	–25	–16	–170	–40
1756	8 Aug 1975	17^h30^m	–50°	–4	14	70	100
7858	29 Jun 1982	22^h0^m	–15°	–3	–4	–80	–30
7903	16 Jul 1982	22^h20^m	–15°	–12	–8	–50	–20

Table 5.3: Schmidt plates scanned to search for Taurid asteroids, and expected angular motions, in ″/hr, of main-belt and Encke trail (first 2 plates) and resonant swarm (last 5 plates) asteroids.

nificantly between orbits; indeed they sometimes overlap the ranges for main-belt asteroids, but only to a very small degree, so that we do have a high chance of being able to distinguish them from the main-belt asteroids.

For each of the 7 plates, a plate taken of the same field at a different time was selected for comparison. In two cases, a second plate was not contained in the Schmidt library and so the appropriate field was taken from the ESO or Palomar collection. Because the two members of a pair of plates are in general taken at different dates, the line of sight through the Solar System is different and so a different number of asteroids appear. The main purpose of the extra plate is to check whether a trail-like image is an asteroid or a galaxy.

The 7 plates of interest and some of the comparison plates were systematically scanned using a microscope at magnification 6.4× and the lengths and orientations of trails due to asteroids noted. Not all the comparison plates were scanned for asteroids; those that were are listed in Table 5.4.

		Plate centre		Main-belt	
Plate	Date	α	δ	$\dot{\alpha}$	$\dot{\delta}$
5391	9 Oct 1979	21^h16^m	–25°	7	8
12195	26 Sep 1987	22^h24^m	–20°	–23	0
3508	17 Aug 1977	23^h0^m	–30°	–29	–19

Table 5.4: As Table 5.3, but for comparison plates rather than plates on which Taurid Complex asteroids were being searched for.

All the plates were taken in the blue region of the spectrum, except one comparison red plate taken on the same night as one of the blue plates of interest. The limiting stellar magnitude is about 22.5 for a 60 minute exposure. There are ex-

pected to be slight variations in limiting magnitude between plates due to differences in sky conditions and line of sight through the atmosphere. Various small regions of pairs of plates of the same part of the sky were enlarged and photographed and the same images seemed to be present in both.

5.2.2 Main-belt asteroids

Despite the fact that they represent nearly all the asteroids on the plates, main-belt asteroids are incidental to this investigation. Our objective is to derive, for each plate, a limiting magnitude for the Taurid asteroids we are looking for. However, checks on number counts of main-belt asteroids (by comparison with expected numbers based on asteroid surveys) should confirm that no serious errors are being made.

The limiting magnitude for asteroidal images is less than that for stellar images (*i.e.* the stars can be seen fainter) owing to trailing loss, the asteroid being a moving object. The trailing loss is a function of angular motion of the asteroid but not of exposure time of the plate, so that variations in the exposure time (between 45 and 75 minutes for the plates scanned) do not affect the limiting asteroid magnitude. The widths of most of the trailed asteroidal images measured are 30–40 μm. The plate scale is 14.9 μm/$''$ and so the width is about 2.5$''$. Therefore if the length over which the image is trailed, in 1 hour, is 25$''$ we expect a trailing loss of 2.5 magnitudes so that the limiting magnitude is 20. This is the figure we shall use in Section 5.2.3, though we shall first check that it seems reasonable, as follows. We accept that our adopted figure may be out by, say, 0.5 magnitudes.

Ishida *et al.* (1984) fitted data from their survey (54 fields of 6° square) using a model that included various parameters to allow for heliocentric distance and latitude distributions and albedos of different asteroid types in their derivation of a size distribution. Their survey went down to an asteroidal magnitude of 19. Unlike Ishida *et al.*'s (1984) paper, it is not the purpose of this work to derive size distributions of main-belt asteroids as precisely as possible. A few rough comparisons against their number counts can confirm that the limiting magnitudes we choose to adopt are realistic. We shall be taking the trailing loss entirely as a function of angular motion. The alternative would be to try to allow for differences between the plates (due to sky conditions, *etc.*) by normalising based on the number of main-belt asteroids present; however, errors in fitting a model prediction of number count to the observed number (in which there will inevitably be a certain random component) would probably result in over-compensation.

The numbers of asteroids found on the various plates, which are 6.4° square, are listed in Table 5.5. The angular motions have been rotated from equatorial

Plate	t_e	$\lambda - \lambda_\odot$	β	$\dot{\lambda}$	$\dot{\beta}$	Number
4393	70	188°	–8.7°	–33	0	146
(5391)	65	118°	–8.7°	8	6	54
10265	70	246°	–9.3°	16	–8	70
(12195)	71	148°	–9.3°	–20	8	113
1559	45	258°	–21.7°	38	–20	6
(3508)	75	190°	–21.7°	–33	–7	36
1633	60	210°	–30.3°	–26	–7	14
1756	60	129°	–26.7°	–3	13	2
7858	60	229°	–2.6°	–4	–3	21
7903	60	218°	–4.3°	–14	–3	46

Table 5.5: Numbers of asteroids found on Schmidt plates. The plate numbers in parentheses were each of the same field as a plate of interest and used for comparison. t_e is the exposure time in minutes. λ & β are the ecliptic coordinates of the plate centre, $\lambda_\odot$ the longitude of the Sun. The expected average motion of main-belt asteroids is given in $''$/hr, the standard deviation being 5–10$''$/hr.

coordinates (Tables 5.3 and 5.4) to ecliptic; apparent slight inconsistencies in the rotation between Table 5.3 and 5.4 are because the angular motion of each asteroid used to give the statistic in Table 5.3 was rotated and then the mean calculated, rather than simply rotating the vector given in Table 5.3. It may be seen that for values of $|\ \lambda - \lambda_\odot - 180°|$ less than 50–55°, the Earth is overtaking the asteroid and $\dot{\lambda} < 0$. For values >50–55°, the component of the Earth's velocity at right angles to the direction of observation is smaller and the Earth is overtaken by the asteroid. As regards $\dot{\beta}$, it is towards the ecliptic (*i.e.* positive, since $\beta < 0$ for all these plates) when the Earth is moving away from the asteroid, *i.e.* when $\lambda - \lambda_\odot < 180°$.

If the trailed length of an asteroidal image is $\lesssim 15''$ then there starts to be a significant chance that I miss it when I scan the plate. The risk increases the shorter the trailed image as it becomes less clearly identifiable as an asteroid. This problem will have affected the number counts on plates 5391, 1756, 7858 and 7903 to varying degrees. A further problem with plate 1756 was the huge number of stars present, the field being near the galactic plane. Vignetting will have a small effect on the number of observable asteroids near the edges of the plate, but it is fair to neglect this during the course of the present approximate calculations. The main parameters affecting the number counts are β (the asteroid density increasing near the ecliptic) and $|\ \lambda - \lambda_\odot - 180°|$. This latter quantity, being correlated with the angular motion, affects the trailing loss; also the nearer $\lambda - \lambda_\odot$ is to 180°, the

closer the Earth to the part of the asteroid belt being observed and so the smaller the limiting diameter corresponding to the same limiting magnitude. Ishida *et al.* (1984) found that a bottom-heavy distribution was needed at the appropriate sizes (down to 1 km or so) to explain such observed number count variations. For angular motions of 35–40″/hr (*cf.* Ishida *et al.*) I am assuming the limiting magnitude will be ∼19.5 and this seems in reasonable accord with the fact that I seem to find, say, twice as many asteroids as they do for plates at similar $|\lambda - \lambda_\odot - 180°|$ and β (see their Table 1), though precise details of course depend on the size distribution. At any rate, it seems acceptable to proceed with the calculation of limiting magnitude as a function of angular motion as planned.

5.2.3 Taurid Complex asteroids

We first see whether there are possibly Taurid Complex asteroids in addition to the main-belt asteroids visible on the plates. In their absence, we derive bounds on the number density in the Taurid swarm and Encke trail.

The lengths and orientations of trailed images were checked to see if any plausibly corresponded to Taurids. For example, plots of the $\dot{\lambda}$ and $\dot{\beta}$ distributions for asteroids on plate 4393 are shown in Figure 5.5. We note that an angular motion of

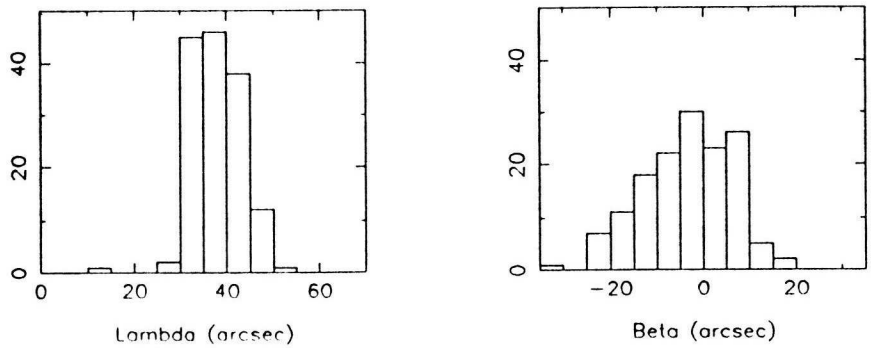

Figure 5.5: Distributions of λ and β components of trailed asteroid images on plate 4393.

$(\dot{\lambda}, \dot{\beta})$ is indistinguishable from $(-\dot{\lambda}, -\dot{\beta})$. In working out the sign of the β motion in Figure 5.5, $\dot{\lambda} < 0$ has been assumed. The exposure time being 70 minutes, the expected trail length is ∼38″ (see Table 5.5). The distribution is seen to be what is expected for a population of main-belt asteroids. There is one much longer trailed image not plotted (see below).

We now summarise what was found on each plate.

Firstly, the 2 plates aimed at observing the Encke trail:

Plate 4393: One asteroidal image had an α component of $\sim 160''$ and cannot be due to a main-belt asteroid; however it is too long even to be an Encke trail asteroid, as well as not having quite the right orientation. It is also in a region of the plate away from the Encke trail orbit.

Plate 10265: Images well fitted by main-belt distribution.

and secondly, the 5 plates aimed at observing the resonant swarm:

Plate 1559: Consistent with main belt.

Plate 1633: Main belt.

Plate 1756: The only 2 asteroids found seem to be main-belt.

Plate 7858: Main belt.

Plate 7903: Nearly all the asteroids are main-belt. One image was $\sim 120''$ long and cannot have been a main-belt asteroid. Neither could it have been a Taurid as it was nearly vertical whereas asteroids in the proposed swarm should have been from about 14–28° to the horizontal. It may well have been an Earth-crossing asteroid.

It would have been most convincing if several Encke trail / resonant swarm asteroids had appeared on a single plate; indeed it would have been ideal if a bimodal distribution in lengths and orientations of trails were found, corresponding to populations of main-belt and Taurid asteroids. As it happened, there were no likely identifications of Taurids. On one or two plates, a small proportion of calculated Taurid orbits had motions matching those of main-belt asteroids so that some of the images could actually be Taurids. However, there is no particular reason to think so since they would have been expected, more likely, to be distinguishable from main-belt images (that they should be was one criterion in the plate selection). We shall presume that no Encke trail or swarm asteroids appeared on the plates inspected.

Though each field contained a range of three-dimensional spatial positions where objects on Taurid orbits would be, we shall adopt a single representative Taurid asteroid for each plate. Its angular motion will yield its apparent magnitude, from which we can derive the limiting diameter of asteroids that could have been detected. This will depend on the heliocentric and geocentric distances of the asteroids, and on assumptions about albedo and also effects of the phase angle of the observation. We can then use the dynamical work (which tells us what proportion of Encke trail or swarm appears on the plate) to extend the answers to the whole trail/swarm.

Firstly, then, we derive the diameters. We are taking the limiting magnitude as being 20 for angular motions of 25″/hr and scaled appropriately for different angular motions (listed in Table 5.3). The radius-magnitude relation (*e.g.* Luu & Jewitt 1988) is given by

$$pa^2 = 2.25 \times 10^{16} r^2 \rho^2 10^{0.4(m_\odot - m)}$$

where p is the albedo, a the radius in km, r the heliocentric and ρ the geocentric distance in AU, $m_\odot$ the apparent magnitude of the Sun (–26.09 in blue; Allen 1973) and m the apparent magnitude of the asteroid. The derived asteroid diameters using p=0.1 and 0.01 are given in Table 5.6. The diameters probably should be increased

				p=0.1	p=0.01
Plate	m	r	ρ	D	D
4393	18.7	2.4	1.4	3.4	10.7
10265	19.6	1.9	1.3	1.8	5.7
1559	19.6	1.6	1.1	1.2	3.8
1633	17.9	1.6	0.7	1.6	5.0
1756	18.3	1.6	0.7	1.5	4.7
7858	18.7	2.2	1.5	3.5	11.1
7903	19.2	2.9	2.0	5.0	15.8

Table 5.6: Minimum diameters D in km of Taurid asteroids that would have been detectable on Schmidt plates, for albedos p=0.1 and 0.01.

by a factor of ∼1.5 because of the phase angle (see, *e.g.*, Bowell *et al.* 1989), which is of order 20° for most of the plates.

Though these calculations are only meant to give a rough idea, it seems that the asteroids of interest would need to be quite a few km in size. Regarding the Encke trail, plate 4393 contained the part of the orbit that was ∼65–75° in mean anomaly behind Encke, thus *the* part of the orbit where the best-fit models of Section 3.3 place the parent object. Thus we could place a constraint on the size of the trail parent of ∼5 km, but the approximate nature of the above calculations and the great uncertainty in albedo probably cannot be reasonably taken as excluding an object as large as, say, 20 km simply because it was not detected on this Schmidt plate. Plate 10265 contained a less favourable part of the orbit (just behind the visible trail that IRAS observed).

The 1975 observations were directed to points comparatively close to the Earth and did not contain a very wide variety of swarm orbits. It would have been encouraging if the lunar meteoroid swarm could have been shown to extend up to, say, >2 km asteroids, but it is probably fair to say that the fields contained only ∼1%

of possible swarm orbits, so that the lack of successful detections does not place a particularly powerful constraint on the number of asteroids in the whole swarm.

The 2 plates taken in 1982 each contained parts of the swarm $\sim 10^\circ$ in mean anomaly but with a reasonable range present of the other angular orbital elements. Nevertheless we are still thinking in terms of well under 10% of the swarm appearing on the plate, and the derived asteroid diameters were quite a few km. Given that the Taurid Complex as a whole probably only contains of order 100 asteroids of 1–2 km diameter (based on the few presently known), it is perhaps not too surprising that no comparatively large asteroids in the swarm turned up.

To summarise, it was worth scanning a few plates because of how useful it would have been to discover a few asteroids associated with the Encke trail or resonant swarm. However, the size distribution limits derivable on the occurrence of negative results to the searches are not very strong constraints. It would require substantial effort to scan a large number of plates and it may be desirable in future to choose times carefully at which to have plates taken of particularly preferred fields.

5.2.4 A fragmented parent object?

In various places we have mentioned the possibility that the Taurid parent is no longer present as a single large object but rather a gravitationally bound cluster of smaller asteroids and meteoroids. This could have either of two effects regarding its detectability on photographic plates. The total surface area for a given mass would increase so that the cluster would reflect more light than the single object. The question is whether the spatial extent of the cluster would be large enough so that the optical depth would be sufficiently reduced to make it less clearly visible.

A calculation of the size of the sphere of influence of the cluster is of interest. We write M and R for the mass and radius of the meteoroid cluster and $M_\odot$ and r for the mass of and distance from the Sun. Comparing the self-gravity of the cluster and the tidal force of the Sun, it is quite easy to derive

$$\frac{R}{r} = \left(\frac{M}{2M_\odot}\right)^{1/3}$$

(see, *e.g.*, Öpik 1976). Checks on the distances of the closest approaches to the planets expected during $\sim 10^4$ yr (Section 3.1.2) show that the tidal disruption is greatest due to the Sun, at perihelion.

For example, for a 10^{18} g ($\sim$10 km) object, taking $r \approx 5{\times}10^7$ km gives $R \approx$ 300 km so that the cluster would subtend $<1''$ at 1 AU and still effectively be a point source. A 10^{20} g ($\sim$50 km) object, which could hardly have been missed

photometrically, would have $R \approx 1500$ km. Now, let us suppose we wish to "hide" an object from view by breaking it up and that for the pieces to be hidden they must firstly be below some fixed size, *e.g.* $\leq$5 km (a typical value of D from Table 5.6), and secondly be spaced sufficiently so that they do not collectively behave as point sources. For the second condition, we shall say that we want only one 5 km object per circular area of the sky of radius 300 km. The number of 5 km objects into which we fragment the parent is proportional to M but the available area on the sky is only proportional to $M^{2/3}$ so that it becomes progressively more difficult to hide a larger parent object. Our calculation of the cluster's tidal radius showed that, let alone a 5 km asteroid, it is not possible even to hide a 10 km object (10 km being one of the larger D's in Table 5.6) by breaking it up so that it appears rather difficult to appeal to this precise explanation for why nothing was found on the Schmidt plates.

On the other hand if we imagine a scenario in which a fragmentation occurring at a larger value of r (*e.g.* 3 AU, 10$\times$ the above) yields a cluster of asteroids which though coherent is not gravitationally bound around the entire orbit but which interacts gravitationally at the point of fragmentation, thus tending to prevent its dispersal, then we may use a value of R that is 10$\times$ greater. The area on the sky is 100$\times$ greater. Performing calculations in the same simplified way as above, we find, *e.g.*, that by breaking a parent into objects of diameter 2 km we may hide a body as large as 10 km. If 5 km is the limiting visible asteroid size then a parent as large as 100 km could be hidden. Of course, the parent is not miraculously going to break up into objects all of the same size and so true possible sizes should be rather less than the values calculated. Nevertheless this appears a viable explanation for the lack of discovery to date of the Taurid parent.

5.3 Conclusions and future work

The Taurid Complex has been known for some time to be of considerable importance in the inner Solar System and the aim of this work was to discover details about the Taurids' dynamical evolution. We now have a plausible picture of a parent object in its late evolutionary (devolatilised) phase having been in a resonant orbit for the past $\sim$10 kyr during which it has fed meteoroids into both a resonant swarm and the Taurid stream as a whole. The Taurid stream is also shown, by way of some simple statistical tests, to extend to objects as large as km-sized asteroids. The best estimates of the mass of the stream suggest that in this way the Taurid parent has

acted as the primary replenishing source for the zodiacal meteoroid complex during this time. The resonant swarm consists of low-velocity ejecta; the mechanism for feeding the stream as a whole, deduced from meteor orbit distributions, appears to be that comparatively large fragments (1 m and above, say) split from the parent near perihelion and many of these undergo catastrophic fragmentation in the asteroid belt.

The most desirable achievement for the future, which a search of photographic plates unfortunately did not succeed in doing, is to find the parent of the complex (provided it still exists). The idea that it may lie within a bright dust trail discovered by IRAS has been shown to be tenable, though this certainly requires further study. Comet Encke (present mass $\sim 10^{17}$ g) has usually been assumed to be the parent object, though an unseen companion was suggested by Whipple & Hamid (1952).

There is no doubt that there is much valuable information in historical records, *e.g.* in the 11th century the Taurids were the most powerful meteor shower, with the Northern branch significantly more active than the Southern (Astapovič & Terenteva 1968). Indeed there was an enhancement of the fireball flux over a few centuries reaching a peak in the 11th century and a comparison with the number of observed comets demonstrates that it cannot simply be ascribed to variations in the effort devoted to recording astronomical phenomena (Clube 1986). More recent analysis of Chinese astronomical records (Hasegawa 1991) suggests concentrations in the 5th and 15th centuries. Some of these enhancements could be indicative of concentrations of meteoroids near the orbit of the parent object which will intersect the Earth's at similar times to times of nodal crossing of the parent itself. (There may also be major objects in the stream other than the parent.) This could provide invaluable constraints on the resonant swarm model of Chapter 3 or the model of the Taurid stream as a whole in Chapter 4 and should certainly be borne in mind in future work when considering the orbit of the parent. Much of the present investigation has proceeded on the basis that the Encke dust trail discovered by IRAS is the location of the parent of swarm and Taurids, and aspects of the results that are independent of this assumption have been distinguished from those that are not. It may be that future confirmation of the swarm radiant being, for example, north of the ecliptic at the pre-perihelion intersection with the Earth will mean that the relevance of the IRAS trail has to be re-evaluated and it may be that a source object in a different orbit is in better accord with the observations of many centuries ago.

Future observations of the dust trail, to see if it really is directly associated with Comet Encke, would be very useful, as would any future detections (and non-

detections in other years) of the proposed resonant swarm at either of the correct ranges of dates. An important opportunity to confirm or disprove the resonant swarm theory comes in June 1992.

An interesting future study making use of the wealth of meteor data available would be to try to extend the dynamical modelling to the orbits that are more spread out, the work in Chapter 4 having concentrated on the core of the stream. An equally precise model would be difficult because of the increased dispersion, but one would hope that it would still be possible to detect and explain various orbital elements distributions/trends in terms of a model that includes meteoroids that precess more quickly and perhaps also covers a longer timescale. Such dynamical studies would be done primarily computationally, this work having shown what planetary models are sensible to adopt for studies on the Taurids, but analytical methods will always be useful for providing explanations of integration results.

Apollo asteroids are being discovered at an ever-increasing rate and it should be possible to draw even stronger statistical conclusions in future regarding the importance of giant comets in replenishing the Earth-crossing asteroid population. In sufficient numbers, Taurid asteroid orbits could prove as useful as meteor data in deriving models of past evolution of the stream.

In a wider context, dynamical studies of planet-crossing orbits of comets and asteroids are important and indeed they are presently being pursued by many researchers (*e.g.* see Milani *et al.* 1989, Hahn & Bailey 1990, Nakamura & Yoshikawa 1991). Knowledge of the details of capture from cometary into sub-Jovian orbits, as happened for the Taurid parent, would be useful, as would a model that could explain most of the Jupiter family of comets as deriving from a single giant comet (the Taurid parent) that split before its capture into a sub-Jovian, high-eccentricity orbit.

Topics connected with the Taurid Complex and the Taurid progenitor are no doubt going to recur in many guises, relating to asteroids, comets, meteoroids and dust, in the years to come.

References

Alexander, S. (1850). "On the classification and special points of resemblance of certain of the periodic comets; and the probability of a common origin in the case of some of them." *Astron. J.,* **1,** 147–150.

Allen, C.W. (1973). *Astrophysical Quantities* (3rd edition), University of London.

Almond, M. (1951). "The summer daytime streams of 1949 and 1950. III. Computation of the orbits." *Mon. Not. R. Astron. Soc.,* **111,** 37–44.

Alvarez, L.W., Alvarez, W., Asaro, F. & Michel, H.V. (1980). "Extraterrestrial cause for the Cretaceous-Tertiary extinction." *Science,* **208,** 1095–1108.

Astapovič, I.S. & Terenteva, A.K. (1968). "Fireball radiants of the 1st–15th centuries." *Physics and Dynamics of Meteors (IAU Symp. No. 33),* eds Kresák, Ľ. & Millman, P.M., Reidel, Dordrecht, Holland, pp. 308–319.

Babadzhanov, P.B. & Obrubov, Yu.V. (1987). "Evolution of meteoroid streams." *Interplanetary Matter,* eds Ceplecha, Z. & Pecina, P., Czechoslovak Academy of Sciences, Ondřejov, pp. 141–150. (= *Publ. Astron. Inst. Czechoslov. Acad. Sci.,* **67 (2),** 141–150).

Babadzhanov, P.B., Obrubov, Yu.V. & Makhmudov, N. (1990). "Meteor streams of Comet Encke." *Sol. Sys. Res.,* **24,** 12–19. English translation. Russian original in *Astron. Vestn.,* **24,** 18–28.

Babadzhanov, P.B., Wu, Z., Williams, I.P. & Hughes, D.W. (1991). "The Leonids, Comet Biela and Biela's associated meteoroid stream." *Mon. Not. R. Astron. Soc.,* **253,** 69–74.

Bailey, M.E. (1984). "Is there a dense primordial cloud of comets just beyond Pluto?" *Asteroids, Comets, Meteors,* eds Lagerkvist, C.-I., & Rickman, H., Uppsala University, Uppsala, Sweden, pp. 383–386.

Bailey, M.E. (1985). "The problem of the $1/a$ distribution and cometary fading." *Dynamics of Comets: Their Origin and Evolution (IAU Colloq. No. 83),* eds Carusi, A. & Valsecchi, G.B., Reidel, Dordrecht, Holland, pp. 311–317.

Bailey, M.E., Clube, S.V.M. & Napier, W.M. (1990). *The Origin of Comets,* Pergamon, Oxford.

Bigg, E.K. & Thompson, W.J. (1969). "Daytime photograph of a group of meteor trails." *Nature,* **222,** 156–158.

Blitzer, L. (1959). "Lunar-solar perturbations of an Earth satellite." *Amer. J. Phys.,* **27,** 634–645.

Bone, N.M. (1989). "1988 Taurids live up to reputation." *Astronomy Now,* **3 (4),** 6–7.

Bone, N.M. (1991). "Visual observations of the Taurid meteor shower." *J. Brit. Astron. Assoc.,* **101,** 145–152.

Bowell, E., Hapke, B., Domingue, D., Lumme, K., Peltoniemi, J. & Harris, A.W. (1989). "Application of photometric models to asteroids." *Asteroids II,* eds Binzel, R.P., Gehrels, T. & Matthews, M.S., University of Arizona Press, Tuscon, Arizona, pp. 524–556.

Brecher, K. (1984). "The Canterbury swarm: ancient and modern observations of a new feature of the Solar System." *Bull. Amer. Astron. Soc.,* **16,** 476. Abstract.

Brigham, E.O. (1974). *The Fast Fourier Transform,* Prentice-Hall, Englewood Cliffs, N.J.

Brouwer, D. (1947). "Secular variations of the elements of Encke's Comet." *Astron. J.,* **52,** 190–198.

Brouwer, D. & Clemence, G.M. (1961). *Methods of Celestial Mechanics,* Academic Press, N.Y.

Brown, J.C. & Hughes, D.W. (1977). "Tunguska's comet and non-thermal ^{14}C production in the atmosphere." *Nature,* **268,** 512–514.

Brown, E.W. & Brouwer, D. (1932). "Tables for the development of the disturbing function with schedules for harmonic analysis." *Trans. Astron. Obs. Yale Univ.,* **6,** 67–157.

Brown, E.W. & Shook, C.A. (1933). *Planetary Theory,* Cambridge University Press.

Burns, J.A., Lamy, P.L. & Soter, S. (1979). "Radiation forces on small particles in the Solar System." *Icarus,* **40,** 1–48.

Carusi, A., Kresák, Ľ., Perozzi, E. & Valsecchi, G.B. (1985). *Long-term Evolution of Short-period Comets,* Adam Hilger, Bristol.

Clube, S.V.M. (1986). "Giant comets or ordinary comets; parent bodies or planetesimals." *Proc. 20th ESLAB Symposium on the Exploration of Halley's Comet (ESA SP-250), Vol. 2: Dust & Nucleus*, eds Battrick, B., Rolfe, E.J. & Reinhard, R., ESA, Noordwijk, Holland, pp. 403–408.

Clube, S.V.M. (1987). "The origin of dust in the Solar System." *Phil. Trans. R. Soc. Lond.,* **A 323,** 421–436.

Clube, S.V.M. (1988). "Dust and star formation in a hot differentiating medium." *Dust in the Universe,* eds Bailey, M.E. & Williams, D.A., Cambridge University Press, pp. 327–335.

Clube, S.V.M. (ed.) (1989). *Catastrophes and Evolution,* Cambridge University Press.

Clube, S.V.M. (1990). "Giant comets and their role in history." *The Universe and its Origins,* ed. Singer, S.F., Paragon House, N.Y., pp. 145–161.

Clube, S.V.M. (1991). "Large scale perturbations of the terrestrial atmosphere: some considerations relating to the role of cometary trails and disintegrating meteoroids." *Adv. Sp. Res.,* **11 (6),** 63–66.

Clube, S.V.M. & Asher, D.J. (1990). "The evolution of proto-Encke: dust bands, close encounters and climatic modulations." *Asteroids, Comets, Meteors III,* eds Lagerkvist, C.-I., Rickman, H., Lindblad, B.A. & Lindgren, M., Uppsala University, Uppsala, Sweden, pp. 275–280.

Clube, V. & Napier, B. (1982a). *The Cosmic Serpent,* Faber & Faber, London.

Clube, S.V.M. & Napier, W.M. (1982b). "Spiral arms, comets and terrestrial catastrophism." *Q. J. R. Astron. Soc.,* **23,** 45–66.

Clube, S.V.M. & Napier, W.M. (1984). "The microstructure of terrestrial catastrophism." *Mon. Not. R. Astron. Soc.,* **211,** 953–968.

Clube, S.V.M. & Napier, W.M. (1986). "Mankind's future: an astronomical view. Comets, ice ages and catastrophes." *Interdisciplinary Sci. Rev.,* **11,** 236–246.

Clube, S.V.M. & Napier, W.M. (1987). "The cometary breakup hypothesis re-examined: a reply." *Mon. Not. R. Astron. Soc.,* **225,** 55P–58P.

Clube, V. & Napier, B. (1990). *The Cosmic Winter,* Basil Blackwells, Oxford.

Cohen, C.J. & Hubbard, E.C. (1965). "Libration of the close approaches of Pluto to Neptune." *Astron. J.,* **70,** 10–13.

Dermott, S.F., Nicholson, P.D., Burns, J.A. & Houck, J.R. (1984). "Origin of the Solar System dust bands discovered by IRAS." *Nature,* **312,** 505–509.

Dermott, S.F., Nicholson, P.D. & Wolven, B. (1986). "Preliminary analysis of the IRAS Solar System dust data." *Asteroids, Comets, Meteors II,* eds Lagerkvist, C.-I., Lindblad, B.A., Lundstedt, H. & Rickman, H., Uppsala University, Uppsala, Sweden, pp. 583–594.

Dohnanyi, J.S. (1969). "Collisional model of asteroids and their debris." *J. Geophys. Res.,* **74,** 2531–2554.

Dohnanyi, J.S. (1976). "Sources of interplanetary dust: asteroids." *Interplanetary Dust and Zodiacal Light (IAU Colloq. No. 31; Lecture Notes in Physics* **48***),* eds Elsässer, H. & Fechtig, H., Springer-Verlag, Berlin, pp. 187–205.

Dohnanyi, J.S. (1978). "Particle dynamics." *Cosmic Dust,* ed. McDonnell, J.A.M., Wiley, Chichester, pp. 527–605.

Donnison, J.R. (1986). "The distribution of cometary magnitudes." *Astron. Astrophys.,* **167,** 359–363.

Dorman, J., Evans, S., Nakamura, Y. & Latham, G. (1978). "On the time-varying properties of the lunar seismic meteoroid population." *Proc. Lunar Plan. Sci. Conf.,* **9,** 3615–3626. (= *Geochim. Cosmochim. Acta (Suppl.),* **10,** 3615–3626).

Dormand, J.R. & Prince, P.J. (1978). "New Runge-Kutta algorithms for numerical simulation in dynamical astronomy." *Cel. Mech.,* **18,** 223–232.

Drummond, J.D. (1981). "A test of comet and meteor shower associations." *Icarus,* **45,** 545–553.

Drummond, J.D. (1991). "Earth-approaching asteroid streams." *Icarus,* **89,** 14–25.

Duennebier, F.K., Nakamura, Y., Latham, G.V. & Dorman, H.J. (1976). "Meteoroid storms detected on the Moon." *Science,* **192,** 1000–1002.

Everhart, E. (1972). "The origin of short-period comets." *Astrophys. Lett.,* **10,** 131–135.

Everhart, E. (1977). "Evolution of comet orbits as perturbed by Uranus and Neptune." *Comets, Asteroids, Meteorites: Interrelations, Evolution and Origins (IAU Colloq. No. 39),* ed. Delsemme, A.H., University of Toledo, Toledo, Ohio, pp. 99–104.

Explanatory Supplement to the Astronomical Ephemeris, Her Majesty's Stationery Office, London (1961).

Fechtig, H. (1982). "Cometary dust in the Solar System." *Comets,* ed. Wilkening, L., University of Arizona Press, Tuscon, Arizona, pp. 370–382.

Fechtig, H. (1984). "The interplanetary dust environment beyond 1 AU and in the vicinity of the ringed planets." *Adv. Sp. Res.,* **4 (9),** 5–11.

Fonk, S.G. (1951). "Tauriden radiant 1951." *De Meteoor,* **7,** 35–36. In Dutch.

Fox, K. (1984). "Numerical integration of the equations of motion of celestial mechanics." *Cel. Mech.,* **33,** 127–142.

Fox, K., Williams, I.P. & Hughes, D.W. (1983). "The rate profile of the Geminid meteor shower." *Mon. Not. R. Astron. Soc.,* **205,** 1155–1169.

Frank, L.A., Sigwarth, J.B. & Craven, J.D. (1987). "Reply to 'Comment on "On the influx of small comets into the Earth's upper atmosphere, II. Interpretation" by L.A. Frank, J.B. Sigwarth & J.D. Craven' by S. Soter." *Geophys. Res. Lett.,* **14,** 164–167.

Froeschlé, C. & Greenberg, R. (1989). "Mean motion resonances." *Asteroids II,* eds Binzel, R.P., Gehrels, T. & Matthews, M.S., University of Arizona Press, Tuscon, Arizona, pp. 827–844.

Fujiwara, A., Cerroni, P., Davis, D., Ryan, E., Di Martino, M., Holsapple, K. & Housen, K. (1989). "Experiments and scaling laws for catastrophic collisions."

Asteroids II, eds Binzel, R.P., Gehrels, T. & Matthews, M.S., University of Arizona Press, Tuscon, Arizona, pp. 240–265.

Ganapathy, R. (1983). "The Tunguska explosion of 1908: discovery of meteoritic debris near the explosion site and at the South Pole." *Science,* **220,** 1158–1161.

Gautier, T.N., Good, J.C. & Hauser, M.G. (1986). "The geometry of the zodiacal dust bands." *Adv. Sp. Res.,* **6 (7),** 91–94.

Goldstein, H. (1980). *Classical Mechanics* (2nd edition), Addison-Wesley, Reading, Massachusetts.

Gonzalez, R.C. & Wintz, P. (1977). *Digital Image Processing,* Addison-Wesley, Reading, Massachusetts.

Gradie, J. & Veverka, J. (1980). "The composition of the Trojan asteroids." *Nature,* **283,** 840–842.

Greenberg, R. (1977). "Orbit-orbit resonances in the Solar System: varieties and similarities." *Vistas Astron.,* **21,** 209–239.

Grün, E., Zook, H.A., Fechtig, H. & Giese, R.H. (1985). "Collisional balance of the meteoritic complex." *Icarus,* **62,** 244–272.

Gustafson, B.Å.S. (1989). "Geminid meteoroids traced to cometary activity on Phaethon." *Astron. Astrophys.,* **225,** 533–540.

Gustafson, B.Å.S., Misconi, N.Y. & Rusk, E.T. (1987). "Interplanetary dust dynamics. III. Dust released from P/Encke: distribution with respect to the zodiacal cloud." *Icarus,* **72,** 582–592.

Hahn, G. & Bailey, M.E. (1990). "Rapid dynamical evolution of giant comet Chiron." *Nature,* **348,** 132–136.

Hartmann, W.K., Tholen, D.J. & Cruikshank, D.P. (1987). "The relationship of active comets, 'extinct' comets, and dark asteroids." *Icarus,* **69,** 33–50.

Hartmann, W.K., Tholen, D.J., Meech, K.J. & Cruikshank, D.P. (1990). "2060 Chiron: colorimetry and cometary behavior." *Icarus,* **83,** 1–15.

Hartung, J.B. (1976). "Was the formation of a 20-km-diameter impact crater on the Moon observed on June 18, 1178?" *Meteoritics,* **11,** 187–194.

Hartung, J.B. (1991). "Giordano Bruno, the June 1975 meteoroid storm, Encke and other Taurid Complex objects." Preprint.

Hasegawa, I. (1991). "Historical variation in the meteor flux as found in Chinese and Japanese chronicles." Preprint.

Hawkins, G.S. (1956). "A radio echo survey of sporadic meteor radiants." *Mon. Not. R. Astron. Soc.,* **116,** 92–104.

Hawkins, G.S. & Southworth, R.B. (1961). "Orbital elements of meteors." *Smithson. Contrib. Astrophys.,* **4,** 85–95.

Helin, E.F. & Shoemaker, E.M. (1979). "The Palomar planet-crossing asteroid survey, 1973–1978." *Icarus,* **40,** 321–328.

Hindley, K.B. (1972). "Taurid meteor stream fireballs." *J. Brit. Astron. Assoc.,* **82,** 287–298.

Hughes, D.W. (1978). "Meteors." *Cosmic Dust,* ed. McDonnell, J.A.M., Wiley, Chichester, pp. 123–185.

Hughes, D.W. (1990). "The mass distribution of comets and meteoroid streams and the shower/sporadic ratio in the incident visual meteoroid flux." *Mon. Not. R. Astron. Soc.,* **245,** 198–203.

Hughes, D.W. (1991). "Comet Halley's outburst." *Mon. Not. R. Astron. Soc.,* **251,** 26P–29P.

Hughes, D.W. & McBride, N. (1989). "The mass of meteoroid streams." *Mon. Not. R. Astron. Soc.,* **240,** 73–79.

Hughes, D.W., Williams, I.P. & Fox, K. (1981). "The mass segregation and nodal retrogression of the Quadrantid meteor stream." *Mon. Not. R. Astron. Soc.,* **195,** 625–637.

Humes, D.H., Alvarez, J.M., O'Neal, R.L. & Kinard, W.H. (1974). "The interplanetary and near-Jupiter meteoroid environments." *J. Geophys. Res.,* **79,** 3677–3684.

Hunt, J., Fox, K. & Williams, I.P. (1986). "Asteroidal origin for the Geminid meteor stream." *Asteroids, Comets, Meteors II,* eds Lagerkvist, C.-I., Lindblad, B.A., Lundstedt, H. & Rickman, H., Uppsala University, Uppsala, Sweden, pp. 549–553.

Ishida, K., Mikami, T. & Kosai, H. (1984). "Size distribution of asteroids." *Publ. Astron. Soc. Japan,* **36,** 357–370.

Jones, J. (1986). "The effect of gravitational perturbations on the evolution of the Taurid meteor stream complex." *Mon. Not. R. Astron. Soc.,* **221,** 257–267.

Jones, J. & Hawkes, R.L. (1986). "The structure of the Geminid meteor stream – II. The combined action of the cometary ejection process and gravitational perturbations." *Mon. Not. R. Astron. Soc.,* **223,** 479–486.

Joss, P.C. (1973). "On the origin of short-period comets." *Astron. Astrophys.,* **25,** 271–273.

Kamél, L. (1991). "The evolution of P/Encke's light curve: no secular fading, a vanishing perihelion asymmetry." *Icarus,* **93,** 226–245.

Kaufmann, P., Kuntz, V.L.R., Pase Leme, N.M., Piazza, L.R., Vilas Boas, J.W.S., Brecher, K. & Crouchley, J. (1989). "Effects of the large June 1975 meteoroid storm on Earth's ionosphere." *Science,* **246,** 787–790.

Kresák, Ľ. (1968). "Structure and evolution of meteor streams." *Physics and Dynamics of Meteors (IAU Symp. No. 33),* eds Kresák, Ľ. & Millman, P.M., Reidel, Dordrecht, Holland, pp. 391–403.

Kresák, Ľ. (1978). "The Tunguska object: a fragment of Comet Encke?" *Bull. Astron. Inst. Czechoslov.,* **29,** 129–134.

Kresák, Ľ. (1980). "Sources of interplanetary dust." *Solid Particles in the Solar System (IAU Symp. No. 90),* eds Halliday, I. & McIntosh, B.A., Reidel, Dordrecht, Holland, pp. 211–222.

Kresák, Ľ. (1987). "Aging of comets and their evolution into asteroids." *The Evolution of the Small Bodies of the Solar System,* eds Fulchignoni, M. & Kresák, Ľ., Elsevier, Amsterdam, pp. 202–216.

Kronk, G.W. (1984). *Comets: A Descriptive Catalog,* Enslow, Hillside, N.J. & Aldershot.

Kronk, G.W. (1988). *Meteor Showers: A Descriptive Catalog,* Enslow, Hillside, N.J. & Aldershot.

Kuiper, G.P. (1951). "On the origin of the solar system." *Astrophysics,* ed. Hynek, J.A., McGraw-Hill, N.Y., pp. 357–424.

Laskar, J. (1988). "Secular evolution of the Solar System over 10 million years." *Astron. Astrophys.,* **198,** 341–362.

Lindblad, B.A. (1973). "The distribution of $1/a$ in photographic meteor orbits." *Evolutionary and Physical Properties of Meteoroids (NASA SP-319),* eds Hemenway, C.L., Millman, P.M. & Cook, A.F., NASA, Washington, D.C., pp. 175–181.

Lindblad, B.A. (1987). "The IAU Meteor Data Center in Lund." *Interplanetary Matter,* eds Ceplecha, Z. & Pecina, P., Czechoslovak Academy of Sciences, Ondřejov, pp. 201–204. (= *Publ. Astron. Inst. Czechoslov. Acad. Sci.,* **67 (2),** 201–204).

Lovell, A.C.B. (1954). *Meteor Astronomy,* Oxford University Press.

Luu, J.X. & Jewitt, D. (1988). "A two-part search for slow-moving objects." *Astron. J.,* **95,** 1256–1262.

Luu, J. & Jewitt, D. (1990). "The nucleus of Comet P/Encke." *Icarus,* **86,** 69–81.

Marsden, B.G. (1972). "Nongravitational effects on comets: the current status." *The Motion, Evolution of Orbits, and Origin of Comets (IAU Symp. No. 45),* eds Chebotarev, G.A., Kazimirchak-Polanskaya, E.I. & Marsden, B.G., Reidel, Dordrecht, Holland, pp. 135–143.

Mazaud, A., Laj, C., de Sèze, L. & Verosub, K.B. (1983). "15 Myr periodicity in the frequency of geomagnetic reversals since 100 Myr." *Nature,* **304,** 328–330.

McCrosky, R.E. & Posen, A. (1961). "Orbital elements of photographic meteors." *Smithson. Contrib. Astrophys.,* **4,** 15–84.

McFadden, L.A., Gaffey, M.J. & McCord, T.B. (1984). "Mineralogical-petrological characterisation of near-Earth asteroids." *Icarus,* **59,** 25–40.

McFadden, L.A., Tholen, D.J. & Veeder, G.J. (1989). "Application of photometric models to asteroids." *Asteroids II,* eds Binzel, R.P., Gehrels, T. & Matthews, M.S., University of Arizona Press, Tuscon, Arizona, pp. 442–467.

McIntosh, B.A. & Hajduk, A. (1983). "Comet Halley meteor stream: a new model." *Mon. Not. R. Astron. Soc.,* **205,** 931–943.

Milani, A., Carpino, M., Hahn, G. & Nobili, A.M. (1989). "Dynamics of planet-crossing asteroids: classes of orbital behavior. Project Spaceguard." *Icarus,* **78,** 212–269.

Murray, C.D. (1982). "Nodal regression of the Quadrantid meteor stream: an analytic approach." *Icarus,* **49,** 125–134.

Murray, C.D., Hughes, D.W. & Williams, I.P. (1980). "The effect of orbital evolution on the influx of Quadrantid meteoroids." *Mon. Not. R. Astron. Soc.,* **190,** 733–741.

Nakamura, T. & Yoshikawa, M. (1991). "Cosmo-dice: dynamical investigation of cometary evolution." *Publ. Nat. Astron. Obs. Japan,* **2,** 293–383.

Napier, W.M. (1984). "The orbital evolution of short period comets." *Asteroids, Comets, Meteors,* eds Lagerkvist, C.-I., & Rickman, H., Uppsala University, Uppsala, Sweden, pp. 391–395.

Neftel, A., Oeschger, H. & Suess, H.E. (1981). "Secular non-random variations of cosmogenic carbon-14 in the terrestrial atmosphere." *Earth Plan. Sci. Lett.,* **56,** 127–147.

Newburn, R.L. & Spinrad, H. (1985). "Spectrophotometry of seventeen comets. II. The continuum." *Astron. J.,* **90,** 2591–2608.

Newhall, X.X., Standish, E.M. & Williams, J.G. (1983). "DE 102: a numerically integrated ephemeris of the Moon and planets over forty-four centuries." *Astron. Astrophys.,* **125,** 150–167.

Oberst, J. (1989). "Possible relationship between the Farmington meteorite and a seismically detected swarm of meteoroids impacting the Moon." *Meteoritics,* **24,** 23–28.

Oberst, J. & Nakamura, Y. (1991). "A search for clustering among the meteoroid impacts detected by the Apollo lunar seismic network." *Icarus,* **91,** 315–325.

Oeschger, H. & Beer, J. (1990). "The past 5000 years history of solar modulation of cosmic radiation from ^{10}Be and ^{14}C studies." *Phil. Trans. R. Soc. Lond.,* **A 330,** 471–480.

Olsson-Steel, D. (1986). "The origin of the sporadic meteoroid component." *Mon. Not. R. Astron. Soc.,* **219,** 47–73.

Olsson-Steel, D. (1987a). "Asteroid 5025 P-L, Comet 1967 II Rudnicki, and the Taurid meteoroid complex." *The Observatory,* **107,** 157–160.

Olsson-Steel, D. (1987b). "Planetary close encounters: probability distributions of resultant orbital elements and application to Hidalgo and Chiron." *Icarus,* **69,** 51–69.

Olsson-Steel, D. (1987c). "The dispersal of the Geminid meteor stream by radiative effects." *Mon. Not. R. Astron. Soc.,* **226,** 1–17.

Olsson-Steel, D. (1988). "Identification of meteoroid streams associated with Apollo asteroids in the Adelaide radar orbit surveys." *Icarus,* **75,** 64–96.

Oort, J.H. (1950). "The structure of the cloud of comets surrounding the solar system and a hypothesis concerning its origin." *Bull. Astron. Inst. Neth.,* **11,** 91–110.

Öpik, E.J. (1963). "The stray bodies in the solar system. Part I. Survival of cometary nuclei and the asteroids." *Adv. Astron. Astrophys.,* **2,** 219–262.

Öpik, E.J. (1976). *Interplanetary Encounters,* Elsevier, Amsterdam.

Pittich, E.M. (1972). "Splitting and sudden outbursts of comets as indicators of nongravitational effects." *The Motion, Evolution of Orbits, and Origin of Comets (IAU Symp. No. 45),* eds Chebotarev, G.A., Kazimirchak-Polanskaya, E.I. & Marsden, B.G., Reidel, Dordrecht, Holland, pp. 283–286.

Porter, J.G. (1952). *Comets and Meteor Streams,* Chapman and Hall, London.

Porubčan, V. (1968). "Separation of meteor showers from the sporadic background." *Bull. Astron. Inst. Czechoslov.,* **19,** 327–337.

Porubčan, V. & Štohl, J. (1987). "The meteor complex of P/Encke." *Interplanetary Matter,* eds Ceplecha, Z. & Pecina, P., Czechoslovak Academy of Sciences, Ondřejov, pp. 167–171. (= *Publ. Astron. Inst. Czechoslov. Acad. Sci.,* **67 (2),** 167–171).

Quinn, T., Tremaine, S. & Duncan, M. (1990). "Planetary perturbations and the origin of short-period comets." *Astrophys. J.,* **355,** 667–679.

Quinn, T.R., Tremaine, S. & Duncan, M. (1991). "A three-million year integration of the Earth's orbit." *Astron. J.,* **101,** 2287–2305.

Roosen, R.G. (1970). "The Gegenschein and interplanetary dust outside the Earth's orbit." *Icarus,* **13,** 184–201.

Roosen, R.G., Berg, O.E. & Farlow, N.H. (1973). "Dust storms in space?" *Evolutionary and Physical Properties of Meteoroids (NASA SP-319),* eds Hemenway, C.L., Millman, P.M. & Cook, A.F., NASA, Washington, D.C., pp. 223–226.

Roy, A.E. (1978). *Orbital Motion,* Adam Hilger, Bristol.

Scholl, H. & Froeschlé, C. (1988). "Gravitational breaking of meteor streams in resonance with Jupiter." *Astron. Astrophys.,* **195,** 345–349.

Schubart, J. (1968). "Long-period effects in the motion of Hilda-type planets." *Astron. J.,* **73,** 99–103.

Scotti, J.V., Rabinowitz, D.L. & Marsden, B.G. (1991). "Near miss of the Earth by a small asteroid." *Nature,* **354,** 287–289.

Sekanina, Z. (1972). "A model for the nucleus of Encke's Comet." *The Motion, Evolution of Orbits, and Origin of Comets (IAU Symp. No. 45),* eds Chebotarev, G.A., Kazimirchak-Polanskaya, E.I. & Marsden, B.G., Reidel, Dordrecht, Holland, pp. 301–307.

Sekanina, Z. (1973). "Statistical model of meteor streams. III. Stream search among 19303 radio meteors." *Icarus,* **18,** 253–284.

Shoemaker, E.M. (1983). "Asteroid and comet bombardment of the Earth." *Ann. Rev. Earth Plan. Sci.,* **11,** 461–494.

Shoemaker, E.M. & Wolfe, R.F. (1986). "Mass extinctions, crater ages and comet showers." *The Galaxy and the Solar System,* eds Smoluchowski, R., Bahcall, J.N. & Matthews, M.S., University of Arizona Press, Tuscon, Arizona, pp. 338–386.

Singer, S.F. & Stanley, J.E. (1980). "Submicron particles in meteor streams." *Solid Particles in the Solar System (IAU Symp. No. 90),* eds Halliday, I. & McIntosh, B.A., Reidel, Dordrecht, Holland, pp. 329–332.

Smoluchowski, R., Bahcall, J.N. & Matthews, M.S. (eds) (1986). *The Galaxy and the Solar System,* University of Arizona Press, Tuscon, Arizona.

Sonett, C.P. & Suess, H.E. (1984). "Correlation of bristlecone pine ring widths with atmospheric ^{14}C variations: a climatic-Sun relation." *Nature,* **307,** 141–143.

Southworth, R.B. & Hawkins, G.S. (1963). "Statistics of meteor streams." *Smithson. Contrib. Astrophys.,* **7,** 261–285.

Stagg, C.R. & Bailey, M.E. (1989). "Stochastic capture of short-period comets." *Mon. Not. R. Astron. Soc.,* **241,** 507–541 & microfiche MN 241/1.

Steel, D.I. (1992). "Additions to the Taurid Complex." *The Observatory,* **112** (in press).

Steel, D.I. & Clube, S.V.M. (1991). "The small comet hypothesis." Preprint.

Steel, D. & Lindblad, B.A. (1992). "The meteor orbit database." *Sp. Sci. Rev.,* to be submitted.

Steel, D.I., Asher, D.J. & Clube, S.V.M. (1991a). "The structure and evolution of the Taurid Complex." *Mon. Not. R. Astron. Soc.,* **251,** 632–648.

Steel, D., Asher, D.J. & Clube, S.V.M. (1991b). "The Taurid Complex: giant comet origin?" *The Origin and Evolution of Interplanetary Dust (IAU Colloq. No. 126),* ed. Levasseur-Regourd, A.C., Kluwer Publishing, Tokyo (in press).

Štohl, J. (1968). "Seasonal variation in the radiant distribution of meteors." *Physics and Dynamics of Meteors (IAU Symp. No. 33),* eds Kresák, Ľ. & Millman, P.M., Reidel, Dordrecht, Holland, pp. 298–303.

Štohl, J. (1984). "On the distribution of sporadic meteor orbits." *Asteroids, Comets, Meteors,* eds Lagerkvist, C.-I., & Rickman, H., Uppsala University, Uppsala, Sweden, pp. 419–424.

Štohl, J. (1986). "The distribution of sporadic meteor radiants and orbits." *Asteroids, Comets, Meteors II,* eds Lagerkvist, C.-I., Lindblad, B.A., Lundstedt, H. & Rickman, H., Uppsala University, Uppsala, Sweden, pp. 565–574.

Štohl, J. (1987). "Meteor contribution by short-period comets." *Astron. Astrophys.,* **187,** 933–934.

Štohl, J. & Porubčan, V. (1987). "On applicability of meteor stream membership criteria." *Interplanetary Matter,* eds Ceplecha, Z. & Pecina, P., Czechoslovak Academy of Sciences, Ondřejov, pp. 163–166. (= *Publ. Astron. Inst. Czechoslov. Acad. Sci.,* **67 (2),** 163–166).

Štohl, J. & Porubčan, V. (1990). "Structure of the Taurid meteor complex." *Asteroids, Comets, Meteors III,* eds Lagerkvist, C.-I., Rickman, H., Lindblad, B.A. & Lindgren, M., Uppsala University, Uppsala, Sweden, pp. 571–574.

Sykes, M.V. (1988). "IRAS observations of extended zodiacal structures." *Astrophys. J. (Lett.),* **334,** L55–L58.

Sykes, M.V. (1990). "Zodiacal dust bands: their relation to asteroid families." *Icarus,* **85,** 267–289.

Sykes, M.V. & Greenberg, R. (1986). "The formation and origin of the IRAS zodiacal dust bands as a consequence of single collisions between asteroids." *Icarus,* **65,** 51–69.

Sykes, M.V. & Walker, R.G. (1991). "Constraints on the diameter and albedo of 2060 Chiron." *Science,* **251,** 777–780.

Sykes, M.V., Lebofsky, L.A., Hunten, D.M. & Low, F. (1986a). "The discovery of dust trails in the orbits of periodic comets." *Science,* **232,** 1115–1117.

Sykes, M.V., Hunten, D.M. & Low, F.J. (1986b). "Preliminary analysis of cometary dust trails." *Adv. Sp. Res.,* **6 (7),** 67–78.

Sykes, M.V., Greenberg, R., Dermott, S.F., Nicholson, P.D., Burns, J.A. & Gautier, T.N. (1989). "Dust bands in the asteroid belt." *Asteroids II,* eds Binzel, R.P., Gehrels, T. & Matthews, M.S., University of Arizona Press, Tuscon, Arizona, pp. 336–367.

Sykes, M.V., Lien D.J. & Walker, R.G. (1990). "The Tempel 2 dust trail." *Icarus,* **86,** 236–247.

van Diggelen, J. & de Jager, C. (1955). "On some recently observed fireballs." *Meteors,* ed. Kaiser, T.R., Pergamon, Oxford, pp. 162–167. (= *J. Atmos. Terr. Phys. (Spec. Suppl.),* **2,** 162–167).

Weissman, P.R., A'Hearn, M.F., McFadden, L.A. & Rickman, H. (1989). "Evolution of comets into asteroids." *Asteroids II,* eds Binzel, R.P., Gehrels, T. & Matthews, M.S., University of Arizona Press, Tuscon, Arizona, pp. 880–920.

Wetherill, G.W. (1967). "Collisions in the asteroid belt." *J. Geophys. Res.,* **72,** 2429–2444.

Wetherill, G.W. (1988). "Where do the Apollo objects come from?" *Icarus,* **76,** 1–18.

Whipple, F.L. (1940). "Photographic meteor studies. III. The Taurid shower." *Proc. Amer. Phil. Soc.,* **83,** 711–745.

Whipple, F.L. (1950). "A comet model. I. The acceleration of Comet Encke." *Astrophys. J.,* **111,** 375–394.

Whipple, F.L. (1951). "A comet model. II. Physical relations for comets and meteors." *Astrophys. J.,* **113,** 464–474.

Whipple, F.L. (1967). "On maintaining the meteoritic complex." *The Zodiacal Light and the Interplanetary Medium (NASA SP-150),* ed. Weinberg, J.L., NASA, Washington, D.C., pp. 409–426.

Whipple, F.L. (1991). "The activities of comets related to their aging and origin." Preprint.

Whipple, F.L. & Hamid, S.E. (1952). "On the origin of the Taurid meteor streams." *Helwan Obs. Bull.,* **41,** 1–30.

Whipple, F.L. & Hamid, S.E. (1972). "A search for Encke's Comet in ancient Chinese records: a progress report." *The Motion, Evolution of Orbits, and Origin of Comets (IAU Symp. No. 45),* eds Chebotarev, G.A., Kazimirchak-Polanskaya, E.I. & Marsden, B.G., Reidel, Dordrecht, Holland, pp. 152–154.

Wright, F.W. & Whipple, F.L. (1950). "The photographic Taurid meteors." *Harv. Coll. Obs. Tech. Rep. No. 6.*

Wyatt, S.P. & Whipple, F.L. (1950). "The Poynting-Robertson effect on meteor orbits." *Astrophys. J.,* **111,** 134–141.

Yeomans, D.K. & Chodas, P.W. (1989). "An asymmetric outgassing model for cometary nongravitational accelerations." *Astron. J.,* **98,** 1083–1093.

Yoshikawa, M. (1989). "A survey of the motions of asteroids in the commensurabilities with Jupiter." *Astron. Astrophys.,* **213,** 436–458.

Acknowledgements

First, and most, thanks to my supervisor, Victor Clube for all the help, encouragement, advice and ideas he has given me. He and Bill Napier introduced me to the subject (not really that long in the past, but more years ago than I like to think); without them I would never have found out how fascinating it all is.

Much of the work described in Chapter 4 resulted from collaboration between Duncan Steel, Victor and myself, and I have learned a lot from Duncan even though the electronic mail connection between here and Australia could be guaranteed to break down just when we needed it urgently.

I have been lucky enough to share an office with Graeme Waddington, the "Great Wading Demon", who has always been willing to provide help on a variety of things.

A short series of classes on solar system dynamics given by James Binney and Tom Quinn proved very instructive in general and in particular enabled me to present the theory on resonant orbits near the start of Chapter 3.

I wouldn't know what a telescope was if it ran me over in the road; nevertheless I have been interested in genuine observational data even if I didn't obtain it. Thanks to David Morgan, Mike Read and Sue Tritton of the U.K. Schmidt Telescope Unit regarding photographic observations and to Helen Walker and Gill Pearce regarding infra-red.

Discussions with Mark Bailey have been very useful. For one thing, they led to my discovering a bug in the program that was used to generate most of my results. Not that it would have undermined the thesis, I hasten to add.

This work would not have got beyond Chapter 1 without computers, which seem to be life-support systems for most astronomers nowadays. Our department has been fortunate indeed to have Tony Lynas-Gray and Ivan Bishop keeping the whole system in order.

No-one can survive without money and I was supported by a research studentship from the Science and Engineering Research Council.

Taurid complex A psychological condition that leads those it afflicts to believe that there is an extremely big comet presently disintegrating in the inner Solar System.